
# Soft Computation Using Electro-Active Polymer Hydrogels

PhD

**School of Biological Sciences, Biomedical Engineering**

Vincent Strong

**February 2024**

# Soft Computation Using Electro-Active Polymer Hydrogels

**Vincent Strong**

## Abstract

Active matter systems have long been explored for computational potential, utilising their unique behaviours for esoteric applications. Electroactive Polymer (EAP) hydrogels are an active matter material currently explored as soft robotic actuators, however not yet explored for their potential computational potential as a form of active matter. Interesting alternate computing mediums exist but studies have yet to present significant framework for materials integrating computation with physical action. This study exploits EAP responses, finding that EAP behaviour can be utilised for automaton and reservoir computing frameworks.

Through reproduction of previous EAP works memory-like behaviour was found within the EAPs, confirming their potential as computational resources, given appropriate framework. Under sequential electrical stimulation, the EAP mechanical responses were represented in a probabilistic Moore automaton framework and expanded through shaping the reservoir's energy landscape. The EAP automaton reservoir's computational ability was compared with digital computation to assess EAPs as computational resources, showing that the EAP's computation via reaction to stimuli can be presented through automaton structures, revealing a potential bridge between and controller in EAP's. This computation was then further expanded through additional inputs. Through this exploration similarities in behaviour between EAP hydrogels and biological neurons were discovered, among these were evidence of the Free Energy Principle (FEP), raising the question; by applying theories of Biological Neural Network (BNN) learning, such as FEP active inference, to learning within a different medium whose behaviour is also governed by FEP, can emergent learning be achieved with alternative mediums? EAP hydrogels were embedded in the simulated game-world of Pong via custom Multi-Electrode Arrays and feedback between motor commands and stimulation. Through performance analysis within the game environment emergent learning was observed, driven by ionic behaviours of the hydrogels. These observations enforced the theories of FEP within learning and its ability to allow learning in other mediums.

# Declaration

I confirm that this is my own work and the use of all material from other sources has been properly and fully acknowledged.



Vincent Strong

# Acknowledgements

I would like to thank Process Vision Ltd and managing director Paul Stockwell for funding this project, without which this would not have been possible. I thank my supervisors, Dr Yoshikatsu Hayashi and Prof. William Holderbaum for their supervisory guidance and for the discussions and insights gained though our meetings. I thank members of the Brain Embodiment Lab (BEL) and Health and Life Science (HLS) lab for their help in using the laboratory spaces throughout my project. My gratitude goes to the university support team and my mentors Sanja Quayle and Susan Lawrence, for their encouragement and continued help thought my university life both academically and personally. My appreciation goes to my parents Christine and Tony Strong for their support through my university life. Lastly, I would also like to thank my friends, with special thanks to Harry Thorpe for helping me maintain a balance between my university and Process Vision work life.

# Contents

# Chapter 1

# Introduction

Computation exists in many forms, from traditional logic based in electronic hardware to biological brains in nature. Because of the many forms it can take computation can be conceptualised in many ways, making the definition of what is and is not computation difficult. The Oxford English Dictionary defines computation as "The action or process of computing, reckoning, or counting; arithmetical or mathematical calculation; an instance of this" [1]. All processes can be modelled mathematically. Meaning that any process, artificial or natural, can be represented as a mathematical calculation in some form and so can be considered computation. For the purpose of this study, computation is defined generally as any type of arithmetic or non-arithmetic calculation that follows a well-defined model or algorithm [2, 3, 4]. This definition can be refined on in terms of application to align with the goals of the project. This refined definition conceptualises computation as "the processing and transduction of information toward a task". The form that this information takes or the way in which the processing of said information supports the task is irrelevant, as long as the processing that occurs is useful to the task and the goal of the task is well defined. Although these definitions may seem vague, this only serves to highlight the varied forms in which computation can present.

In recent research alternative forms of computing are being used more and more frequently to achieve computation and calculations significantly more efficiently [5, 6]. These explorations of alternative mediums have become especially promising in the field of soft robotics through the implementation of smart materials [7, 8]. These materials are capable

of reacting to environmental conditions and have been implemented to reduce the need for more traditional algorithm based robotic control systems, allowing simpler soft robots to be far more capable. These smart materials are applied through implementation of theories derived form computation in nature, referred to as embodied and morphological computation [9, 10, 11].

Morphological and embodied computing are theories that explore the unique computation that occurs through the intrinsic integration of hardware and software, most often illustrated via the codependency of body and brain in nature. These theories present the idea that the brain uses the body as an extension to its computational ability, and it is only though this reliance that its unique learning and adaption capabilities are achieved [12, 13]. The most prevalent forms of computation in the world are those found in nature, all of which employ concepts of morphological and embodied computing in their function. There have been several successful implementations of these unique forms of computation within modern problems. For example, mycelium mold as maze solvers [14], chemical reactors as logic gates [15, 16], and water ripples used for image analysis [17, 18]. As morphological and embodied computing concern the body, the bodies' material composition is key to achieving the desired behaviour. The most prevalent field concerning these materials is that of active matter.

Active matter materials are composed of many active agents which consume energy to drive mechanical forces [19, 20]. The complex interaction between these agents are what generate the interesting behaviour of the material, behaviour that can often be exploited for computation. This exploitation has been implemented for a number of purposes, however one of the most interesting with application to robotics is that of learning [21, 22]. This learning occurs through a form of memory that exists in active matter materials, agents coming to represent this memory and learning occurring as the agents interact. Ionic Electro-Active Polymer (EAP) hydrogels are one such active matter material [20] that has recently shown promise in computing for this reason [23], if given an appropriate application and framework.

Ionic EAP hydrogels have long shown promise in soft robotics as actuators [24]. These materials change shape in response to stimulation via an electric field, with ions acting as active agents. However, these ions also interact with many other morphological and

environmental factors, such as the polymer structure, temperature, water concentrations. Furthermore, due to the compliant nature of the hydrogel and possibilities of different shapes ionic EAPs offer almost infinite complexities in behaviour that have yet to be fully explored in computation. This study seeks to answer two main questions in regards to these areas of research: By utilising a materials, such as ionic EAPs, that offer more complex behaviour, over that of the materials currently studied within morphological and embodied computation, can more complex forms of emergent computation be achieved? Furthermore, what can this exploration highlight about the method in which greater forms of computation could be achieved from other such similar materials?

## 1.1 Problem Statement

Active matter has for some time been classified as a material within the field of soft robotics as soft matter [25]. Through this classification there have been a significant number of studies into the integration of body and control in soft robotics utilising active matter materials [26, 27, 28]. These studies use the theories of morphology and embodied computation to allow the robot's body structure to be used as a computational resource in its own control [29, 30]. However, very few current soft robotic studies of morphological computing attempt to exploit potential learning and emergent properties of active matter in these applications [21]. This gap in application is due to a lack of exploration into materials capable of both emergent learning and soft robotic actuation, and lack of an applicable theoretical framework that is able to integrate both of these attributes [21]. Although all current studies and applications have offered unique computational potential and robotic applications, this only scratches the surface of what could be possible with more complex active matter soft robotic materials. This study aims to contribute to this under explored area of soft robotic and active matter research.

## 1.2 Aims and Objectives

The aim of this work is to show that EAP hydrogels, and by extension other similar materials, can be used uniquely in computational applications. Furthermore, how they could, through use in these applications, offer potentially more efficient solutions that

might otherwise be overlooked or missed via other more conventional, digital, means of computation. This overarching aim was broken down into the following sequential goals which are achieved through this study, each contributing to the research field:

1. Establish the theoretical mechanisms driving the EAP hydrogel, and the behaviours, resulting from these mechanism, useful to computation.

2. Through initial experimentation, develop the initial interfacing procedure to extract this useful behavior for computation tasks.

3. Develop an initial framework for potential application of the computationally useful behavior to a computational task, validating this framework through simulation.

4. Via the simulated results refine the framework to allow the application to a real-world task, validating the refined framework with application to a live real-world task.

## 1.3 Thesis Structure

This thesis is comprised of several experiments undertaken during research while working towards the main aims of the project, to demonstrate EAP hydrogels in a real-world computation task and show the emergent benefits. The chapters of this thesis are organised and described, along with their respective contributions, as follows:

**Chapter 1 Introduction.** Introduces the topic and goals of the thesis and overall structure.

**Chapter 2 Literature Review.** Covers background literature and information which introduces the fields of study covered within this work and provides the necessary understanding to the reader throughout the rest of the thesis.

**Chapter 3 Reproducing EAP Hydrogel Actuation Results.** Through the reproduction of previous work in EAP hydrogel, establishes the mechanics, properties, and the experimental procedures needed to explore the computational abilities of EAP hydrogels. Through this chapter the current methods in the field for synthesising,

actuating, and recording EAP hydrogels are refined and expanded on to create a reproducible methodology that can be applied to a much wider range of hydrogel shapes.

**Chapter 4 Electro-Active Polymer Gels as Probabilistic Reservoir Automata for Computation.** Initially explores the computational application of the unique mechanics within EAP hydrogels by developing and validating an initial automaton reservoir framework via a probabilistic Moore automata, designed to harness the EAP hydrogel's response to an electric field. Through this chapter a new Probabilistic Moore Automata framework is developed. This framework allows the application of the unique behaviour of active matter materials in computation and calculation problems.

**Chapter 5 EAP Hydrogel Inspired Neural Network.** Further explores the potential of computational application, by comparing the similarities between EAP hydrogels and biological computation to allow the EAP hydrogels to be more fully utilised via neural learning techniques. Through this chapter an experimental 3 electrode EAP hydrogel actuation method and model is constructed. This model shows the applicability of weights to alter swelling rates within EAP hydrogels using similarities to neurons behaviour as the starting framework.

**Chapter 6 Learning Behaviour When Embodied in a Simulated Game-World.** Builds on the previous chapter by developing and validating a method to show how the potential learning behaviour of EAP hydrogels can be better exploited, via theories of the free energy principle and active inference, leading to emergent learning behaviour when embodied in a simulated game-environment. Through this chapter a unique electronic interface is developed to integrate the EAP hydrogel as a computational resource within a task. The experiments and results in this chapter show the computational benefit and learning capability of the EAP material used in this way. This chapter also contributes to the theories of FEP and active inference by showing the applicability of these theories even when applied to an entirely different medium.

**Chapter 7 Conclusion.** Addresses the initial aims that were met through this work, highlighting the contributions and discussing possible future work.

## 1.4 Publications

There have been several publications as a result of the research undertaken in this project. These have contributed to the field through the aims of the project as described in this thesis. The publications are listed below:

- Active Matter as a Path Planning Interpreter - Published in the 2nd IMA Conference on Mathematics of Robotics [31].
- Electroactive Polymer Gels as Probabilistic Reservoir Automata for Computation - Published in the journal iScience via Cell Press [23].
- Electro-active Polymer Hydrogels Exhibit Emergent Learning When Embodied in a Simulated Game-Environment - Currently under review by the journal Cell Reports Physical Science, via Cell Press, as of the date of this thesis.

# Nomenclature

| | |
|---|---|
| $\alpha$ | Actions |
| $\alpha_{gain}$ | Gain parameter, $\alpha_{gain} \in \mathbb{R}$ |
| $\bar{\theta_{\boldsymbol{I}}}$ | Mean angle for input sequence, $\boldsymbol{I}$, $\bar{\theta_{\boldsymbol{I}}} \in \mathbb{R}$ |
| $\bar{c}$ | Mean value of $c$, $\bar{c} \in \mathbb{R}^{+}$ |
| $\bar{k}_l$ | Mean output state label given by the input sequence labeled $l$, $\{\bar{k}_l \in \mathbb{Z} \mid 0 \leq \bar{k}_l \leq 26\}$ |
| $\bar{R}$ | Ideal gas constant, $\bar{R} = 8.315J \cdot mol^{-1} \cdot K^{-1}$ |
| $\boldsymbol{\Theta}_i$ | Processed angle, $\boldsymbol{\Theta}_i \in \mathbb{R}$ |
| $\boldsymbol{\Theta}_{max}$ | Maximum output angle of gel, Degrees |
| $\boldsymbol{\Theta}_{min}$ | Minimum output angle of gel, Degrees |
| $\boldsymbol{I}$ | Input Sequence, $\boldsymbol{I}(l) = (\boldsymbol{I}_1, \boldsymbol{I}_2, \boldsymbol{I}_3)$ |
| $\boldsymbol{I}_i$ | Input symbol, $\{\boldsymbol{I}_i \in \Sigma\}$ |
| $\boldsymbol{O}_I$ | Output sequence, $\boldsymbol{O}(k) = (\boldsymbol{O}_1, \boldsymbol{O}_2, \boldsymbol{O}_3)$ |
| $\boldsymbol{O}_i$ | output symbol, $\{\boldsymbol{O}_i \in \Gamma\}$ |
| $\chi^*$ | Interaction coupling parameter, $\chi^* \in \mathbb{R}^{+}$ |
| $\chi_0$ | Polymer–ion interaction, $\chi_0 \in \mathbb{R}^{+}$ |
| $\chi_1$ | Polymer–solvent interaction, $\chi_1 \in \mathbb{R}^{+}$ |

$\delta$ Transition relation

$\epsilon$ Absolute permittivity of material, $\epsilon \in \mathbb{R}^{>0}$

$\Gamma$ Output alphabet, $\Gamma = \{-1, 0, 1\}$

$\hat{p}$ Power of the coefficient, $\{\hat{p} \in \mathbb{Z}^{\geq 0}, \hat{p} \leq r\}$

$\iota$ Initial state, $\iota \in S$

$\lambda_{\perp}$ Cell swelling degree, $\lambda_{\perp} \in \mathbb{R}^{+}$

$\mu$ Internal states

$\mu_U$ Mean of $U$, $\mu_U \in \mathbb{R}^{>0}$

$\Omega$ Number of microstates, $\Omega \in \mathbb{Z}^{+}$

$\omega$ Output function

$\Phi$ Normal distribution

$\phi$ Volume fraction, $\phi \in \mathbb{R}^{+}$

$\phi_0$ Initial volume fraction, $\phi_0 \in \phi$

$\Pi_c$ Counterions osmotic pressure, Pascals

$\Pi_p$ Polymer-polymer affinity negative pressure, Pascals

$\Pi_{ela}$ Rubber elasticity density, $\Pi_{ela} \in \mathbb{R}^{+}$

$\Pi_{osm}$ Osmotic pressure, Pascals

$\Sigma$ Input alphabet, $\Sigma = \{-1, 0, 1\}$

$\sigma^2$ Variance, $\sigma^2 \in \mathbb{R}^{>0}$

$\sigma_U$ Standard deviation of $U$, $\sigma_U \in \mathbb{R}^{>0}$

$\theta$ Bending angle, Degrees

$\theta_i$ Angle after symbol $i$, $\theta_i \in \mathbb{R}$

$\theta_{actu}$ Actuation angle, Degrees

$\theta_{rest}$ Resting angle, Degrees

$\upsilon$ Solvent concentration, $\upsilon \in \mathbb{R}^{+}$

$\varphi$ Concentration, Substance per unit volume

$\widetilde{s}$ Sensations

$\widetilde{x}$ Environmental states

$A$ Surface area of electrode, $A \in \mathbb{R}^{+}$

$a$ Gain minimization parameter, $a \in \mathbb{R}$

$a_i$ Actuation coefficient $i$, $a_i \in \mathbb{R}$

$a_{\hat{p}}$ Coefficient associated with the power $\hat{p}$, $a_{\hat{p}} \in \mathbb{R}$

$A_{PMA}$ Probabilistic Moore Automata, $A_{PMA} = (S, \Sigma, \Gamma, \delta, P, \omega, \iota, )$

$b_i$ Trend fitting coefficient $i$, $b_i \in \mathbb{R}$

$b_{ni}$ coefficient $i$ of trend $n$, $b_{ni} \in \mathbb{R}$

$c_0$ Undeformed polymer elastic density, $c_0 \in \mathbb{R}^{+}$

$c_i$ Number of occurrences of the $i^{th}$ element of $O$, $c_i \in \mathbb{Z}^{+}$

$C_{cont}$ Continuity adjustment, $C_{continuity} = -0.5$

$C_{ties}$ Adjustment due to tied ranks, $C_{ties} \in \mathbb{R}^{>0}$

$D$ Diffusion constant, $D \in \mathbb{R}^{+}$

$d$ Distance between opposing electrode plates, $d \in \mathbb{R}^{+}$

$D_{kl}$ Kullback–Leibler divergence, $D_{kl} \in \mathbb{R}^{>0}$

$e$ Electron charge, $e = 1.602 \times 10^{-19} C$

$F$ Free energy, $F \in \mathbb{R}^{>0}$

$F_{con}$ Faraday constant, $F_{con} = 9.649 \times 10^4 C \cdot mol^{-1}$

$i$ Input symbol, $\{i \in \mathbb{Z}^{\geq 0}, i \leq N\}$

$J$ Diffusive flux, $mol/cm^2 - s$

$k$ State label representation of $\boldsymbol{O}$, $\{k \in \mathbb{Z} \mid 0 \leq k \leq 26\}$

$k_B$ Boltzmann constant, $k_B = 1.381 \times 10^{-23} m^2 \cdot kg \cdot s^{-2} \cdot K^{-1}$

$k_e$ Coulomb constant, $k_e = 8.988 \times 10^9 N \cdot m^2 \cdot C^{-2}$

$K_{rank}$ Set of unique ranks with ties, $K_{rank} \in \mathbb{R}$

$k_{rank}$ Rank, $k_{rank} \in K_{rank}$

$l$ State label representation of $\boldsymbol{I}$, $\{l \in \mathbb{Z} \mid 0 \leq l \leq 7\}$

$m_i$ Ion and water Concentration of cell $i$, $m_i \in \mathbb{R}^{>0}$

$N$ Sentence length, $N \in \mathbb{Z}^{\geq 0}$

$n$ Size of dataset, $n \in \mathbb{Z}^{>0}$

$O$ Set of elements in $Q$ without repetitions, $O \in Q$

$o$ Number of samples in $O$, $o \in \mathbb{Z}^+$

$p$ P value, $p \in \mathbb{R}^{>0}$

$Q$ Sample used in distribution, $\{Q \in \mathbb{Z} | 0 \leq Q_i \leq 1000\}$

$q$ Number of samples in $Q$, $q \in \mathbb{Z}^+$

$R$ Norm of Residuals, $R \in \mathbb{R}$

$r$ Degree of the polynomial, $r \in \mathbb{Z}^{\geq 0}$

$r_i$ Resting coefficient $i$, $r_i \in \mathbb{R}$

$R_s$ Lowest ranked sum value, $R_s \in \mathbb{R}^{>0}$

$r_{elec}$ Distance of ion from electrode pair, $r_{elec} \in \mathbb{R}^+$

| | |
|---|---|
| $S$ | Set of Probabilistic Moore Automata States |
| $S_{ent}$ | Entropy, $S_{ent} \in \mathbb{R}^{>0}$ |
| $S_{i,j}$ | State, $S_{i,j} \in S$ |
| $T$ | Absolute Temperature, $T \in \mathbb{R}$ |
| $t$ | Time, Seconds |
| $t_{k_{rank}}$ | Number of ties for the ${k_{rank}}^{th}$ rank, $t_{k_{rank}} \in \mathbb{Z}^{>0}$ |
| $U$ | U statistic, $U \in \mathbb{R}^{>0}$ |
| $u$ | Free energy, $u \in \mathbb{R}^{>0}$ |
| $u_c$ | Chemical gradient energy, Joules |
| $u_e$ | Electric field energy, Joules |
| $u_p$ | Electric potential energy, Joules |
| $v_e$ | Voltage of electrodes, $v \in \mathbb{R}$ |
| $v_i$ | Ion voltage potential in cell $i$, $v_i \in \mathbb{R}$ |
| $v_m$ | Monomeric unit volume, $v_m \in \mathbb{R}^+$ |
| $w$ | Weight, Seconds |
| $x$ | Distance over which ion motion is measured, $x \in \mathbb{R}^+$ |
| $z$ | Z score, $z \in \mathbb{R}$ |

# Chapter 2

# Literature Review

## 2.1 Introduction

The research pursued in this study covers many different fields. Computation as a subject itself is extremely diverse, influencing and influenced by areas of study from physics and mathematics to biology, chemistry, and philosophy. This study, however, focuses on the practical application of computation through alternate mediums such as EAPs, utilising theories of computation across these subjects to achieve unique and useful results.

The concept of achieving computation in alternate mediums is referred to as "unconventional computing", and can encompasses countless fields of computational research. Unconventional computing can take almost any form from physical and mechanical systems, to fluidics [32, 33], to atomics and quantum computing [34], to biological system such as DNA [35] and chemical computing [36, 15]. A key feature of this field of study is, through the utilisation of these alternate mediums, solutions that would not initially be obvious in more traditional approaches can be achieved, often with unique benefits. This approach of uniquely efficient computing is key to the goals of this project, with many soft robotic materials falling into the realm of unconventional computing themselves.

Many of the fields of unconventional computing covered in this study are relatively new resulting in a disproportionate distribution of literature across topics to review. To support this diversity of fields and subjects, this literature review aims to present an evaluation of the relevant background information and state of the art as it relates to this

study.

This review chapter is broken down into two main sections. The first section focuses on the explanation of active matter EAP hydrogels that are the focus of this study as an alternative computational medium. The section describes their established and state of the art use in the field as well as the mechanics that make them promising in the applications pursued through this study. The second section starts from a higher-level point of view of computation and gradually narrows down into the specific fields associated with the alternate computing topics covered in this study. Initially covering computation broadly, demonstrating how varied forms of computation can exist, while examining computational structures and fields relevant to this study. This is followed by specific computational structures that align with the advantages of active matter in computation, covering various theories in neural network application and learning both artificially and biologically.

## 2.2 Section I - Active Matter and Soft Robotics for Computation

The Oxford English Dictionary defines a machine as "A complex device, consisting of a number of interrelated parts, each having a definite function, together applying, using, or generating mechanical or (later) electrical power to perform a certain kind of work (often specified by a preceding verbal noun)" [37]. This definition applies to more than just the traditional mechanical or electrical apparatus. The definition can apply to many natural systems and alternate materials that have gained traction in fields of robotics and unconventional computation. One such material field within unconventional computing that has been gaining notoriety, and the field that is most aligned with this thesis, is that of active matter. This part of the literature review will lay the background of active matter then go on to review its current use in the field. This aims to give an overall view of the application of active matter within soft robotics and explain why EAP hydrogels were the clear choice, of active matter material, in pursuit of this studies goals.

### 2.2.1 Active Matter

Active matter is a field of material science that has recently made great strides in the use of alternate materials in novel applications. Principles of active matter have existed since 1600s, with Isaac Newton holding the notion "Nature contains foci of activity, agents whose spontaneous working produces results that cannot be accounted for by the mechanical philosophy's only category of explanation: particles in motion" [38, 39]. These theories have since evolved into the understanding of today. Today, examples of active matter are explored in areas from bacterial colonies [40] and bio-polymers [41] to self-propelled particles [42, 43] and active fluids soft robotics [44], with active matter as a classification of soft matter only recently widely accepted [25].

Active matter materials today are defined as materials that are composed of many active agents which consume energy to drive mechanical forces [19, 20]. As these constituent elements, "agents", continually consume energy the system is intrinsically out of thermal equilibrium and breaks time reversal symmetry [45, 46]. Importantly, for the purpose of this study, these active agents, although independent, influence each other leading to a form of parallel and emergent computation. This feature has been exploited in some chemical processor systems utilising Belousov–Zhabotinsky (BZ) reactions [22, 47].

BZ reactions are a classic example of non-equilibrium thermodynamics and thus exemplify active matter. A solution of an acid and bromine is created (typically malonic acid and potassium bromate). When mixed, the interaction between chemicals creates standing waves of reactions that propagate across the surface interacting with each other [48].

In the study by Parrilla-Gutierrez, Sharma, and Tsuda, et al [22] a grid of fluidically connected cells each containing BZ reactions was constructed. This grid was used as a matrix of parallel chemical oscillators. Each cell could be mixed via a controllable motorised stirrer to provide inputs to the system, while a camera used image analysis techniques to extract the chemical oscillation as output. This system was then used to encode letter characters for machine learning. Although the system was able to effectively encode the data, effectively doing pre-emptive calculations to improve efficiency of the machine learning algorithm, it was limited to a passive role in the learning process. The

system in this study was shown to have memory. However, this memory was not used to its fullest potential, only being used to encode short term historical information. This limited exploitation of memory is emphasised by complexity of the methodologies used to apply input to, and extract output from the BZ system. Input required translation of signals into stirring commands before they could interact with the reactions, while outputs required non-trivial image analysis processes to extract the useful information. The complexity of these methodologies result in additional layers of abstraction between the computational behaviour of the BZ system and the larger machine making use of this computational resource, limiting efficiency.

The computational potential of active matter materials is evident, although the choice in material is key to the possibilities of application. Memory, although not required (as in ANNs), when utilised in computation greatly expands the potential problems that can be solved [49, 50, 51], and is common in some form to all active matter systems. With the advent of active matter's classification within soft robotics, many other forms of active matter material which display these uniquely computational behaviours have been explored, and offer behaviours that are significantly easier to interface with.

### 2.2.2 Soft Matter Technologies

Within the field of soft robotics, active materials, or soft matter, have been widely applied with the goal to emulate or exceed the versatile behaviours and properties of naturally occurring materials and organisms [8, 52, 21]. There has been much emerging interest in synthesizing active matter to serve as smart materials and structures capable of operating autonomously around people [8]. Due to this the current field of soft matter materials is vast, and, given the large number of forms active matter can take, extremely varied in terms of material type. The current field of soft matter can be summarised into a few main categories of material; elastomers, polymer composites, fluids, and gels [52]. There is, however, overlap between these categories as applications of soft matter technologies utilise multiple different techniques to accomplish robotic goals. These categories are rooted in the material technologies commonly used throughout the field of soft robotics. As stated, this study focuses on the application of these soft matter materials toward achieving the same emergent computing capabilities of active matter systems. In this sub-section of the

literature review, I will cover current state of the art examples within the categories of soft matter, showing their pros and cons toward the aims of emergent computing, and conclude with the chosen technology.

**Elastomers**

Elastomers are by far the most common material technology used within soft robotics; they are rubbery polymers that are mechanically compliant with high elastic strain limits. Elastomers and other soft polymers used in soft robotics typically undergo large strains, due to this their the stress response is typically nonlinear [52]. It is through this non-linear response that active elastomers have been applied within soft robotics, utilising materials whose stress response is influenced by additional stimuli. Active elastomers utilise the unique stress response to induce passively useful behaviour in the robot body, often presenting as adaptivity in complex task environments [53].

The study by Chortos, Mao, and Mueller, et al [54] used 3D printing to construct custom bundles of dielectric elastomers suited to specific tasks. Dielectric elastomers, also referred to as Electro-Active Polymers (EAPs), are elastomers whose stress strain relationship is altered through the application of electricity. By carefully designing the arrangement of dielectric bundles, the behaviour of the printed actuator was pre-programmed. Through their use of 3D printing technology the possible programmed shape deformations were far more customisable than any previous approach. The actuators were capable of high frequency, 700 Hz, actuation with cycle lifetimes, 2.6 million cycles, exceeding what current soft actuators are capable of. Although these materials were shown to be robust and capable soft actuators. Their computational ability was limited to that which they were pre-programmed with during manufacture, as they were not designed with computation in mind.

The study by Zhang, Ke, and Jiang, et al [26] developed a programmable elastomer sheet for origami robots. Origami robots are soft robotic structures that actuate via folding motion. The elastomer chosen in the study swelled when a solvent is applied. By using a laser to selectively engrave grooves on the surface of the elastomer sheet the shape change induced by swelling could be programmed. This programmed information can be thought of as akin to memory, once programmed the material remembers the states it is to

transition into. Using a laser, the density of programable information is extremely high, allowing for the possibility of very complex programmed behaviours. This study differs from the previous one in that the sheets could be reprogrammed. Once engraved the sheets were re-coated to fill in the engraved ridges, the surface could then be re-engraved with the new programmed motion. Although this material was able to be reprogrammed it still required significant processing to accomplish. Because of this, much like in the previous example, the computational ability is limited to that set when the material is programmed.

The study by Chung, Parsons, and Zheng, et al [55] developed novel elastomer actuators that deformed in response to a magnetic field. An elastomer is doped with a magnetic particle to imbue the material with magnetically reactive properties and allow deformation under magnetic fields. As with the previous examples, the response of the elastomer is programmed through the specific arrangement of magnetically responsive elastomers with non-magnetic elastomers. This means that like the previous examples the material is only capable of the calculations defined during its construction but also has a memory like element. However, unlike electric stimulation or solvents, magnetic fields are much easier to shape and allow operation of the material from a distance. The study discusses the benefits of this technology in non-invasive medical applications. With regard to computation, an application not pursued in the study, the additional degrees of freedom afforded by this means of stimulation allow for a larger range of input variation and thus larger output variation. This larger variation in input and output could mean a greater potential for more complex computational behaviour.

The study by Tracz, Wille, and Pathiraja, et al [56] took a different approach to introducing active elements into elastomer based soft robotics. Building on previous work by the same research group [57], the team built pneumatic logic devices. These devices functioned similarly to transistors, allowing different air flow rates in one channel based on the pressure of an input channel. Unlike the other examples mentioned the elastomers themselves were not active, it was through the structure that active elements were enabled, allowing the structure to react to input and transduce an output. The computationally significant aspect of these devices was their ability to be used in conjunction with eachother to form logic circuits. Through complex arrangements of these logic devices, the team

suggests that purely elastomer based soft robots could perform automated tasks without the need for silicon based control systems. Although this approach is promising, in terms of active elastomer application, it is, ironically, quite rigid. The circuits would need to be designed for a specific task, and once set could not be updated, limiting computational versatility in the learning focused context of this project.

Although these materials showed great benefits as active actuators, their computational ability is limited. This is understandable as many were not designed with the goal of computation in mind. In terms of computation, the key drawback of soft matter technologies involving elastomers is intrinsically linked to their main benefit. It is through their construction that they are programmed, essentially given a form of memory. Memory is a key element of computation [49, 50, 51], and would be required in some form in the chosen technology. However, the computational behaviour of these actuators is defined in construction, as they are programmed through the design of their morphology. Although this programming can be exceedingly complex, and can allow for a wide range of possibilities in computation, it is fixed. This means that the kind of learning behaviour found in other active matter examples, such as the study by Parrilla-Gutierrez, Sharma, and Tsuda, et al [22] mentioned in the previous subsection, would not be possible with elastomers.

**Polymer Composites**

Polymer composite technologies build on the mechanisms of elastomers by constructing devices from various types of elastomer and polymer each with their own mechanisms and responses to stimuli. It is through the interaction between these varying mechanisms that this type of soft matter archives unique active behaviour. This technology is also not limited to composites between polymers but also other materials, some approaches using imbedded metals and even electronics to allow for interesting applications.

The study by Park, Mondal, and Treadway, et al [58] utilises channels of liquid metal within a stretchable elastomer to create a soft, compliant, variable capacitor. The study poses applications for these devices as sensors and stretchable electronics. It focuses primarily on the procedure and materials used to create the precise and defined channels in the elastomer. However, the compliance of the technology as a sensor introduces a

great degree of freedom in interaction with its environment. The application to stretchable electronics creates an interesting avenue of implementing complex computation via more traditional electronic architectures.

The study by Jin, Lin, and Kiani, et al [59] used a similar combination of liquid metal and elastomers. How their applications differs, however, is in the use of temperature as the driving mechanism. The elastomer structure was doped with thermochromic pigments, these pigments react in response to temperature by changing color. Liquid metal was also embedded within the elastomer which redistributed as the structure was stretched or otherwise deformed. The liquid metal alters the heat transfer within the elastomer structure which then presents as a color change in the pigments. Through the design of specific channels the flow of liquid metal was able to be designed into tactilely triggered logic circuits. This inclusion of logic circuitry introduced an interesting, computationally significant, secondary active feature to the already active material composite, with the possibility of complex color changing responses to touch.

The study by Binysh, Wilks, and Souslov [60] designed devices capable of "snapping" between shapes, through the elastocapillary phenomena. This phenomenon occurs through surface tension, the same phenomena responsible for the shape of water droplets. By surrounding an elastic material (core) with a negatively tensioned material (shell) the resultant composite can be capable of snapping between steady state forms. This state change can be triggered by a number of environmental conditions such as temperature, pH, etc. The interaction between tension of the core and shell result in interesting shape changes that could be employed computationally. The study shows that these theories can be applied in both the macroscopic and microscopic scales, resulting in potential self-controlling soft micro-robotic devices using this technology. However, the study only simulates the materials and although potential methods are given, they have yet to be tested making implementation difficult.

The study by Bastola, Rodriguez, and Behl, et al [61] constructed biologically inspired cactus robots utilising active elastomers to react to environmental conditions. The technologies used in this example overlap with other categories as hydrogels were used in conjunction with elastomers to achieve the desired result. Hydrogels were applied over an elastomer core, the rigidity of the overall composite was dependent on the volume of

the hydrogel. The core resembled a star shape, based off of a cactus stem. When the gel volume is low the star is able to deform and bend freely, when the gel volume is high the star is held in its uniformly distributed position resulting in a more rigid structure. The volume of the gel is affected by air moisture and temperature, this means that the robotic cactus is able to alter is rigidity in response to environmental factors much like that of the biological counterpart. This behaviour can be thought of as a kind of computation of environmental factors. Although limited, the robot is responding by calculating the appropriate flexibility in relation to the environment.

Although the more complex properties of these technologies highlight avenues for interesting computational applications the same drawback of single material elastomers remain, the function is programmed at construction. The kind of emergent computation that has been shown in other active mater examples, such as the study by Parrilla-Gutierrez, Sharma, and Tsuda, et al [22], relies on the interaction of many active agents. The constraints applied by the elastomers limit these interactions, making behaviour more predictable. This predictability makes the technology more desirable as an actuator but vastly limits its potential exploitation as a computational resource. This kind of behaviour was most successfully achieved in swarms [62, 63] and by extension active fluids [22, 64]. Fluids, however, have been implemented as soft matter materials.

**Fluids**

Fluids within soft robotics can refer to a variety of mediums from gasses to liquids [52]. The body acts to direct the force produced by the accumulation of these fluids into useful motion and behaviour. In this way they are similar to composite technologies. However, to distinguish categories, the fluidic technologies discussed here are differentiated by the direction of influence. In these examples the fluid actively deforms the surrounding body, as opposed to the other way around as in previous elastomer composite examples. In active soft matter applications, these fluids are typically responsive to external or internal forms of stimuli. Mediums such as ferro and conductive fluids are used as well as various chemical reactions, leading to the unique behaviour of active matter occurring in a soft robotic body.

The study by Wehner, Truby, and Fitzgerald [65] designed a soft robot octopus that

used microfluidic logic to actuate. A reaction between two chemicals generates gas which is used to expand and contract the integrated soft actuators. The body is inlayed with microfluidic logic in the form of integrated valves and channels. In this way the motion of the robot is looped, allowing for a motion cycle and locomotion. The robot is essentially programmed via the arrangement of internal valves and channels that result in the microfluidic logic. The complexity of the program is limited by the implementable density of valves. As with previous examples, the fact that the program is set in construction limits the computational ability. However, the methodology is capable of far more complex behaviour, compared to the simpler elastomer structures, though the use of chemical reactions, chemical reactions having shown capability for computation with correct implementation [15]. The computation shown in this study is directed by the microfluidic logic. However, as this logic cannot be changed later the potential for emergent computation is limited.

The study by Garrad, Soter, and Conn, et al [33] utilised similar fluidic circuits within an number of robotic structures, where the study differs significantly is in the application. These circuits were used for sensory and control functions within the larger structure. The fluidic structures interfaced with electronic circuity, acting as a form of integrated soft feedback control for the actuation system. One of the structures explored in the study was a softworm. The worm's body was designed to allow the pressure of a fluid, in an embedded tube, to contract the body, as the body contraction propagated along the body the worm locomoted. The pressure propagation was controlled by an electronic pump, electrodes where embedded in the tube that made contact with the fluid. When contact was made an electronic signal altered the direction of the pump. This meant that the fluid itself, and the body structure of the worm, controlled the actuation. By changing the electrode placement the gait of locomotion could be altered. The study also explored the application of these techniques to more complex logical circuits opening a considerable expanse of possibilities of integrated soft computing, where complex actions can be taken by robots whose own body structure define their behaviour.

The study by Fan, Jiang, and Li, et al [27] created a shape changing soft robotic structure, that does not require an outer supporting body, using ferrofluid. The robot body is entirely composed of a ferrofluid solution, this fluid is magnetic and can be influenced

by magnetic fields. Using electromagnets, the body can be influenced to change shape and move. In the study the robot was navigated through a maze of varying shaped openings. By altering the shape of the robot, it was able to pass through each of the openings and navigate sections that a solid body robot would not have been able to. The active matter element of this robot is present in the bodies' ability to morph in reaction to the magnetic field and environment. Although computation was not the goal of the study, the material does show potential in this application. The magnetic fields act as an input to the body, providing a problem to be solved. The morphology of the body then solves this problem by changing its shape, the final shape of the body is the solution to the problem. This presents an interesting computational paradigm that allows for "re-programming" during operation by simple altering the magnetic field. For the application of self-contained robots there are drawbacks however, as the fluid can only be controlled by electro-magnets external to the environment that the root is navigating, requiring significant supporting infrastructure.

Fluids show considerably more potential in computation through their greater variation in responses and complexity. Greater variability allows for greater potential outputs and allows the material to represent more complex computations. However, interfacing with these materials is difficult, requiring significant external infrastructure, or a specially designed body to direct the fluid, both requiring significant time and energy in implementation and limiting versatility in application. The polymer-based materials were much easier to interface with but lacked the same computational potential. Gels can be thought of as a solution to this problem.

#### Gels

Gels are a recently emerging popular material within soft robotics for actuation and electronics. Gels are binary fluid-solid systems [66] and can be thought of as combining the material properties of polymers/elastomers and fluids. The polymer volume fraction is typically only enough to provide structural integrity ($\approx 1 - 10\%$). The gel is also commonly bicontinuous, with the solid and fluid phases forming connected networks, influencing each other, much like the different materials in composite polymers however with much greater complexity. Gels can be infused with a variety of different fluids, from water to ionic solutions.

The study be Kim, Hanna, and Byun [67] developed a soft matter disc capable of transitioning between 3-dimensional shapes. This disc is comprised of a hydrogel that swells and de-swells under changes in temperature. The crosslinking in the chosen gel can be tuned through irradiation dose. By altering the crosslinking the shape change response to temperature can be tuned. The study used lithography to apply the radiation in specific patters over the surface of the gel disc. This application is similar to the laser etching used in the study by Zhang, Ke, and Jiang, et al [26]. However, hydrogels are capable of considerably higher volume changes due to their much lower polymer volume fraction. As with the laser etching study this methodology apply behaviour to the gel disk similar to memory, however, the response is hard programmed during creation.

The study by Hong, Almomani, and Montazami [68] explores ionic EAP hydrogels as a strain sensor. Ions within the EAP hydrogel rearrange when the gel is subject to strain. This was shown to generate a detectable electric field. This application utilises the imbalance of thermodynamics common to all active matter materials to transduce strain into a readable electric signal. Due to the compliance of the hydrogels, these sensors allow for strain in almost any direction to be detectable. The ability to sense the direction of strain is dependent on the arrangement of electrodes used to sample the generated electric field. These sensors were shown to have high sensitivity, demonstrating a very versatile strain sensor that could be applied in all manner of soft robotic applications and even wearable technologies. The transduction of information can be thought of as a type of computation, preforming calculations to transpose data from one form to another. This example senses environmental information but does not react to it, although it demonstrates computational potential it does not display any potential for emergent behaviour.

The study by Yoshida [28] further explores the benefits of hydrogels as active matter materials in application as a computational medium. As in the study by Parrilla-Gutierrez, Sharma, and Tsuda, et al [22], BZ reactions were utilised within hydrogels to create a self-oscillating hydrogel structure. This study utilized the self-oscillating BZ reaction coupled with the shape changing ability of hydrogels to construct a “walking” hydrogel robot via propagating shape change. The BZ reaction creates a propagating wave of pH gradient, which causes the collapse of the hydrogel. The element of this study that enforces the computational nature of active matter, lies in the control method. The hydrogel was, in

essence, controlling itself. The BZ reaction was self-propagating and self-regulating with the motion taken by the gel robot dictated by the three-dimensional shape the hydrogel was constructed in and how the BZ reaction propagated down said shape. The shape of the gel was essentially acting as a form of programming, controlling the robot's motion path. This was further controlled by altering the concentration of the reactants in the BZ reaction. Through careful selection of these variables, the motion was "pre-programed" into the robot structure, allowing the robot's own morphology to control its motion removing the need for a designated control system. This example shows the potential of this single active matter material to combine both the cognition and actuation elements. Where the robotic platform demonstrated in this study is lacking, is in environmental interaction. Once constructed, the robot cannot react to environmental influence and thus limits its application in many robotic tasks. However, as demonstrated by the study by Hong, Almomani, and Montazami [68], EAP hydrogels can react to external stimuli if the proper framework is implemented.

Hydrogels show the most adaptable application to computation. Hydrogels can be stimulated by a variety of means, pH, temperature, electric fields, ect, this allows for many more possible input and output frameworks when compared with other soft matter technologies. Gels also employ the same computational potential as found with active matter fluids while being contained in a structure that is much easier to implement. This containing structure also does not impose the limitations found in fluid soft matter implementations such as the study by Wehner, Truby, and Fitzgerald [65]. Memory is also possible as with other elastomer technologies. However, the examples thus far have only explored "hard" memory programmed into the structure of the material at construction. However, ionic hydrogels are capable of presenting a short term memory in their behaviour.

### 2.2.3 Ionic EAP Hydrogels

Ionic EAP hydrogels, as explored in the study by Hong, Almomani, and Montazami [68], have been shown to present a form of memory in their behaviour [20, 23], although an attribute not yet explored in soft robotic applications. Ionic hydrogels are an active matter material [20] showing promise in soft robotics as soft actuated materials (SAMs) [69, 24]. Originally demonstrated to have reversible shape phase transitions by Tanaka, Fillmore,

and Sun, et al [70] in 1978, recent studies have shown the potential for these materials' behaviour to be used in computation [23] given an appropriate application and framework.

As an active matter material and ionic EAP, free floating ions act as the active agents. The application of stimulation causes an increase in free energy. The free-floating ions then seek to minimise this free energy through migration causing changes in the polymer structure [71]. As the ions migrate [72] they draw water molecules with them, this causes changes in the water distribution within the polymer. As the ions collect on one side, the hydrogel swells and deforms [20] [73].

The computational behaviour presents itself in these active matter examples via memory based behaviour in their actuation. Rate of deformation reduces as the swelling increases and more energy is needed. Because of this hysteresis affect [74], the accumulative swelling of the gel due to electric stimulation diminishes. As such, each deformation has influence on further deformations much like the memory presented in chemical computing applications [15, 65]. This hysteresis means, as with other active matter systems, previous responses to stimuli affect future responses leading to the memory-like function [20, 75].

There are many different forms of stimulation that can initiate this structural "collapse" and shape change; pH [76], salt [77], solvent [78], heat [79], humidity [80], electric [81] or magnetic field [82, 83], and light [84]. This versatility in how they are interacted with, along with their compliance, are the driving factors in their current popularity in soft robotic applications [69].

These same factors make them a promising active matter material that is capable of actuation, sensing, and computation. The attractiveness of these materials within soft robotics and morphological computing is furthered by the versatility in interaction methodologies. The current use of these materials in biomedicine and soft robotics demonstrates some of the many possible paths of research that exploit these unique attributes.

### Current Use in Soft Robotics

Ionic EAP hydrogels are regularly used in biomedical applications as a delivery medium for drugs and tissue engineering [85, 86, 87]. EAP hydrogels also exhibit strong biomimetic behaviour with biological muscles [88, 89]. This has led to their recent application in robotics as artificial muscles [73]. However, as with any material there are benefits and drawbacks

that can be balanced through the method of application, such as high compliance but low force output [90].

The study by Otake, Kagami, and Kuniyoshi, et al [91] explores the kinematics of EAP hydrogels for applications in biomimetic robots. In order to approach the problems of solving kinematics in a compliant body, the motion of the gel was restricted to one plane. A rectangular bar of gel was used with plates, providing the electric stimulation, affixed opposite each other on one end. As the electric field is applied the gel bent in a consistent arc. This methodology allowed the motion to become more predictable and concise, but restricted the compliance and potential of the soft body, thus not making full use of its possible degrees of freedom.

Alternatively, in the study by Otake, Kagami, and Inaba, et al [24] a robotic starfish was built. The robot itself was entirely composed of the EAP hydrogel and suspended in a tank of water. The stimulation was applied via an electric field through plats attached to the walls of the tank. This arrangement allowed for complex motion to be achieved in the robot, making the most of the compliant soft body. However, as the field is applied externally, the method becomes very difficult to use in applications outside of a lab environment. Additionally, the robot is also very difficult to control, with control in the study resembling a more manual or "brute force" approach.

These applications combined with the soft matter gel studies explored earlier [68, 28], demonstrate the balance required in utilising the actuation potential of the ionic EAP hydrogels. Freedom of motion must be balanced with ease of control.

### 2.2.4 Section I - Conclusion

From the technologies explored in this section of the literature review Ionic EAP hydrogels offer the most adaptability and potential complexity when applied as a computational resource. The example studies of this section have demonstrated that ionic EAP hydrogels, as an active matter material, have the potential to act as, actuator [91, 24], sensor [68], and computational resource [28]. Through the framework in which they are applied, each of these aspects can be utilised. However, as yet, these applications have been limited to simple tasks such as basic locomotion or sensing and have yet to be exploited together. This limitation is imposed by the framework in which they are applied. Through the

exploration and application of more complex computational theories and structures, could greater exploitation of potential and greater complexity in application be achieved?

## 2.3 Section II - Computation

This study's focus is on the application of computing within the unique mechanics of active materials. Computation, however, spans many fields of study, from algorithmic mathematics to hardware design and biological simulation [92, 3], and exists in many different forms, from the more obvious electronic devices to mechanical interactions and living systems [92, 3, 93, 2, 94]. Natural computation is a term used to encompass many of these forms of unconventional computing based, in part, off the concept that all processes in nature can be interpreted as forms of information processing. Natural computing can be broken into three main branches: computing inspired by nature, simulation and emulation of nature by means of computing, and computing with natural materials [94, 95, 96]. These branches have come to include examples of cellular automata [97], artificial immune systems [98], evolutionary computation [99], and swarm intelligence [62], to name a few. Additionally, all of the examples of computation covered within this review fall somewhere into the realm of natural computing via one or more of these branches.

The variation in form means that computation can be defined in many different ways. However, for the purposes of this study, computation is defined generally as any type of arithmetic or non-arithmetic calculation that follows a well-defined model or algorithm [2, 3, 4].

In traditionally digital computation systems, the hardware, that performs the arithmetic or non-arithmetic calculation, and software, that implements the well-defined model or algorithm, are separate [100]. This separation allows for a diverse range of operations to be possible within the same architecture. However, the unique active materials utilised within this study have no separation [101]. This lack of separation is also common to many natural computational systems, the most prominent being the biological brain, the "software" exists in the structure of the "hardware". This concept is called embodied computation and serves as the base theory used to exploit computational behaviour in the materials pursued by this study. This part of the literature review will cover this approach

to computing by laying out background understating and reviewing current examples in applying these theories.

### 2.3.1 Embodied and Morphological Computation

To fully understand the current field of embodied computation, first its origin must be explained. Embodied computation stems from theories of embodied cognition in neuroscience and philosophy. Embodied cognition as a theory originated in the early 20th century from philosophers Martin Heidegger and Maurice Merleau-Ponty [102], and more recently by Pfeifer and Bongard [11] via embodied intelligence. Embodied cognition holds that an agent's cognition is not independent from the body in which the cognition inhabits but inexplicably connected. In other words, cognition, rather than being the result of abstract representations of the world, is strongly influenced by aspects of an agent's body [13, 11]. In this way cognition is embodied within the whole of the agent and not just the "brain". The cognition of the agent is shaped by the environment in which it inhabits. However, the agent interacts with the environment through its body, therefore the cognition of the agent is also directly influenced by the form of the agent's body [103, 104, 105, 106]. The dynamic and reciprocal coupling between brain (cognition, or control), body, and environment are thought to be responsible for the brain's ability to adapt and effectively control the body through learning [107]. It is through these theories that embodied computation was formed with the aim to achieve these same results.

Embodied computation/intelligence employs concepts of embodiment in the context of computation rather than cognition. In reality, even traditional digital systems are subject to embodied computation as the possible computations are limited by the hardware in which it is embodied [101, 108]. However, due to the abstraction between hardware and software as different layers this is minimised in traditional digital systems. Recent work exploring embodied computation has found that by embracing the intrinsic link between hardware and software, more complex and efficient computation is possible. These exploitations have allowed relatively simple constructs to perform complex tasks by offloading computational load onto the morphological structure of the body, making use of materials not normally associated with providing any computational benefit. Morphological computing is a recent field that emerged from the utilisation of these concepts of

embodied computation in application, most significantly in robotics.

It should however be highlighted that embodied intelligence and morphological computation are not interchangeable, and conceptualise computation within the body in different ways. Embodied intelligence forms the concept that the observed intelligence of an agent is not just a result of the brain or control mechanism that drives it, but also the influence of the body structure of said agent on the driving control mechanism. The way in which an agent senses and interacts with the world influences the actions that it would take, altering its cognition/intelligence. The field of Embodied intelligence itself being a study into the tight coupling between an agent body and brain [11, 109]. Morphological computing, on the other hand, is the offloading of certain processes, to be performed by the body, that otherwise would have to be performed by the brain [11]. An agent exhibiting embodied intelligence will also exhibit morphological computing within its body, but the inverse is not always the case. In essence embodied intelligence requires the tight linking between body and mind, whereas morphological computing only requires the body. Implementations of morphological computing usually being achieved through outsourcing aspects of control tasks to a robot's body, to be handled through the emergence of functional behaviours via inherent properties such as compliance, resonance, damping, and friction [110, 111]. Within applications of engineering and robotics, morphological computing has resulted in the pursuit to achieve some form of embodied intelligence through connecting a system's body and mind [112, 11].

- Soft robotic arms – A study by Nakajima, Li,Hauser, and Pfeifer [113] utilised the inherent properties of a soft octopus arm in its control. In this example sensors were placed down the length of the arm to record the bending shape, and a motor with a single degree of freedom was placed at the base of the arm. A target oscillation frequency was given for the arm to move. The system used the sensed bending motion of the arm to tune the weights of a summing algorithm that fed back into the driving motor. The output weights were tuned to achieve a target oscillation frequency, creating a feedback loop where the soft-body's own response dictated future behaviour. In this way the compliance of the arm was used as an element in its own control, the "calculation" of the bending trend generated by the arm

in response to the motion of the motor was used in place of a control algorithm. This was first explored in simulateion in the study by Nakajima, Hauser, Kang, and Guglielmino, et al [9].

- Soft burrowing robot – A study by Sadeghi, Tonazzini, and Popova, et al [114], followed up by a study by Laschi and Mazzolai [115], used a snake-like compliant robot to move through earth. The end effector of the compliant body naturally tends toward the softer earth. This allows a robot to find the most efficient route through soil without external control. Here the morphology of the robot body is used to calculate the most efficient path, resulting in a more compact and robust system.

- Universal gripper - A study by Brown, Rodenberg, Amend, and Mozeika, et al [116] developed a form of universal gripper. Most grippers rely on finger like mechanism to apply even pressure over the surface of an object and support it. However, many objects consist of uneven surfaces that require complex finger arrangements, with equally complex control and coordination algorithms, in order to support the object. The designed in this study used a compliant bag filled with small beads. When the bag was placed on an object it conformed to a surface's shape. A vacuum was then pulled on the bag causing it to retract over the internal beads and become rigid in the new conformed shape. This allows the gripper to apply maximum surface area over the object while gripping it and allows for a great variety of grippable surfaces. In this example the compliant bag essentially does "calculations" as it conforms to the object. A task that would require complex kinematic equations to apply equal force are effectively achieved by the unique morphology of this design.

- Passive robotic walkers – Developed by McGeer [117], passive walkers exemplify morphological computing, maintaining balance and locomotion due to their structure. The structures walk through the careful design of weights and joints without the need for any external control system or active feedback. Essentially as the robot moves the morphological structure calculates how to best move the limbs through its mechanical implementation, this provides its own self-balancing passive feedback control system.

- Spider silk computers – A project by Hauser and Vollrath [118, 119], utilising the unique and complex signal processing attributes of spider webs for computation. Spiders catch prey through their webs. These webs act as a form of sensor array transmitting information, such as location, size, speed, etc, back to the spider via vibrations. Although the vibrations are simple it is through the structure of the web and the way in which the spider interprets the vibrations that a significant amount of information can be extracted. The arrangement of the webs essentially allows for the signal processing calculations to occur, these calculations are programmed in the morphology of the webs structure.

- Physarum machine - The physarum machine, or slime mould computer, [120] made popular by A. Adamatzky. Adamatzky, in combination with many partners, used slime moulds to compute railway and road networks between major cities [121, 122, 123]. The slime mould grows to reach food and attempts to do so by the most optimised route. By creating a scale map of the geographical topology and placing food at the representative locations of major cities, the slime mould is able to "compute" most optimised route between those locations. The generated route can then be implemented as transport routes. Through utilising this alternate medium the most optimised route can be found with minimal simulation and modeling, allowing for much more efficient computing of the same task. The use of these mediums also offers interesting possibilities for emergent intelligence [124], resulting in solutions that would not initially be obvious in more traditional approaches. These features of uniquely efficient computing and emergent behaviour are key to the goals of this project, with many soft robotic materials falling into the realm of unconventional computing themselves.

Each of these examples use the inherent properties of a physical body/structure to stand in for control that would normally be handled externally. As described in embodied cognition and computing, cognition arises from bodily interactions with the world and depends on the kinds of experiences that come from having a particular body [125]. However, embodied cognition also highlights that this influence does not occur in one direction. Although the body influences cognition, the cognition is responsible for actions taken by

the body. In this way, the cognition causes changes in the body. As shown from the examples of morphological computation this bidirectional influence is exploitable, although the degree to which it can be exploited is highly dependent on the specific example. This raises issues in determining when morphological computing can or should be employed for a given system.

A study by Zahedi and Ay [126] sought to quantify the impact of morphology on a system in an effort to address this issue. Through the base model of a general sensorimotor loop as the example of a morphological structure, 2 main concepts were proposed to quantify morphological influence: Negative effect of the action, and Positive effect of the world. To summarise these concepts, the first is a measure of how the action of a an agent alters the next world state, the second is a measure of how the previous state of the world effects the next state of the world. If only one concept is true, for a given system, then no morphological effect occurs. Morphological influence depends on a balance between these concepts where the next state of the world is altered by both the actions of the agent and the world itself, which in turn effect the next actions of the agent. These concepts where further explored in application to theories of synergy of body and brain [127], and DC-motor driven models of hopping movements [128]. The employment of these concepts provides encouraging basis for validity of morphological computing techniques as a quantifiably exploitable resource.

Morphological computing as a field shows that useful computation can be exploited in alternative mediums such as EAPs, however the implemented approach to computation is heavily dictated by the material chosen. Implementations of morphological computing often involve custom frameworks to best make use of the unique behaviours of said material. There are, however, commonalities in computation, features found in all computational systems that are required to perform computations. By exploring these commonalities and how they are used for computation in established computational frameworks, these frameworks can be adapted to the active material utilised in this study via theories of morphological computing. One feature common to all computation mediums is memory [49, 50, 51]. The most common memory based computational structure is that of the automata [129, 3].

### 2.3.2 Automata

Automata are a computational structure that process information in sequence according to a set of programmed rules [3]. Information in and out of the automaton must follow a language definition, comprised of a set of defined symbols (or words) with defined grammar to form a sequence (or sentence) [3, 4]. The language dictates what the automaton accepts as input and what the automaton gives as output. The output can belong to an entirely separate language to the input and be as simple as acceptance or rejection of certain inputs. Given the simplicity of this structure it can be applied as a framework to almost any problem of computation, and can be used to represent models both artificial and natural.

One of the simplest automata frameworks is that of the Elementary Cellular Automaton (ECA) developed by Stephen Wolfram [97]. ECAs are one-dimensional cellular automaton that use a set of rules to determine the next state of each cell based on that cell's current state and the state of its neighbours. Compared to other forms of cellular atuomata, ECAs differ in that there are only two symbols, and each rule only looks at three adjacent cells, this leads to a limited rule-sets with only 256 possible ECA configurations. One of the most unique features of this automata is that, despite is very simple structure, it is capable of very complex behaviour. Within ECAs there are rule-set configuration that have been found to be Turing complete. Because of their spacial aspect, cellular automata have been used to model many natural and real-world systems from societal economics and geography [130], to mollusc shell formation [131].

The ability for automata to represent real-world systems is not uni-directional, there are physical systems that exhibit behaviour similar to that of automata. This application of automata to alternative computing mediums was recently examined in the paper by Dueñas-Díez and Pérez-Mercader [15]. In this study, chemical reactors were used to construct logic gates under an automaton structure. Chemicals were assigned symbols and used as inputs while measurable changes, such as colour and pH, were used as outputs with the interaction between chemicals acting as the automaton. Through this framework the chemical reactors were able to act as Turing complete automata and replicate simple logical gate structures. However, this approach was limited in its application to simple

computational structures. Utilising the chemical reactors required careful selection of the chemicals themselves in order to achieve the desired computational response. This prevents the approach from being applicable to other forms of alternative computing, such as active materials, as the automaton framework structure is inextricably tied to the specific reactions used. Although the chemical reactions are simple, in order to "program" the automata for a different task, the chemicals would need to be re-selected, essentially rebuilding the framework from scratch. Alternatively, if a more complex base medium was chosen, such as EAP hydrogels, then more complex automaton structures could be applied allowing for more varied application while using the same automaton framework structure.

Although limited, the study [15] shows that the versatility in automata make it an ideal starting point when dealing with alternate computation mediums. The vast forms of automata available, provide frameworks that can conceptualise the behaviour of a number of mediums into a computational space. There are many paradigms of programming within automata, from the selection of the input/output language to the structure of states and transitions. The following section will discuss some of the more generalised automata and how their structures would allow for alternative mediums to be used computationally.

**Finite-state Machines**

Finite-state machines (FSM) are a subcategory of automata and the most commonly implemented structure or "simple" machines. They are defined as an abstract machine that can be in exactly one of a finite number of states at any given time. FSMs transition from one state to another in response to inputs and provide outputs [132, 129, 3]. FSMs are the most basic form of automata and so provide the most versatility when used as a starting framework for the application of alternate mediums to computation. Although this summarises the basic framework of FSMs, there are many different forms, each with features applicable to certain scenarios. For the purpose of utilising the behaviour of an alternate medium for computation, as is the aim of this study, transducer automata allow for the application of established chemical/physical behaviour to a computational scheme.

Transducers produce output based on input and/or state. They are often used in control applications and extensively in the field of computational linguistics [133]. Among

control and computational applications there are two main forms of transducer FSM automata used, the Mealy machine and the Moore machine.

The Mealy machine was developed in 1955 by George H. Mealy [134]. As with other FSMs this machine moves between states according to inputs received, each transition has an assigned output which is given when the transition occurs. As the output is derived from the transition, which is essentially a convolution of inputs and states, the use of a Mealy machines often leads to a reduction in the number of states compared to other FSMs. Mealy machines are also generally more efficient due to the reduction in states. However, as the output occurs on the transition independent from any clock pulse, it can be difficult to integrate with traditional digital computation. In terms of the research for this thesis, this method of output would also make it difficult to align with the behaviours of alternate computing mediums. For example, in EAPs the transition would be the motion from one state to another. To fit the EAP behaviour into the Mealy structure the transitional motion would need to be encoded into a symbol representation. Due to the compliant nature of EAPs and the amount of variation in motion, this transition would be extremely difficult to define discreetly.

The Moore machine was developed in 1956 by Edward F. Moore [135]. As with other FSMs this machine moves between states according to inputs received. However, alternate to the Mealy machine, Moore machines give outputs at each state. This means that there are usually either less outputs or more states than in Mealy machines. The advantage of the Moore model is a simplification of the behaviour, as output only depend on states. As outputs are given at each state, synchronisation is much easier and allows for simple integration with other computational structures. Indeed, Moore machines have been used to embody many fundamental computational building blocks such as edge detectors and binary adding machines [136]. This means that by using them as a foundation, any framework generated already has a strong base in computational logic allowing for easier implementation within applications. In terms of this study and EAPs, the shape would represent the output and, although still subject to the compliance and inherit variation, is significantly easier to discretise into distinct states and outputs than transitional motion.

The automaton structures covered thus far are deterministic although not all applications of automata are. Through automata structures, even highly dynamic systems

can be simplified into sets of rules given a large enough rule set [4]. This means any non-deterministic machine, such as active materials, can be represented by a deterministic automaton given enough complexity. However, this method of representation can be extremely inefficient for highly complex systems, such as those found in nature [92] and many active materials, as the size of the deterministic automata becomes unmanageable. More efficient representation can be accomplished via non-deterministic and probabilistic automata.

### Probabilistic Automata

Probabilistic automata are a generalization of non-deterministic finite automaton that traverse states based on probability distributions converted to weighted state transitions [137, 138, 139]. Due to their generalisation, probabilistic automata can be applied to a significant number of applications, often used in statistical modelling [140]. Probabilistic computing, or stochastic computing, has been a field of interest since the 1960s. Probabilistic frameworks allow for more efficient computation with high error tolerance [141], when compared to deterministic models, and allow for broader ranges of computations [142]. The error tolerance becomes extremely beneficial when interfacing with active materials, whose behaviour is often subject to significant variation. One of the most common forms of probabilistic automata is that of the Markov chain.

Markov chains are a stochastic model developed by Andrey Markov in 1906 [143], describing a sequence of possible states, or events, in which the probability of each state depends only on the previously inhabited state [144]. This model is often used in automata as a non-deterministic structure. Markov chains are used throughout statistical modelling in fields from physics [145], and biology [146, 147], to economics [148, 149]. However, Markov chains are limited to applications where it can be assumed that the dynamics are time-invariant, and no relevant history need be considered which is not already included in the state description [150, 151]. Additionally, Markov chains do not traditionally take inputs, or give outputs beyond the currently inhabited state. Lacking the ability to transduce information, severely limits computational applications of the structure.

Markov chains offer an efficient structure to model probabilistic behaviour of active matter. However, they do not allow for the incorporation of input sequences and so cannot

be directly integrated as part of a computational process. Moore automata, however, take inputs and aligns them with computational structures synchronously. It has been shown in previous work that every Markov chain can be simulated via a sufficiently complex Moore automata [152]. Additionally, this has been extended to generalised probabilistic automata [153]. Building on this work, through the combination of behavioural features in these automata and modelling frameworks, behaviours of potential active matter computational mediums could be represented in a computational context.

These automaton frameworks provide a flexible and robust computation scheme that can be used to represent the active material's behaviour in a computational context. However, they are generalisations driven by sequential logic. Active matter is inherently parallel, driven by many simultaneous active agents [15]. So it stands to reason that a fundamentally sequential framework, while robust, may not fully exploit the computational ability of active material. However, there is a computational structure that emerged from early work in automata that is also inherently parallel, neural networks.

### 2.3.3 Artificial Neural Networks

Artificial neural networks (ANNs) are a computational structure inspired by applying concepts of automata to the structure of biological neural networks in the organic brain. ANNs were developed with the aim of achieving, computationally, similar levels of complex calculation as found in the biological brain. The biological brain is inherently parallel in its approach to information processing [154, 155], as is the behaviour of active materials. Through understanding how ANNs model this means of processing, a framework that is coupled more deeply to the core mechanics of active matter behaviour can be designed, and the computational potential better exploited.

ANNs are one of the oldest approaches to machine learning, their practical use dating back to the 1960s [156]. The original work that led to the practical artificial neural network started in 1940 with Warren S. McCulloch and Walter Pitts, who, using automata theory, sought to model the function of neurons resulting in the McCulloch-Pitts neural model [157]. Since the early conception of ANNs, there have been many developments in the field improving on speed, efficiency, and accuracy [158]. These developments have led to various algorithms and networks structures such as Multilayer Perceptron Networks

(MLP) [159], Growing Neural Networks (GNN) [160], and Convolutional Neural Networks (CNN) [161]. All these algorithms enhance the computational ability of the ANN structure in order to approach more complex tasks. These structures, as with all implementations of ANNs, are typically only implemented in software making adaptation to active material behaviour difficult. However, ANNs have also been implemented effectively through the use of specially designed hardware to accelerate processing, known as Hardware Neural Networks (HNNs) [162, 163].

These hardware implementations take many architectural forms and implement many ANN algorithms. Implementations have used digital [164], analog [165], optical [166], and gate arrays [167], as well as many more. The breadth of HNN implementations shows the precedence for ANN frameworks to exist closer to a physical hardware. However the majority of HNN implementations are designed with a specific ANN algorithm in mind [162]. This approach makes it difficult to apply the architectures of HNNs to active mater materials. Additionally, as approximations of BNNs, these implementations are not capable of the same emergent learning found in their biological inspiration or in other active matter applications, as they are limited by their hardware implementation [162, 168]. However, within the field of ANNs and HNNs there is an implementation of machine learning that expands this implementation dependency, reservoir computing.

**Reservoir Computing**

Reservoir computing is an ANN field, initially derived from Recurrent Neural Network (RNN) frameworks but now applied more broadly to many other applications. The dynamics of a fixed non-linear system, called a reservoir, are used as part of a neural network, mapping input and output signals to higher dimensional space [5]. One of the key features of reservoir computing is the versatility in possible reservoirs that can be implemented. The first forms of reservoir computing, also called classical reservoir computing, utilised RNN based reservoirs, linking back to its conceptual framework. The standout structures of these initial implementations were Echo State Networks (ESNs) [169] and Liquid State Machines (LSMs) [170].

ESN reservoirs are structured as a hidden layer of fixed and sparsely connected (¡1%) RNN [169]. Alternatively, LSMs utilise spiking neural networks [170]. These network

structures incorporate time into the operating model and more closely mimic the structure of biological neural networks [171]. In both cases the networks are randomly connected, randomly initialised, and fixed during training. The main benefit of these structures, allowing their use in reservoir computing, is that, when training, only the nodes that connect the network to the output layer need to be trained. The key difference between these structures is in how they implement the transmission of data between nodes. Whereas ESNs are based on the more traditional RNN structure of neurons firing at each propagation cycle, LSMs fire continually encoding data in the rate of firing. The main interest of using LSMs instead of ESNs comes from their similarity to biological neural networks, and the advantages that can offer when approaching problems that are traditionally very easy for biological brains. Although the implementation of LSMs can be more complex than ESNs, the LSM's intrinsic incorporation of time in transmission of data within the network offers great benefit when approaching pattern recognition in the temporal domain [172], a feature not found in ESNs. It is through the incorporation of additional dimensions in data transmission that more complex computation is possible, approaching the complexity of the biological brain.

Both ESNs and LSMs can be implemented in software and, as such, are extremely versatile and flexible in their application to problems. However, in more recent developments within the field reservoirs are typically physical systems exhibiting complex behaviour, such as active matter systems, used to encode and transduce data. Physical systems are, by their very nature, more rigid in how they can be implemented, limiting the versatility of problems they can be applied to. However, physical systems offer a significant advantage in two areas, efficiency and complexity of data transmission. As physical systems these reservoirs effectively act as analog computers [173], allowing for much greater efficiency in data transduction and offering many other dimensions to data encoding. For this reason if a problem can be approach via a physical reservoir, the implementation can result in considerably more optimised solutions.

The main reason for reservoir computing is that the encoding performed by these reservoirs embodies computation not possible within a typical ANN structure. For this reason reservoir computing is an ideal framework to be used in applying the computational potential of active material to computing applications. In order to understand how this

application can be accomplished their structure and examples of their current use in the field must be reviewed.

Reservoir computing structures consist of three main layers, excitation layer, reservoir, and readout layer. The excitation layer encodes network input into reservoir stimulation. The readout layer interprets reservoir responses into usable data using weights to allow performance tuning and optimisation. The weights of the neurons in the readout layer are tuned to achieve learning in the system much like in standard RNNs. To be used as a reservoir, a physical system needs to present two properties: non-linearity and memory [174]. Provided with the properties, the reservoir can be any kind of medium that encodes temporal problems into higher dimensions creating recurrent connections in data [175]. There are many examples of this in recent studies involving alternative methods of computation. Here, several examples are listed to give a snapshot of the breadth of this field.

- Bucket image encoding – A study by Fernando and Sojakka [17] used water ripples in a bucket as a reservoir to encode data for a variety of purposes including logical XOR calculations and speech recognition. In this example data was fed into the water bucket reservoir via weighted vibration motors. The way in which the ripples interacted created a resulting waveform that was enhanced via a back-light and recorded by a camera. The recorded information was in essence an encoded form of the information given to the water bucket, much like any morphological image processing. However, the water system was able to perform this encoding much more efficiently than any digital software. In this case the bucket of water was used as a computational resource.

- Fiber optic speech recognition – A study by Larger, Soriano, and Brunner, et al [176] used a length of optical fibre as a reservoir to introduce a time delay and gain in audio feedback. The audio was first encoded into light signals and transmitted down the length of the optical fiber. The signals take time to transmit down the fiber as they are reflected, this introduces a time delay. The delayed signals were then combined with those being transmitted at the beginning of the optical fiber. The way in which these signals interacted with each other created data encoded with

historical information. This data was then used to improve speech recognition, as in speech sounds are given in a meaningful sequence where each sound always related to those that came before. In this example the optical fiber was able to preform encoding live on the signal as it was transmitted creating a much more efficient speech recognition system.

- Protozoa driven computer – A study by Ushio, Watanabe, and Fukuda, et al [6] used ecological and population dynamics of a unicellular protozoa organism as a reservoir. Time series data from other ecologically based systems was fed into the reservoir by controlling the temperature of the organism culture. The encoded information was extracted as population dynamics and showed the ability to predict near future of chaotic dynamics and emulate nonlinear dynamics. This studies' aim was to show that biological systems can be used computationally. In essence a small scale ecological system, capable of being run in a lab environment, was used to predict the outcomes of much larger scale ecological systems, that couldn't be run in a lab environment, more efficiently than computer simulations would allow.

Through all these examples, the reservoir was able to encode data into a form more efficiently, and with less processing time, than a digital computer or simulation. By using the unique properties of the medium to perform calculations on the information, machine learning based on that information was easier to perform via the readout layer. The computations performed by the reservoir are embodied through a form of short-term memory utilising time base interference. EAP gels have also been shown to contain memory like behaviour [20, 23]. This further confirms the appropriate application of reservoir computing within the studies' aims for active matter computing.

However, in these examples the reservoir acts essentially as a static black box separate from the recurrent learning mechanisms contained within the readout layer. The reservoir encodes inputs into outputs to make learning easier but learning itself does not occur within the reservoir. To achieve any form of emergent learning an active matter reservoir would need to be capable of learning itself, in parallel to the readout layer. Within the field of reservoir computing this has been approached through adaptive reservoirs, reservoir systems whose dynamics can be altered to better achieve solutions. As with

any implementation of learning, these systems utilise a learning algorithm to apply the alterations to the reservoir, through altering its structure or dynamics in some way. There are many different implementation examples of these learning algorithms within the more classical reservoir computing structures. A study by Chatzidimitriou and Mitkas [177] utilised neuro-inspired evolutionary algorithms to restructure echo state networks with very promising approximations of real life tasks. Similarly a study by Hoerzer, Legenstein, and Maass [178] utilised a reward system based on Hebbian learning to achieve adaption in chaotic neural networks. As with the previous study, this approach used theories of neuro-inspired learning, such as neuro-plasticity, to implement adaptive learning in a generic network model. Through the strengthening of connections in response to a reward based framework, the system was able to create complex computational structures without direct supervision.

These examples show how learning is possible within the reservoir structure, however only examples where the concept was approached via software and simulation. Physical reservoirs offer considerably more obstacles in implementation, as methods and impact of restructuring vary from medium to medium. A study by Lee, Wei, and Stenning, et al [179] approached this through a chemical reservoir whose dynamics where dependant on temperature and magnetic fields. By altering these controls the reservoir was able to access entirely different computational spaces and could be applied to a greater range of tasks. Although this method allowed for much larger flexibility in task application, while maintaining the computational benefit of its analog nature, the possibility of learning was not explored.

Many of the adaptive reservoir structures that employ learning rely on biologically inspired algorithms, such as Hebbian and synaptic learning. Applying these theories to physical reservoirs is difficult and highly dependent on the reservoir's medium. There is however an example of physical reservoirs where the implementation of biologically inspired learning techniques become simple, biological neural networks [180].

### 2.3.4 Biological neural networks

To understand how biological neural networks are applied as reservoirs, the mechanics that result in learning in biological neural networks must be understood. Computation

in biological systems takes place via biochemistry [181, 4], chemicals and stimuli acting as inputs, with the interaction of these chemicals acting as the process, and the resulting substrates or energy released as the output. Learning in biological systems takes place via a process called neural plasticity. Neural plasticity refers to the nervous system's ability to change activity in response to intrinsic or extrinsic stimuli by reorganizing its structure, functions, or connections [182]. Essentially, this is the capacity of the nervous system to modify itself, functionally and structurally, in response to experience [183]. By stimulating BNNs with encoded task information, neurons will form pathways in response.

Integration between grown neuron cultures and electronic interfaces have been explored as computational devices [184], referred to as organic or 'wetware' computers. Wetware computers are usually implemented through control of network plasticity, achieved via application of patterned or random stimulation [185]. By controlling plasticity, the rate of network reorganisation is controlled. A feedback loop is implemented where the network is 'punished' by increasing plasticity or 'rewarded' by reducing plasticity [186, 185].

A study by DeMarse and Dockendorf [187], used lab grown neuron cultures as a computational resource for flight control stabilisation in a flight simulator. The outputs used to control the plane were selected randomly, using controlled neural plasticity via patterned stimulation to enforce desirable connections. The system showed capability to learn but was prone to over learning, where weights in the network became saturated. This means that although the BNN reservoir was able to learn independently it still required a governing framework/interface to manage learning and prevent saturation.

A study by Kagan, Kitchen, and Tran, et al [188], used lab grown neuron cultures as a computational resource to control an agent in a simulated game environment. An electrode array was used for bidirectional communication between the neuron culture, acting as the reservoir, and a computer containing the game Pong. Environmental inputs, such as the location of the ball, are supplied to the neurons as electrical feedback acting as the excitation layer. Outputs were recorded from the neurons firing and sent to the computer. The outputs were then encoded, so that they could be used to control the paddle in Pong game. This encoding of neuron firing acts as the reservoir readout layer. The readout layer was tuned via altering the mapped association between locations in the neuron culture and the effect of output from those locations on paddle motion. Rally lengths were used as

the performance metric within a closed loop which managed neural plasticity. The BNN (referred to as DishBrain) improved in ability while playing the game as plasticity was altered. The improved game performance shown in the study was attributed to emergent learning, driven by strengthening in synaptic junctions. The learning shown in this study, although present, was only possible once the readout layer was tuned via a reward-based learning algorithm carried out on the computer, external to the neutral culture.

These studies lead to interesting paradigms of learning achievable through application of learning theories in biological systems. However, all demonstrate that, even when utilising a reservoir medium capable of independent learning, a suitable framework that can govern, optimise, and direct that learning is required. The method of controlled plasticity demonstrated in the study by Kagan, Kitchen, and Tran, et al [188] is derived from theories of emergent intelligent behaviour in biological brains via the Free Energy Principle (FEP) [189, 190, 191]. All systems can be summarised via free energy equations, however, some systems better embodied the thermodynamics of FEP than others. The imbalance of thermodynamics that attribute active matter with their unique behaviour can themselves be attributed to an imbalance in free energy [45, 46]. The theories of FEP as applied to emergent intelligent behaviour have, as of yet, only been applied to biological neural systems. However, given the applicability of FEP theories to active matter systems, can similar emergent learning be achieved within a non-biological active matter material? To achieve this the interfacing mechanism would need to be properly designed for the unique behaviour of the active matter reservoir, while accounting for FEP as the driving mechanism. In order to accomplish this the specific considerations of FEP as a learning theory must be understood.

### FEP Learning in Biological Neural Networks

FEP and active inference are recently proposed theories for action, perception, and learning. Much of the most recent work on these theories, in relation to the biological brain and neurology, has been headed by Karl Friston [192, 193, 194, 195]. One such review by Friston [189] covers this application of FEP to BNNs. In this review, FEP is formulated to connect concepts of free energy, as used in information theory, with concepts used in statistical thermodynamics and suggests that any self-organizing system that is at equi-

librium with its environment, must minimize its free energy [189, 196, 197]. This is a formulation of how adaptive systems resist a natural tendency to disorder [197, 198]. FEP interprets learning as an agent bounding it's maximum surprise or entropy, limiting free energy by entering states that alter sensed information [192, 197, 199, 191]. The review conceptualises this in terms of biology, through a feedback loop between internal states, of the brain, and external states, of the environment. In this feedback loop, internalised environmental information is continually improved by actions altering the environment, causing ordered interaction between the agent's internal states. The process created by this feedback loop is referred to as active inference.

In active inference, an internal generative pseudo model predicts inputs representing the environment [189, 196, 193], continually updating the internal model to match external events. The review highlights the similarity between this process and Bayesian inference, a common structure used to apply learning in statistics [200] and interpret learning in biology [201]. As sensed inputs, different from those expected via the model, are received, free energy increases. The system seeks to reduce free energy by the most direct means. This presents as the self-organisation of neural connections [202, 203]. As inputs influence the structural change, the new structure is representative of the inputs, and, by inference, is representative of the environment the inputs came from. Restructuring presents behaviourally as either, action to reduce the difference between the internal model and sensed environment by making the environment match the model or, by altering the internal model to better reflect the environment. In this theory, BNNs hold 'beliefs' about the state of the environment, and learning behaviour emerges by minimising internal free energy through either, updating these beliefs, or taking action to change the environment to match these beliefs [196, 204].

The developed ordering of internal states, conceptualised by active inference in the review, is known as self-organisation, feedback corrects deviations from an ordered configuration [205, 206]. In BNNs self-organisation presents through the reconfiguration of synaptic pathways [207, 208]. These pathways are altered through the interaction of many compounding mechanisms, involving electrical, chemical, and physical systems that act on both the micro and macro scales. To compare to active matter materials, this reorganisation occurs in the distribution of active agents. To summarise, this extremely complex

system as purely the minimisation of free energy could be considered an oversimplification. By obscuring the complexity, the nuance of how learning occurs is also obscured. In more recent studies by Parr and Friston [204, 196], the model of free energy in application to learning has been refined, and the theories have been shown to hold merit in application to practical BNN learning problems as in the study by Kagan, Kitchen, and Tran, et al [188]. Although, as demonstrated by the studies, biological neural networks can be modelled via free energy, there are other materials, such as EAP hydrogels and active matter materials, whose mechanics and behaviour are more directly embodied via free energy equations and thermodynamics.

### 2.3.5 Section II - Conclusion

There are many fields of computation which focus on the use of unconventional mediums as control resources. Embodied and morphological computing are such fields that employ the physical structure of the medium in its control. Through theories of embodied cognition, these fields have shown the ability of the body of "machines" to effectively control themselves without the need for distinctly separate or external control mechanisms. Further to these, new branches of neural network theories, stemming from these explorations of embodiment via automaton theory, have been developed leading to reservoir computing. Through the use of a reservoir structure many complex mediums have been explored for their computational benefits, used primarily to encode data into a form more easily learnt by traditional ANN structures. However, through the use of cultured BNNs as reservoirs, learning has been shown to be achievable in the reservoir itself.

The learning achieved in these examples is attributed to theories of learning via FEP and active inference. These theories conceptualise learning within the biological brain as the minimisation of free energy through feedback between the internal states of the brain and the external states of the environment. The simplification of leaning in the brain to free energy equations, however, obscures the vast complexities resulting from compounding mechanising and structures. These theories of learning have been shown to hold merit in application to BNN computational problems but the abstraction of FEP when compared to the complexities of the biological brain raise an interesting question. If a material, whose mechanics and behaviour more closely embodies free energy minimisation equations, was

used in a computational application, could the same emergent learning and computational ability be achieved more directly?

## 2.4 Conclusion

This literature review highlighted the many intersecting fields involved in the forms of alternate computing this study focuses on. Active matter is a rapidly developing field with interesting applications within smart materials and computing, with one such promising material showing this computational application being ionic EAP hydrogels. This literature review also highlighted the many computational frameworks that have been used within the field of alternate computing, from the basic automata to more complex reservoir techniques. Within computation, concepts of emergent learning were also covered, theories that allow relatively simple structures to achieve complex computational feats. The computational examples covered here, lay the background, serving as the framework that is built on to achieve the desired emergent computing behaviour within soft matter materials to be applied further into this study.

The next chapter starts the process in pursuing the aims of this study by, initially reviewing the driving mechanics of EAP hydrogels, replicating the actuation achieved in previous works, and initially discussing how the responses observed could be applied to a computational structure.

# Chapter 3

# Reproducing EAP Hydrogel Actuation Results

## 3.1 Introduction

The first step in using EAP hydrogels in the application of computation is establishing their mechanics, properties, and the experimental procedures needed to explore these properties.

This chapter aims to lay this foundation, first through the explanation of EAP mechanics via the physical chemistry concepts regarding EAP hydrogel behavior. Secondly, by establishing the base experimental features required to explore EAP hydrogel behavior, defining initial procedures and apparatus through experimentation with the aim to reproduce the actuation properties of EAP hydrogel materials established in current literature. This also includes refining the synthesis procedure for the selected EAP hydrogel, based on the procedures from current literature, for the requirements of the experiments within this study.

Lastly, by performing initial experiments to reproduce and record the EAP hydrogel actuation behavior already established in the current literature and make initial observations in experimental results as to EAP applications within computation.

## 3.2 Physical Chemistry Mechanics within Hydrogel EAPs

The EAP hydrogel structures consist of three main components; the polymer network, the water, and the free-floating negative ions, as shown in figure 3.1 section A. The hydrogen within the water molecules is attracted to negatively charged ions, this means that as the ions move the water follows. As the hydrogel is a polymer structure it is flexible and allows for stretching. If ions are manipulated to concentrate in a specified areas of the hydrogel, then the water also concentrates in that area. This causes an inhomogenous distribution of water that leads to collapse and swelling in apposing areas of the hydrogel. This manipulation can be achieved through the application of electric fields, as the ions themselves are charged they are pulled by the electric field toward the electrodes. However, as a soft body EAP hydrogels do not actuate linearly. The magnitude of energy required to change the shape of the hydrogel by a set amount increases as the shape deviates from its norm, resulting in a hysteresis of motion and requiring unique control schemes when used in actuation applications [209, 210]. Depending on the specific arrangement of electrodes, the ions can be manipulated to gather within a specific place in the hydrogel, causing localized swelling, or leave the hydrogel, causing deswelling of the overall gel demonstrated in figure 3.1 section B. This behavior constitutes the base mechanism that has been exploited, within the current literature, for actuation. One of the initial studies on this behavior was that by Tanaka titled “Collapse of gels in an electric field” and explored the deswelling behavior [71].

There are, however, many interconnected mechanisms that allow the behavior to occur. The motion of the ions results from the changing balance of forces between several physical and chemical mechanics within the hydrogel as electric stimulation is applied. There are two main systems working in parallel to determine hydrogel shape, a system determining the shape of the hydrogel based on ion and water content, and a system determining the ion’s motion through the hydrogel based on the electric field. These systems can be approximated by considering the hydrogel as a one-dimensional series of cells, as shown in figure 3.2 section A and B.

The first system acts on each cell and functions as the equilibrium between three forces, that act to determine the shape of the hydrogel based on the local concentration of

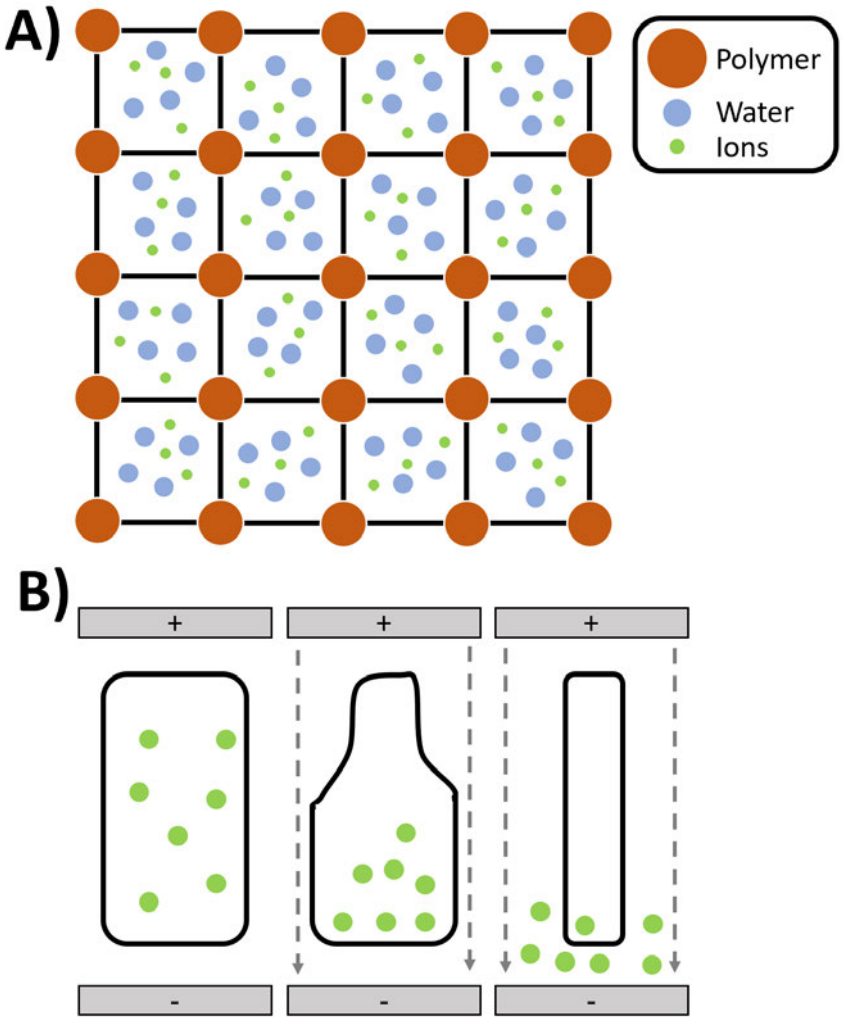


Figure 3.1: **A)** Representation of the structure of an EAP hydrogel. Showing the polymer chains, water molecules, and ions with homogenous distribution. **B)** Represented progression of ion movement and resultant hydrogel shape change while under electric field.

water and ions. These forces are; the positive osmotic pressure of counterions, the negative pressure due to polymer-polymer affinity, and the rubber elasticity of the polymer network [70]. These forces are visualized in figure 3.3 section A for a single cell. Positive osmotic pressure of counterions, $\Pi_c$, results from a chemical gradient of counterion concentration from inside to outside the cell. This force pushes to expand the cell and equalize the gradient. Negative pressure of polymer-polymer affinity (or attraction/interaction), $\Pi_p$, results from the chemical bonds as a result of the cross-linking and charged attractive forces between polymer chains in the network. This force pulls to collapse the cell and reduce the space between polymers. These forces can be simplified into a single term for overall osmotic pressure $\Pi_{osm}$, via Flory Huggins theory for mixing to account for the interaction between the solvent and the polymer [211]. $\Pi_{osm}$ is defined in equation 3.1, where $\phi$ is the volume fraction, $\upsilon$ is solvent concentration, $\chi_0$ is the polymer–ion interaction, $\chi_1$ is the polymer–solvent interaction, and $\chi^*$ is the interaction coupling parameter. The rubber elasticity, $\Pi_{ela}$, acts as a force in both directions, acting to keep the structure in an equilibrium state. Elasticity, oppose to polymer-polymer affinity, is entropic in nature resulting from the random interlaced distribution of polymer chains determined by the change in strand conformations during the network deformation. Elasticity is defined in equation 3.2 [211, 212], where $c_0$ is the density of elastic strands in the undeformed polymer network, $v_m$ is the volume of a monomeric unit, $\lambda_\perp$ is the degree of swelling of the cell, and $\phi_0$ is the initial volume fraction.

$$\Pi_c + \Pi_p = \Pi_{osm} = -(\phi + \ln(1-\phi) + (\chi_0 + \chi_1\phi)\phi^2) + \chi^*\upsilon\phi \tag{3.1}$$

$$\Pi_{ela} = c_0 v_m \left( {\lambda_\perp}^{-1} - \frac{\phi}{2\phi_0} \right) \tag{3.2}$$

As the concentration of ions and water changes within the cells, the equalization of these formulations such that $\Pi_{osm} = \Pi_{ela}$ lead to change in the volume fraction and thus change in the shape. As ions and water molecules gather the osmotic pressure increases, the elastic force then increases to match this and prevent water from leaving the EAP hydrogel, as the elastic force increases the volume fraction increases and the cell swells.

The second system acts on the ion and water molecule migration between cells and

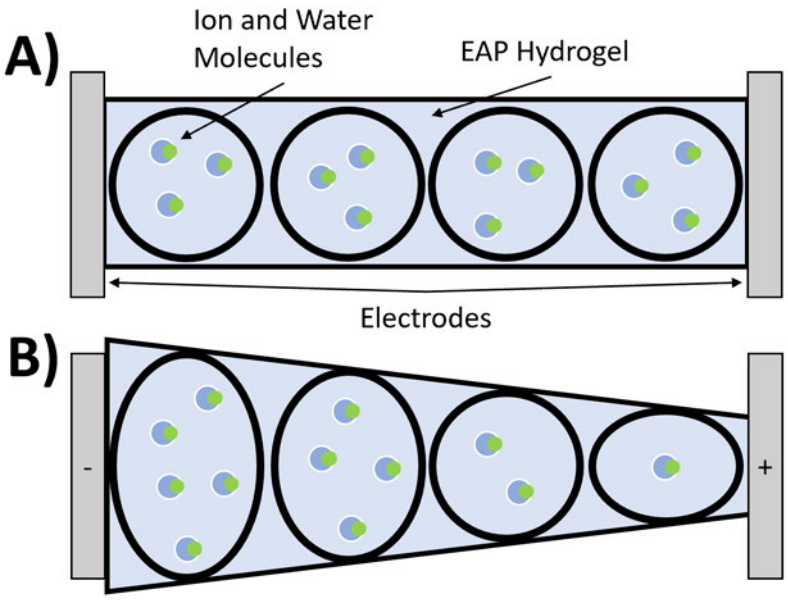


Figure 3.2: One-dimensional representation of the EAP hydrogel as a series of circular cells. **A)** Shows the EAP hydrogel without any stimulation, ions and water molecules are homogenously distributed and so all cells are of the same size. **B)** After stimulation the electric field causes ion and water molecules to migrate from right to left. The collection of water molecules within the left most cells causes swelling and an overall shape change of the hydrogel.

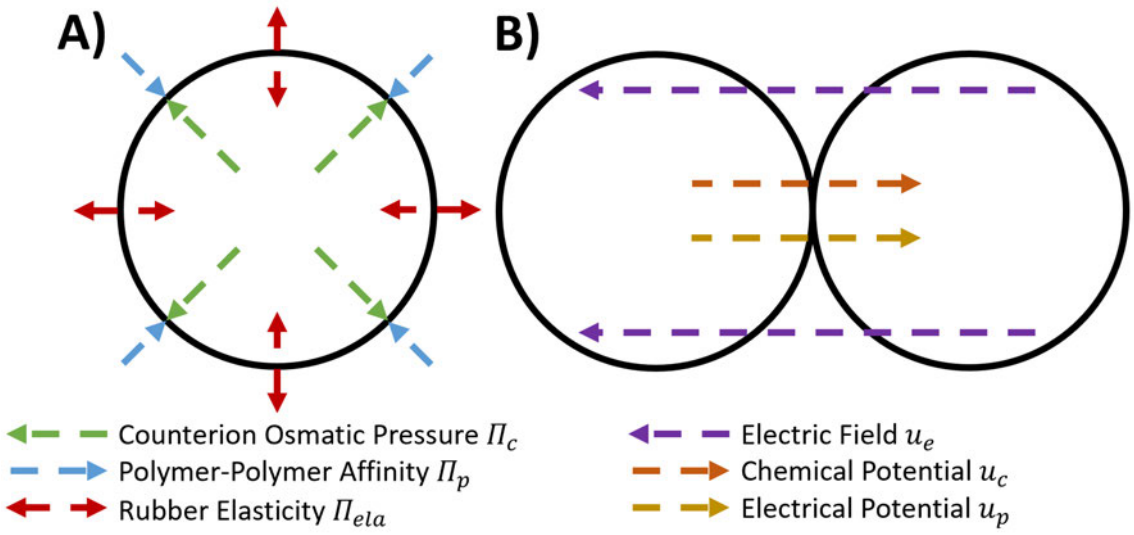


Figure 3.3: **A)** Representation of equalisation between osmotic pressure and rubber elasticity in a "cell" of the EAP hydrogel. **B)** Representation of resultant force between the electric field and electro-chemical potential of the ions and water molecules across "cells".

functions as an equilibrium between three forces. These forces are due to; the electric field on the ions and water molecules migrate across all cells, the chemical gradient of ions and water molecules between cells, and the electrical potential gradient of ions between cells. As discussed earlier, the ion and water chemical gradient is also a component of the osmotic pressure $\Pi_c$. This linking between systems is indicative of the complex coupling between the mechanics that govern the EAP hydrogel's behaviour. This equalization across cells is shown in figure 3.3 section B. These forces can be defined in terms of energy gradient using Frick's first law of particle diffusion [213], shown in equation 3.3, to quantified rate of ion and water molecule diffusion between cells.

$$J = -D\frac{\delta\varphi}{\delta x} \tag{3.3}$$

Frick's first law describes diffusive flux $J$ between regions of high concentration to low concentration. Equation 3.3 is written in terms of concentration gradient, where $\delta\varphi$ is the change in concentration, $\delta x$ is the distance over which the energy gradient acts, and $D$ is the diffusion constant. This law can also be written in terms of energy gradient, shown in equation 3.4, where $\delta u$ is the change in energy, $\bar{R}$ is the ideal gas constant and $T$ is the absolute temperature. The equalization of forces as energy is represented in equation 3.5, where $u_e$ is the energy due to the electric field, $u_c$ is the energy due to the chemical concentration gradient, and $u_p$ is the energy due to the electrical potential gradient via ion concentration.

$$J = \frac{D}{\bar{R}T}\frac{\delta u}{\delta x} \tag{3.4}$$

$$\delta u = u_e + u_c + u_p \tag{3.5}$$

$$u_e = k_e\frac{v_e \epsilon A e}{dr_{elec}} \tag{3.6}$$

$$u_c = \bar{R}T\ln\left(\frac{m_2}{m_1}\right) \tag{3.7}$$

$$u_p = eF_{con}\left(v_1 - v_2\right) \tag{3.8}$$

The electric field energy $u_e$ can be defined via Coulomb's law, using electric potential energy and capacitance to derive the imposed charges of the electrode pair on the ions, as the two apposing plates can be thought of as a large capacitor with the EAP hydrogel acting as the dielectric material. This is defined in equation 3.6, where $k_e$ is the Coulomb constant, $v_e$ is the voltage of electrodes, $\epsilon$ is the absolute permittivity of the EAP hydrogel material, $A$ is the surface area of the electrodes, $e$ is the charge of the particles being affected which in this case is the ion charge which is equal to electron charge, $d$ is the distance between apposing electrodes, and $r_{elec}$ is the distance of the ion from the electrode pair. The chemical gradient $u_c$ can be derived from the Gibbs free energy representation of entropy as the ratio between concentration increases [214]. This is shown in equation 3.7, where $m_1$ and $m_2$ represent the concentration of ions and water molecules in the current cell and cell ions are migrating to respectively. The electrical potential $u_p$ is derived via the Gibbs free energy derivation of cell potential [214]. This is shown in equation 3.8, where $F_{con}$ is the Faraday constant, $v_1$ represent voltage potential due the ions in the current cell , and $v_2$ and the represent voltage potential due the ions in the cell being migrating to. Due to Coulomb's law, as the ions approach the inversely charged electrode and enter the next cell the associated energy component $u_e$ increases resulting in a larger flux $J$. However, as the concentration on ions and water molecules within that cell increases the opposing electro chemical energy component $u_c + u_p$ also increases. These two opposing forces change at very different rates, the difference in magnitude being a key factor of the hysteresis component. As the ions migrate under the influence of the electric field, eventually $\delta u$ is minimised as the opposing factors balance.

Through the combination of these systems the rate at which ions migrate is controlled and the shape which the EAP hydrogel take due to the change in concentration changes. This interpretation is, however, a simplification. In actuality, there are many additional components that contribute to the complexity of the hydrogel's EAP behavior such as terms associated with, how the deformation of the gel's polymer structure and charged monomer strands interfere with ion migration, how pH and ionic gradient outside of the hydrogel affect swelling, and how these interconnected systems behave in a 3-dimensional setting. These additional terms also influence factors of other terms such as diffusion coefficients and permittivity of the hydrogel material, resulting in extremely complex behavior

as energy is minimised. This complex behavior can only be fully explored via practical experimentation.

## 3.3 Base Actuation Experimental Setup Decisions

To initially reproduce the EAP hydrogel actuation results currently seen in the field, the experimental procedure must be defined. Although current literature shows the actuation of EAP hydrogels, the procedures vary and the intended applications differ from those of this study. The computational goals of this study require two important factors to be considered in the experimential design:

- Definition of input and output structures – to investigate computational ability, what is considered the input and output of the hydrogel must be well defined in the experimental procedure so that the EAP hydrogel's behaviour can be integrated into a computational structure.

- Consistent synthesis of the EAP hydrogels – for a resource to be useful computationally it must be consistent. To allow consistency in hydrogel performance to be assessed any inconsistencies via experimental procedure must be minimised.

The factors are less important when investigating the EAP hydrogels as purely actuation devices. These factors can be satisfied though consideration in the definition of the experimental structure and procedure. These considerations are highlighted in the proceeding subheadings.

### 3.3.1 Experimental Structure

The first experimental aspect to be addressed is the input out structure, to asses the EAP material as a computational resource. The experimental structure must provide a means to control input and output of the EAP hydrogel is such a way as it can be applied to a computational architecture. Although many parameters influence the actuation behaviour (temperature, pH, ion content, etc), electrical stimulation is by far the easiest to control and as such input is simply the stimulation applied by the electric field. The structure of the stimulation, polarity, strength, etc., can be decided based on the computational

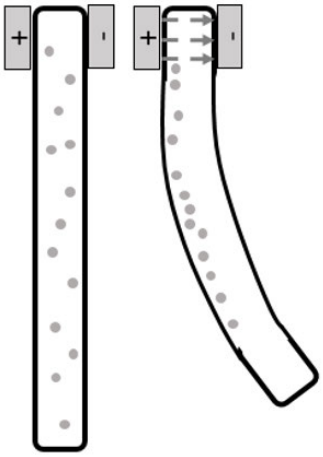


Figure 3.4: Diagram showing how ion migration due to controlled electric field can cause bending motion.

structure being tested in future experiments. Thus the experimental setup must allow for this variation in the application of stimulation, it must be possible to alter polarity during an experiment without interrupting the hydrogel's behaviour. This can be accomplished via a power supply with removable supply leads and allowing for time in the application procedure to swap polarity if necessary, this aspect can be further explored when the computational structure to be applied is defined in future chapters.

The output would require an encoding of the EAP's actuation motion into a computational architecture. As a soft medium this motion can vary wildly. However, to simplify the encoding the EAP hydrogel's possible actuation motion can be restricted through controlling the EAP hydrogel's shape and the stimulating electric field shape. The simplest controlled motion EAP's are capable of is bending, this can be achieved by using a rectangular hydrogel and placing opposing electrodes, touching the hydrogel, at one end [73]. Through application of the electric field ions are drawn to one side of the electrode pair and induce swelling at that location, through asymmetric swelling a bending motion is induced, as shown in figure 3.4. The bending motion can easily be measured as an angle by placing a camera to record the motion perpendicular to the EAP hydrogel. This footage can be analysed later to asses bending motion and apply any required encoding.

Although the EAP hydrogels exhibit actuation, the force of said actuation is small. In the desired application of computation actuation force is not a factor as the hydrogels are not used as actuators. However, this must be considered in the experimental design

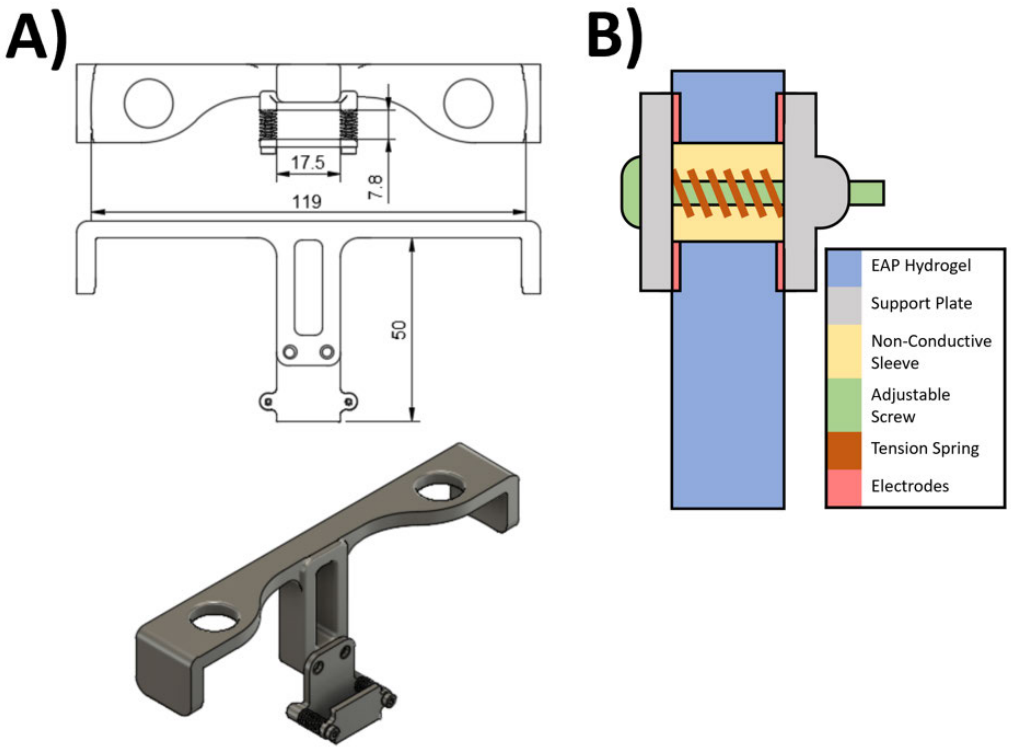


Figure 3.5: **A)** Diagram of suspension apparatus designed to hold electrodes onto gel as specified locations within the neutral buoyancy solution. **B)** Diagram of suspension apparatus used to secure the hydrogel. The adjustable screw and tension spring allows the gel to be secured regardless of variation in width. The sleeve prevents inadvertent conduction through the screw.

as the weight of the hyrogel can impact motion range, reducing the possible outputs that can be recorded. This can be addressed by placing the hydrogel in a solution to provide neutral buoyancy, this significantly reduces the impact of gravity, and the hydrogels own weight, on motion and maximises useful output. The hydrogel then must be suspended within the solution with electrodes at the correct positions. A suspension apparatus was designed to achieve this which can be seen in figure 3.5. The distance between electrodes is adjustable to the width of the hydrogel and holds the sample at the centre of a beaker that can be filled with the solution.

With these considerations defined the structure of the experimental apparatus is shown in figure 3.6 section A as a diagram and section B as a picture of the actual setup.

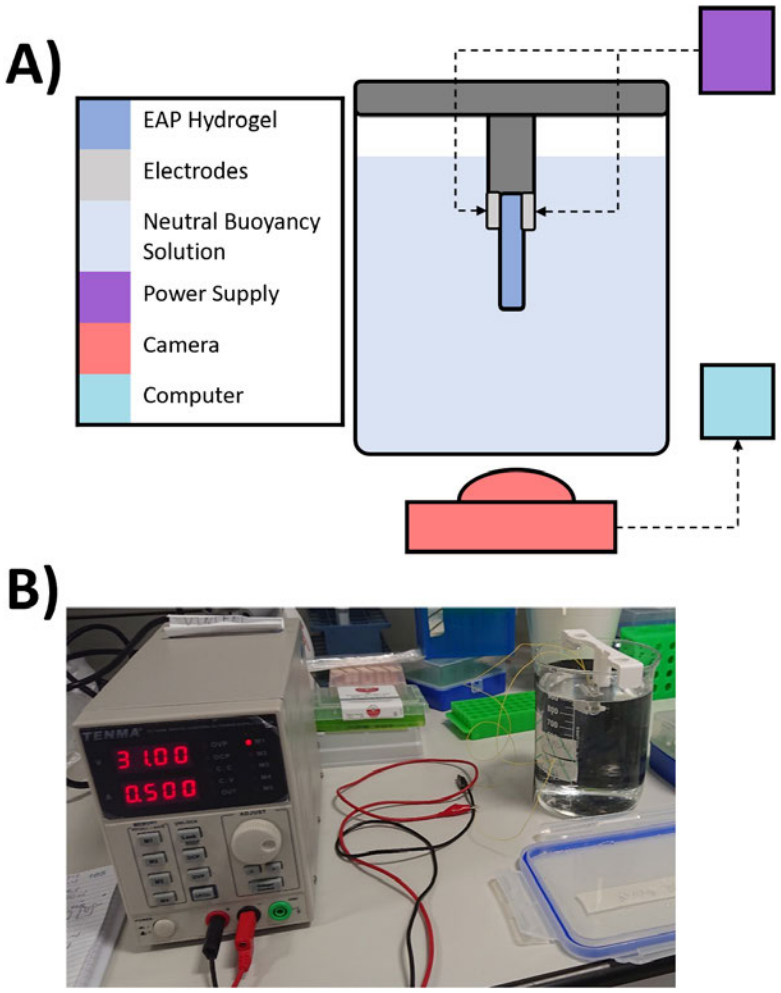


Figure 3.6: **A)** Diagram of base experimental setup with legend. The camera is placed perpendicular to the EAP gel's motion. **B)** Picture of experimental setup described in section A.

### 3.3.2 Hydrogel decision

There are many EAP hydrogel materials that have seen experimentation within the field of soft robotics, each of these materials have their own strengths and weaknesses when used in actuation but must be assessed in relation to the guiding key factors mentioned at the introduction to this chapter section. From initial investigation into the current literature two main materials were found to have promising capabilities, Carrageenan, and Polyacrylamide. For each of these materials an initial electric stimulation was applied via foil pressed to the surface to observe reactions, judging applicability based on structural durability and degree of shape change.

#### Carrageenan

Carrageenan is an anionic polymer extracted from red seaweed [215] that has seen some use in biomedical applications due to its nontoxicity and biodegradability [215, 216]. Carrageenan is naturally ionic, containing the negatively charged ions required for EAP actuation. Carrageenan is a polysaccharide and forms hydrogels at room temperature through entanglement of the helical polymer chains, because of this they are very easy to work with making them a worthwhile choice for experimentation. There are three main commercial classes of carrageenan [217]:

- Kappa forms strong, rigid gels in the presence of potassium ions, and reacts with dairy proteins.
- Iota forms soft gels in the presence of calcium ions.
- Lambda does not gel, is used to thicken dairy products.

For the purposes of this experiment carrageen that was predominantly kappa and lesser amounts of lambda (C1013) was sourced. Various concentrations of carrageenan were made into hydrogels with 3% providing the ideal flexibility and mouldability, the synthesized gels for 6% and 3% are shown in figure 3.7 section A and B respectivly. However, with application of an initial electric field the carrageenan hydrogel broke down without displaying the required shape change behavior. This is most likely due to the process in which the polymer structure forms. Polymer chains are dispersed in water with

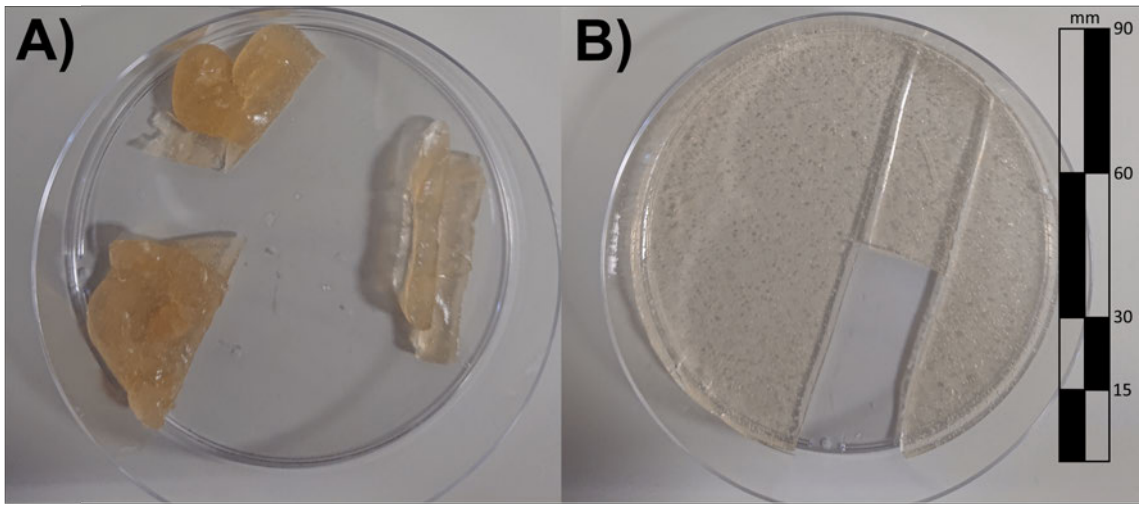


Figure 3.7: Samples of Carrageenan hydrogel made with different concentrations of powder, moulded in a 90 mm diameter petri dish. An approximate scale bar is included for reference. **A)** Carrageenan hydrogel with 6% carrageenan powder to water content. This ratio did not mould to the desired shape, clumping into usable chunks. **B)** Carrageenan hydrogel with 3% carrageenan powder to water content. The ratio moulded to the desired shape of the dish, cutting the gel into strips provided samples to be tested.

heat and as they cool contract into entangled hydrogel structures. The electric field causes electrolysis within the on the surface of the hydrogel and causes an increase in heat within the system, this heat causes breakdown in the polymer structure and thus is not suitable in this application. This observation does however highlight the necessity of stability within the hydrogel polymer structure for this application.

### Polyacrylamide

Polyacrylamide is a water-soluble synthetic linear polymer made of acrylamide [218]. Polyacrylamide is used extensively in EAP hydrogel studies [71, 24] and finds use in various biomedical applications as a drug release medium [219, 220] and for electrophoresis due to its chemical inertness [221]. Polyacrylamide hydrogels polymerise via free radical polymerisation [70] of four chemicals. Acrylamide, the linear constituent; N,N'-methylenebisacrylamide, the tetrafunctional cross-linking constituent; and ammonium persulfate and N,N,N',N'- tetramethylethylene diamine (TEMED), the initiators, dissolved in water. The polymerised hydrogels can then be ionised through hydrolysis in a TEMED solution, where acrylamide groups are converted to acrylic acid groups some of which ionise in water [70, 71] as shown in figure 3.8. Polyacrylamide undergoes thermal degra-

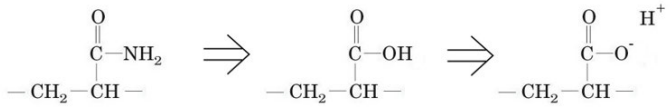

Figure 3.8: Chemical reaction for the hydrolysis of the polymer leading to hydrogen ions.

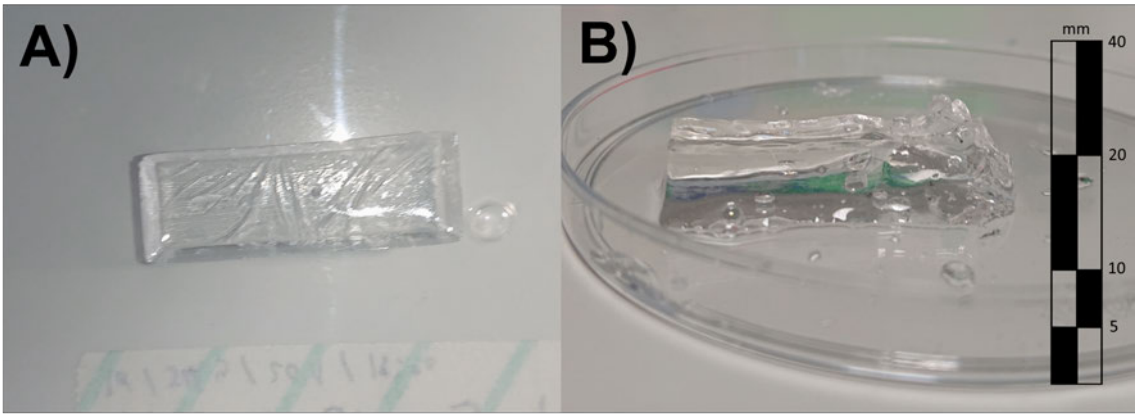


Figure 3.9: Moulded samples of polyacrylamide hydrogel. An approximate scale bar is included for reference. **A)** Polyacrylamide gel synthesised into strips ready to be used in initial tests. **B)** Polyacrylamide gel sample after stimulation via electric field with visible swelling on the right side.

dation at 175 to 300°C [218, 222], this makes it a much more suitable medium for EAP as it resists degradation due to heat generated via electrolysis. The polyacrylamide samples were synthesised using the quantities described in [70], with the synthesised hydrogel shown in figure 3.9 section A. With initial application of the electric stimulation there was no significant degradation, the hydrogels maintaining a cohesive structure allowing for further electrical stimulation to be applied. With the initial stimulation shape change was observed on the hydrogel's surface, as seen in figure 3.9 section B.

From these initial tests it is clear that polyacrylamide is the most applicable choice and will be used in all experimentation within this study. With the hydrogel material decided the specific synthesis procedure must be defined, allowing for replicable consistent hydrogel samples used to generate reliable results.

### 3.3.3 Polyacrylamide Hydrogel Synthesis

With Polyacrylamide selected as the EAP hydrogel, the specific synthesis procedure must be refined for reliability. The base procedure and chemical ratios were replicated from "Phase Transitions in Ionic Gels" [3], as these ratios are well established to work in appli-

cations of EAP actuation [71]. The chemical quantities for 100ml of water are as follows:

- Acrylamide – 5g
- N, N'- Methylenebisacrylamide – 0.133g
- Ammonium Persulfate – 40mg
- N, N, N, N-tetramethylethylenediamine (TEMED) – 240 µl

The solution can then be moulded into whatever form is required by the experiment. As mentioned earlier, a key consideration for these experiments is the input-output structure, as the output is defined in the actuation of the hydrogel. The larger the range of output from the hydrogel's actuation the more possible outputs will be able to be recorded. Because of this, the hydrogels need to be big enough to exhibit a large range of actuation, while being small enough that their own weight does not inhibit motion. Using the results of the paper "Electrochemical properties and actuation mechanisms of polyacrylamide hydrogel for artificial muscle application" [73] the width was selected as 10mm as this showed the best bending behavior. 30mm was chosen as the length to allow for easier measuring of bending angle over the referenced paper. Moulds were created with these dimensions consisting of two parts, a base and wall section shown in figure 3.10 section A as dimensional drawings and section B as printed components. This arrangement allowed the hydrogels to be moulded, as shown in figure 3.10 section C, and easily removed without damage. This arrangement also allows for the easy cleaning of the mould between gel samples to prevent cross-contamination between batches. A seal is made between the two mould parts using plastic wrap, which also provides a flat surface for the bottom of the gel to conform against, reducing variation in surface texture.

Any small bubbles in the solution during polymerisation can cause voids within the moulded gel, to avoid these the solution must be de-gasses via a vacuum chamber before being placed in the mould. Additionally, the length of time required for the hydrogels to fully polymerise depends on the size of the gel, however this polymerisation does not always occur homogenously. As the distribution of chemicals within the solution cannot be guaranteed to be homogenous the free radical polymerization will start in regions, this means that as the polymerisation progresses voids can be left where there aren't sufficient

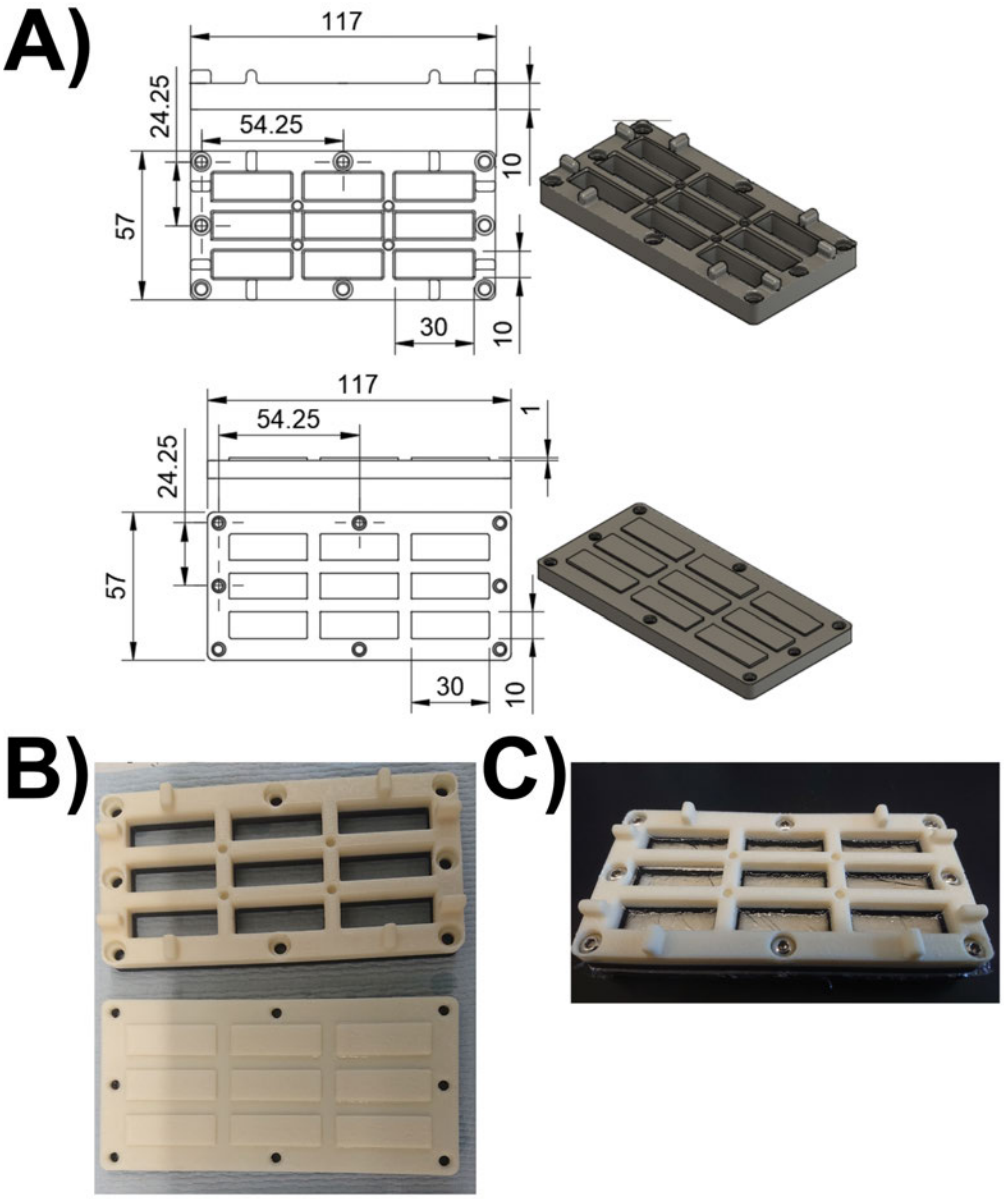


Figure 3.10: **A)** Diagram of hydrogel mould dimensions for walls and base. **B)** 3D printed hydrogel mould components, walls and base. **C)** Assembled hydrogel mould with polyacrylamide hydrogels moulded inside.

chemicals to form a polymer chain. This can be avoided by initializing the polymerisation process evenly over the surface of the solution when in the mould. For polyacrylamide, polymerisation starts as the solution reaches a reactive temperature of above 23-25 degrees centigrade [223], by heating the base of the mould this starts the polymerisation evenly across the cross-sectional area of the hydrogel and means that voids can be mitigated.

After being removed from the mould, although the hyrogels are fully polymerised, they are not their final size. The hydrogels must first be allowed to equalise within distilled water to achieve their final water content [71, 70]. This takes place over 24 hours at which point the hydrogels are removed. With fully formed hydrogels synthesized, they must be ionized to induce the electro-active properties. This is achieved through hydrolysis by placing the hydrogels in a TEMED-water solution. A solution of 1.2% was used as this has been shown to work well in EAP applications [71]. The hydrogels were left in the solution for 7 days. Based on previous papers this duration is sufficient to cause enough ionization within the hydrogel to achieve the majority of shape change behaviour [70]. The hydrogels are then washed to remove any remaining chemicals and stop the hydrolysis process, then placed in an airtight container. Once polymerised, polyacrylamide hydrogels are inert and, provided they are stored in such a way as to not lose moisture and not far above room temperature, they have a shelf life of a few weeks. The step by step procedure for the synthesis is included in the appendix under section A.1.1 "Step by Step Polyacrylamide Hydrogel Synthesis Procedure".

### 3.3.4 Electrode Material

With the EAP material and synthesis procedure defined, there are still some aspects of the experimental procedure that need to be addressed. Shape change is triggered by electric stimulation. This stimulation is applied through contact electrodes as shown in figure 3.5 section A and figure 3.6 section A, however different electrode materials will react differently within the application. Several electrodes materials were considered for the experimental procedure, keeping in mind the key factor of repeatability. First materials were compared based on the galvanic series, this being used as a measure for rate of corrosion in electrolysis. The electrodes would need to span the entire width of the gel to allow for even deformation, this size requirement limits the selection to more common

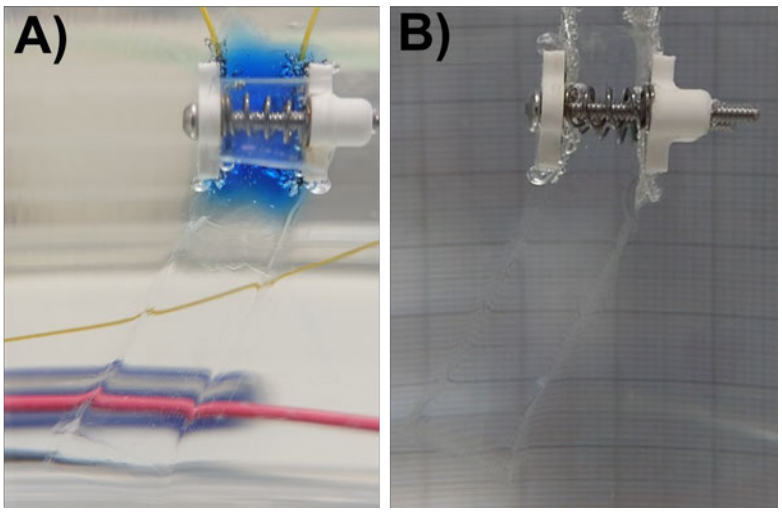


Figure 3.11: **A)** Stimulated polyacrylamide hydrogel with contact electrodes made of copper tape. There is significant colour change in the gel due to the copper oxide produced by the corrosion of the electrodes. **B)** Stimulated polyacrylamide hydrogel with contact electrodes made of aluminium tape. The corrosion of the electrodes appears to have no visible effect on the gel.

materials such as copper, aluminium, zinc, etc. as cost becomes a consideration. All materials at this point in the galvanic series will undergo corrosion in the application of the electric stimulation and as such they must be easily replaced between each experiment. To this effect metal tapes were considered as the electrode material, these are easily sourced in a variety of metals and allow for easy replacement within the experimental apparatus.

Metal tapes are available most commonly in copper and aluminium. Copper is higher in the galvanic series so should undergo less corrosion. However, both were tested on gel samples to compare degradation over application of the stimulation. From this experimentation copper reacted more heavily on the hydrogel, causing blue copper oxide to disperse throughout the area between the electrodes, as shown in figure 3.11 section A. In contrast aluminium did not lead to any visible dispersion though the gel, as seen in figure 3.11 section B. This is likely due to aluminium being more reactive with air and so already having a thin layer of aluminium oxide over the electrodes surface. It is possible that the dispersion of copper oxide would interfere with the migration of hydrogen ions as copper oxide, itself, is ionic. For these reasons aluminium was chosen as the electrode material.

With the electrode material selected the method for attachment must be defined. The electrodes cannot be secured with any additional adhesive that would interfere with

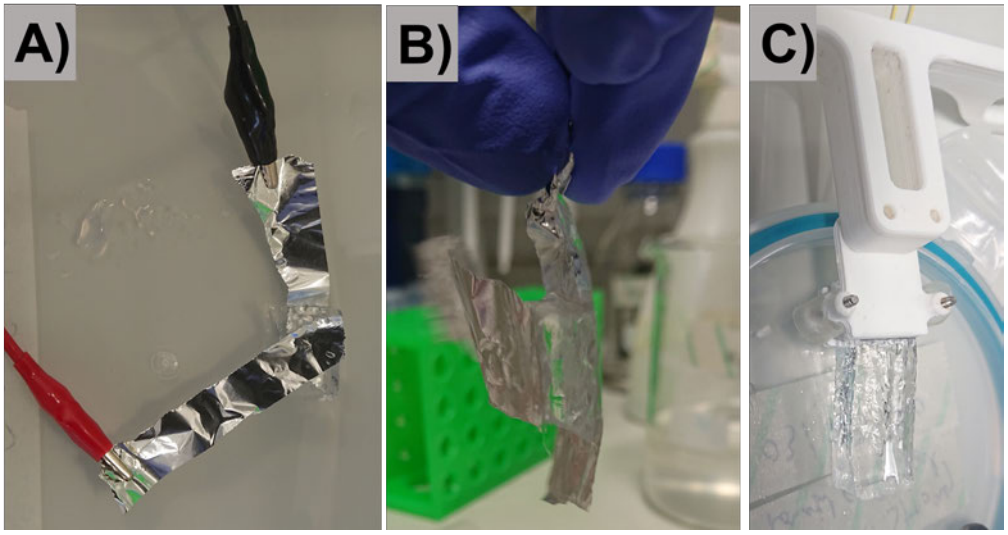


Figure 3.12: **A)** Initial test of adherence of aluminium electrodes to polyacrylamide hydrogel. **B)** Demonstration of electrode adherence, gel is entirely supported by adherence to aluminium electrode. **C)** Demonstration of how gel is secured within support apparatus.

the electrical conductivity. However, as the hydrogels are extremely compliant they also cannot be held in place by compression alone. Through experimentation of electrode materials, it was found that by applying a small stimulation voltage to the hydrogels via the electrodes, prior to placement within the neutral buoyancy solution, the electrodes can be adhered to the hydrogel surface, as shown in figure 3.12 sections A, B, and C. By applying the voltage in both polarities for 10 seconds the negatively charged polymers are partially drawn into the surface texture of the electrodes, this bonds the materials enough for the hydrogel to be suspended in the solution and apply further stimulation to induce shape change.

### 3.3.5 Salt Concentration

By applying the experimental aspects previously defined, stimulation can be reliably applied to the EAP hydrogels to cause shape change and actuation. However, with distilled water used as the suspension solution shape change is minimal and inconsistent. Previous studies have shown that shape change can be maximised through the use of an ionic solution to enhance the chemical/osmotic gradient between the hydrogel and its surroundings [71, 70], due to the change in the absorption property of the hydrogel [224]. Changing solution pH or solvent composition can induce shape change within the hydrogel via the

osmotic pressure. This method is used to induce total shape change across the entire surface in many studies [70, 73]. However, in this experiment shape change should only be induced by electrical stimulation so the pH and solvent composition should remain neutral. For this reason, sodium chloride salt was used to alter the ionic content of the solution as it does not result in a chemical reaction with any component of the experiment and so should not induce a pH change.

Various sodium chloride concentrations were tested in application of the ionic solution. Higher ionic concentrations resulted in faster actuation as the gel underwent electrolysis, however higher concentrations also resulted in faster corrosion of the electrodes. With more in depth experimentation of ionic concentrations and recording of the gel bending reaction, the concentration could be optimised to maximise performances. This is, however, unnecessary within this study. All hydrogels will be compared against each other so for this application the concentration only needs to provide a sufficient range of motion without causing total degradation of the electrode before the completion of the experiment. Through experimentation it was found that 0.08% salt provided this balance.

By recording the electric current draw of various concentrations of sodium chloride salt in distilled water, using the experimental setup shown in figure 3.13 section A, the conductivity of the ionic solution was found against salt concentration. These conductivity results are shown in figure 3.13 section B and C, from this graph 0.08% salt gives a conductivity of 0.29 S/m.

### 3.3.6 Output Extraction

Now that shape change can be reliably induced within the EAP hydrogel, the method for extracting the output must be defined. In this experimental arrangement the output is provided by the degree of bending achieved by the EAP hydrogel and is recorded via a camera over the course of the experiment, as shown in figure 3.6 section A. The hydrogels are transparent making accurate measurements extremely difficult while suspended in the ionic solution. However, when the hydrogel is placed against a black background, the transparent hydrogel appears as a cloudy blue, as shown in figure 3.14 section A. This is due to Rayleigh and Mie scattering [225] induced by the size of the polymer molecules interfering with the visible light that passes through, thus allowing the hydrogel to be

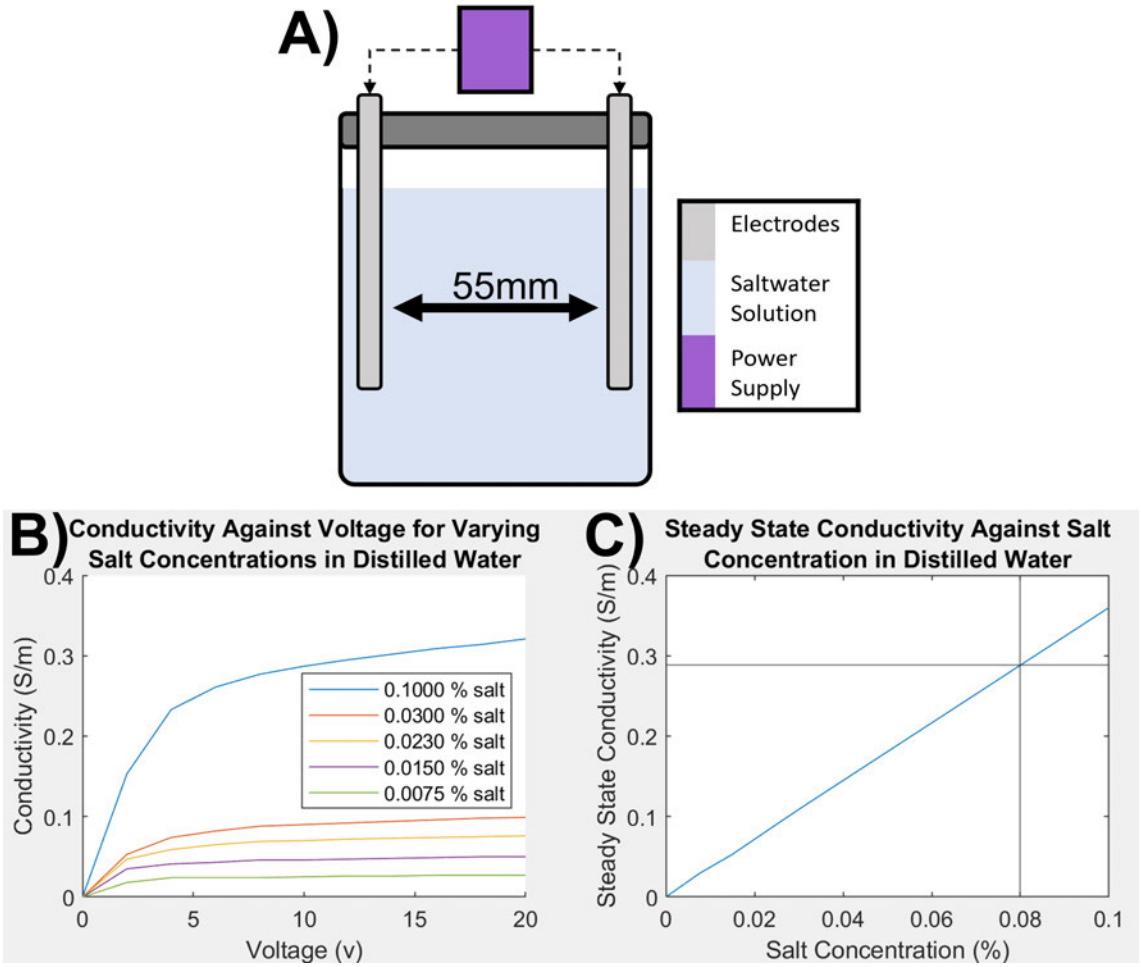


Figure 3.13: **A)** Experimental setup used to collect conductivity data from salt concentration, using aluminium plates spaced 55mm apart and with a surface area facing the opposing plat of 0.00467 $mm^2$. **B)** Conductivity against voltage in varying saltwater concentrations. **C)** Stabilised conductivity of saltwater concentrations. The concentration of 0.08% used with the stimulation of the EAP hydrogel shows a conductivity of 0.29 S/m.

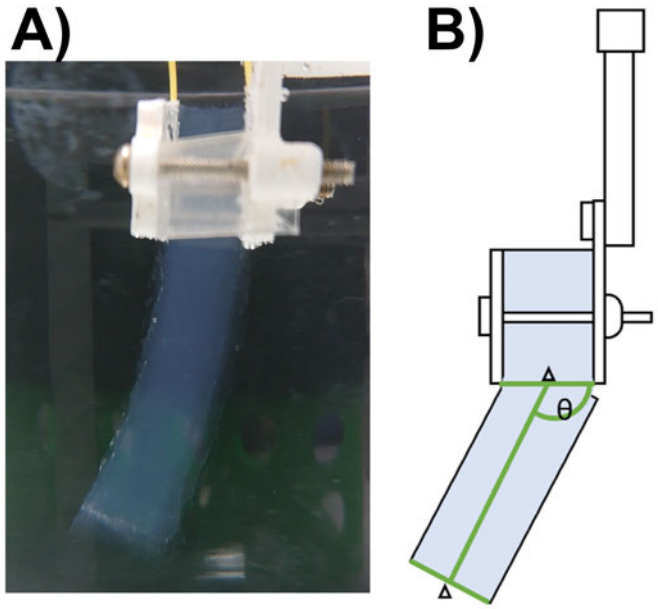


Figure 3.14: **A)** An example of Rayleigh and Mie scattering [225] in the polyacrylamide hydrogel when placed in front of a black background. **B)** Diagram showing process of measuring bending angle. Angle is measured from base of suspension apparatus using the center of the gel at that location and the center of tip of the gel. This provides the most repeatable measurement of angle for the soft body gel.

more easily recorded via the camera.

With the hydrogel's motion recorded, the bending angle can be measured using the suspension apparatus and electrode mounting point as the origin. The angle of the hydrogel is measured as shown in figure 3.14 section B. The angle of the hydrogel is measured at time t=0 as a baseline and all further angles are measured as a difference from this baseline to show total bending motion of the individual gel sample.

## 3.4 Initial Shape Change Results

With the experimental setup fully defined, initial experimentation can be undertaken to ensure that the experimental setup is capable of replicating the actuation behaviour of other EAP studies. Two experiments were performed in tandem to assess the replication of results and set the ground work for future experimentation. The actuation mechanics were tested via application of the electric field to the EAP hydrogel, and recording of the bending rate trend. Along side this, the rate of relaxation was also recorded from the EAP hydrogel, measuring the time the hyrogel takes to return to a completely un-actuated

position after stimulation is removed.

### 3.4.1 Actuation Experiments

To test the actuation mechanics a voltage was applied to the polyacrylamide gel using the procedure define in the previous section. 31V was applied to the gel for 270 seconds, with the positive electrode placed on the left and negative electrode on the right. The hydrogel's motion was recorded via a camera and then translated into bending angles, using the methods shown in figure 3.14 section B, at 30 second intervals. Figure 3.15 section A shows the extent to which the EAP hydrogel was able to bend in this time, reaching a maximum bending angle difference of 42 degrees from baseline. This alone shows that this experimental setup is able to replicate the actuation ability. For reliability, this experiment was run a further 2 times on new hydrogel samples. The results of this were plotted in figure 3.15 section B and showed an s-curve trend with an origin of (0,0), which is consistent with trends observed in other EAP hydrogel research [226, 227]. A best fit line, as defined in equation 3.9, was applied to the plot. The application of this best fit line was done using the Matlab Curve Fitting app [228] and gave the coefficients $a_1$, $a_2$, and $a_3$ as -35.66, 158.4, and 29.09 respectively.

Equation 3.9 was used in this instance because it best represented a simplified version of the real world bending behaviour. The bending of the hydrogel, measured as an angle from its starting position, followed an s-curve, starting at 0 then bending initially at a faster rate before slowing down as it reached its maximum bending angle. The exponential function $\frac{a_1}{1+e^{\left(\frac{(t-a_2)}{a_3}\right)}}$ used here provided a response that matched the behaviour of the hydrogel when under stimulation even beyond the bounds of the experiment, representing the constant state of the hydrogel both before the stimulation is applied and after the maximum point of bending is reached via applied stimulation. The negative exponential component $-\frac{a_1}{1+e^{\left(-\frac{a_2}{a_3}\right)}}$, ensured the function started at the origin of 0,0 in alignment with the fact the angle is measured as an offset from its starting position. The use of this function also meant that only 3 coefficients were needed to fit the curve and allowed for easier fitting to the recorded data. All these factors contributed to the use of this function to best represent the EAP hydrogel bending behaviour, and to provide a robust model that would have suitable versatility for future applications within this study.

$$\theta_{actu}(t) = \left(\frac{a_1}{1 + e^{\left(\frac{(t-a_2)}{a_3}\right)}}\right) - \left(\frac{a_1}{1 + e^{\left(-\frac{a_2}{a_3}\right)}}\right) \tag{3.9}$$

The trend visible in figure 3.15 section B, through the best fit line, shows a clear hysteresis in motion. The hydrogel's motion shows an initially slow increase in bending speed as the ions start to move, as more ions collect the hydrogel bends more. As more of the ions collect the area reaches a saturation point, the rate of bending decreases as fewer ions enter the area. Eventually the area becomes completely saturated, and the bending angle reaches a steady state point. This behaviour results in a slight "lag" in motion and causes the observed hysteresis.

The hysteresis response is expected given the exploration of system mechanisms at the beginning of this chapter, and the changing difference in magnitude between opposing forces within the hydrogel as swelling occurs. Initially the forces within the hydrogel resulting from rubber elasticity and polymer-polymer affinity are considerably higher than the forces imposed by the electric field, as shown in figure 3.3 section A. As a result, the initial rate of swelling is low. Eventually these forces are overcome as the swelling rate increases, however at the same time the electrochemical potential resulting from increased ion concentration also increases, as shown in figure 3.3 section B. This increases the forces opposing the electric field and causes the rate of swelling to reduce.

The hysteresis and resulting trend of motion, when under consistent stimulation, means that the rate at which the hydrogel bends is directly correlated to the amount of time the hydrogel has been bending for. In other words the amount that the hydrogel will swell in the next instance is directly related to how long it has been under stimulation, and how much it had already swelled in the previous instance.

### 3.4.2 Deswelling Experiments

To test the rate of deswelling or "relaxation" in the hydrogel, stimulation was applied to the hydrogel for 270 seconds to saturate the hydrogel, as in the previous experiment, then stimulation was removed. A camera was placed in front of the hydrogel and set to record the motion with the angle recorded every 30 seconds over the course of 2000 seconds. This

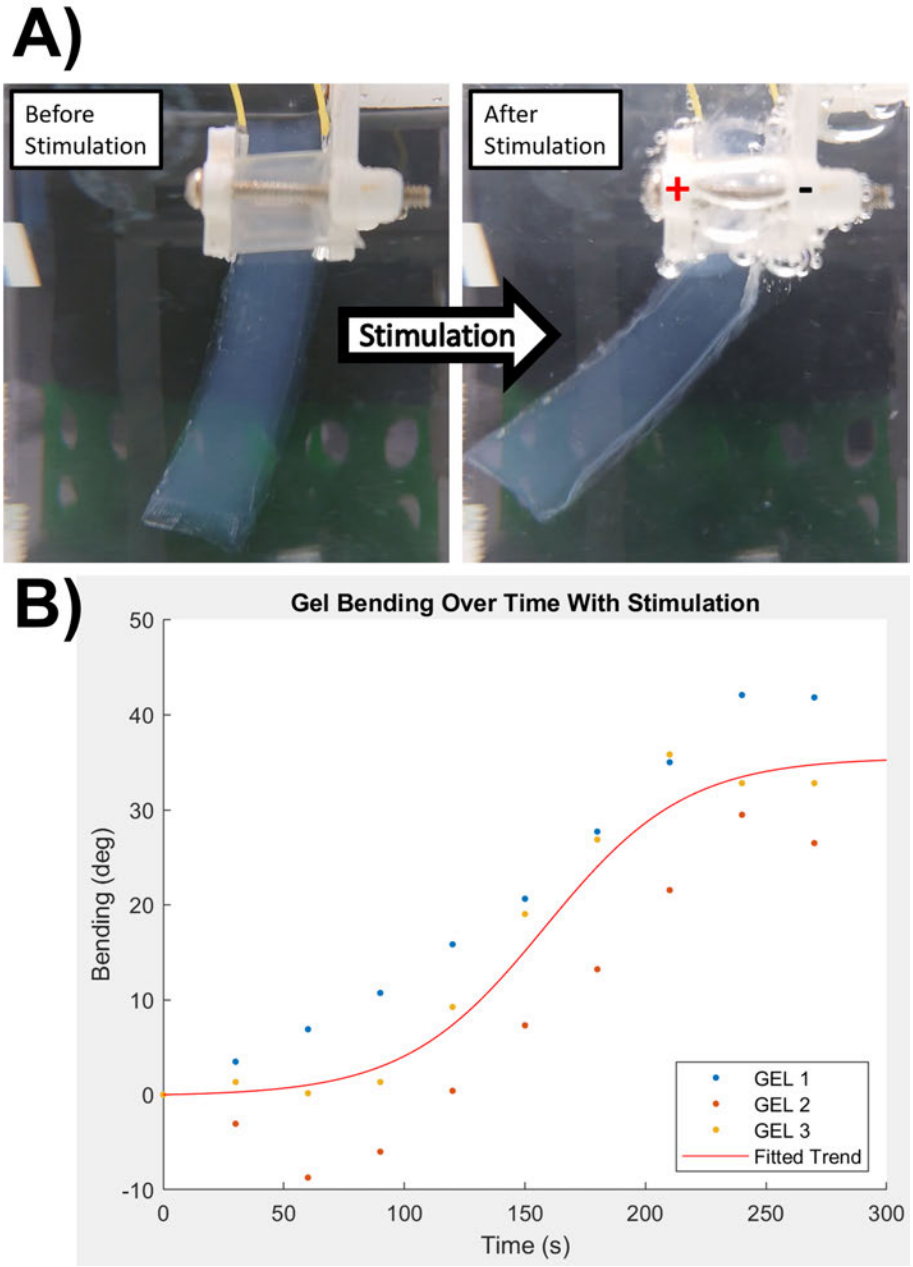


Figure 3.15: **A)** Comparative images showing the EAP hydrogel before and after stimulation with obvious actuation induced by swelling in the gel. 31 volts was applied with the positive cathode on the left and negative anode on the right, labelled in after stimulation image. **B)** Measured bending angle over time with application of electric stimulation. Angle is measured as difference from starting position. An exponential best fit line was applied to the data using the Matlab Curve Fitting app [228], and shows the trend follows an s-shape.

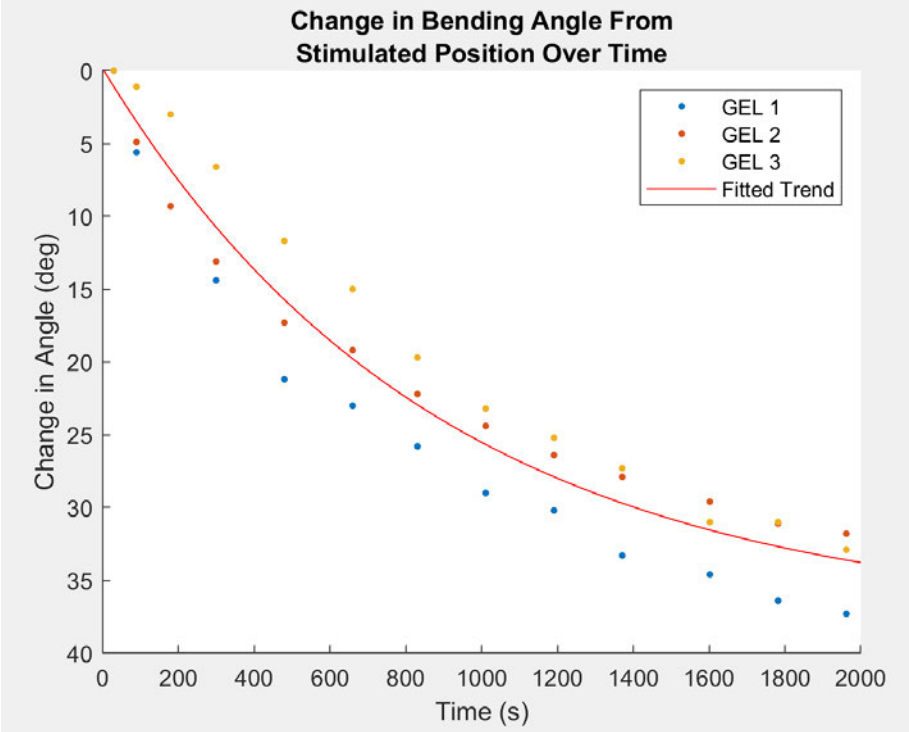


Figure 3.16: Plot of hydrogel relaxing after 270 seconds of stimulation has ended. As different hydrogels reached different positions after stimulation, therefore having different starting positions for relaxation, the angle is recorded as a difference from the fully actuated position. The y axis is inverted to show the relaxation curve consistently with figure 3.15. An exponential best fit line was applied to show the trend using the Matlab Curve Fitting app [228].

experiment was preformed 3 times with a new hydrogel sample each time. These results are shown in figure 3.16 with an exponential best fit line as defined in equation 3.10. The application of this best fit line was done using the Matlab Curve Fitting app [228] and gave the coefficients $r_1$, $r_2$, and $r_3$ as -37.88, -0.001135, and 37.69 respectively.

$$\theta_{rest}(t) = r_1 e^{r_2 t} + r_3 \tag{3.10}$$

Although the time the hydrogel was left to relax for did not allow for the hydrogel to completely return to a relaxed state, as seen in figure 3.16, the trend can be extrapolated. The point at which the hydrogels motion is less than 0.001 degrees per second would be after 4000 seconds. From this data it is obvious that the time taken for the hydrogel to swell under stimulation is significantly lower than time taken to relax after swelling, at a

ratio of 1:6.8 seconds.

## 3.5 Chapter Conclusion

This chapter served to establish the base experimental procedures, and define the components of experimental structure used to investigate the computational abilities of the EAP hydrogels within the rest of this study. This chapter also provided the initial experimental results confirming the actuation behaviour of the EAP hydrogels within the forementioned experimental structure. It was shown that the EAP hydrogel actuated following an s-shaped hysteresis. This means that a stimulation applied for a set time would have a different affect on the hydrogel's motion depending on the total length of stimulation that was applied up until that point. This behaviour can be interpreted as a form of memory, where previous states of the hydrogel influence future ones. Combined with the large difference between stimulation and relaxation time, as shown in figure 3.15 section B and figure 3.16, the "memorised" states would exist in the hydrogel for a significant length of time, allowing for interactions between states. This memory behaviour provides a clear path for EAP hydrogel's use as a resource within computation that will be explored in the following chapters.

# Chapter 4

# Electroactive Polymer Gels as Probabilistic Reservoir Automata for Computation

## 4.1 Introduction

The previous chapter explored the base mechanics of EAP hydrogels and established a reliable experimental procedure. Through this experimentation interesting memory like behaviour was observed in the bending response induced by stimulation. As described in the previous chapter, through the application of electric fields, the ions move causing changes in the polymer structure [71]. A hysteresis is induced by changes in the polymer structure and causes subsequent stimulations to generate less actuation [74]. This hysteresis means previous responses to stimuli affect future responses leading to a memory function.

The clear memory behaviour is promising in the application of EAP hydrogels as a computational resource. In order to investigate if it is possible to combine actuation and control, a computational structure is needed that these behaviours can be exploited through. The most common memory based computational structure is that of the automata, the simplest being deterministic. However, active matter systems such as EAP

hydrogels are non-deterministic, as each input can lead to several outcomes. Nevertheless, even highly dynamic systems can be simplified to sets of rules given a large enough rule set [4]. Probabilistic automata are a generalization of non-deterministic finite automaton that traverse states based on weighted state transitions [137, 138]. The probabilistic automaton structure allows large complex systems to be simplified into state machines, where probability distributions are converted to weighted state transitions [139]. These automata fit real world behaviour of complex bodies such as active matter systems but do not traditionally take inputs. However, Moore Machine automata are a type of finite-state transducer (FST) automata [135] that traverse states based on sequential inputs, giving an output at each state. Through the combination of behavioural features in these automata frameworks, EAP hydrogels, and other such morphological systems, could be represented in a computational context as a probabilistic Moore automaton.

Using the conventional computing techniques of Moore machine automata as a base gives a head start in framework development through the wealth of knowledge in the field of automata computing. Additionally, the probabilistic elements can provide a broader computational landscape, when compared to more convectional computational structures. Although these automaton frameworks provide a flexible and robust computation scheme, the true potential lies in exploiting the inherent parallel processing of active matter [15]. Neural networks are an inherently parallel computational construct but are typically implemented in software or specially designed hardware, reservoir computing expands this implementation dependency.

Reservoir computing is inspired by Recurrent Neural Network (RNN) frameworks where the dynamics of a fixed non-linear system, called a reservoir, is used as part of a neural network to map input and output signals to higher dimensional space [5]. The reservoir feeds into a layer of neurons known as the output layer. The weights of these output neurons are tuned to achieve learning in the system much like in standard RNNs. The reservoir can be any kind of medium that can encode temporal problems into higher dimensions to generate recurrent connections between data [175]. For example, water ripples in a bucket have been used as a reservoir to encode image data for pattern recognition [17].

As with morphological computing, the key use of reservoir computing systems is to

exploit alternative computation mediums to solve problems that would otherwise be inefficient for traditional computing [175]. In automaton theory the automaton is designed to accomplish a specific task through the definition of its language [3]. Automaton structures are limited by the language that they use. However, using reservoir computing as an additional layer that alters the automaton language to suit a given task, could expand the capabilities of the system. Given the morphological nature of physical reservoir computing, can physical reservoir computing be combined with probabilistic Moore automata to supplement short comings and allow the full free energy landscape of the active matter systems, such as EAP hydrogels, to be utilised.

In summary, EAP hydrogels exhibit memory behaviour and thus show potential in computational application. Utilising the ubiquitous computational frameworks of automaton, the computation of other active matter systems has been exploited as shown in chemical examples [15]. With more appropriate automaton frameworks, such as probabilistic Moore automaton, can EAP hydrogels be exploited for computation beyond the currently explored EAP technologies. Furthermore, utilising additional morphological computing structures such as reservoir computing, is it possible to further utilise the potential of such an active matter medium.

This chapter explores the application of the unique mechanics within EAP hydrogels by developing and validating a automaton reservoir framework, designed to harness the EAP hydrogel's response to an electric field. First, using the mechanical responses of the ionic EAP hydrogel under an electric field, to study the memory mechanics present within its behaviour in more detail. Second, applying this memory to develop a probabilistic Moore machine automata structure and evaluated this structure against the hydrogel's responses to stimuli. This allowed analyse of the hydrogel's computational potential as an automata. Third, expanding the automata framework through reservoir computing and thresholding to construct a hybrid automaton-reservoir system capable of beneficial computation.

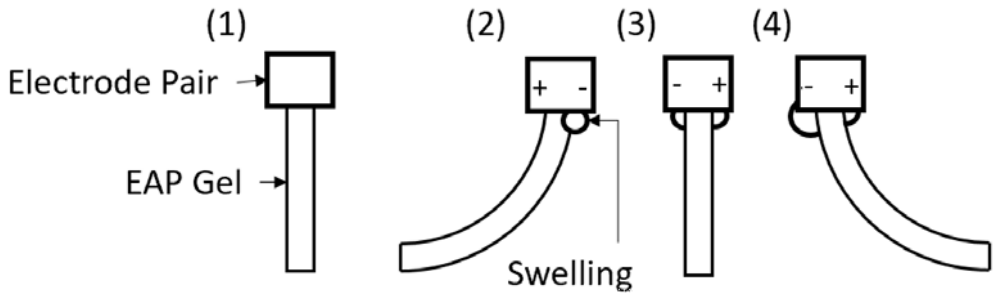


Figure 4.1: Diagrams demonstrating the experimental set-up and effect of compound antagonistic swelling; (1) Experimental set-up with the placement of electrodes on gel, (2) Bending of the gel upon application of electric field, (3) Equalized bending upon electric fields application in the opposite direction, (4) Further bending by continuing application of electric field.

## 4.2 Memory Mechanics Through Ion Migration

Although the memory exhibited in the EAP hydrogel's benign behaviour is promising, the specific mechanics through which this memory emerges must first be clarified. Through this clarification the limits and application methods of the memory within computation can be better understood, allowing for better incorporation within the potential automaton framework.

The memory results from the hysteresis [73] in polymer structure as ion and water molecule migration induces bending. This hysteresis effect is easily observed in the trend of the EAP hydrogel's bending motion, and the difference in time scale between bending and relaxation, both observed in the previous chapter. Due to this, if a series of stimulations were applied, of consistent length and strength, each consecutive stimulation would cause less localised swelling in the gel than the previous. Since each consecutive stimulation causes less and less volume change, each deformation has influence on further deformations. The influence of sequential swelling can be seen in figure 4.1. Given a constant migration rate of ions into a local polymer network, the localised rate of swelling gradually decreases creating the hysteresis effect [74]. As the memory is driven by ion and counterion concentrations, it's function can be further explored through recording these concentrations. This can be achieved via measuring the voltage potential across the gel as electric stimulations are applied, as voltage potential is directly proportional to the

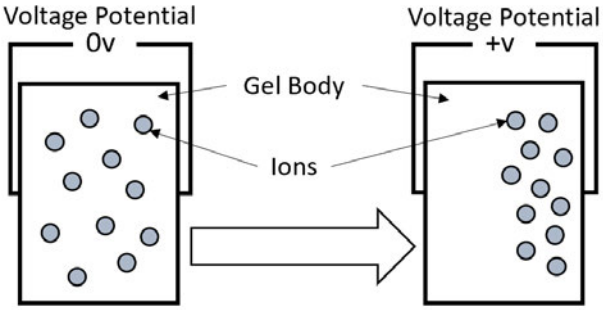


Figure 4.2: Diagram showing how inhomogeneous distribution of ions causes change in the voltage potential between gel's surfaces.

distribution of ions. A concentration of charged ions at one electrode creates a potential much like an ion battery [229], demonstrated in figure 4.2. Therefore by recording the voltage potential and electrical current against time as stimulation induces bending in the EAP hydrogel, the memory mechanics can be evaluated.

### 4.2.1 Experimental Design

The Polyacrylamide gels were synthesised using the methodology detailed the previous chapter, moulded into strips for actuation. The gels were then suspended in the sodium chloride ionic solution (0.08%) using the procedure detailed in the previous chapter, between aluminium electrodes as shown in figure 4.3 section a and b. A camera is used to record the bending angle of the hydrogel as in the previous chapter, using the suspension apparatus as the origin to measure from as shown in figure 4.3 section c.

Sequences of voltages are used to stimulate the gel, -31 V referred to as 1 and +31 V referred to as -1, across the 6.4mm width of the gel, with polarities applied as shown in 4.3 section b. 31 volts was used as it was the maximum output of the power supply and caused swelling in the gel at a reliable rate during experimentation. A INA219 electric current sensor is placed in line with the driving voltage, recording electric current and voltage potential values with time stamps to align with the video data. Due to the polarity in which the electric current sensor was applied the recorded voltage potential appears inverted, however this does not impact experimental results. This voltage potential measurement system does introduce some noise but does not effect the collected results [230]. Eight stimulation sequences are applied to the gel representing every combination of positive and negative stimulations in a 3-input sequence (-1-1-1, -1-11, -11-1, -111, 1-1-1, 1-11,

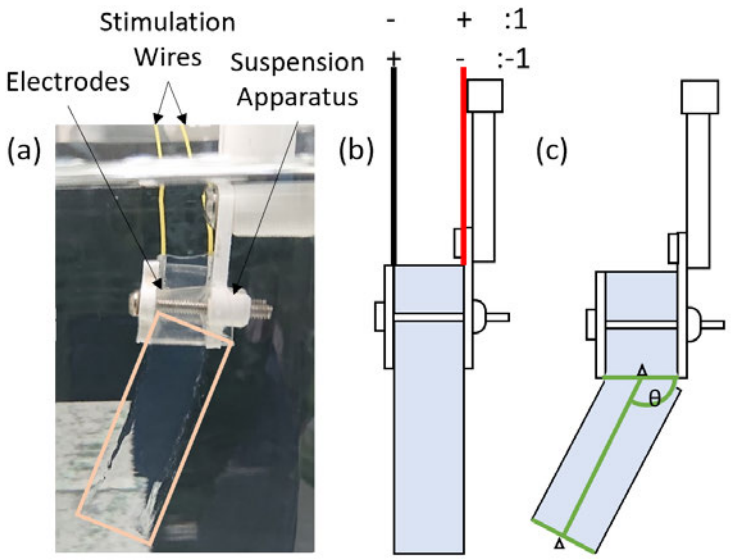


Figure 4.3: **a)** EAP gel suspended within the solution; gel is highlighted by yellow outline. 3D printed apparatus holds the gel on electrodes at set height within the solution, yellow wires provide power to electrodes for stimulation. **b)** Diagram showing the symbol representation of stimulation polarity, 1 is +31 V and -1 is -31 V. **c)** Diagram showing how gel bending angle is measured against base of suspension apparatus and gels mid-point at tip.

11-1, 111).

- For each experiment fresh aluminium electrodes were applied to the suspension apparatus with wires affixed behind the electrodes.
- The gel was placed between electrodes with both sides touching the gel shown in figure 4.3 section a and b. A voltage of 31v was applied in both polarities twice for 10 seconds each time to adhere the gel to the electrodes by pulling the charged gel polymer into the texture of the electrode. 10 seconds was found to be the shortest time needed to adhere the electrodes.
- The suspension apparatus along with the gel were placed in a beaker of sodium chloride solution shown in figure 4.3 section a.
- The camera was adjusted to place the gel in centre view parallel to the suspension apparatus.
- The video recording was started along with the voltage potential recording. A sequence of stimulations were applied to the gel, each stimulation applied for 90 seconds

with 10 second breaks between stimulations to allows for change in polarity if necessary. A stimulation length of 90 seconds was used as it was found to be the shortest time allowing visible bending to occur, as seen in figure 3.15 section B.

- The video was segmented into a set of pictures representing the output of each stimulation, with an initial image used as the gel at t=0.

The code used to analyse the data collected from these experiments can be found in the repository 10.5281/zenodo.7274655 in folder "Experiment _1-Memory _Mechanics _Through _Ion _Migration _and _Voltage _Potential _Measurement".

In addition to these steps temperature and humidity can affect the response of EAP hydrogels. The elastic properties of the gel are a function of temperature [71, 70]. As the osmotic pressure difference between the polymer networks and ionic solution drives the swelling, changes in the hydrogel's water content change the degree to which it can swell, as well as altering the mechanical properties of the material [231]. For this reason, the purified water used in the ionic solution, although not temperature controlled during the experiment, is from a temperature controlled source (22C), so the experiments would always start at the same temperature. As the gels rely on water molecules to swell the hydrogel's water content also affects the response and as such so can humidity. Suspension in the ionic solution prevents the influence of ambient humidity on the gels during experimentation. The gels are also stored in watertight containers in between experimentation to maintain moisture content until use.

### 4.2.2 Results

Figure 4.4 shows two sequences of positive and negative stimulation of (-1,1,1,-1) and (-1,-1,-1,1), with the electric potential (voltage) presented against time. In figure 4.4) pictures of the gel's responses at the different time-steps were labelled from 0 to 4. Gel behaviour for the stimulation sequence observed in figure 4.4) section A is described corresponding to these labelled time steps below:

0. At t=0s, the gel has yet to be stimulated and was at default position.

1. At t=10s, negative stimulation (31v) was applied for 90s placing anode on right until t=100s. Positively charged ions were drawn to negative electrode (right) pulling

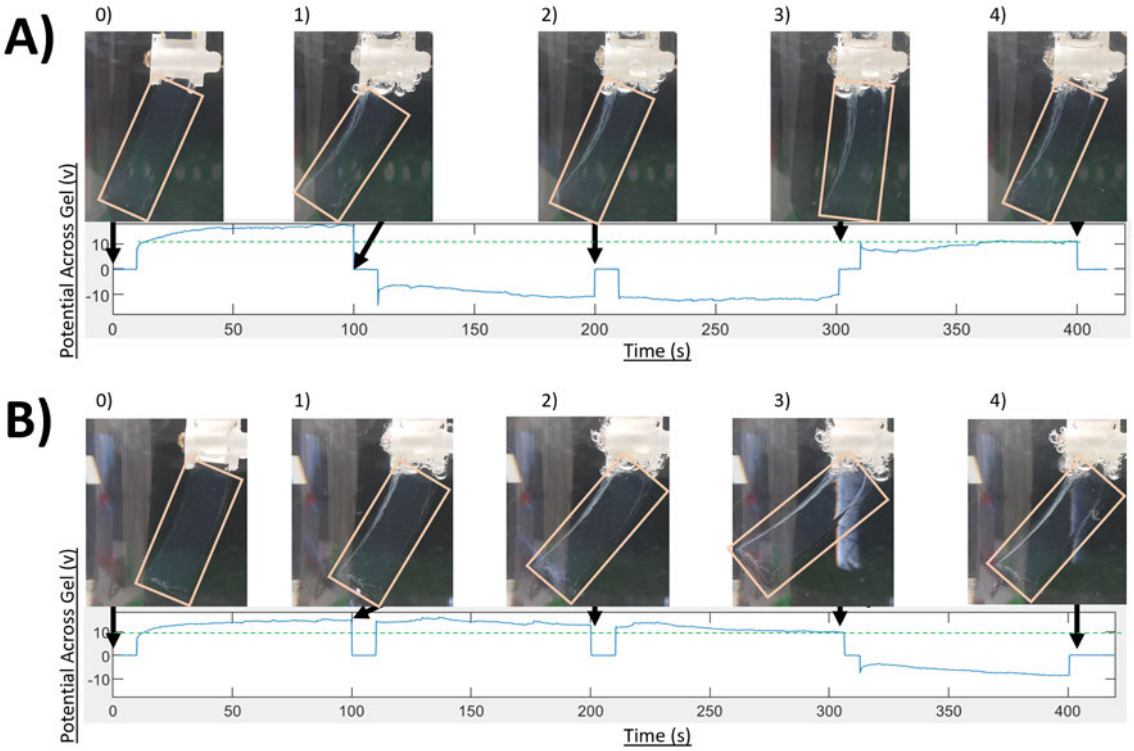


Figure 4.4: Voltage potential across gel over time. Key frames from recorded video illustrate bending at t=0, t=100, t=200, t=300 and t=400 (seconds) and labelled as 0,1,2,3,4 respectively. A green dashed line is used to compare the voltage potential at the end of a stimulation with that at beginning. **A)** The sequence applied in the experiment show is -1,1,1,-1. **B)** The sequence applied in the experiment show is -1,-1,-1,1.

water molecules with them causing swelling and the gel to bend to the left. There was an immediate rise in voltage potential provided by electric field, as ions gather on right the voltage potential increases further.

2. At t=110s, positive stimulation (31v) was applied for 90s placing anode on left until t=200s. There was an immediate drop of voltage potential shown in the figure at t=110s caused by application of the electric field. Ions were currently towards right, so voltage potential starts higher (closer to 0 as shown on graph). Ions were pulled to left electrode causing voltage potential to decrease as they gather causing swelling on the left and bending the gel toward the right.

3. At t=210s, positive stimulation (31v) was applied for 90s placing anode on left until t=300s. Ions continued to move towards left electrode causing further swelling on left, further bending the gel to the right. The voltage potential continues from its value in the previous stimulation as the ion distribution remains. The hysteresis effect can be seen in this change in voltage potential. The voltage potential first plateaus, then starts rising towards 0, as the minimum limit of voltage potential reduces. The limits of the voltage potential (directly related to the swelling amount via ion migration) reduce over continuous stimulation by the hysteresis effect.

4. At t=310s, negative stimulation (31v) was applied for 90s placing anode on right until t=400s. Ions moved back towards right electrode causing swelling and the gel to bend slightly left, but less, due to the hysteresis effect caused by the change in ion distribution as a result of swelling. Voltage potential raised as ions gather but due to the hysteresis, the level of the potential was less than that achieved by the initial stimulation (shown by the dashed green line).

The stimulation sequence observed in figure 4.4) section B shows the same memory mechanics, and is described corresponding to these labelled time steps below:

0. At t=0s, the gel has yet to be stimulated and was at default position.

1. At t=10s, negative stimulation (31v) was applied for 90s placing anode on right until t=100s. Positively charged ions were drawn to negative electrode (right) pulling

water molecules with them causing swelling and the gel to bend to the left. There was an immediate rise in voltage potential provided by electric field, as ions gather on right the voltage potential increases further.

2. At t=110s, negative stimulation (31v) was applied for 90s placing anode on right until t=200s. Ions continued to move towards left electrode causing further swelling on left, further bending the gel to the right. The voltage potential continues from its value in the previous stimulation as the ion distribution remains. The voltage potential first plateaus, then starts fall towards 0, as the minimum limit of voltage potential reduces, showing the hysteresis effect. The limits of the voltage potential (directly related to the swelling amount via ion migration) reduce over continuous stimulation by the hysteresis effect.

3. At t=210s, negative stimulation (31v) was applied for 90s placing anode on right until t=300s. Ions continued to move towards left electrode causing further swelling on left, further bending the gel to the right. The voltage potential continues from its value in the previous stimulation as the ion distribution remains. The hysteresis effect progresses further as the potential continues to fall towards 0, as the minimum limit of voltage potential reduces.

4. At t=310s, positive stimulation (31v) was applied for 90s placing anode on left until t=400s. There was an immediate drop of voltage potential shown in the figure at t=320s caused by application of the electric field. Ions were currently towards right, so voltage potential starts higher (closer to 0 as shown on graph). Ions were pulled to left electrode causing voltage potential to decrease as they gather causing swelling on the left and bending the gel toward the right.

### 4.2.3 Discussion

The results of figure 4.4, described in the previous section, show how the voltage potential always continues from the previous point when breaks in stimulation are introduced leading to short term memory. These results also showed how the electric field induced swelling is subject to the hysteresis. This presents through the reduction of the maximum and minimum voltage potentials as a function of consecutive stimulations. The voltage

potential necessary to induce the same angle of bending was altered with each stimulation as a function of time, influenced by previous simulations leading to a response tantamount to long term memory. Now that the memory function has been established through the dynamical responses of the gel, a suitable framework is required to utilise the memory for computation.

## 4.3 Applying EAP gel to a Probabilistic Moore Machine Automata

The previous section shows how EAP gels exhibit memory. As stated in the introduction, one of the most common memory based computational frameworks is the automata. As a next step, we map electric stimulation and mechanical responses of the gel onto the automata framework to examine the computational ability of the hydrogels. Electric stimulation is considered as the input to the automata system, and the bending angle as the system output. Using this input-output relation, we apply the memory function, attributable to the dynamical responses of the gels, as an automata. Further, in this context, the gel acts as an interpreter, converting one language to another [232]. As an interpreter the gel converts input stimulations to output postures through the memory function. The memory function of the gel acts as a set of defined instructions. This framework also follows the structure of a transducer automaton [233].

Due to the highly dynamic nature of the EAP gels, their responses to the electric stimulation have variation in terms of bending angles. A probabilistic automata was used to take account of this variation in behaviour and provide an additional dimension in behaviour. In probabilistic automata each state transition has a probability of occurring, this means that two identical probabilistic automata would have variations in outputs [137, 138] mimicking variations between gel instances. We consider that this form of automata can be mapped onto the EAP gel behaviour, because the output angles are not purely determined by the input stimulation but also determined by probability as a result of the highly complex dynamics of the hydrogels in an ionic solution.

Automata utilise symbolic representations of inputs and outputs. For example, the output series can represent words in the sentences that are translated by the automata.

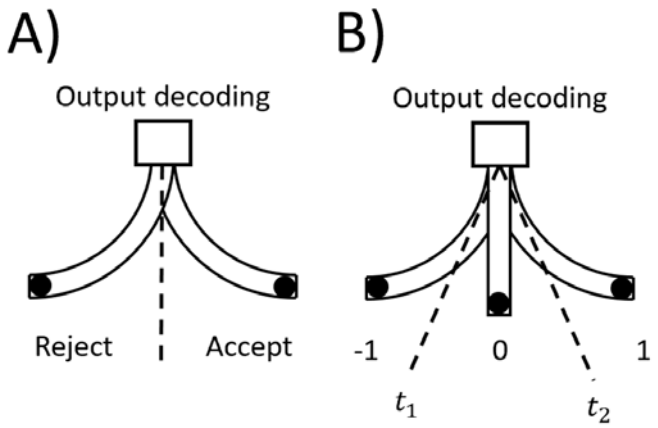


Figure 4.5: Illustrated encoding of resultant bending angle through Application of the thresholds to determine the output series. **A)** Simple acceptance or rejection with one threshold. **B)** Simple symbolic encoding with two thresholds.

In automata the input and output sentences can utilise different grammar rules and thus represent different languages [3, 234], this is also the case for the hydrogel. The inputs and outputs of the hydrogel require different encoding rules as they represent different energy forms, electrical stimulation and mechanical motion, different encoding rules mean different grammar rules and so different languages.

To fully utilise the gel in an automata framework, we first define these languages in the input and output series of the EAP gels. The gel's behaviour must be broken down into finite states by applying discrete time intervals, defining characters, words, and sentence within the context of gel's response to a series of electric stimuli as follows; input to the system is voltage applied to the gel as electric stimulation. In this study we used three input states with set magnitude; negative (-31v), neutral (0v), and positive (+31v) simplified into the symbol set of $-1, 0, 1$ respectively. The state of the system is defined as the bending angle of the gel under the electric field, and can be mapped, through thresholds, to an output symbol. A demonstration of this mapping is shown in figure 4.5 section A, output symbols were set by applying zones over the full movement range. Defining more zones to categorise the bending angles creates an output language with more output symbols, giving higher resolution. However, this higher resolution is at the cost of accuracy due to the probabilistic nature of the hydrogel as an automaton. These thresholds act to define the output symbols, converting an analogue input-output system to a discreet representation adapted to an automaton framework. The thresholding

algorithm was used to generate the grammatical structure of the output symbol series. For this study, three thresholding zones were used: left, centre, right as $-1, 0, 1$ respectively to generate the output symbols as shown in figure 4.5 section B.

To utilise these automaton languages a suitable automaton framework is required that is probabilistic and takes inputs for state transitions. Moore machine automata are a restricted type of finite-state transducer, whose output are determined only by its current state [135]. This behaviour closely matches the EAP gel's automaton behaviour, given the constructed language definitions. Moore machine automata are, however, deterministic for a given initial state and input pair, a deterministic finite automaton (DFA) has exactly one next state.

The dynamical responses of the EAP gels are non-deterministic or probabilistic, however, a probability component can be introduced to the Moore machine definition in order to create a Probabilistic Moore Automata (PMA). The PMA can be defined using an adapted Moore machine definition that includes a probability component $P$ mapping probabilities to the transition function. This is shown in equation 4.1 as a 7-tuple system.

$$
\begin{aligned}
&A_{PMA} = (S, \Sigma, \Gamma, \delta, P, \omega, \iota,) \ \textit{Where}: \\
&\quad \bullet \ \boldsymbol{States}\ S = \{S_{01}, S_{11}, S_{12}, \ldots, S_{NI}\}, I = 2^N \\
&\qquad\qquad \textit{where } S_{i,j} \in S \textit{ for} \\
&\qquad\qquad \{i \in \mathbb{Z} \mid 0 \leq i \leq N\} \textit{ and } \{j \in \mathbb{Z} \mid 1 \leq j \leq I\} \\
&\qquad\qquad \textit{, and } N \textit{ is the sentence length } N \in \mathbb{Z}^{\geq 0} \\
&\quad \bullet \ \boldsymbol{Input\ alphabet}\ \Sigma = \{-1, 0, 1\} \\
&\quad \bullet \ \boldsymbol{Output\ alphabet}\ \Gamma = \{-1, 0, 1\} \\
&\quad \bullet \ \boldsymbol{Transition\ function}\ \delta : \Upsilon \times \Sigma \to \Upsilon \\
&\quad \bullet \ \boldsymbol{Transition\ probabilities}\ P : \delta \to \mathbb{R}^+ \\
&\quad \bullet \ \boldsymbol{Output\ function}\ \omega : S \to \Gamma \\
&\quad \bullet \ \boldsymbol{Initial\ state}\ \iota = S_{0,1}
\end{aligned}
\tag{4.1}
$$

For every symbol in the input sentence, the active matter moves to the appropriate state based on the probability of the transition, and gives the output associated with that

state. The output function $\omega$ defines the encoding that maps from state to output via thresholding, translating gel bending angle to output symbol.

To evaluate the application of the probabilistic automaton on the EAP hydrogel, the gel is stimulated using the defined input sentence, and the responses compiled. In this experiment $N$ was set to 3, as stimulation beyond that point led to no significantly measurable response from the EAP gel. Thus, the input and output sequences were defined as the 3 element vectors $\{\boldsymbol{I}(l) : \boldsymbol{I}(l) = (\boldsymbol{I}_1, \boldsymbol{I}_2, \boldsymbol{I}_3), \boldsymbol{I}_i \in \Sigma\}$ and $\{\boldsymbol{O}(k) : \boldsymbol{O}(k) = (\boldsymbol{O}_1, \boldsymbol{O}_2, \boldsymbol{O}_3), \boldsymbol{O}_i \in \Gamma\}$ respectively, where $i$ is the $i^{th}$ symbol in the vector. $l$ & $k$ are labels for the input and output state respectively as a result of the sequence vector, given by equations 4.2 and 4.3.

In equation 4.2, $l$ is the integer labelling the state of the input vector $\boldsymbol{I}$ and $\boldsymbol{I}_i$ is the $i^{th}$ symbol in $\boldsymbol{I}$, for example, $\boldsymbol{I(5)} = [1, -1, 1]$ and $\boldsymbol{I(2)} = [-1, 1, -1]$. In equation 4.3, $k$ is the integer labelling the state of the output vector $\boldsymbol{O}$ and $\boldsymbol{O}_i$ is the $i^{th}$ symbol in $\boldsymbol{O}$, for example $\boldsymbol{O(5)} = [-1, 1, 0]$ and $\boldsymbol{O(21)} = [1, 0, -1]$. The experiments seek to create a generalised framework to overcome inconsistencies between gels, and so, each series of 8 input permutations is repeated with a different batch of gels.

$$l = \sum_{i=1}^{N} 2^{i-1} \left(\boldsymbol{I}_i + 1\right) / \, 2 \tag{4.2}$$

$$k = \sum_{i=1}^{N} 3^{i-1} \left(\boldsymbol{O}_i + 1\right) \tag{4.3}$$

### 4.3.1 Experimental Design

The input sentences are applied to the gel using the same sequential stimulation procedure and apparatus as in the Memory Mechanics experiment of the previous section. Every permutation of input symbols (8 sequences) is applied to a new gel so that sequences have no influence on each-other. This is because there is no guarantee that, in practice, previous stimulation on a gel will not affect future behaviour even after significant rest time.

Each path was then repeated a further 8 times resulting in 64 separate experiments to collect enough data to establish results consistency in every path through a 3-symbol tree. These input sequences are applied with the same voltage and timing as in the

Memory Mechanics experiment following the same reasoning. Stimulation lengths of 90 seconds were used per input, with 10 second breaks to change electrode polarity. Values used for concentration, voltage, and times can be altered to change the gel's response to input sequences but requires more detailed experimentation to analyse the best conditions, beyond the scope of this thesis.

Once data is collected the video is segmented into a series of images, representing the end of each input symbol and one at t=0 used to find the change in bending angle. As bending occurs over the length of the gel the angle is measured using the midpoint at the gel's tip and the edge of the suspension apparatus, shown in figure 4.3 section C.

All data analysis was performed using code written in the Matlab environment. The code used to analyse the data collected from these experiments can be found in the repository 10.5281/zenodo.7274655 in folders "Experiment _2-Applying _EAP _gel _to _a _Moore _Machine _Automata" and "Experiment _3-Applying _Moore _Reservoir _Hybrid _to _Collected _Data".

### 4.3.2 Results

Each series of 8 different input sequences creates its own state tree of gel postures which are compared with each other to evaluate consistency and repeatability. One such state tree is shown in figure 4.6 and depicts the change in gel posture with different input sequences as a directed automata graph.

To effectively judge consistency of the dynamical responses between gel samples, some post-processing is needed to filter noise from unavoidable inconsistencies between experiments, e.g., positioning of gel, gel surface texture, slight synthesis differences between batches, etc. The procedure is designed to minimise inconsistencies. To filter noise in the current setup, a gain $\alpha_{gain}$ and offset $\theta_0$ parameter are used to reduce the effect of differences in surface texture that cause initial bending in the gel at t=0 [235]. The use of these parameters also reduces the effect of differences in synthesis between batches due to differences in chemical ratio changing in elasticity [236], respectively. The specific use of this filtering can be found in the appendix section A.2.1 "Post-Processing Experimental Results to Reduce Variance", the reduction in variance via the post-processing can be seen in the appendix table A.1. From this filtering the variance [237] in output angles for each

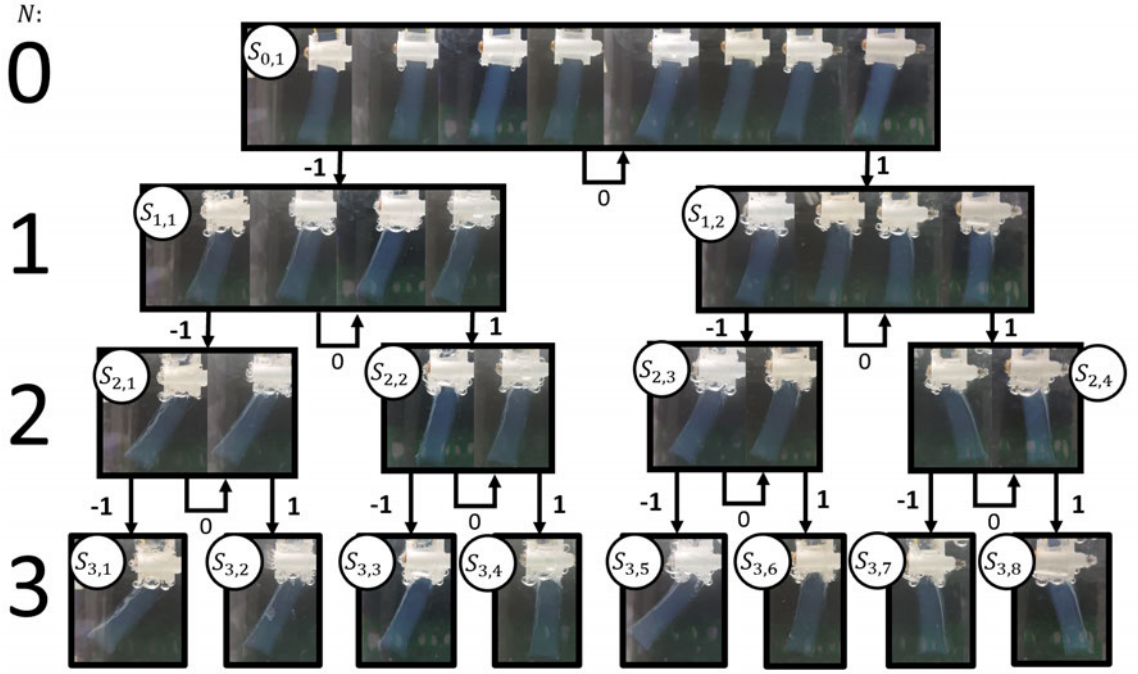


Figure 4.6: Automata directed graph for a 3-symbol system (N=3). 8 gels were run to explore each sequence and branch of the directed graph. At each stage of the sequence the gels are shown side by side in the same order for each layer. Each $S_{i,j}$ node represents a state of the machine where $i$ denotes the layer (or symbol in the case of the input/output sequence) and j denotes the path that led to that state for that layer, with $S_{0,1}$ as the initial state, also defined in equation 4.1. Each node has 3 input paths; -1 and 1 lead to subsequent states, 0 representing no input leads back to the same state.

input sequence was reduced. Thresholds are used to categorize the continuous output into a symbol list to be used in an automaton context, as represented by the output function $\omega$ in equation set 4.1 and defined by equation 4.4, where $\boldsymbol{O}$ is the output symbol, $\boldsymbol{\Theta}$ is the post-processed output angle, $t_1$ and $t_2$ are thresholds 1 and 2 respectively. A smaller symbol list allows for reduced variance, but also, reduces computational ability as fewer symbols can be used to represent computed results. Likewise larger symbol lists allow for more complex computation but are more sensitive to gel composition [238]. There needs to be a balance between computation and predictability.

$$\boldsymbol{O} = \omega\left(\boldsymbol{\Theta}, t_1, t_2\right) = \begin{cases} -1 & \boldsymbol{\Theta} < t_1 \\ 0 & t_1 \leq \boldsymbol{\Theta} \leq t_2 \\ 1 & \boldsymbol{\Theta} > t_2 \end{cases} \tag{4.4}$$

To apply the collected data to the probabilistic automaton structure, $t_1$ and $t_2$ must be set in equation 4.4. Selection of output thresholds alter the response of the gel as an automaton. To assess the automata's ability under different values of $t_1$ and $t_2$, the following criteria was used for optimisation:

- Maximize predictability: Achieved by maximizing the probability that each $\boldsymbol{I}$ vector will consistently result in the same $\boldsymbol{O}$ vector between activations of the probabilistic Moore machine.

- Maximize computational range: Achieved by realising equal distribution of output symbols in the $\boldsymbol{O}$ vectors generated by the probabilistic Moore machine.

- Maximize computational versatility: Achieved by maximizing the number of unique $\boldsymbol{O}$ vectors given by the probabilistic Moore machine across all $\boldsymbol{I}$ vectors.

Through the optimisation of these criteria the thresholds were found to be -7.8 and 2.7 for threshold 1 and 2, respectively. A more detailed definition of the optimisation function approach and results can be found in the appendix section A.2.2 "Optimisation of Output Encoding Thresholds to Maximize Automaton Response", the results of the optimisation of these criteria can be seen in the appendix figure A.1. From these thresholds a bias

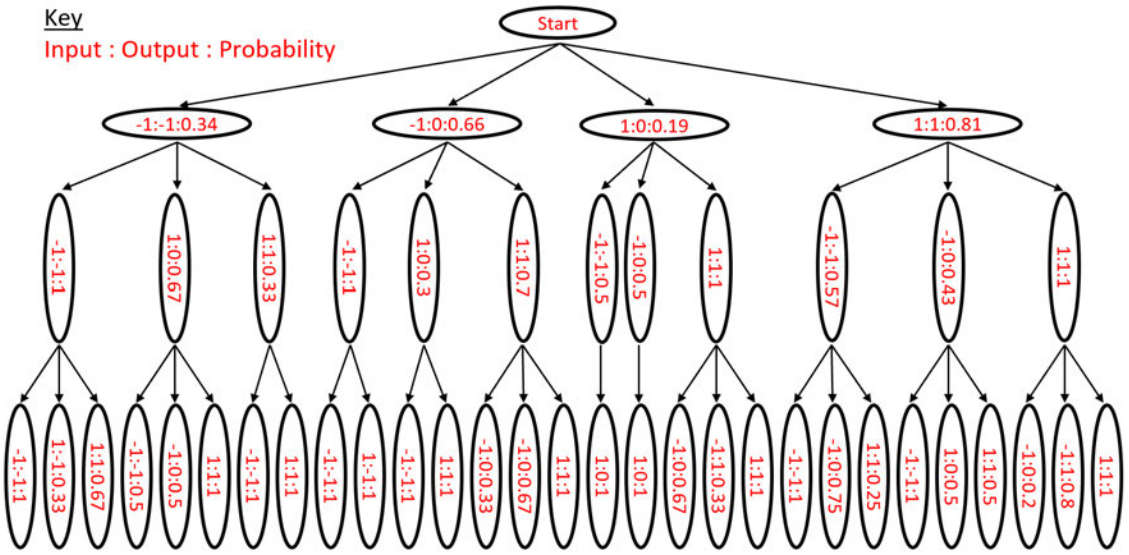


Figure 4.7: The directed graph of the probabilistic automaton using thresholds -7.8 & 2.7 for thresholds 1 ($t_1$) & 2 ($t_2$) respectively (as found through threshold optimisation detailed in the appendix section A.2.2 "Optimisation of Output Encoding Thresholds to Maximize Automaton Response" and figure A.2). The starting state that the gel inhabits is labelled as "Start", each following node depicts a possible state which is labelled in red with the following format (Input, the input symbol that lead to this state from the previous state) : (Output, the output symbol given from entering this state) : (Probability, the probability that this state would be entered given the input symbol)

can be observed towards one direction as the negative threshold is much larger than the positive. This is likely due to the orientation of the gel in the moulding process, the bottom has contact with the mould surface while the top is open leading to a difference in surface texture. However, as all gels are made consistently this shouldn't affect the validity of the results.

The optimised thresholds were used to generate a transition tree from the experimental data and generate the probability transitions as shown in figure 4.7. The probabilistic directed graph is of figure 4.7, showing the probability that each transition path will be taken given a certain input symbol and the function of the hydrogel as a non-deterministic automata.

### 4.3.3 Discussion

The resultant EAP hydrogel PMA, represented in figure 4.7, shows a promising complexity in the automata's output response and rule structure, with threshold selection able to tune the ability of the automaton.

When designing automata, the complexity of the program (rule set) is limited by the range of possible responses. This is also limited by the grammar of the language via timing and symbol selection. with shorter stimulations output variation between different sequences would be lower. With fewer stimulations, there are fewer possible combinations of symbols. It is possible to expand the rule set by altering the grammar of the language, in this case through the chosen timing of stimulation. Although the timing used in this study was the minimal timing possible to achieve bending, longer stimulations and breaks could be used. If the breaks were long enough for resting to occur as shown in figure 3.16, then the number of stimulations, and thus symbols, per sequence could be extended allowing for more complex behaviour. This is however beyond the scope for this chapter but can be explored in future work.

However, through a probabilistic state system, the possible responses are far more versatile. There is, however, a trade-off, the automaton has a much wider range of computational capacity (able to output more complex sequences) at the cost of accuracy giving less determinable results. This means that the use of such a computational resource needs to be fit for purpose regarding application and computational ability. In the next section, to broaden the computational ability, we expand the framework to better embody the mechanisms of the hydrogel as a computational reservoir.

## 4.4 Probabilistic Moore Automata as a Computational Reservoir

The PMA is rich in dynamics, allowing information storage through memory of the EAP hydrogel. Each state of the directed tree acts as a non-linear node encompassing the behaviour of the non-linear units (active ions) as shown in figure 4.7. This network of nodes behaves similarly to a neural network and, more specifically a reservoir. Reservoir Computing is a framework that maps input signals into higher dimensional computational spaces through the dynamics of a fixed, non-linear system called a reservoir [5]. Reservoir computing is a derivation of recurrent neural networks and as such implements the ability to learn. In reservoir computing learning takes place through the optimisation of output encoding [175]. The encoding functions are altered until the result best embodies the

function desired for the intended application.

Reservoir computers allows for highly dynamic analog systems to be used in computation, allowing them to perform computations that would otherwise be slower or less accurate on digital computers [175]. These computers are, however, less versatile than current digital systems as the selection of a reservoir is dependent on the intended application. For example, the ripples in a vibrating water source have been used to encode image data more efficiently than conventional digital computers [17].

A reservoir computing layout consists of 3 main components; excitation layer, reservoir, and readout layer [5], these components are described in table 4.1.

Table 4.1: Description of reservoir computing components with application within the EAP gel network

| **Component** | **Description** | **Application to Gel** |
|---|---|---|
| Excitation layer | Input to the reservoir, converting from defined input symbols to stimulations in the reservoir network. | Inputs are defined as -1,1 and are applied via electrical stimulation across the width of the gel. This is the same system as the excitation layer used in the Moore Machine framework. |
| Reservoir | Fixed, non-linear system that is used to map inputs to higher dimensional space. | EAP hydrogel suspended in the ionic solution via surface electrodes, stored as a virtual database through the PMA. |
| Readout layer | Output from the reservoir. Converts from the reservoir network to defined output symbols. This layer is tuned to train the reservoir computing network. | Bending angle of the gel as viewed from the side perpendicular to the electric field, binarized (thresholded) into the defined output symbols of -1,0,1. Tuning is performed through the optimisation of thresholds. |

A reservoir in this context must be made up of individual, non-linear units, and capable of storing information [239] much like the PMA has already presented. In the field of physical computing, reservoirs produce multiple outputs in order to provide a rich nonlinear in interaction with the surrounding environment. For example, down the length of an octopus arm [9, 29] or the location of ripples in a vibrating water source [17, 18].

In contrast, in the current implementation of the EAP hydrogel framework, there is only one physical output via the bending angle of a single EAP gel. However, through using the PMA, additional outputs are given over temporal space. Each symbol of the output

sequence of the PMA constructed in the previous section represents an instance in the EAP hydrogels motion. Thus, using the temporal responses of the hydrogels, we can utilise multiple outputs over the duration of the motion path. Figure 4.7 shows this temporal sampling as each layer of the tree represents a different step of time in the automaton's operation. Figure 4.7 also shows each path has an associated transition probability that increases the dimensionality of the automaton. This means the relatively simple EAP system can be used as a reservoir via the generated PMA, providing the required multiple outputs via temporal sampling and higher dimensions via the probability element.

The similarities between the PMA and reservoir computing frameworks allow for techniques of reservoir computing to be used to expand the computational ability of the PMA by using it as a reservoir. To apply this reservoir framework to the EAP gel-based PMA, the reservoir computing components must be defined in terms of the EAP gel system, these comparisons are shown in table 4.1.

The main concept of reservoir computing is to utilise the non-linear behaviour of a physical system to do computations that would require an approximated mathematical model to calculate [175] via conventional purely digital/binary computation systems, such as microcontrollers or personal computers. For the PMA to have value as a reservoir, its behaviour must embody computations that would otherwise be less effective when modelled via conventional digital computational means.

The mechanics of the EAP hydrogels showed continuous probabilistic responses upon electrical stimulation, which were discretised to fit the automaton framework. Although many examples of reservoirs in morphological computing are physical, like the gel, reservoir computing's origins lie in virtual representation [239]. Virtual reservoirs can take the form of modelled systems, such as artificial neural networks, such as ESNs [169] and LSMs [170], or as a database of responses from physical reservoirs. The discretised probabilistic automata transitions from the previous section, as shown in figure 4.7, have potential as a virtual database reservoir that can be used to validate the EAP hydrogel PMA as a reservoir computer. The use of a virtual database reservoir allows for faster analysis of the complexity of a PMA reservoir based on EAP hydrogel.

In order to utilise the PMA network, as shown in figure 4.7, as a database reservoir the input and output sequences need to be simplified to allow for easier comparison to

conventional digital computation. For the purpose of simplification, the input and output sequences are represented by the state labels $l$ and $k$ described in equations 4.2 and 4.3 for input and output sequences, respectively. The PMA takes a sequence of inputs ($\boldsymbol{I}$) and maps them to a sequence of outputs ($\boldsymbol{O}$) utilising a network of weighted transitions. Using the state labels $l$ and $k$ the PMA becomes a non-linear integer mapping function based on the PMA's probability distribution, derived from the recorded responses of the EAP hydrogel. The non-linear function of the integer mapping becomes the database representation of the EAP hydrogel reservoir, where the output layer is adjusted through tuning the thresholds $t_1$ and $t_2$ in the output function $\omega$, as defined in equation 4.4.

In the function of the PMA, the thresholds served to binarize the analog output of the gel to fit a sequential symbol language. However, in the context of a reservoir tuning the output layer, through the adjustment of $t_1$ and $t_2$, tunes the probabilistic mapping between input and output states. By tuning this probabilistic mapping, the function of the reservoir can be controlled to serve a purpose. In more general terms, the reservoir as a whole embodies a large energy landscape of probability maps, but through the adjustment of the output layer can be tuned to a specific probability mapping that can be used within a computational application.

An example of a single probabilistic mapping condensed from the reservoir via the thresholds $t_1 = -7.8$ & $t_2 = 2.7$ is represented in figure 4.8, where the input and output sequences are denoted by their state labels. Shown in figure 4.8, for each input state, each output state has a probability of occurrence. For each input state, there is a single leading output state that has a much higher probability of occurrence than the other output states. With a larger dataset, it is likely that these outcomes converge further, and this leading output state will become more pronounced as the minor differences in gel synthesis and experimental procedure become less impactful on the final results.

This framework provides a virtual reservoir representation of the complex continuous function of the EAP hydrogels computation. By tuning the thresholds, the reservoir provides a mapping function of 8 input states to 27 possible output states. However, for the EAP reservoir to be useful as a computational medium it must be capable of performing certain computational tasks more efficiently than purely digital/binary based hardware alternatives. The EAP reservoir is structurally simple, comprising of only 3

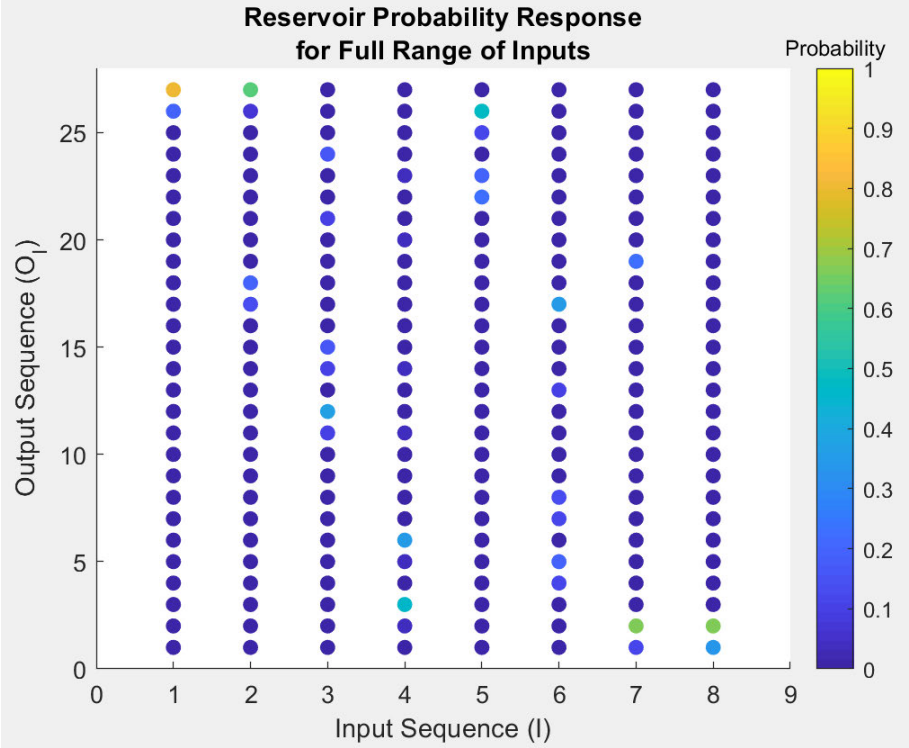


Figure 4.8: Probability of each output integer given an input integer using thresholds -7.8 & 2.7 for thresholds 1 & 2, respectively. The probability is shown as a colour representing a number between 0 and 1.

layers in the automaton, although the analog nature allows infinite combinations of input and output sequences when continuous values are considered. For example, by changing the input/output language through the adjustment of the stimulation voltages or output bending angle thresholds. A digital computer would never be capable of exactly representing an analog system, but in practice an approximation of analog results is often sufficient. Any commonly used digital computing system can represent a function through models stored in memory. Given a digital system with enough memory, any analog system could be approximated sufficiently to be used in a given task. To compare the EAP reservoir with digital systems the question is, how large would the memory of a digital system need to be to accurately represent the EAP reservoir. A comprehensive answer to this comparison depends on the application, but by comparing the mapping functions generated by the EAP reservoir with a model commonly used in digital computation systems the difference in memory usage can be visualised and the value of this application assessed.

### 4.4.1 Experimental Design

One of the simplest forms of model that is used within digital computation systems is the polynomial. Because of polynomial's simplicity they can be represented on any form of digital computer hardware, from simple microcontrollers to complex cluster computers. All digital systems use memory to store functions, in the case of the polynomial it's the coefficients that require memory space to be stored. The mapping function generated by tuning the thresholds of the reservoir can be compared to the polynomial representation of the same function, comparing the memory usage and accuracy of the representation in each case. In the physical reservoir the mapping functions are continuous like the hydrogel but have been discretised for the purpose of simplifying the initial framework. This discretisation also allows for virtual reservoir storage and more direct comparison to digital computation. If the polynomial requires as much memory as used by the mapping function, generated from the virtual representation of the reservoir, then for that function the reservoir is more efficient in memory usage than the digital polynomial representation. Which is to say the hydrogel computation is more efficient than the same computation achieved utilising digital computation methods. The memory used in the representation can be correlated to the number of coefficients required to represent the model. As there are only 8 possible inputs, using 8 coefficients (7th degree polynomial) would essentially create a lookup table and be no more computationally advantageous than the virtually stored EAP reservoir. For this reason polynomials with degrees from 0 to 6 will be tested and their performances assessed.

There are many different modelling methods with some far more optimised, however different methods require different hardware to run. Polynomials, as one of the simplest modelling techniques, can be implemented on any hardware. This means that using polynomials as the comparison allows the assessment of the hydrogel reservoir to be hardware agnostic, allowing for a more generalized conclusion for this initial investigation. Additionally, the EAP reservoir already represents the free energy landscape of the physical system which, in this case, is used to generate the computation, selected by tuning the thresholds. The hydrogel does not have to generate this energy landscape as it is inherent to its structure, whereas in the digital system a computer must generate the landscape

representation through the calculation of the polynomial approximations. Since the computational resources used to generate the polynomial approximations of the EAP reservoir have no counterpart in the hydrogel's computation, they will be ignored when comparing efficiency.

To assess the entire free energy landscape of the EAP reservoir, each combination of thresholds needs to be converted to a reservoir instance and represented digitally for evaluation. To accomplish this a database of PMA reservoir instances is made containing the probability distribution (as shown in figure 4.8) of the reservoir at every threshold combination. This uses the same threshold range as used in the threshold optimisation earlier in the study, using the minimum to maximum angle reached as the bounds (-31.3 and 29.3) with a step of 0.5 degrees. The thresholds are applied with equation 4.4 where $t_1$ and $t_2$ are the thresholds constants for that iteration of the automata.

$$\bar{k}_l = \left\lceil \left( \sum_{k=0}^{3^N} P\left(k,l\right) k \right) + 0.5 \right\rceil \tag{4.5}$$

$$\bar{\boldsymbol{k}} = (\bar{k}_0, \bar{k}_1, \ldots, \bar{k}_l, \ldots, \bar{k}_{(2^N-2)}, \bar{k}_{(2^N-1)}) \tag{4.6}$$

To represent each EAP reservoir instance in the database as a series of polynomials, the probabilistic component will need to converted to analog outputs. To this aim, we obtain the average output label for each input sequence using equation 4.5, based on the assumption the probability transitions converge as predicted from the interpretation of figure 4.8. Equation 4.5 defines how the probability distribution of output labels for a given input label are averaged to a single output label to create a one-to-one mapping that the polynomial can attempt to model as a continuous function. $\bar{k}_l$ is the average output state label representation $k$ for the input sequence labelled $l$ as found from equation 4.2, the average output labels are stored as a vector $\bar{\boldsymbol{k}}$ defined in equation 4.6 where $\{\bar{k}_l \in \mathbb{Z} \mid 0 \leq \bar{k}_l \leq 26\}$. As with the PMAs definition before $N = 3$. In equation 4.5 $P(k,l)$ gives the probability that the output state $k$ is given when the PMA receives the input sequence $l$, as derived from the probability distribution of PMA outputs for a given set of thresholds.

$$f(l) = \sum_{\hat{p}=0}^{r} a_{\hat{p}} l^{\hat{p}} \tag{4.7}$$

$$k = \lceil f(l) + 0.5 \rceil \tag{4.8}$$

$$\underset{(a_0,\ldots,a_{\hat{p}},\ldots,a_r)}{\arg\min} \sum_{l=0}^{2^N-1} |f(l) - \bar{k}_l|^2, \tag{4.9}$$

$$\text{subject to: } a_{\hat{p}} \in \mathbb{R}, a_{\hat{p}} \in [-100, 100]$$

With the EAP reservoir instances converted to a series of analog mapping functions, they can now be represented via polynomials. The generalised polynomial used to represent the continuous EAP reservoir mapping functions is defined in equation 4.7. The polynomial is fitted to the averaged reservoir mapping using the minimization equation 4.9 for a given degree $r$. $f(l)$ is the input to output transition function that maps input values $I$ to output values $O$, the result of $f$ is rounded to the closet integer (to correspond with the integer representation of output sequences) as shown in equation 4.8. $\hat{p}$ is the power, $a_{\hat{p}}$ is the coefficient associated with the power $\hat{p}$ and $r$ is the degree of the polynomial.

The number of coefficients used to represent a polynomial function is representative of the memory required to store that function. So, by fitting polynomials, with various numbers of coefficients, to the averaged continuous EAP reservoir mapping, and analysing how well each degree of polynomial fit the actual EAP reservoir mapping, the effectiveness of representing the EAP reservoir digitally can be assessed.

Fitting was performed using the polyfit function in Matlab [240]. Polyfit uses least-squares minimization via the discriminant of the Vandermonde matrix to find polynomial coefficients of the specified degree, that most closely represents a given dataset. For each fitted polynomial, the norm of residuals for the error of $\bar{k}_l - k$ is calculated to represent the accuracy of the fitting for the polynomial $f$ given the inputs $\boldsymbol{I}$ and average reservoir outputs $\bar{O}_I$. Each averaged reservoir instance in the database is then fitted to a polynomial using degrees from 0 to 6 to visualise how effective digital systems can represent the free energy landscape of the PMA reservoir.

### 4.4.2 Results

Using the validation method, the graphs in figure 4.9 were generated using the degrees 0, 2, 4 and 6 (graphs for 1,3 and 5 found in the appendix figure A.2). As described earlier, each pair of threshold values is used to generate a PMA reservoir instance via the output layer, and a polynomial is fitted to the resultant mapping function of these reservoirs. These graphs show a norm of residuals heat map for the fitted polynomials against the threshold values in the output layer of the PMA reservoir.

More coefficients allow the polynomial to fit the PMA reservoir's mapping function better, which is to be expected. The bounds of the tested thresholds (-31.3 and 29.3 for $t_1$ and $t_2$ respectively) are always the points of lowest error. This is expected as these thresholds represent the extremes of the reservoir. As -31.3 and 29.3 are the maximum and minimum angles achieved by the gel, if the thresholds were set to these values all output angles would be in a single segment of the thresholded ranges (as shown in figure 4.5), meaning all input sequences would result in the same output sequence. The 'texture' of the heat maps in figure 4.9 have consistent patterns of vertical and horizontal lines. These lines are a good representation of changing sensitivity in the reservoir's response to threshold selection. As the thresholds move closer to recorded output angles of the gel, the impact of the change in threshold value on the reservoir's structure becomes more significant.

From the graphs in figure 4.9, the fitted polynomials required a significant number of coefficients to be close in ability, with pronounced error present until a polynomial of 4th degree was used. As the number of coefficients approaches the number of possible input sequences, the polynomial becomes a direct mapping and offers no computational efficiency over the reservoir. This observation gives insight into the kind of hardware memory required to represent the EAP reservoir based on the number of coefficients used.

The reservoir mapping function being fitted is a sampled average approximation of the true EAP hydrogel function, reducing the probability component, and using only a 3-symbol input sequence $\boldsymbol{I}$ with a 2-symbol language. This means that given the simplest form of the EAP reservoir, where the probability function converges causing a simplification of the probability component, the reservoir function would still not be able to be

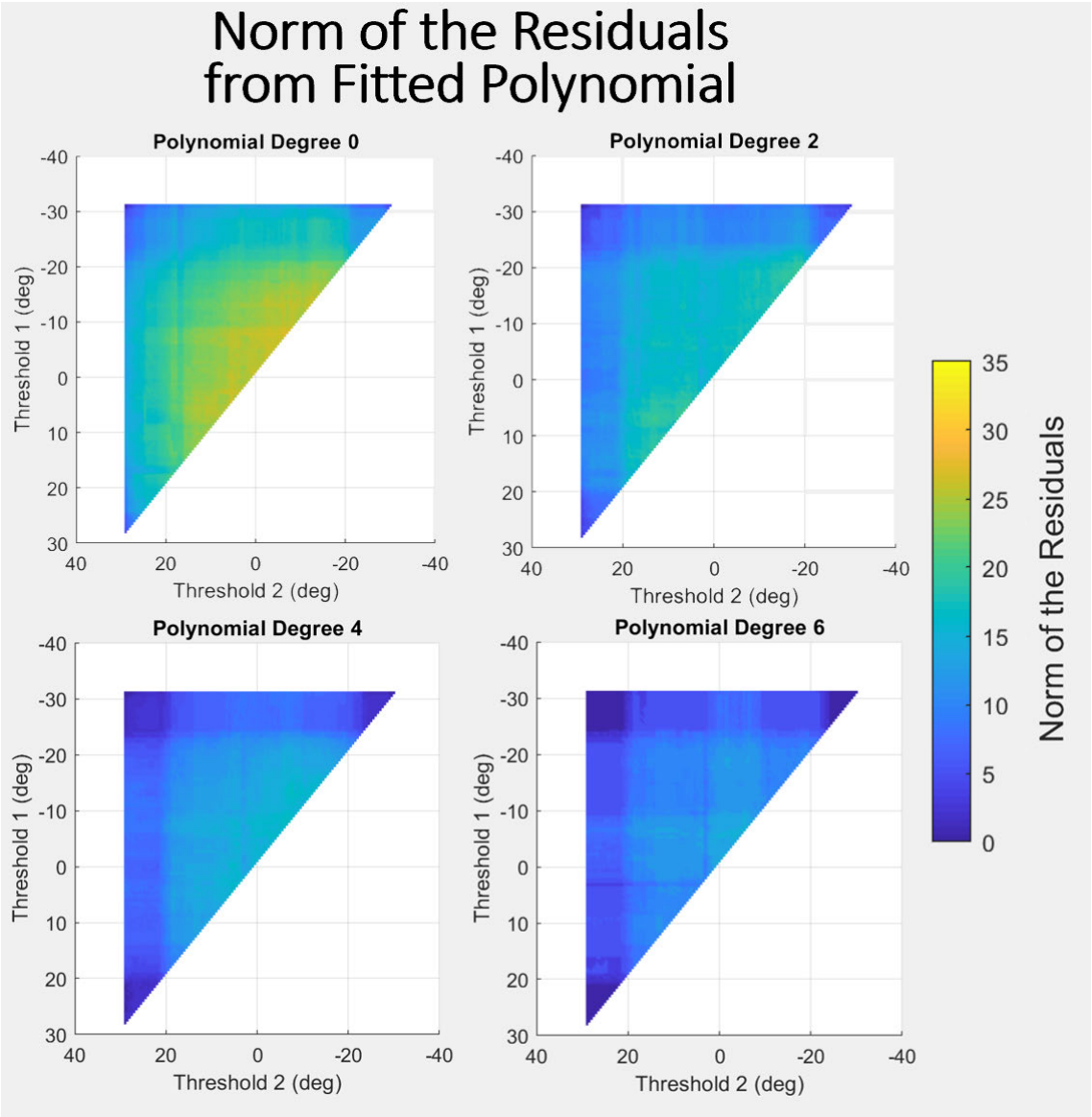


Figure 4.9: Heat map for the norm of residuals error of fitted polynomials, against the threshold values used in the output layer of the PMA reservoir instance that the polynomial is fitted to. Each pair of threshold values is used to generate a PMA reservoir by being applied to the output layer and a polynomial is fitted to the mapping function of these reservoirs. These graphs show the results of polynomial fitting for polynomial degrees 0, 2, 4 and 6 with graphs 1, 3 and 5 found in the appendix figure A.2. The colour bar shows the relative norm of residual values.

represented by the digital computational method without significant error. From this, it is likely that a purely digital representation of the EAP reservoir in computer hardware, such as with a computer modelling method similar to polynomial representation, would not be able to efficiently replicate the high complexity and rich dynamics of the EAP hydrogel reservoir. This ineffectiveness would be even more pronounced when input and output languages of higher complexity and larger vocabulary are used to encode the responses of the EAP gel.

Utilising the reservoir in an application provides an interesting problem, as the task the reservoir's calculation contributes to needs to be possible within the computational landscape of the PMA reservoir. Given a system where events lead to outcomes with certain probabilities of occurrence, such a system can be simplified into a PMA structure. It is unlikely that the probabilities will match that of the EAP hydrogel PMA, but this is where using the PMA as a reservoir allows for it to contribute to computation. The EAP hydrogel PMA provides an energy landscape that can be tuned to a given application by changing the interpretation of the response. Altering the output language definition allows this high dimensional space to be sampled appropriately for the purpose.

### 4.4.3 Discussion

In summary, the sequence of stimulations can be encoded into input sequences, then the output language can be continually altered until the same probability response of the replicated system is observed. Once the input language is defined, this refinement of the output language can be performed virtually. The complexity of the output language does not matter as long as, through its definition, the desired system probabilities are present within the resultant mapping function. In this way the full range of the reservoir may not be used, but the computation it accomplishes can be used to represent/predict the behaviour of the replicated system.

## 4.5 Chapter Conclusion

This chapter assessed the computational ability of EAP hydrogels. First through the exploration of the underlying mechanics of the memory behaviour. then application of

these mechanics to a framework designed using a Probabilistic Moore Automaton (PMA), by constructing a sentence structure for the input stimuli and output response of the gel. Experimental data was collected to generate a PMA, stored as a database of EAP responses. The automaton EAP gel system was shown to be capable of computational tasks, utilising the form of memory in the gel's complex dynamics observed in the previous chapter. Through the PMA structure, unique output sequences were generated from the input sequences.

The theory of computation was then expanded to allow for more complex calculation, combining the PMA framework with reservoir computing to form a hybrid system. Reservoir Computing allows the network of active agents within EAP gels to embody a form of parallel processing. The PMA provides a rich free energy landscape that can be tuned to applications through the adjustment of the input and output language definitions. Through analysis of this energy landscape, given the input and output languages defined in the PMA, the reservoir was shown to be capable of functions that would prove difficult to model via traditional digital computational alternatives with the same analog efficiency. However, the automaton structure is inherently discrete due to the symbolic representation of the input and output languages. The behaviour and mechanics of the EAP hydrogel are, by their nature, analog, thus to fully utilise the computational potential of the EAP hydrogel the framework used must also be analog. The following chapter explore this analog approach to EAP hydrogel integration, building on the concepts and framework developed here.

# Chapter 5

# EAP Hydrogel Inspired Neural Network

## 5.1 Introduction

The previous chapter confirmed that EAP hydrogels are capable of computation via automaton structures. This was accomplished through utilization of the complex dynamic mechanics that mimic memory like behavior via inherent parallel computing. However, through application of the automaton framework the input-output relationship of the EAP hydrogel was fit into the discrete domain of automaton computation. EAP hydrogels are, by their nature, analog and continuous. If the computational and learning abilities of EAP hydrogels are to be fully exploited, then the structure used to interpret computation must employ analog techniques. The most commonly employed paradigms of analog computer are those of biology. Biological neurons and neural structure allegories are commonly used in the field of computing to achieve tasks that would be impossible by any other means.

This chapter explores the similarities between EAP hydrogels and biological computation in order to develop the base understanding and evaluate the shared behaviors that would allow computational potential of EAP hydrogels to be more fully utilized via neural learning techniques. Firstly, through initial observations of similarities in mechanics and revaluation of EAP hydrogel motion behavior from previous chapters in the context of neuron behavior. Secondly, through the collection of additional experimental data and then

further exploring the neuromimetic behaviors, specifically those associated with learning such as neural plasticity. Lastly, evaluating the observations made in this chapter to understand how the implementation of the EAP hydrogel within computation can be altered to better exploit the computational abilities.

## 5.2 Comparisons Between EAP Hydrogel and Biological Neurons

As has been established in previous chapters, the motion of ions within EAP hydrogels, and thus the deformation, can be controlled by manipulating the shape of the electric field [241, 24]. With a basic layout of two opposing electrodes, as described in the previous chapters, the hydrogel bends parallel to the electric field when stimulation is applied.

To summarize the mechanics explored in previous chapters, the localised swelling of the EAP hydrogel essentially acts as a water balloon. As the water molecules gather, the combined pressure eventually overcomes the elasticity of the polymer network and the hydrogel expands. As the hydrogel expands in a localized area, more and more water molecules are needed in that area to expand the hydrogel further until it reaches an equilibrium and can't swell anymore. Without the electric field the ions and water molecules are no longer under an external force. The combined elasticity and entropy cause the water and ions to redistribute back to their homogeneous distribution within the hydrogel. This is called back-relaxation [242].

This behaviour shows striking resemblance to that of biological neurons. As in biological neurons the action of the entity is driven by the flow of ions, in the case of the hydrogel the flow of ions causes bending motion, in the case of biological neurons the flow of ions causes action potentials. Additionally, in both cases this flow of ions is caused by the introduction of charges to the, otherwise, resting state of the system. Withing biological neurons the voltage gated ion channels are closed, preventing the flow of ions, until a charge is introduced by a connected neuron [243]. Within the hydrogel the flow of ions is prevented by the equalisation of the forces as shown in figure 3.3 sections A and B, until an electric field is introduced to offset this equalisation and drive ion motion. Similarly the bending motion of the hydrogel is comparable to the thresholded firing of the biological

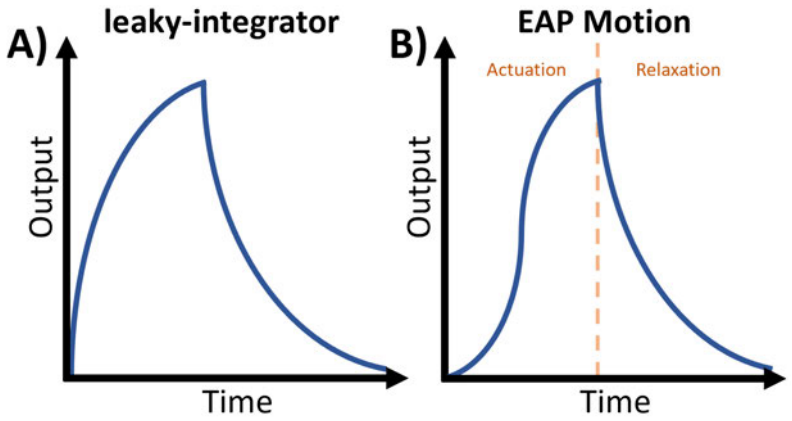


Figure 5.1: **A)** Representation of the leaky-integrator model commonly used in the modelling of neuron behaviour. **B)** Representation of the approximate leaky-integrator model constructed using the EAP hydrogel actuation (with stimulation) and relaxation (without stimulation) behaviour, as shown in figure 5.2, separated by the dashed line. Time is not represented as a consistent scale.

neurons. Where biological neurons fire once a significant number of ions have gathered, so too do the hydrogels bend only after enough ions and water molecules have gathered to offset the balance of osmotic pressure, as described in equations 3.1 and 3.2. The inverse power of the degree of swelling in equation 3.2 shows that, although there is no distinct threshold, the change in osmotic pressure results in a sudden change in volume once the pressure imbalance is high enough. Similarly the function of back relaxation after bending stimulation, shows close resemblance to the refractory period exhibited in biological neurons. Based on these similarities it stands to reason that the hydrogel's behaviour can be simplified into a model commonly used for neurons, the leaky-integrator model.

$$\frac{\delta x_{potential}}{\delta t} = -A_{leak} x_{potential} + C_{input} \tag{5.1}$$

$$x_{potential}(t) = k_{inital} \exp^{-A_{leak} t} + \frac{C_{input}}{A_{leak}} \tag{5.2}$$

The leaky-integrator model, represented simply in figure 5.1 section A, is one of the most common approximations used to model the behavior of biological neurons [244, 245]. The model can be represented by the differential equation 5.1 and general solution in equation 5.2. Where $x_{potential}$ is the output and in the case of the neuron neural potential, $t$ is time, $A_{leak}$ is the rate of leak, $C_{input}$ is the input, and $k_{inital}$ is a constant encoding

the initial condition. The main components of the leaky-integrator model are explained in terms of neural behaviour and EAP behaviour in table 5.1, with reference to the equation components. Although originally used to model simplified biological neuron behaviour, the leaky-integrator model is now more commonly used in artificial neural networks, with significant application to echo state networks/machines [169] within reservoir computing.

Table 5.1: Description of leaky-integrator model components in terms of neurons and EAPs with reference to the differential components of equation 5.1 and solution components of equation 5.2.

| **Name** | **Neural Component Description** | **Differential Component** | **Solution Component** | **EAP Equivalent** |
|---|---|---|---|---|
| Integrator | Raise in internal potential as connected neurons fire | $C_{input}$ | $\frac{C_{input}}{A_{leak}}$ | The base bending behavior under stimulation. Meaning the trend of the EAP hydrogel's bending motion. |
| Leaky | Decline in potential when no firing takes place | $-A_{leak}x_{potential}$ | $k_{inital}\exp^{-A_{leak}t}$ | The behavior of the hydrogel when under no stimulation after reaching maximum bending. Meaning the trend of the EAP hydrogel's relaxation motion. |

Although this initial linking shows similarities, to properly show the comparison some questions about the EAP hydrogels behaviour must be answered. How does the EAP hydrogel's rate of motion change with time and what are the limits of said motion? How does this compare to the integrator aspect of the leaky-integrator neuron model? What is the trend of the relaxation motion and how fast is the recovery period? How does this compare to the leaky aspect of the leaky-integrator neuron model? The trend of EAP hydrogel motion under stimulation and rest was initially investigated in Chapter 3 under section "Initial Shape Change Results". These results can now be applied in the context of neuron comparison. When under stimulation, it was found that the motion followed

an s-curve, as shown in figure 3.15. The observed trend showed an initial "ramp up" not found in the common integrator model. However, the asymptotic relationship to the maximum bending angle fits the integrator model in terms of behavior. Furthermore, the resting behavior after stimulation, as shown in figure 3.16, shows a trend that matches that of the leaky component of the leaky-integrator model. These plots are shown side by side in figure 5.2. By combining the trend shapes for actuation and relaxation, the leaky-integrator model for the EAP hydrogel becomes as shown in figure 5.1 section B. Although the EAP hydrogel leaky-integrator has slight differences, the majority of behavior mirrors that of the neuron model. These similarities should allow for nuromimetic behavior from the EAP hydrogel.

In addition to the similarity in leaky-integrator behavior, there are additional ways in which the EAP hydrogel acts as an allegory for neuron behavior. Through connections between neurons, the firing of a presynaptic neuron can either excite or inhibit the firing of the post synaptic neuron [246, 247]. In this comparison, the electric field applied to the hydrogel is representative of the firing of connected neurons. Due to the controllable polarity of the stimulation used to actuate the EAP hydrogel, the EAP hydrogel has the ability to cause bending in apposing directions. This means the hydrogel can represent both the excitatory and inhibitory inputs present in biological neurons [246, 247]. Furthermore, biological neurons create spikes when a threshold is met, continuing the chain of voltage spikes through the network. The spiking is often modelled by the leaky-integrate and fire model [248]. Although the EAP hydrogel cannot create a potential as an output, the behavior can be implemented using external logic applied to the bending angle of the hydrogel, such as the thresholding approach shown in the previous chapter. Once the bending angle reaches a set threshold the spike can be created via the logic and propagated to connected nodes.

Compared to biological and artificial neural responses, the EAP hydrogels appear to exhibit the same behavior, however, in both comparisons there are limits. The EAP hydrogels have a significantly slower response time when compared to biological and artificial counterparts due to the large scale of the EAP system. From figure 3.16 the EAP hydrogels appear to have refractory periods in excess of 2000 seconds, while biological neurons have average periods of around 20ms [249]. This means that EAP hydrogels cannot be

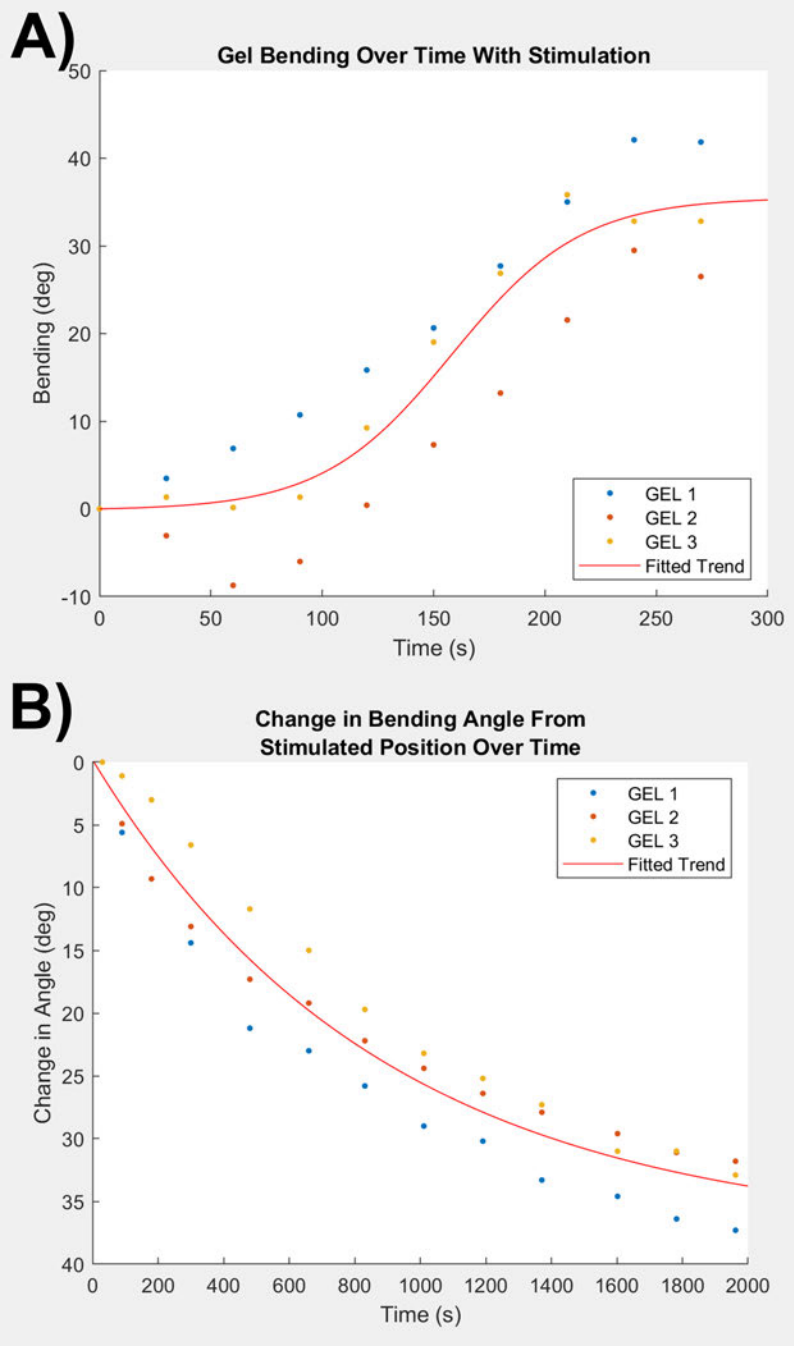


Figure 5.2: **A)** Measured bending angle over time with application of electric stimulation, as shown in figure 3.15 section B. Angle is measured as difference from starting position. An exponential best fit line was applied to the data using the Matlab Curve Fitting app [228], and shows the trend follows an s-shape. **B)** Plot of hydrogel relaxing after 270 seconds of stimulation has ended, as shown in figure 3.16. As different hydrogels reached different positions after stimulation, therefore having different starting positions for relaxation, the angle is recorded as a difference from the fully actuated position. The y axis is inverted to show the relaxation curve consistently with figure 3.15. An exponential best fit line was applied to show the trend using the Matlab Curve Fitting app [228].

used as direct replacements in those specific applications. However, the behavior of EAP hydrogels may offer beneficial complexities not currently found in SNNs when implemented artificially. However, to implement the EAP hydrogel artificially as an SNN one element that allows for learning in neural networks is still required, neural plasticity.

## 5.3 Neural Plasticity Via Weighted Ion Migration

Neural plasticity reinforces or weakens neural pathways by altering the effect, or weight, that incoming signals have on the rise or fall of the internal potential. The rate of ion migration in EAP hydrogels primarily results from the shape and strength of the stimulating electric field. Through the same mechanics that cause bending, the rate at which it bends can be controlled.

The migration of ions to a local area causes the collection of water molecules in that local area, resulting in bending in the hydrogel. The amount of bending is directly proportional to the quantity of ions gathered in the local area, and the rate of bending is directly proportional to the rate of ion migration under the electric field. The ion velocity is determined by the electric field strength and the ion's drift velocity in the hydrogel medium [241, 250]. In keeping with the biological neuron analogy, the electric field strength of applied stimulation is constant. However, the electric field shape can be altered through the manipulation of additional electrodes, effectively allowing the flow of ions to be controlled by controlling the distance ions need to travel to cause bending.

Adding an additional weight electrode, as shown in figure 5.3 section A, introduces an additional degree of freedom. By applying an electric potential between the weight electrode and the actuation electrodes, as shown in figure 5.3 section B.1, the ions in the lower section of the EAP hydrogel can be pulled into the top active area between the actuating electrodes without causing bending action. With this higher concentration of ions between the actuation plates, when the bending stimulation is applied the bending rate is increased as there are more ions present to induce bending. Actuation however cannot be induced concurrently with weight application as all electrodes are required for weight application.

Through this method, a weight can be applied to the EAP hydrogel that reinforces the

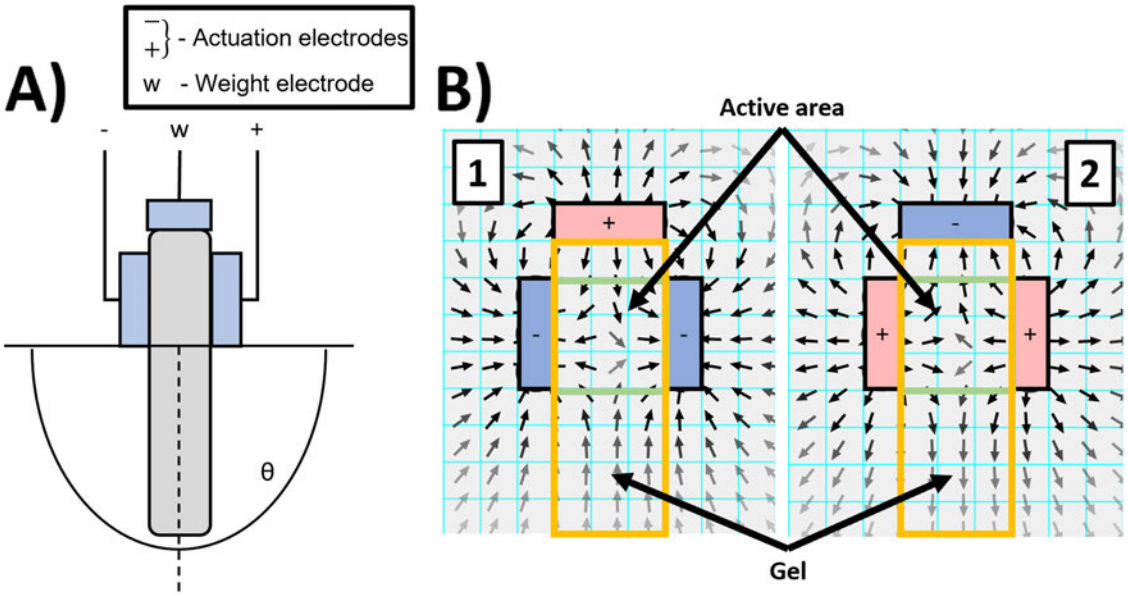


Figure 5.3: **A)** Three electrode arrangement diagram showing positive, negative and weight electrodes. Bending angle is denoted by theta. **B)** Electric field distribution with electrode polarities. Weight is applied by applying a positive voltage to the "Weight" electrode and a negative voltage to the "Actuation" electrodes, this causes the electric field polarity observed in diagram 1, drawing ions into the "Active area" for amplified actuation. These polarities can also be reversed to cause ions to leave the "Active area". As all electrodes are needed to apply the weight, actuation cannot be induced concurrently with the application of weight.

effect of incoming stimulations on the rate of bending, acting in close approximation to weight reinforcement in biological neurons. In the EAP hydrogel the weight application is not automatic with firing coordination. It can, however, be introduced using simple external logic as is intended for thresholding bending output into potential spikes.

In contrast to weight reinforcement, this additional degree of freedom does not allow for weakening to the bending rate. As shown in figure 5.3 section B.2, this arrangement does not provide enough directed force to move the ions out of the active area between the actuation plates. Even with these limitations the EAP, hydrogel provides a close approximation of the biological neuron's behavior.

### 5.3.1 Ion Migration Represented Through Electric Current Draw

To show how the three-electrode arrangement works as a means to alter ion distribution within the EAP hydrogel, a means of measuring ion concentration in the active area is required. When a voltage is applied to the EAP hydrogel, the stimulation induces a electric current draw in the power supply. This electric current draw is influenced by the distribution of ions throughout the hydrogel, as the distribution affects conductivity of the hydrogel. For example, as the ions are influenced by the electric field they move from their homogeneous distribution causing the distance between ions to increase. This causes the conductivity of the hydrogel to reduce thus reducing the electric current draw. By recording this change in electric current in response to stimulation, the change in ion distribution in relation to weight application can be explored.

The polyacrylamide hydrogels were suspended in the sodium chloride solution using aluminium electrodes defined in the previous chapters. A new suspension apparatus was designed to hold the three electrodes on the surface of the hydrogel, as shown in figure 5.3 section A. The new suspension apparatus is detailed in a dimensional drawing and rendering in figure 5.4. A weight was applied to the hydrogel as a continuous voltage of 31V using both the actuation electrodes as negative and the weight electrode as positive, as shown in figure 5.3 section B.1. A INA219A electric current sensor placed in series, recording electric current draw over time. This experiment was repeated 5 times across different EAP hydrogel samples to ensure reproducible results.

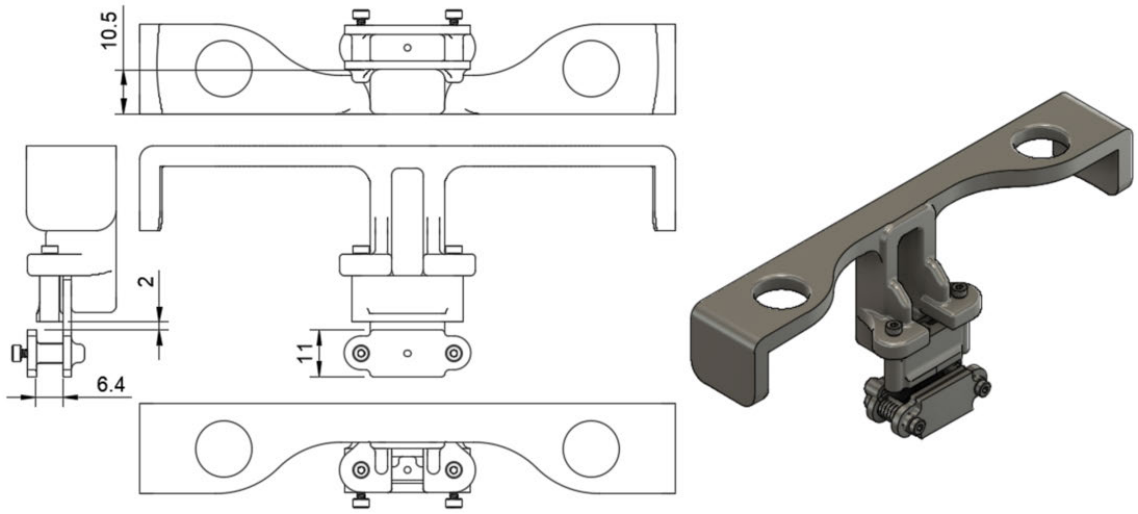


Figure 5.4: Dimensional drawing and rendering of 3 electrode suspension apparatus. The base design from the previous 2 electrode version was used with an additional weight electrode added on top.

### 5.3.2 Results

Figure 5.5 shows the affect of the weight over time, with a clear stabilization following an exponential trend. From this, the weight appears to have a saturation point within the hydrogel which can be modelled using the exponential function shown in equation 5.3, where $I$ is the electric current draw in mA, $t$ is the time in seconds and $c_1$, $c_2$ and $c_3$ are the coefficients. This equation was applied to the recorded data using the curve fitting application of Matlab [228], $c_1$, $c_2$ and $c_3$ were found to be 151.9, -0.04691, and 17.88 respectively.

$$I = c_1 e^{c_2 t} + c_3 \tag{5.3}$$

The exponential shape of figure 5.5 shows a similar behavior to the leaky-integrator as the effect slowly stabilizes under a constant step input. The exponential shape of the trend closely resembles the leaky component of the leaky integrator model, as described in equation 5.2 and table 5.1. This further highlights the similarities in behaviour between neurons and the EAP hydrogel on a mathematical level. In this case $k_{inital}$ can be related to $c_1$ and $A_{leak}$ can be related to $C_2$. This similarity is expected as the same mechanism is

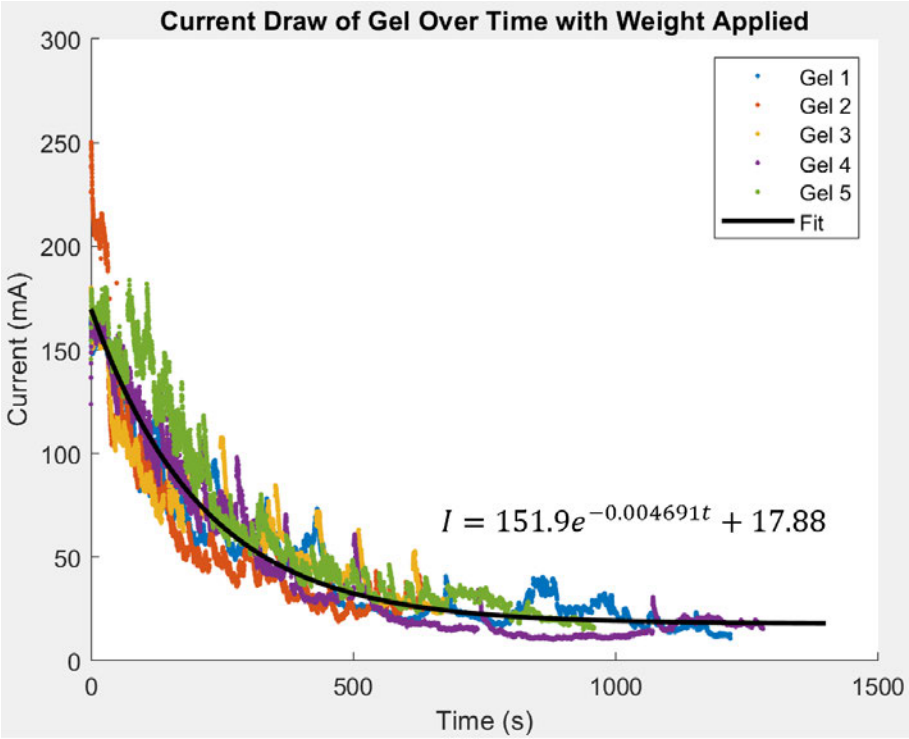


Figure 5.5: The electric current draw from power supply over time. 31v was applied to the EAP hydrogel in the configuration shown in figure 5.3 section B.1. This experiment was run 5 times giving N=5, the legend shows the different gel samples used for each experimental run. An exponential best fit line was applied using the curve fitting application of Matlab [228], with the resultant equation labeled on the graph.

responsible for the bending, which also follows leaky-integrator behavior. With the model, the electric current limit is the asymptote of $I$=17.88 mA, and the time it takes for this limit to be reached within 0.01 mA is 220 seconds. This means that after 220 seconds, all ions that can be moved from the rest of the hydrogel will be in the active area between the actuation electrodes.

### 5.3.3 Discussion

From this experiment it has been confirmed that the three-electrode arrangement allows for ions to be moved into the active area by applying a "weight". This was confirmed through electric current measurement, as electric current is proportional to conductivity which is, in turn, proportional to ion concentration. The experiment also showed saturation behavior. In both biological synapses and artificial neurons the weight applied to inputs can become saturated [251, 252]. This happens when a synaptic weight is reinforced to a point where it cannot be reinforced any further, limited by the maximum chemical potential it can hold. This prevents any single neuron from entirely overshadowing other neurons in the network, thus helping to mitigate over-learning. Saturation has been shown to be important to plasticity of biological systems and key to overall learning through ideas of metaplasticity [253]. Saturation has also shown to be beneficial when implemented in artificial learning algorithms [254]. The presence of this saturation behavior further enforces the behavioral similarities between EAP hydrogels and biological neurons and allowed for said behavior to be modelled.

Although this experiment confirms the weight application methodology and saturation behaviour, the degree to which this weight affects bending must still quantified to properly express EAP hydrogel behavior in terms of a neuron. Therefore, the next step in assessing the application of EAP hydrogels as neural proxies becomes the confirmation that the weight's effect on EAP hydrogel output aligns with that of neuron behavior.

## 5.4 Modelling Neuro-Memetic Behaviour Through Experimental EAP Hydrogel Data

To assess the EAP hydrogel's application within neural networks, the observed mimetic behavior must be formalized via collected data. With collected experimental data, a model can be constructed to compare against current artificial neuron algorithms. With the motion and resting behavior gathered in the Chapter 3 and explored here in the context of neural behavior, there is still a key neuromimetic behavior that must be quantified. That is, the effect of different weights on the EAP hydrogel motion path, when weights of differing lengths are applied. Through experimentation the questions of; how is the trend of the motion path influenced, and how does this compare to neuron behavior or artificial neural network implementation, must be answered.

### 5.4.1 Experimental Design

To quantify this behavior, the same experimental structure as defined in Chapter 3 and used in Chapter 4 was replicated here. However, the suspension apparatus was replaced with that shown in figure 5.4 to allow for application of weights. In alignment with the experimental structure of the previous chapters, polyacrylamide hydrogels are suspended in a sodium chloride solution (0.08%), with aluminum electrodes placed on all three electrode surfaces in the arrangement as shown in figure 5.3 section A.

To allow for more reliable control of the additional electrode, a stimulation controller was designed. This controller uses electro-magnetic relays to direct the stimulation to the individual electrodes allowing for each electrode to be in one of three states; positive, negative, or high impedance. In the high impedance state, the electrode is unconnected to the power supply and so has no affect on the electric field shape, allowing for actuation stimulation as before without interference from the new weight electrode. The relays are controlled via a microcontroller connected to buttons that alter the relay arrangement when pressed. This allows the polarity and electrode arrangement to be altered quickly and reliably with minimal human error. The circuit diagram for these controlling electronics is in the appendix figure A.3. The same electronics setup is shown assembled in figure

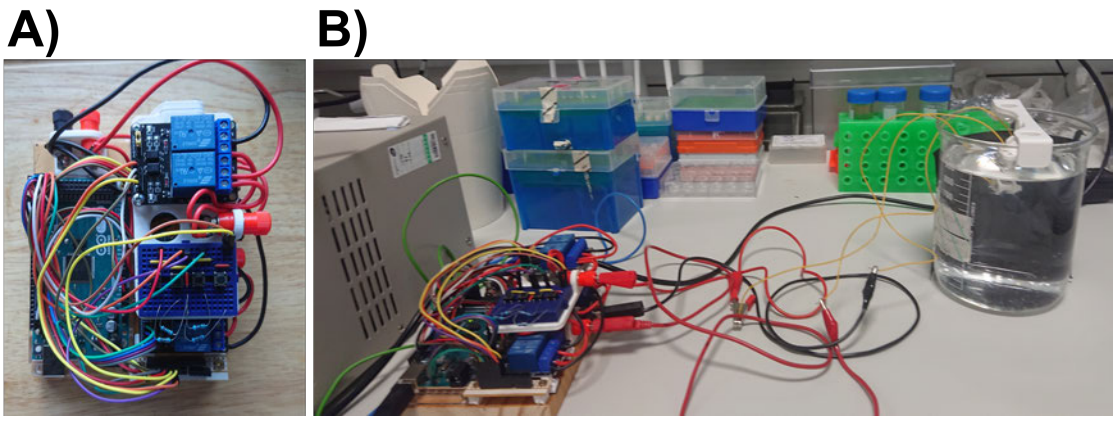


Figure 5.6: **A)** Top view of the driving electronics used to apply stimulation to the three electrodes. A circuit schematic is found in figure A.3. **B)** The driving electronics shown in experimental setup with the EAP hydrogel.

5.6 section A and connected to the suspension apparatus and EAP hydrogel in figure 5.6 section B.

For each experiment a weight is applied to the hydrogel by setting the parallel actuation electrodes as cathodes and the top weight electrode as the anode, as shown in figure 5.3 section B.1. The weight is applied at the start of the experiment before any actuation stimulation is applied. The length of the time the weight is applied is varied to show the effect on the bending rate. After the application of the weight, the EAP hydrogels are left to rest for 10 seconds. Actuation stimulation is then applied across the parallel actuation electrodes with the weight electrode set to a high impedance state. The left electrode is set as the anode and the right electrode as the cathode which causes bending to the right as the ions gather and cause swelling on the left electrode. The actuation stimulation is applied for 240 seconds to give enough time for the effect of the weight to be visible and each experiment is repeated three times to ensure consistency.

Throughout this procedure, a camera is directed at the EAP hydrogel to record the motion. Sample frames are taken from the video along the motion of the hydrogel. These are used to discern the change in angle over time, using the suspension apparatus as the origin to measure from as described in the previous chapters and shown in figure 3.14. These angles are then collated, graphed and analyzed to show the differing EAP hydrogel behavior under different weights. The weights of 45, 90, 135, 180, 225 seconds were tested, with 0 weight already established in the Chapter 3 This range of weights was

deemed enough to explore the full range of effect, as weights in excess of the actuation time would not significantly affect actuation.

### 5.4.2 Results

The plots in figure 5.7 show that for each weight, the bending motion of the EAP hydrogel follows an s-curve, as observed in the Chapter 3 figure 3.15. This response is consistent with trends observed in other EAP hydrogel research [226, 227]. For each of these trends a best fit curve was applied using the same function defined in Chapter 3, equation 3.9, during the actuation experiments. This function was redefined in this chapter for the purpose of modeling the weighted actuation data. This function is shown in equation 5.4 where $\theta$ is the angle, $t$ is time and $b_1$, $b_2$, and $b_3$ are fitting coefficients. This curve was fit to the data using the Matlab curve fitting application [228] utilizing Non-linear Least Squares minimization. The best fit lines are shown in red with in figure 5.7 with the specific coefficient values shown in table 5.2.

$$\theta = \frac{b_1}{1 + e^{\frac{t-b_2}{b_3}}} - \frac{b_1}{1 + e^{\frac{-b_2}{b_3}}} \tag{5.4}$$

$$b_n = b_{n1} e^{b_{n2} w} + b_{n3} \tag{5.5}$$

Table 5.2: Table showing the coefficient values for $b_1$, $b_2$, and $b_3$ for the applied best fit trend defined in equation 5.4 to the plots of figure 5.7.

| **Coefficients** | **Weight (Seconds)** | | | | | |
|---|---|---|---|---|---|---|
| | 0 | 45 | 90 | 135 | 180 | 225 |
| $b_1$ | -35.66 | -49.86 | -60.22 | -51.1 | -61.85 | -55.47 |
| $b_2$ | 158.4 | 121.8 | 109.7 | 94.36 | 98.49 | 107 |
| $b_3$ | 29.09 | 40.3 | 42.44 | 45.32 | 53.42 | 37.69 |

For the neural comparison to hold true, equation 5.4 would need to represent the integrator component of the leaky-integrator model as shown in equation 5.2 and table 5.1. However, the relaxation component is still active within the Hydrogel during stimulation thus in reality equation 5.4 also represents, in part, the leaky component. This accounts for the negative component and exponential denominators of equation 5.4 acting as the decaying factor. This decaying factor is responsible for the hysteresis that acts within the

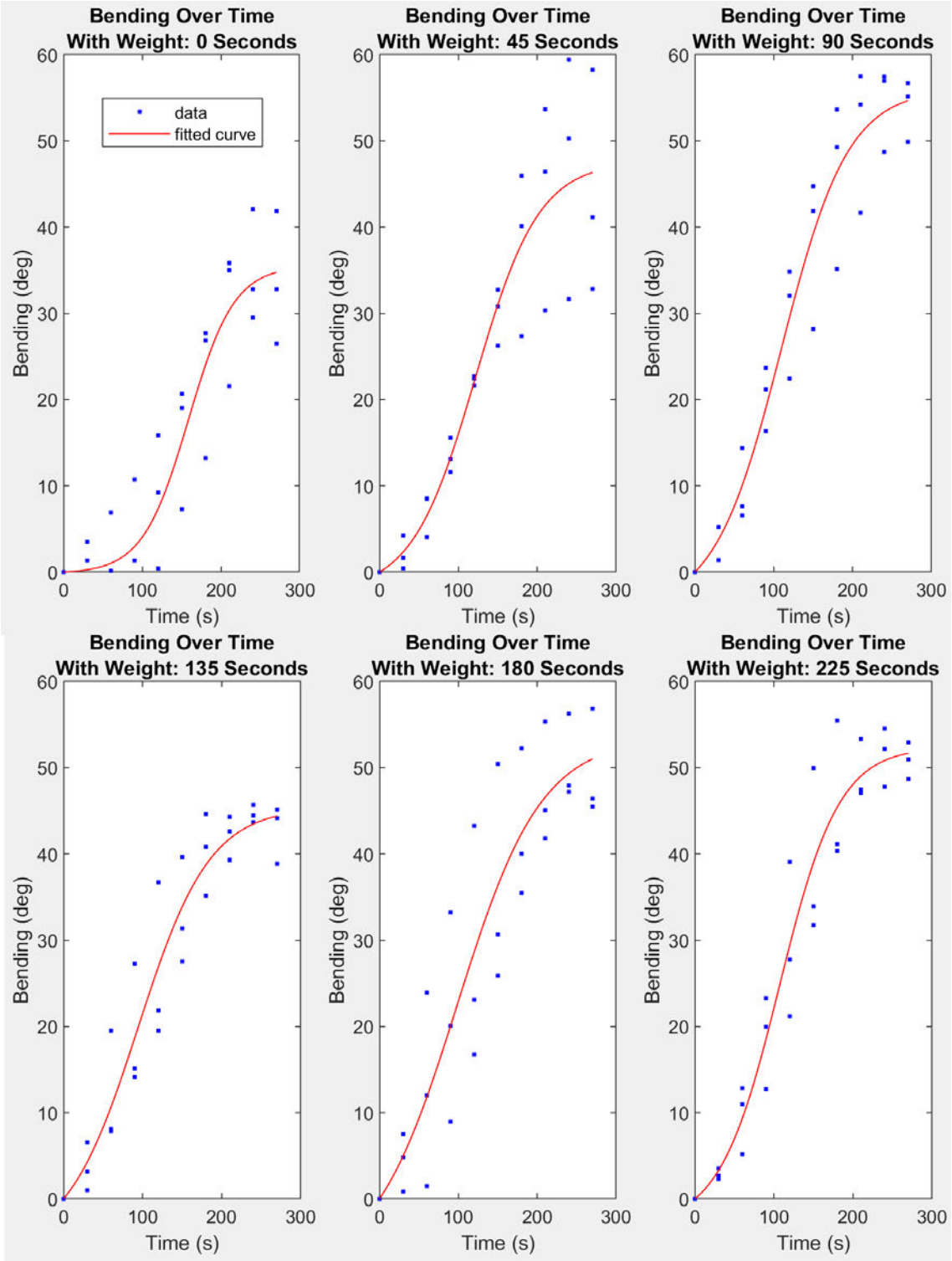


Figure 5.7: A series of plots showing the effect of applied weight on the bending motion of EAP hydrogel, for the weights of 0, 45, 90, 135, 180, 225 seconds. The coefficients of the fitted line can be found in table 5.2.

hydrogels behaviour, and in turn, is also responsible for the memory. By removing this decaying factor the remaining model closely resembles that of the integrator component shown in table 5.1, where $b_1$ represents $C_{input}$ and $1 + e^{\frac{t-b_2}{b_3}}$ represents $A_{leak}$ including the decaying factor. This further highlights the similarities in behaviour between neurons and the EAP hydrogel on a mathematical level.

When looking at the response to weight in figure 5.7, as the weight increases the limit of actuation increases initially showing an average limit of approximately 35 degrees increasing to approximately 55 degrees with a weight of 90 seconds. This increase in limit becomes less consistent with weights in excess on 90 seconds, as seen by the drop in maximum bending angle with weight of 135 seconds. However, after this point the rise in maximum bending angle continues to increase, seen for weights of 180 and 225 seconds. It is possible that the data collected for 45 and 90 second weights was subject to higher variation in hydrogels, perhaps accounting for the larger variance in data points observed in the 45 second weight plot. This may mean that the experimental procedure would benefit from improvements to increase repeatability, additional experimental runs per weight, or additional weights to test. This potential inconsistency means that strong conclusions may not be able to be drawn from the increase in angle limit, however, what is consistent is that as weight increases the initial gradient of the motion trend increases. With application of a large weight, the rate at which the EAP hydrogel initially bends is much faster. These observations in behavioral change with weight can be quantified through modeling of the best fit coefficients.

To model the behavioral change, the coefficients of $b_1$, $b_2$, and $b_3$ shown in table 5.2 were plotted against their corresponding weight. This plot is shown in figure 5.8. A best fit trend was then applied to these trends using the function described in equation 5.5 using the Matlab curve fitting application [228], where $n$ is the motion trend coefficient identifier, and $w$ is the corresponding weight of the coefficient trend. The coefficients of these new trends are shown in table 5.3.

The results of figure 5.8 clearly show a changing motion trend as weight is applied. Although coefficients of $b_1$ and $b_3$ show little change with weight, there is an obvious trend. $b_2$ shows the most significant change, following a clear exponential trend with weight. This aligns with the observations of how initial bending rate changes with application of

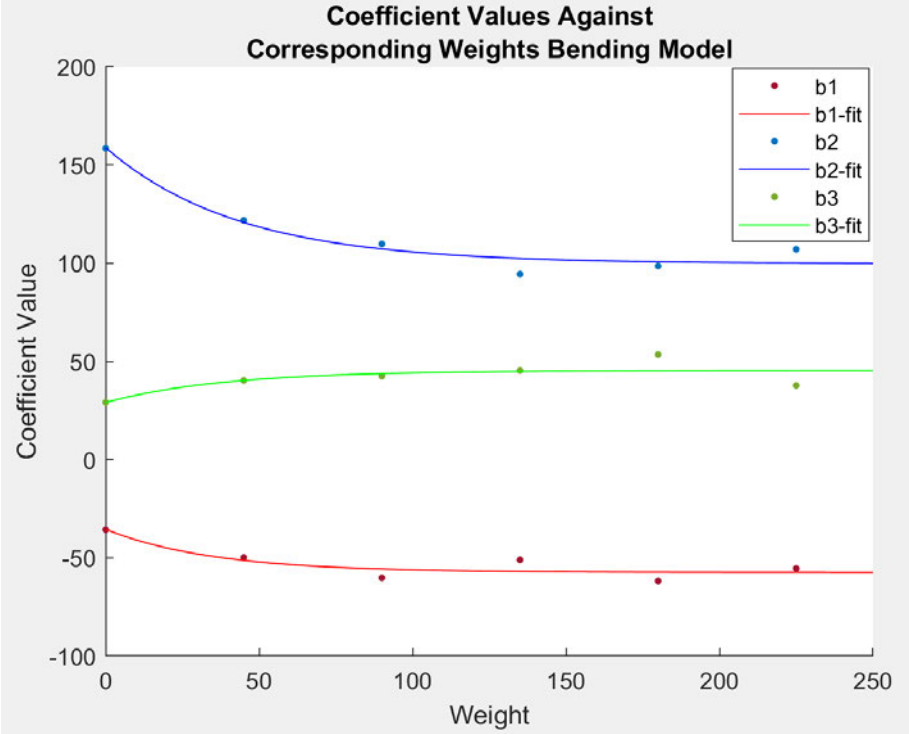


Figure 5.8: A plot showing the coefficients $b_1$, $b_2$, and $b_3$ (from the fitted trends of figure 5.7) with weight $w$ along with the fitted trend using equation 5.5. The coefficients of the fitted line can be found in table 5.3.

Table 5.3: Table showing the coefficient values for $b_{n1}$, $b_{n2}$, and $b_{n3}$ for the applied best fit trend defined in equation 5.5 to the plots of figure 5.8.

| **Coefficients ($n$)** | **Secondary Coefficient** | | |
|---|---|---|---|
| | $b_{n1}$ | $b_{n2}$ | $b_{n3}$ |
| $b_1$ | 21.92 | -0.02851 | -57.41 |
| $b_2$ | 59.02 | -0.02298 | 99.72 |
| $b_3$ | -16.72 | -0.02913 | 45.67 |

weight, as coefficient $b_2$ decreases the initial gradient of the s-curve increases. In all cases the coefficients quickly stabilise. With weights of 129, 160, and 127 seconds, the functions for $b_1$, $b_2$, and $b_3$ are respectively within 2.5% of their asymptotic limits.

To understand the impact of this trend in coefficients on bending behaviour with weight, the system can be modelled using equations 5.4 and 5.5 with the coefficients defined in table 5.3. The results of this model are shown in figure 5.9. The model has been limited to weights from 0 to 160 to show the most significant change in behaviour. Figure 5.9 represents a heatmap of the corresponding weight. Due to the exponential nature of the trends involved, the majority of behaviour change occurs within the initial

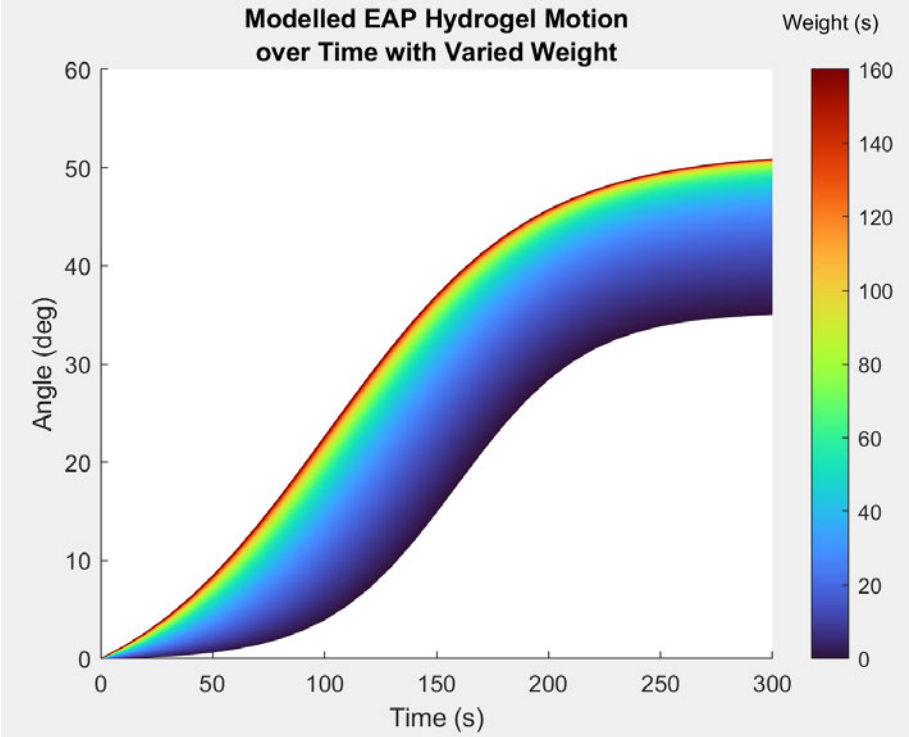


Figure 5.9: Heatmap plot showing the approximate modelled affect of weight on the bending motion trend. Simulated from model defined via equations 5.4 and 5.5 using coefficients defined in table 5.3. The model results are limited between a weight of 0 and 160 to highlight the most significant behaviour.

weight. The model clearly shows that as weight increases the initial rate of bending also increases. However, the decrease in bending rate as it reaches its final bending angle does not change significantly with weight. The model also clearly shows the weight saturation effect as the change in weight has less and less visible affect, visualised by the compressed colour spectrum at the upper end of the plot. It is, however, important to note that the plot represents modelled data, this means that the trend observed in the plot is an approximation of the real world behaviour and may obscure some features or dynamics. These obscured features can however be explored through future work by improving the repeatability of the experimental procedure.

### 5.4.3 Discussion

Through these experiments, the neuromimetic plasticity behavior of the EAP hydrogel was observed and modelled. Equations were formulated that represent how the application of a weight stimulation can cause a change to the rate of bending. Mimicking

how neuroplasticity changes the weight of synaptic inputs in biological neurons and how the weighted inputs of an artificial neurons affect output. Each bending response trend matched those of the leaky-integrator comparison described earlier in the chapter, further confirming the neuromimetic analogy. However, the time scale of the weight application shared the significantly longer timescale when compared to biological neurons. Although this time scale difference would impact direct application, these experiments do show that more information can be encoded into the EAP hydrogel via additional degrees of freedom in the electric field application.

## 5.5 Chapter Conclusion

This chapter served to explore the analog learning capabilities of the EAP hydrogel using biological learning as a comparison. The EAP hydrogels were shown to mimic the behaviour of biological neurons, exhibiting the same leaky-integrator trend in ion motion as is commonly used to model neuron potentials. The EAP hydrogels themselves, in the current bending structure, have refractory periods far slower than biological or artificial neurons, EAP hydrogels taking in excess of 2000 seconds, as shown in figure 5.2 section B, compared to biological 20ms [249]. This vastly longer relaxation period makes applying the current EAP hydrogel structure directly to the neural network structure inefficient, as response times between EAP stimulations would limit effectiveness. However, through understanding of the physical and chemical mechanics, the EAP hydrogel refractory period is dependent on the scale of the hydrogel and distance the ions must travel. Although the refractory period is substantial, the comparative bending time is much shorter by an approximate factor of 10.

Through experimentation, it was also found that, like neurons, the EAP output can be influenced by the application of weight. In the EAP hydrogel this presented as altering the shape of the stimulating electric field, and manipulating the distribution of ions within the hydrogel structure. Although the time scale of this weight application is still outmatched by current neuron implementations, it shows that more information can be encoded into the EAP hydrogel via additional degrees of freedom in the application of the electric field.

The EAP hydrogel was shown to exhibit neuromimetic behaviour. However, the ex-

perimental structure limited the application to learning tasks. With a different structural implementation, can the neuromimetic behaviour of the EAP hydrgoel be utilised for computation and learning while minimising the impact of negative factors highlighted through the experiments of this chapter, such as time scale, refractory period, etc. The neuromimetic behaviour is driven by the motion of ions. However, when output is extracted via bending there are layers of abstraction between the ion motion and output. If ion distributions could be measured closer to the level of the ion migration can the reaction time issues of scale be mitigated. Furthermore, could this more direct integration of individual ion neuromimetic behaviours allow hydrogel polymer structure to be treated as the neural network. Through this analogy, additional degrees of freedom can be added to the electric field allowing the full parallel procession of the ion distribution to be taken advantage of. The following chapter will explore this new approach to the application of EAP hydrogels to computational learning, using the neuromimetic behaviour as inspiration for a new structural implementation.

# Chapter 6

# Learning Behaviour When Embodied in a Simulated Game-World

## 6.1 Introduction

The previous chapter highlighted that adequate exploitation of the EAP hydrogel's computational ability requires analog and continuous interaction between the EAP hydroel and the task. It was shown that the EAP hydrogels could demonstrated significant neuromimetic behaviour, when greater degrees of freedom were applied to the stimulating electric field. BNNs exhibit a great deal of versatility and capability in computation through, among other things, the manifestation of emergent learning behaviour via the interaction of many neurons. Emergent computing is a field inspired by this biological learning behaviour and is described as highly complex processes arising from the cooperation of many simple processes [255], or when behaviour of a system does not depend on its individual parts but on their relationships to one another [256]. Artificial neural networks were developed based on the emergent computing behaviour of biological brains. Both are large complex systems composed of simple machines whose combined interactions lead to complex computation or thought. The expansion of these theories led to

the approach of reservoir computing as explored initially in Chapter 4, where a physical non-linear systems, called a reservoir, is applied as part of the computation process.

If the EAP hydrogel is capable of showing neuromimetic behaviour, it stands to reason that a network of EAP hydrogels could also exhibit emergent learning behaviour. Unfortunately, the integration of many independent EAP hydrogel systems, as experimented with in the previous chapter, is not feasible at any scale that would required for emergent learning. However, although the EAP hydrogel exhibits the neuromimetic behaviour in its motion, the ions migration is the driving force of motion and thus the ion migration is where the neuromimetic behaviour originates. The ions themselves act as the individual agents whose relationships to each other and the surrounding polymer structure result in emergent behaviour. Following this line of thinking is it possible that the EAP hydrogel itself can act as the neuromimetic network and allow for emergent learning behaviour. Furthermore, continuing the work of the previous chapter, through the application of a more continuous computational interface and additional degrees of freedom, can more complex interaction and encoding of information via the electric field be archived, thus allowing for complex and nuanced tasks to be pursued through the application of reservoir computing techniques.

In current theories on learning in biological brains there is president for this approach. A theory of learning gaining much traction is that of the Free Energy Principle (FEP). FEP suggests that any self-organizing system that is at equilibrium with its environment, must minimize its free energy [189, 196, 197]. In BNNs this presents through self-organisation of synaptic pathways [207, 208] via active inference. In active inference, an internal generative pseudo model predicts inputs representing the environment [189, 196, 193], continually updating the internal model to match external events. As sensed inputs, different from those expected via the model, are received, free energy increases. The system seeks to reduce free energy by the most direct means. This presents as the self-organisation of neural connections [202, 203]. This creates a feedback loop where internalised environmental information is continually improved by actions altering the environment, causing ordered interaction between the agent's internal states. This developed ordering of internal states is known as self-organisation, feedback corrects deviations from an ordered configuration [205, 206].

The behaviour of EAP hydrogels can also be defined via free energy, as described in Chapter 3. Using theorise of FEP the neuromimetic behaviour observed in the previous chapter and the memory like behaviour established in Chapter 4 can be explained, as electric fields cause an increase in free energy ions seek to minimise this free energy through migration [71]. Therefore, if both EAP hydrogels and BNNs exhibit behaviour via the FEP, then it should be possible that EAP hydrogels can exhibit the same learning capabilities if embodied in a computation interface feedback loop and applied to an established BNN task. Therefore, if the EAP hydrogel stimulation was representative of an environment, would the redistribution of ions represent an internal model of that environment, similar to the structure of BNNs within the brain?

Although the approach of using the EAP hydrogel as the network is promising, the previous chapter highlighted a key issue. Although neuromimetic behaviour was present in the EAP hydogel responses, the difference in time scale would prevent the direct integration with any useful computational architecture. The large time scale in output results from the time it takes for ions to induce swelling. To cause any observable change in polymer shape a significant number of ions need to migrate to the stimulated region. If a different method of extracting output from the EAP hydrogel's response, that could read ion migration more directly, was employed the time scale for responses could be reduced. This would allow for a faster control loop and significantly easier integration with a more accessible computational framework.

This chapter aims to show how the learning behaviour of EAP hydrogels can be better exploited leading to emergent learning behaviour, similar to that found in BNNs, when embodied in a simulated game-environment. First, by measuring ion concentrations through conductivity of the EAP hydrogel after periods of stimulation a new method of extracting output responses was tested, and the associated ionic memory mechanics enforced. Lastly, the EAP hydrogel is embodied in a simulated game environment of Pong through a custom Multi-Electrode Array (MEA). The game Pong is used as an established task for this study via current work in wetware computers [188]. The game environment is encoded into stimulations provided to the hydrogel, with recorded ion concentrations used as motor commands. Multiple game 'runs' are conducted with this setup and the game performance over time recorded and analysed.

## 6.2 Output Extraction Via Ion Migration and Conductivity Measurement

To use the EAP hydrogel in a computational feedback loop it must have a short enough response time to effectively take actions on a task as it is occurring. Up until this point experiments have used the bending motion as the output, however as shown in Chapters 4 and 5 this response time is much too long for live computation.

As described in previous chapters polyacrylamide uses hydrogen ions as active agents to induce swelling [71]. When enough ions migrate to a specified area the equilibrium between osmotic pressure [211] and rubber elasticity [212] cause changes in the polymer structure. As shown in Chapter 4, the ion motion and its interaction with other mechanics of the EAP hydrogel result in the memory mechanics and computation. Therefore, if the ion distributions can be monitored the computation can be extracted, without the need to induced mechanical motion from the EAP hydrogel, reducing the response time.

Ion concentration can be measured through the conductivity of the EAP hydrogel. As ions collect in a location, and ionic concentration increases, the local conductivity also increases [257]. By applying a small voltage to said location, the electric current draw on the power supply is directly proportional to the conductivity and thus directly proportional to the ion concentration. Utilising two adjacent pairs of electrodes, stimulation can be applied while conductivity is simultaneously measured. This setup is illustrated in figure 6.1. The adjacent electrode pair arrangement also allows stimulation to be applied at the same time that the electric current is measured. This means that input can be given at the same time that output is extracted, allowing the response time and feedback loop period to be even shorter. The experiment also serves to enforce the memory mechanics within this new electrode arrangement. By recording the ion concentrations before and after consecutive stimulations, the "remembered" state caused by the stimulation can be observed in the electric current measurements.

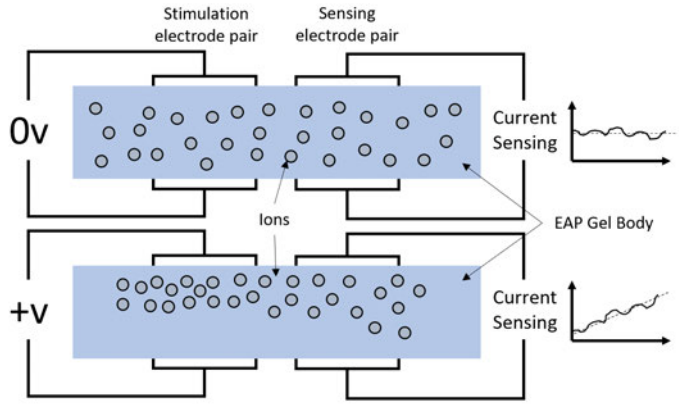


Figure 6.1: Diagrams showing how ion motion is influenced by external stimulation via an electric field and recorded via electric current draw. Under stimulation ions will gather between the electrode pair from elsewhere in the EAP gel. As the concentration of ions in this location increases the conductivity also increases, the increase in conductivity can be measured as an increase in electric current draw when a small voltage is applied in parallel close to this location via a secondary electrode pair.

### 6.2.1 Experimental Design

Using these concepts, a series of stimulations were applied to a polyacrylamide hydrogel sample to demonstrate the new method of output extraction and the memory mechanism. The gels were synthesised using the methodology described in the appendix section A.1.1 "Step by Step Polyacrylamide Hydrogel Synthesis Procedure". The gel was left in a sodium chloride solution (0.08%) to allow the ion concentrations to stabilize and provide consistent starting water concentration within the hydrogel. The gel was then placed between two electrode pairs spaced with a 7mm gap between them. A constant sensing voltage of 2 V was applied to one electrode pair, using a electric current sensor to record the response, while a series of 20 V, across the thickness of the hydrogel (8.5mm), stimulations were applied to the second electrode pair. All stimulations were applied with the same polarity, with the same polarity was used for the sensing voltage applied to the sensing electrode pair. 2 V was chosen as the sensing voltage as it was found to be the minimum voltage required to induce an electrical current high enough to make sufficient use of the electric current sensors resolution. The sensing voltage, as with the stimulating voltage, does induce some breakdown of the hydrogel. However, 20 V was chosen as the stimulating voltage as in practice, with the sensing voltage as 10% of the stimulation voltage, the rate of breakdown induced by the sensing voltage is negligible when compared to that induced

by the stimulation. Through trial and error 20 V was found to be the minimum voltage that induced a significantly measurable rise in electrical current, while also allowing for a long enough hydrogel lifespan to witness the rise and stabilisation in measured electrical current.

Temperature and water content within the hydrogel can affect free energy equilibrium [71]. Temperature alters the elastic properties and rate of ionic motion [70]. As the osmotic pressure difference between the polymer networks and ionic solution drives the swelling, changes in the hydrogel's water content change the degree to which it can swell, as well as altering the mechanical properties of the material [231]. Because of this, temperature and water content must be controlled. To mitigate this as much as possible, the water was taken from a temperature controlled source (approximately 22 °C) to ensure the solution was a consistent temperature and provide the same starting temperature conditions. Furthermore, the gels were stored in water tight containers and left in the ionic solution for the same period of time to ensure the starting water content of the hydrogel was consistent.

### 6.2.2 Results

The results of this demonstration can be seen in figure 6.2. Each segment and the events taking place are described below to represent the memory mechanics through ion migration.

A. The recorded electric current has a default value of approximately 0.8 mA as the EAP hydrogel is inherently conductive.

B. With application of an electric field there is an immediate rise to 2 mA, as the stimulating electric field is picked up by the sensing electrode pair, shown at the beginning of this segment. The stimulation also caused an increase in free energy. As a result, the ions moved toward the electrode to minimise free energy. The electric current draw also rose, as ions collect and conductivity increased, to 2.4 mA. It is important to note that the increase in current is not directly proportional to the number of ions but instead their energy, in essence it is directly related to the velocity/mobility of the ions.

C. Once the stimulation was removed the electric current dropped back to almost default

values. It was however slightly higher than as shown in segment A as the area still contains the migrating ions.

D. Once the stimulation was reapplied, the electric current draw immediately rose back to the point where segment B ended, as the ions still maintained their positions and mobility. As stimulation is applied the ions mobility gradually decreases as they all gather in the destination area. This causes the electric current to also decrease, however the electric current at the end of the segment is still higher than that shown at the beginning of segment B.

E. The stimulation was removed again, and again electric current dropped back to slightly above default values.

F. Once the stimulation was reapplied, the electric current draw immediately rose back to the point where segment D ended as the ions still maintained their positions and mobility. With continued stimulation the mobility continues to decrease, however at an exponentially slower pace as mobility decreases. Halfway through the segment the electric current appears to have stabilised as the mobility cannot decrease any further.

G. The stimulation was removed again, and again electric current dropped back to slightly above default values.

This observed behaviour exhibits a memory like mechanism where a value is "saved" to the EAP hydrogel by the redistribution and mobility of ions within the gel, in response to the increase in free energy. This behaviour can then be seen again at the beginning of segment F where it continues from where segment D finished.

### 6.2.3 Discussion

From this demonstration of memory mechanics, it is evident that changes in the ion distribution/mobility and polymer network can be recorded as electric current draw through the application of a small voltage. This is evidenced by the change in electric current over time as stimulation is applied, altering the ion distribution and polymer network. The demonstration also highlights how the increase in free energy through stimulation

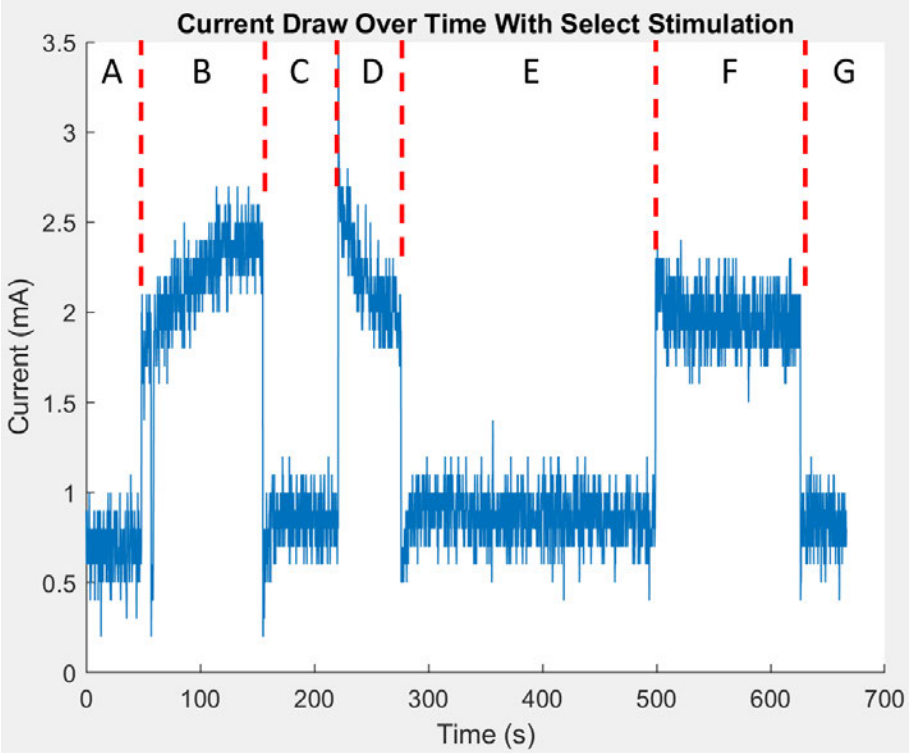


Figure 6.2: This graph shows a sample of recorded electric current draw from 2 adjacent parallel electrodes as described in 6.1. The data has been segmented and labelled **A** through **G** for reference. The sensing voltage (2 V) was applied continually through the entire demonstration, stimulation (20 V across the 8.5mm thick hydrogel) is applied in sections **B**, **D**, and **F**. The recorded electric current has a default value of approximately 0.8 mA as the EAP gel is inherently conductive shown in segment **A**. With application of an electric field there is an immediate rise to 2 mA as the field is picked up by the sensing electrode pair shown at the beginning of segment **B**.

is resolved by the hydrogel through ion migration, and the last state of the EAP hydrogel "remembered" if stimulation is removed. With reapplication of the stimulation the changing electric current continues from the last state recorded during stimulation. From these observations it can be established that the ion concentrations at "sensed" points can be measured, allowing for more direct EAP response extraction. These observations also enforced the memory present in the EAP hydrogel, with the response due to the hydrogel's memory able to be measured in parallel with the application of stimuli. To fully demonstrate this new approach to computational integration, a suitable activity is required, along with a closed loop control structure and hardware to interface with the hydrogel.

## 6.3 EAP Hydrogel Embodied in a Simulated Game-world

The behaviours of the EAP hydrogel can be characterized through free energy minimisation [71]. There are many systems whose mechanics can be represented through free energy minimisation, in computation one of the most significant is that of learning within BNNs [189]. Furthermore, in the most basic sense, biological brains represent information through the self-organisation of neurons as active agents [258]. Similarly, EAP hydrogels can represent information via the distribution and organisation of ions as active agents. Information in BNNs is also stored through many other complex means, however the organisation of neurons serves as a leading mechanism within the BNN system. For the demonstrated memory mechanics to exhibit learning functions, the EAP hydrogel would need to be embodied within a closed control loop, as is present in BNN systems. To induce learning, the hydrogel must be able to influence actions within an environment. The change in environment as a result of those actions must feedback to the hydrogel leading to changes in actions and learning behaviour. To construct this closed loop and quantify learning a suitable activity is required.

The paper "In Vitro Neurons Learn and Exhibit Sentience When Embodied in a Simulated Game-World" [188] used a single player version of the game Pong as the quantifying activity when integrating a BNN with computer architecture. The game provided a virtual environment for the BNN to inhabit and learn from. The method used to interface

the biological neurons with the simulated environment, fits neatly with the reservoir computing framework [5]. In the paper [188] the position of the ball was presented to the neurons through localised stimulation, aligning with the function of the excitation layer in a reservoir computer. The neuron responses were converted to motor commands to control the paddle, aligning with the function of the readout layer. Given the commonalities in the underlying mechanics, in relation to FEP and memory, the performance of computational learning within the EAP hydrogel can be assessed using the same Pong game-based activity, in a simulated game environment, utilising the reservoir computing framework.

The paper did however implement a form of supervised learning through random and patterned stimulation. Theories of FEP, however, do not depend on supervised learning. By implementing a second system that interacts with the BNN a second source of information entropy is present outside the hybrid system. This study seeks to investigate the application of FEP theories of learning to a more purely free energy driven system, as such, to test if learning can be induced self-consistently. The theories of FEP in this study are applied in the context of unsupervised learning.

### 6.3.1 Experimental Design

An MEA was used to interface the EAP hydrogel with a computer system containing the Pong game environment. The array of electrodes were divided into two regions, used to provide stimulus as input to the gel via the application of electric fields at select locations, and record output via the electric current at select locations. This division of regions is similar to how MEAs are currently used in applications [188, 259]. By dividing areas into specific tasks, interference from different tasks happening in the same location is minimised. The layout of these regions can be seen in figure 6.3 section A.

The stimulation region of the gel acts as the stimulation layer of the reservoir framework, consisting of a 2 by 3 array. To translate the ball's position into stimulations the game environment was divided into a 2 by 3 grid, as shown in figure 6.4 section B. The location of the ball in the game environment is sent from the computer to the MEA, as the ball passes through those regions the corresponding electrode pair is activated to stimulate that area. The regions as they are labelled in black in figure 6.4 section B are how they will be referenced throughout this paper.

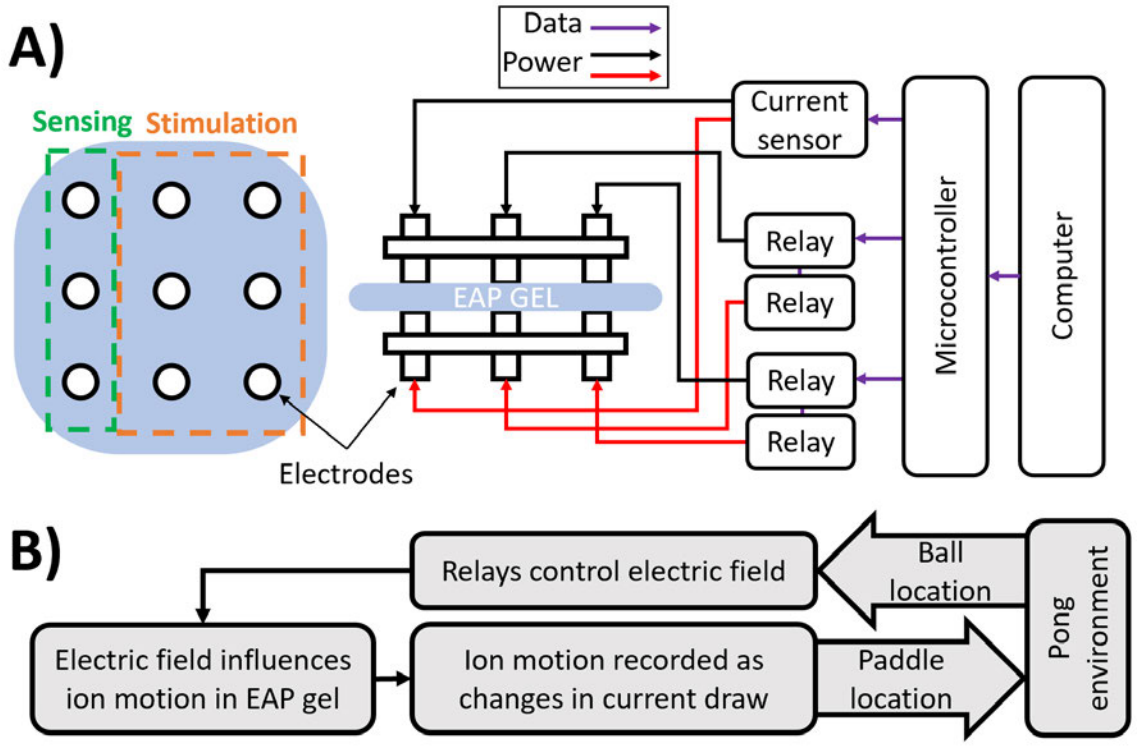


Figure 6.3: System layout of closed loop communication between the computer containing the Pong environment and the EAP hydrogel. **A)** The layout of communication between components in the system and separation of the electrodes into regions. The electrodes are divided into driving, which provide stimulation, and sensing, which measure electric current draw. The driving electrodes are driven by relays that direct the electric field (20 V across the 10mm thick hydrogel disk). The sensing electrodes provide a small voltage (2 V) and the electric current draw is measured by a electric current sensor. Both relays and sensors are coordinated by a microcontroller, which is in turn directed by the computer and Pong game environment. A more detailed circuitry schematic can also be found in the appendix figure A.5. Additionally, an image of the physical hardware can be seen in the appendix figure A.7. **B)** A flow chart of the information path from the Pong environment on the computer to the hydrogel containing the ions.

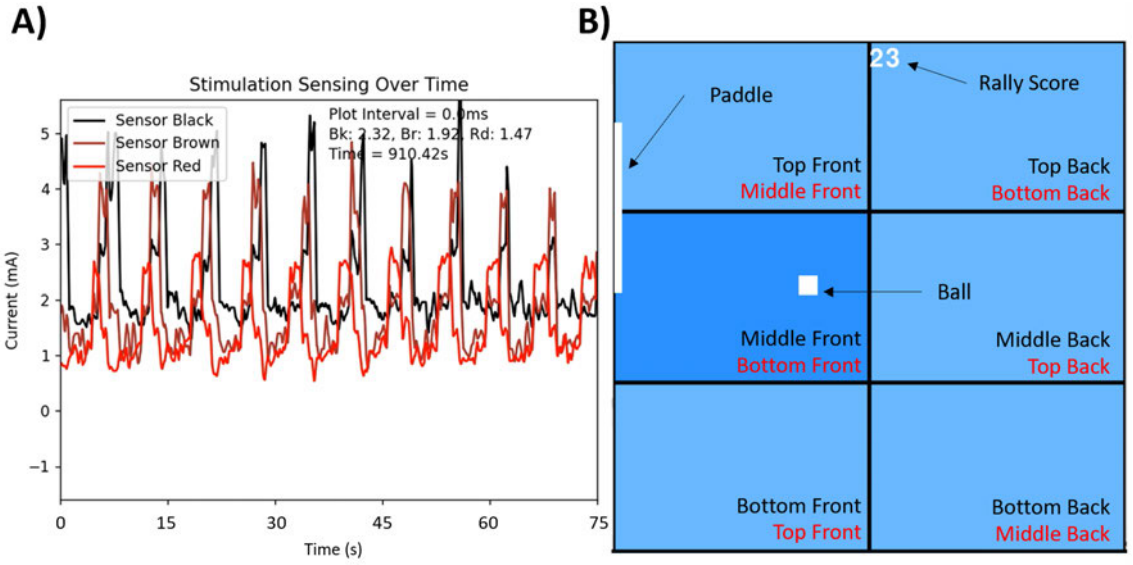


Figure 6.4: Software representation of the Pong game within the computer. **A)** The electric current sensor readings as they are received by the computer. The black, brown, and red lines represent the top, middle, and bottom sensors respectively. The interval between received data is also measures and averages at 0.5 mS, labelled as "Plot Interval". The averaged electric current across the graph for each sensor is measured for the purposes of establishing default values, labelled as "Bk", "Br", and "Rd". The total recording time is also displayed labelled as "Time". These sensor values move paddle in the Pong game environment through conversion to a position based on sensor location, as visualised in figure 6.5. This can be seen on the computer screen along with the apparatus in the appendix figure A.9. **B)** The simulated Pong game environment, 1000 by 1000 pixels, which is separated into 6 regions as described in figure 6.3 section B. When the ball is in a region it will darken and the corresponding electrode pair will stimulate the EAP hydrogel. The score is displayed at the top and resets when the ball hits the left wall behind the paddle. The regions are also labelled in black here for reference within this paper. The paddle is set to 1/3 the environment height (333 pixels). The rearrangement of regions used for the control dataset, where 'vision' is impaired, is indicated by the red region labels. This can be seen on the computer screen along with the apparatus in the appendix figure A.9.

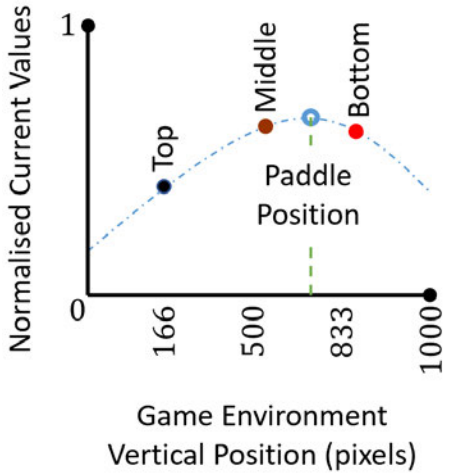


Figure 6.5: An example of the method used to place the paddle based off the electric current readings as measured in figure 6.4 section A, shown here as the same representative colours and labelled with their region locations. The electric current readings are normalised between 0 and 1 and plotted based on their region's centre vertical location. These coordinates are 166, 500, and 833 pixels for the top middle and bottom regions respectively. A 2nd degree polynomial is applied, as indicated by the blue dashed line. The point where the polynomial is at its peak is the maximum predicted electric current, as indicated by the blue circle, and this is where the paddle is placed.

The sensing region acts as the readout layer of the reservoir framework. Electric current sensors were used to measure the electric current draw at the sensing electrodes, utilising the small sensing voltage (2 V) defined in the previous experiment. These electric current values are recorded on screen, shown in figure 6.4 section A recorded in mA, and interpreted into motor commands for the paddle. Recorded electrical current values are normalised using the maximum and minimum electric current values recorded from the hydrogel during the previous experimentation with the apparatus, found to be +3mA and -0.75mA respectively. An electrical current spacial trend is then calculated using these normalized values against their locations represented in the Pong game environment. The sensing electrodes are evenly distributed across hydrogel. When comparing the distribution of sensing electrodes to the regional layout of the simulated environment, this places the point of electrical current measurement at the centre of each region. This means that the measured current correspond to a particular pixel point in the simulated game environment, 166, 500, and 833 pixels for the top middle and bottom sensing electrodes respectively.The electrical current spacial trend is generated by fitting a 2nd degree polynomial to the 3 points of y coordinate (pixels) and electrical current (mA) . The peak of

this trend is the predicted point of highest electric current, and highest ion concentration, in the hydrogel and is where the center of the paddle is placed. This is illustrated in the example in figure 6.5. In alignment with the rules of pong, the paddle is limited to within the game area, meaning it cannot go off screen. The calculated paddle position is constrained to within game to ensure this.

Through this layout of hardware and software, a closed loop was established where the computer outputs the game's environment, represented as ball location, to the MEA applied to the gel as shaped electric fields. In response, the ion concentrations are measured by the MEA as electric current and provided to the computer and the Pong game to move the paddle. This closed loop is outlined in figure 6.3 section B. A more detailed description of the behaviour and implementation of the Pong game, as shown in figure 6.4, can be found in the appendix section A.4.2 "Pong Game Implementation and Behaviour". Similarly, a more detailed description of the hardware implementation, as shown in figure 6.3 section A, can be found in the appendix section A.4.3 "MEA Hardware Implementation and Details". A circuitry schematic and image of the physical hardware can found in appendix figures A.5 and A.7. The full setup of the computer game environment and MEA apparatus can be seen in the appendix figure A.9. The full experimental procedure for each run of the Pong game with the EAP hydrogel, can be found in the appendix section A.4.4 "Pong Game Experimental Procedure". In total 21 separate EAP hydrogel runs were carried out, collecting 3500 seconds of 'game play' for each run before the hydrogel degraded beyond the point of continuing.

From these games several metric were recorded to be used in performance analysis, electric current measurements, stimulation positions, and score. The score, shown in figure 6.4 section B, increases whenever the paddle successfully hits the ball and resets to 0 whenever the ball misses the paddle hitting the wall. All data from these separate runs was combined into a single dataset to view the overall averaged behaviour of the hydrogel and assess the performance as well as the repeatability.

#### Control Experiments Via Interference of Information Translation

A set of control experiments were also undertaken to create a baseline to compare performance against, and further show that the hydrogel's improved performance was a direct

result of the environmental information received. These experiments explore the null hypothesis that the hydrogel's performance increase was not a result of accurate game environment information. The control experiments are designed to accomplish this by interfering with the translation of information between the hydrogel and the simulated game environment. By altering this translation, the hydrogel is presented with information that does not accurately represent the simulated game environment, and thus, the hydrogel would be unable to learn about the environment. There are two key positions within the closed feedback loop, between the hydrogel and game environment, that can be altered, these are labeled in figure 6.6 and described as such:

1. Translation from voltage readings, via ion concentrations at electrodes, to a paddle position within the game environment.

2. Translation from ball position within the game environment to distribution of stimulation positions. Which are then translated into electrical stimulation via electrodes.

Control experiments can be applied by altering the flow of information within the closed feedback loop at either of these key positions;

- Altering the flow of information from the hydrogel to the simulated game environment, via interfering with the translation of information at point 1.

- Altering the flow of information from the simulated game environment to the hydrogel, via interfering with the translation of information at point 2.

At these positions in the closed control loop, there are also two main ways in which information translation can be altered. Either through the manipulation of mapping functions, altering the way in which electrode positions in the hydrogel map to positions in the simulated game environment, or by entirely severing the information path. The latter method would, however, only result in no actions taken by the EAP hydrogel and thus not glean any useful information. Although the EAP is active it does not produce an electric field on its own, and thus requires some stimulation to create the inhomogeneous distribution of the charges necessary to create control signals. Because of this the control experiments should be pursued through manipulation of the mapping functions at the two key points detailed in figure 6.6.

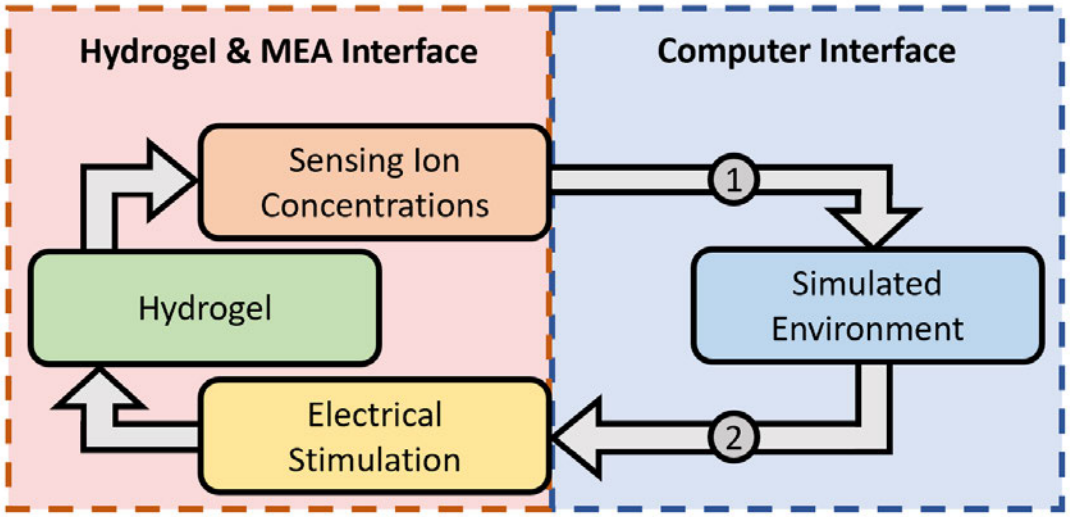


Figure 6.6: Software representation of the Pong game within the computer. Diagram showing the various paths of information within the experimental setup. Representing the flow of information between the MEA and computer systems. The key points of information transduction that can be altered for the purpose of control experiments are labelled as 1 and 2.

In both these control experiment structures, for the null hypothesis to be rejected, the hydrogel would need to exhibit no learning. For this to be true, the hydrogel would need to perform worse than if the paddle was moving randomly. As the paddle is 1/3 the height of the simulated environment, the rejection would require a hit rate below 33%.

The first control, remapping the sensing data, experiment was achieved through simulation, utilising the data collected through running the live experiment. Simulation allows for multiple arrangements of sensing inputs to be tested without the need for multiple hydrogel samples, reducing error due to variation in hydrogel samples. The method of simulation is detailed in the supplementary information section "Control Experiment Surrogate Data Simulation". In this control experiment the sensing regions, as described in figure 6.4 section C, were rearranged from top, middle, bottom to middle, bottom, top. This ensures that all sensing regions are in entirely different areas to prevent overlap between the control and non-control experiments.

The second control experiment, remapping the stimulation data, however, cannot be accomplished accurately in simulation. Due to the complex interference between stimulated regions within the EAP hydrogel this experiment must be performed on the live hydrogel sample. This was accomplished by rearranging the game environment's regional

correlation to the MEA's stimulation electrodes, giving incoherent environmental information to the hydrogel and effectively impairing its 'vision'. The rearrangement of game environment regions can be seen in figure 6.4 section B, indicated by the red region labels.

### 6.3.2 Results

#### Memory Function of the EAP Hydrogels Via Electrical Current Measurement

To show the memory mechanics in the combined MEA and Pong experimental structure, and follow the progression of the learning behaviour, first the measured electric current draw was plotted for each sensing electrode pair. This allowed an initial view of minimised energy in the form of electrical current, and established the time range in which learning occurs. Figure 6.7 represents the combined measured electric current data points of all 21 game runs, with data points sorted against time, averaged using a 600 second moving average window. The electric current initially rises as ions move towards the electrodes. As the ions collect their rate of migration decreases due to the increasing concentration gradient. Eventually, the ions stop moving and the electric current reaches its maximum, shown in figure 6.7 by the vertical purple dashed line. Then the hydrogel breaks down as the electric current falls, eventually leading to breakdown of the polymer structure as a result of electrolysis [260] and impairing connection between electrodes, as shown in the appendix figure A.14. This breakdown marks a cutoff point, after which hydrogel is too degraded for results to be representative of performance, marked in figure 6.7 by the orange vertical dashed line at 2000 seconds. This degradation, and eventual breakdown, is caused by strain resulting from the migration of ions and water molecules under the electric field. As the hydrogel is an EAP its shape is altered by the flow of water in reaction to an electric field. Although the hydrogel is elastic it is relatively fragile, and prolonged shape change causes degradation impacting measurements. Thus, the graphs used to analyse the hydrogel's performance were limited to between 0 and 2000 seconds so to remove any unrelated data.

The hydrogel breakdown occurs at a consistent time in each experimental run, at the point of this breakdown the gel develops a hole and the connection between sensing and

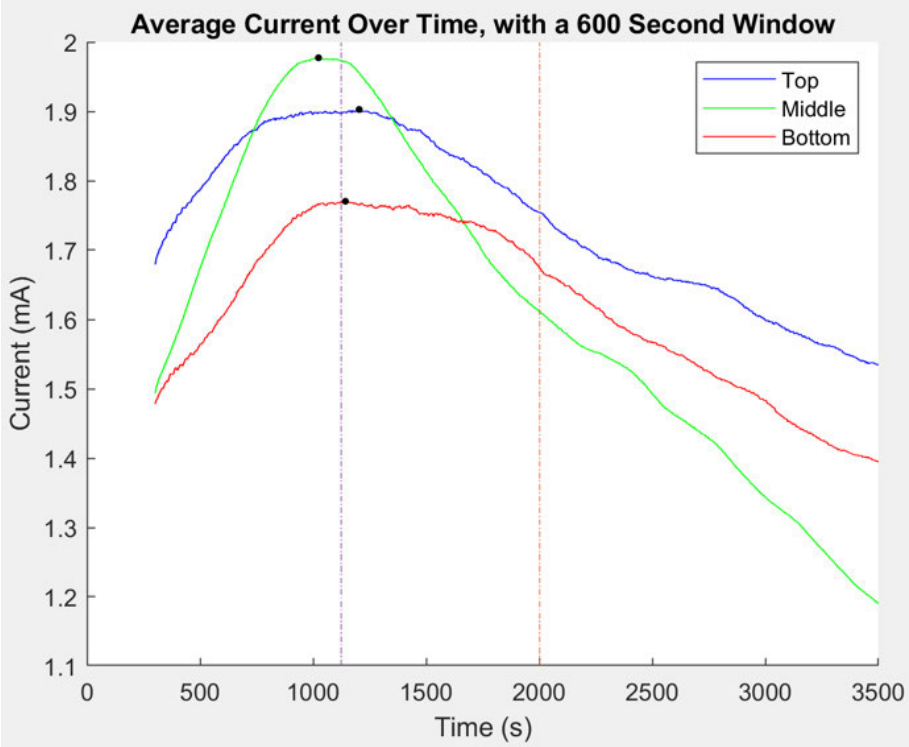


Figure 6.7: The electrical current at each sensor over time for the combined unimpaired dataset of runs, smoothed using a moving average window of 600 seconds. Due to the averaging, data starts at 300 seconds. The point of maximum electric current draw is marked with a black dot. 1203, 1023, and 1142 seconds for top, middle, and bottom respectively. The average point of maximum electric current draw is marked by the purple vertical dashed line at 1122 seconds. The orange vertical dashed line marks the earliest point the EAP gels broke down. Standard error was calculated for each trend from the windowed samples and found to be at maximum, 0.0169, 0.0053, and 0.0116 for the top, middle, and bottom trends respectively.

stimulation fully separates making the point of total breakdown obvious in measurements. The point at which electric current decreases, after the point of maximum electric current, is a result of the gradual structural breakdown leading to total breakdown around 2000 seconds. Through comparison and averaging between experimental runs, this gradual structural breakdown also appears consistent across experimental runs with different hydrogel samples. As the structural breakdown is predictable the impact on measured results is minimal.

### Performance of the EAP Hydrogel Within The Pong Game

To assess the performance of the hydrogel within the Pong game, the hit rate was calculated using the combined data points of the 21 game runs sorted by timestamp, shown in

figure 6.8 as the left axis. 21 experiments were sufficient for reliable results shown via standard deviation analysis, described in the appendix section A.4.5 “Accuracy of Experiment Repetitions”. Due to the boundary conditions of the paddle, the top and bottom regions of the wall were hit more often by the ball than the middle (see appendix figure A.10). As hit rate is different between regions, learning rate may be different between regions. For this reason, the hit/miss data was segmented based on the region in which the hit/miss occurred. Figure 6.8, shows the segmented paddle performance learning curve for the top, middle, and bottom game regions.

For the middle region, the paddle had an initial ball hit rate of 50%, but over the course of the game this rose to maximum of 60%, giving a rise of 10% over 1450 seconds. The middle region shows the greatest improvement in performance.

The top and bottom regions are subject to the boundary conditions leading to a higher initial hit rate, as seen in figure 6.8, as the trend via the measured electric current in those regions is almost linear, seen in figure 6.7. For the bottom region the paddle initially hit the ball approximately four times more often than it missed, hitting 79% of the time. As the bottom region is also a boundary condition this is expected. However, over time this performance did increase up to a maximum of 87% hit rate, showing an improvement of 8% over 1750 seconds.

When compared to the other regions, when the paddle was in the top region it rarely missed the ball. However, when the number of successful paddle hits are summed for each region over the 21 game runs, the paddle hit the ball in the top region 49% of the time while the middle and bottom regions hit the ball 12% and 40% of the time respectively. This distribution can be found in the appendix figure A.11 section A. This distribution follows the distribution of ball hits as found via the appendix figure A.10, the top and bottom regions hitting more often consistently with each other while the middle region hitting far less often. This means that the distribution of paddle hits matches the inherent distribution of the game physics, and furthermore the increased hit rate is not due to the ball spending a higher percentage of time in the top region. However when summing paddle misses the top region has far less occurrences across all experiments. The paddle when in the top region only missed the ball 4% of the time while the middle and bottom regions accounted for 66% and 30% of misses respectively. This distribution can be found

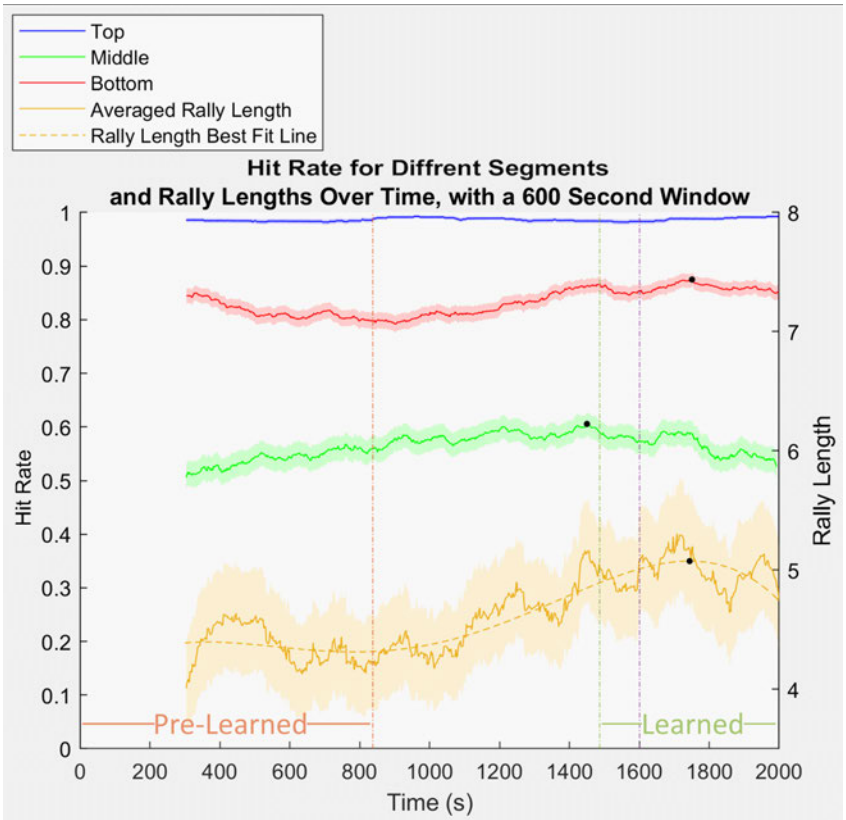


Figure 6.8: *Left Axis:* The hit rate as a hit to miss ratio over time for the combined unimpaired feedback loop dataset, separated based on the region the hit/miss occurred in as described by figure 6.4 section B. Smoothed using a moving average window of 600 seconds, this window size provided the clearest view, additional windows sizes can be seen in the appendix figure A.12. The standard error for each windowed sample is shown by the shaded area. The point of maximum performance is marked on the "Middle" and "Bottom" lines by a black dot, 1450 and 1750 seconds respectively. The average between these times is marked by the purple vertical dashed line (1600 seconds). From the graph, the middle region saw a performance increase of 0.1, from 0.50 to 0.60. The bottom region decreased to 0.79 before increasing to 0.87, from its lowest point this is a performance increase of 0.08. *Right Axis:* The rally length (maximum score before a miss) against time for the combined unimpaired feedback loop dataset. Smoothed using a moving average window of 600 seconds. The standard error for each windowed sample is shown by the shaded area. A 4th degree polynomial best fit line was applied via the MATLAB Polyfit function [240]. This was the minimum order polynomial that fit the trend presented by the data that was not influenced by the periodic peaks of the data. This choice is explained in more detail in the main text. The maximum point of performance is marked by the black dot at 1744 seconds. This marks an increase of 0.8, from 4.3 to 5.1. This data, prior to the application of the moving average, was used to perform a one tailed t-test. From 0 seconds to the vertical orange dashed line (838 seconds), indicates the dataset used to represent before learning, labelled as pre-learning. From the vertical green dashed line (1488 seconds) to the cutoff of 2000 seconds, indicates the dataset used to represent after learning, labelled as learning. The reasoning for the selection of these datasets can be found in the appendix section A.4.6 "Rally Length Subsampling for Learned and Unlearned States".The distributions of these datasets can be seen in the appendix figure A.15.

in the appendix figure A.11 section B. This means that the comparatively high hit rate of the top region is, in actuality, caused by a much lower miss rate than the middle or bottom regions.

From the readings of figure 6.7, the top sensor tended to read higher electric currents than the other regions. These higher electric current readings, and by connection the lower miss rate, are likely due to some bias in the MEA rig construction. However, this bias was consistent through all experiments, including the control experiments. The purpose of this study is to investigate improved performance over time, higher initial performance does not impede game performance analysis provided some change happens over the course of the game. This bias does not impede analysis for the purpose of this study.

From figure 6.8, when in the bottom region the paddle initially hit the ball approximately four times more often than it missed, hitting 79% of the time. As the bottom region is also a boundary condition this is expected. However, over time this performance did increase up to a maximum of 87% hit rate, showing an improvement of 8% over 1750 seconds.

To better show the overall performance increase through the course of the game, a graph was generated of the rally lengths against time. The rally length is a measure of how many times the ball was hit before it was missed, shown as the "rally score" in figure 6.4 section B. The score reached before it resets to zero when missed is the rally length. Each time the ball was missed the rally length achieved was recorded against the time, and plotted using an averaging window of 600 seconds as with the previous plots. Shown in figure 6.8 as the right axis, rally lengths increase over the course of the game. The metric appears to fluctuate more than the hit rate, however, this is due to difference in scale and averaging over the combined scores of many samples, leading to higher variation. This does not impact the conclusion gathered from these results as the standard error follows the same trend.

A fourth-degree polynomial was used, at this point in the analysis there was no clear function that the performance would follow, making a polynomial the logical first choice of best fit function. As can be seen in the data there are a number of peaks, these seem to follow a periodic pattern with a period of approximately 250 seconds with a variation of +/- 100 seconds. This is likely caused by the average length of rally in combination with

the average time between hits, with the variation in period resulting from the variation in rally length throughout the game. As these peaks are likely an artifact of variations in rally lengths, they do not contribute to the overall trend of performance improvement. There is however a clear peak in the overall data trend observed at approximately 1700 seconds. This peak aligns with the peak in hit rate observed in the same figure with a small delay of approximately 150 seconds, a period similar to that of the periodic peaks of the rally lengths trend. As the cause of both the delay and periodic peaks is linked this will be discussed in more detail at the end of this subsection, however a fourth-degree polynomial was used as it captured the overall peak and performance trend without significant influence by the periodic peaks.

This graph clearly shows the ability of the gel to perform within the Pong game before and after the learning period. With this separation of states, before and after learning, the significance of the increase in the hydrogel controlled paddle's performance, via the rally lengths, can be analysed.

The significance of the change in performance can be analysed through a statistical test (using null hypothesis $\alpha = 0.05$) between the rally length before and after the performance increase or "learning". The before learning sample is a subsample from 0 to 838 seconds in the rally length dataset, shown via the vertical orange dashed line in figure 6.8. The after learning sample is a subsample from 1488 to 2000 seconds in the rally length dataset, shown via the vertical green dashed line in figure 6.8. Details on how these ranges were selected can be found in the appendix section A.4.6 "Rally Length Subsampling for Learned and Unlearned States".

Although the pre and post learned values were recorded from the same gel samples, these values were recorded when the hydrogel was in two distinct states. When in the pre-learning state the hydrogel is in the initial stages of the trial, ions still aligning to an almost homogeneous distribution and not yet subject to significant shape change within the EAP. When in the post-learned state the hydrogel's distribution is considerably altered by the ion migration and stimulation induced shape change. Therefore, the variables representing before and after learning can be considered independent, as there is no one-to-one relationship between data points in the two states. Because of this, the statistical significance can be assessed via the p value of sample comparison, using critical limit

theorem and the Mann–Whitney U test. Details on this calculation can be found in the appendix section A.4.7 “Statistical Significance and Mann–Whitney U Test Calculations”.

These calculations give a $p = 0.00041$, placing the probability below 0.05% and rejecting the null hypothesis. This validates the improvement before and after learning as statistically significant, despite any fluctuations between experimental runs, and reinforces the observed increase in hydrogel paddle control ability in the Pong game environment. Showing that the improved hit rate, shown in figure 6.8, was not regions exclusive, but contributed to improved overall game performance.

As mentioned earlier, it can also be observed that the peak in rally length aligns with the average peak in hit rate at approximately 1600 seconds, observed in figure 6.8, with a slight delay of around 150 seconds, if averaging between peaks for bottom and middle. This delay makes sense as the effect of the improved hit rate would take some time to translate to an improvement in rally length, due to the additional layer of abstraction caused by the time taken for a full rally to be completed. As discussed the cause of the delay and periodic peaks in rally lengths are linked due to the similarity in duration.

To understand the cause of the delay first the periodic peaks in rally length must be understood. The plot of rally length over the course of a single game can be thought of as a pulse function, where the height of a given pulse is directly proportional to the distance between it and the previous pulse. With many game runs averaged together these pulses constructively interfere with each other, this means that the periodic peaks are likely a result of this constructive interference between games and likely aligns with the most prominent rally length. To this effect a histogram distribution of rally length can be made to find the most prominent rally, this is shown in figure 6.9 as the left axis. However, as stated the height of the ”pulse” is proportional to its distance from the previous pulse. This means that many short rally lengths can occur in the space of a long one, and thus the most prominent rally length is not necessarily the most common but the most impact full based on height and frequency. This measurement of ”impact” can be found by multiplying the rally’s length by its frequency, and is shown in figure 6.9 as the right axis.

From the plot of rally length impact, two distinct peaks can be seen at rallies of length 3 and 25. To find the period of these rally lengths they can be multiplied by the average

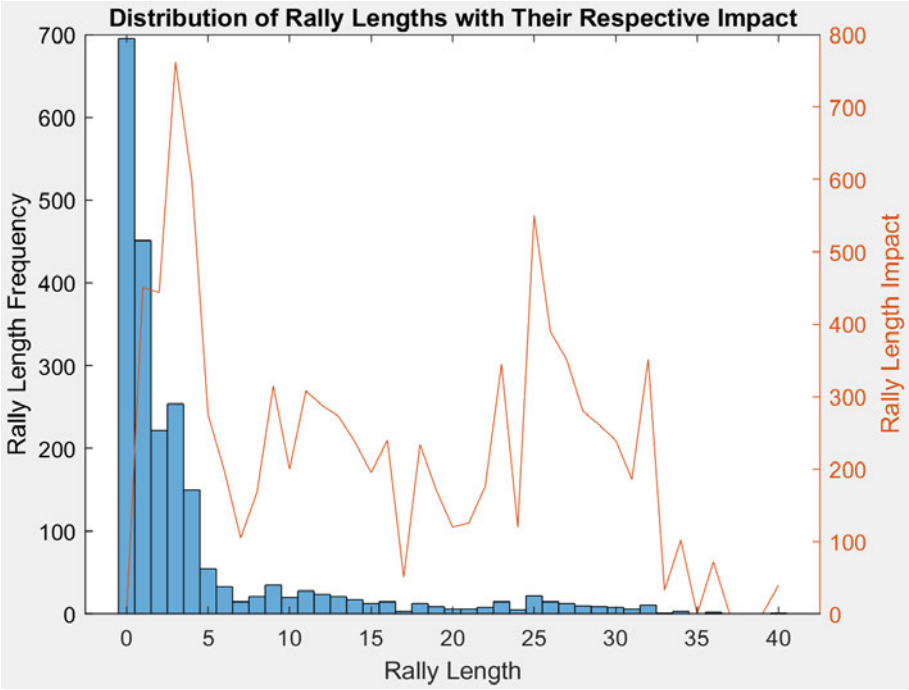


Figure 6.9: *Left Axis:* Histogram representation of the distribution of rally lengths over the course of all combined games. Shorter rally lengths occur far more often, however this is mostly due to the fact that as they are shorter more of them can occur. In order to properly analyze the prominence of each rally length the frequencies need to be normalized using their respective rally lengths. This was done by creating a plot of "impact". *Right Axis:* Impact of each rally length on the averaged rally length, calculated by multiplying each rally length by its frequency. From this plot there are two prominent peaks at 3 and 24 length rallies. Rallies of these lengths appear to have had the most impact on the performance plot shown in figure 6.8.

time between hits throughout all games. The average time between hits was found to be approximately 6 seconds. The peak at rally length 3 gives a period of 18 seconds, this does not match the delay or periodic peaks but may be responsible for the smaller periodic peaks, it is also possible that periodic noise caused by this period was lessened by the averaging preformed on the data and is thus not as prominent. The peak at rally length 25 gives a period of 150 seconds, this matches exactly with the delay between peaks in rally lengths and hit rate, and approximately matches the period of the periodic noise. This enforces the theory that the delay results from the length of the rallies and the layer of abstraction caused therein.

Further to the alignment between peaks in hit rate and rally length, the average peak in hit rate observed in figure 6.8, aligns with the peak electric current measurement observed in figure 6.7, with another delay of around 600 seconds.

This increase in electric current represents the ion distribution of the hydrogel being influenced by the received environmental data, filling the memory similarly to how the memory component was observed in the first section of this paper as electric current measurement. As with the delay between hit rate and rally length, it would take some time for the base level electric current measurements to translate to improved hitting ability, due to the layers of abstraction caused by the mechanics of the game and MEA interface.

Lastly an additional metric was recorded as rally aces, representing the number of times the paddle failed to intercept the ball without a single hit. The graph of this metric is shown in the appendix figure A.16. This graph shows a clear drop in the number of aces aligning with the points of maximum learning as found from the previous metrics of hit rate and rally lengths, occurring at 1706 seconds. The combination of these three metrics shows a clear tendency for performance to increase throughout the course of the game.

#### Game World Performance in Relation to the Free Energy Principal

The results of figure 6.7 and figure 6.8, show the learning capability through the improvement in game performance, via the EAPs control of the Pong paddle. However, the way in which the hydrogel dynamics, through free energy minimisation via ion migration, result in emergent learning is obscured. In other words, how does the change in free energy,

as a result of polymer dynamics (electrostatic interactions between polymers and ions, physical entropy of polymer networks, ion migration, etc) and FEP, alter the paddle's behaviour with respect to ball's position result in increased game performance and emergent learning?

The molecular picture of the free energy is extremely complex, as the already complex EAP system (charged polymer networks interacting with ions and water molecules) [71] is, in this study, open, and coupled to the environmental dynamics of the Pong game through the electrostatic forces externally applied. However, recent theories of FEP can be a leading principal, since FEP incorporates direct coupling, or feedback loops, within the embodied environment and emergent learning process.

FEP is based on the assumption of the 'Bayesian brain' as an "inference generator", predicting environmental dynamics [192]. In FEP systems, agents pursue actions of least surprise to minimise the difference between predictions based on their pseudo internal model of the world and their perception of the world as input. This difference is quantified by variational free energy and is minimised through iterative feedback loops, by actively acting in the embodied environment to minimise distance between the expected and predicted model of the environment [197, 191].

To summarise FEP in context of the EAP hydrogel, minimisation results as the equalisation between three main sources of free energy, shown in equation 3.5. These are; energy on ions due to the electric field, energy due to the ion and water chemical gradient, and energy due to the ion electrical gradient. The electric field application causes a gradient of increased free energy, shifting the point of equilibrium, so ions migrate to minimise this.

The game environment closed loop can be summarised as; measured electric current encoded into paddle motor commands, and the ball's position fed back via electric stimulation to the hydrogel. As the ions migrate to minimise free energy, under the electric field, the redistribution of ions affects the game environment through paddle motion since the paddle's motion alters ball's trajectory through collision. This implementation of closed loop free energy minimisation via environmental information, can be considered the framework of FEP. The results discussed indicate that through feedback, free energy minimisation, and environmental exploration FEP can lead to a form of emerged learning.

To develop the chain of events that culminate in improved performance, the kinematics

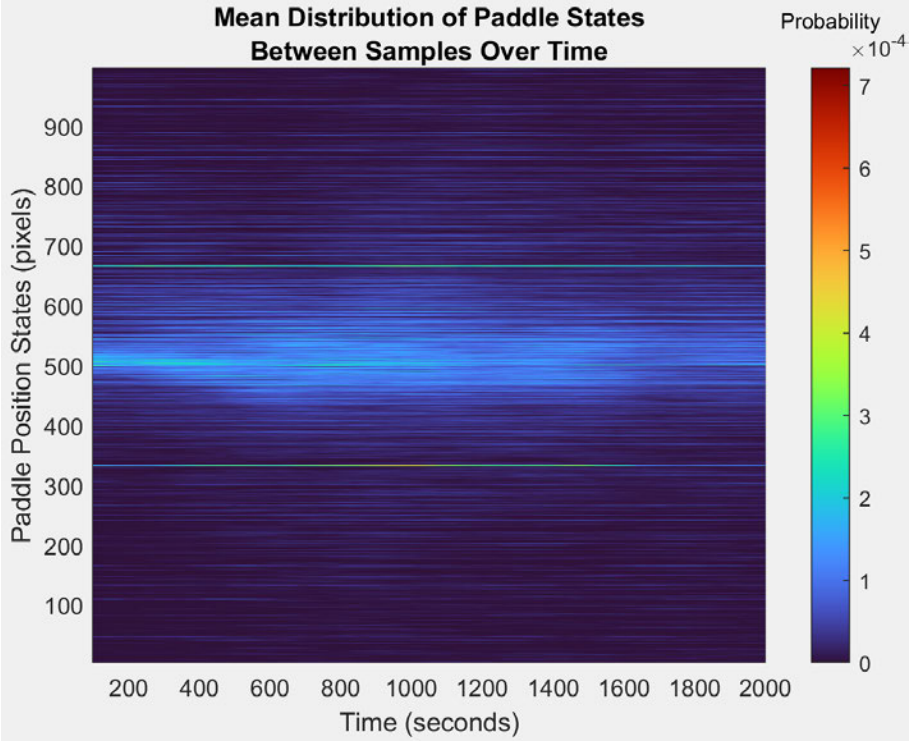


Figure 6.10: The mean distribution of paddle states for all 21 experimental samples, as a heatmap. Each positional state represents the center of the paddle. The positional states shown in the heatmap are prior to the constraints applied to keep the paddle entirely within the game area. This allows the full range of paddle states provided by the hydrogel to be analysed.Distributions were sampled every 20s starting at t=100 using a window of 200s, providing enough data points for accurate representation with minimal sample overlap. The color of each point represents the state probability. States of 0 and 1000 pixels have been omitted, the probability of these states was much higher than others (0.0129, and 0.0177 respectively) due to the boundary conditions, so would obscured the data by scale biasing. An additional set of plots can be seen in the appendix figure A.18, showing individual distributions for the timestamps 200, 400, 600, 800, 1000, 1200, 1400, 1600, 1800, and 2000.

of the paddle were analysed over the course of the game through analysis of the changing distribution of paddle positions over time. This can also be approached through analysing the paddle's motion in response to the ball's location. This analysis is detailed in the appendix section A.4.8 "Paddle Motion and Standard Deviation Analysis".

Both the paddle and ball move in the y-axis, each vertical position the paddle or ball exists in can be thought of as a state that the paddle or ball inhabit. By applying a window to the data the change in positions can be shown as changing state distributions through the course of the game and analysed.

Figure 6.10, shows the mean of the paddle position probability distributions as a func-

tion of time. Individual distributions can be seen in the appendix figure A.18, showing probability distributions for timestamps 200, 400, 600, 800, 1000, 1200, 1400, 1600, 1800, and 2000 using a larger window for direct comparisons of sample distributions. With these figures there is a clear change in the distribution of paddle positions as the game progresses. Initially starting with a large central peak that becomes less pronounced as the gel reaches its maximum performance point at 1800 seconds, as found from figure 6.8, where the distribution becomes more uniform. From this it can be deduced that the distribution of paddle positions changes through gameplay. In line with the principles of FEP this distribution of states can be thought of as a representation of the pseudo internal model, as the paddle's motion mimics that of the ball. Similarly the ball's state distribution represents the actual environment. In figure 6.10 the states of y=0 and y=1000 were omitted as their larger values obscured the rest of the results. These larger values are a result of the boundary conditions and inference function. A plot showing the distribution of paddle state positions resulting from this interaction between boundary condition and inference function can be found in the appendix figure A.17. Through this plot, the secondary peaks visible at y=333 and y=667 can also be explained via this interaction.However to fully explore the learning mechanics, the impact and cause of these boundary conditions must be investigated.

The boundary conditions occur as the paddle cannot pass beyond the edge of the game environment. If the measured electric current trend used to place the paddle, as described in figure 6.5, has a positive gradient toward either edge the paddle will be placed at the edge. This means that there are more combinations of electric current that lead to the paddle being at the edges than in-between. The boundary conditions can be visualised by simulating the paddle with random electric current inputs, using the algorithm described in figure 6.5, and recording the paddle's positional states. A distribution of these simulated results is shown in figure 6.11 section A, this plot shows that with random electric current the paddle has a significant tendency toward either end with a peak distribution in the centre. The shape of distribution at the centre can also be explained as a result of the boundary conditions and is analogous with a depletion force. The boundaries in the paddle's motion act as two point forces with high attraction to the paddle; the forces interact at the mid-point between them creating a peak [261, 262].

With greater resolution, the effect of the boundary conditions could be reduced. However, that is beyond the scope of this study. The distribution shown in figure 6.11 section A is similar in shape to the initial distribution at $t = 100$ in figure 6.10, as the paddle's initial motion is almost entirely influenced by the boundary conditions having yet to gather enough information to diverge.

Although the boundary conditions explain the initial state distribution of the paddle, to understand the change in behaviour the distribution at maximum performance (t=1800) must be assessed. Through the principles of FEP, if the paddle's state distribution represents the pseudo internal model as predictions about the environment, and the ball's state distribution represents the actual environment, the system would seek to minimise the difference between these distributions. Indeed in an ideal Pong game the paddle position should match that of the ball's vertical position at all times. Ideal anticipation of ball dynamics would mean that the paddle's position would be the same as the ball's position once it hits the wall. Essentially the paddle's vertical position would match that of the ball's vertical position with a time offset in relation to the proximity of the ball to the paddle, defined by the degree of anticipation. This means that the paddle and ball should move through the same positions over the course of the game, meaning that the ball and paddle should have almost identical distributions of vertical positional states. By comparing the paddle's state distribution against that of the ball, the paddle's change in behaviour can be assessed against what would be the ideal behaviour and compared to the principles of FEP. This allows analysis of what attributes of the paddle's distribution change to match that of the ball leading to improved performance. The ball's state distribution can be simulated using the Pong game environment. However, the ball resets on missing the paddle which alters the ball's distribution. This means that as performance improves, the ball's behaviour changes as it is hit more and follows different trajectories. This is evident when comparing two simulations of the ball's positional distribution, where the ball is never hit by the paddle and where it is always hit by the paddle, shown in appendix figure A.23. To accurately compare the paddle's distribution to that of the ball, the ball's distribution must represent the behaviour for the ball at the point of maximum performance. At this point the hit rates are 0.98, 0.58, and 0.86 for the top, middle, and bottom regions respectively, shown in figure 6.8. When the ball hits the paddle wall, the

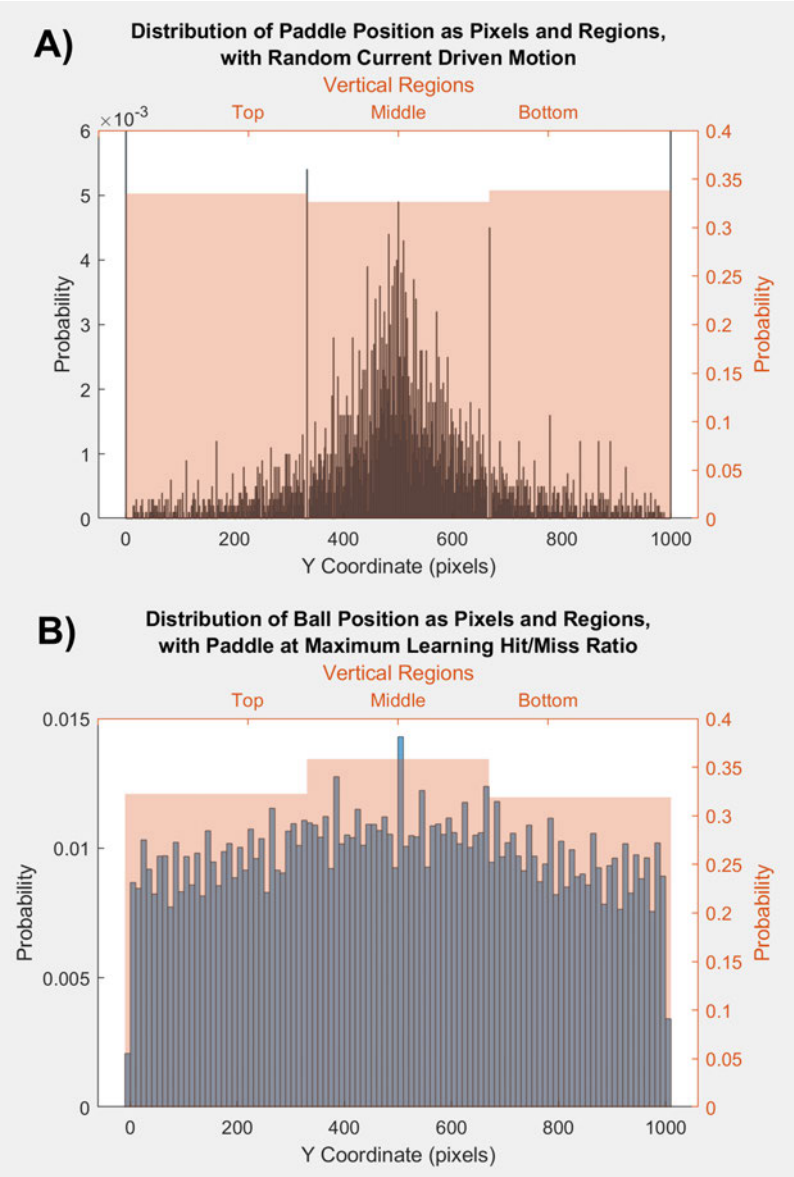


Figure 6.11: Distributions of positional states from paddle and ball simulations. Each plot shows the distribution divided into bins of each state, signified by the blue bars, and divided by regions shown by the orange transparent overlay bars. **A)** The simulated distribution of paddle states generated, using the algorithm described in figure 6.5, with randomised electric current values. 10000 samples were simulated to show the distribution. To allow the central peak to be visible the left y-axis has been limited to 0.006, however the states of 0 and 1000 are higher than the central peak due to the boundary conditions. The states 0 and 1000 have probabilities of 0.2754 and 0.2796 respectively. **B)** The simulated distribution of vertical ball states using the maximum hit rate for each region. The ball was simulated with the same game physics, starting with a random direction and resetting to the centre on a miss. The probability of the ball being intercepted by the paddle was recorded as 0.98, 0.58, and 0.86 for the top, middle, and bottom regions respectively. Each time the ball hit the paddle wall in simulation these probabilities were used to simulate if the ball hit the wall or paddle. As the ball moves the full path of each ball simulation was recorded resulting in 600000 samples, with the travel of each ball simulation before reset lasting on average 245 samples.

ball is either bounced (as if hit by the paddle) or reset (as if hitting the wall) according to the hit rate of the region in which it hits the paddle wall, this simulated distribution can be seen in figure 6.11 section B. From this distribution the ball's vertical motion over the game environment is more uniform than the paddle's initial distribution with fewer unique states (represented as the number of histogram bins), indicative of the predictable ball trajectories. From figure 6.10, the paddle's distribution appears to become more uniform as the central peak becomes less pronounced. Additionally, the number of unique states reduces, also moving closer to the ball's distribution. These observations, however, need to be quantified via metrics representing the behavioural change of paddle and ball motion, as a result of the closed loop interaction them.

There are two main metrics used to analyse the attributes of the paddle and ball's motion distribution, both representative of information entropy within the system aligning with theories of FEP and Bayesian inference [189, 196, 193, 200, 201].

- Number of unique states: The number of unique states/positions the paddle/ball is recorded in within the sample window used to generate the distribution (also represented as the number of histogram bins). Defined in equation 6.2 as $o$, where $Q$ is the sample used to make the distribution, $O$ is the set of elements in $Q$ without repetitions, and $|O|$ represents the cardinality of $O$. Information entropy $S_{ent}$ is a function of unique states $u$. In statistical thermodynamics physical entropy is defined as $S_{ent} = k_B \ln \Omega$ [263], where $k_B$ is the Boltzmann constant, and $\Omega$ is the number of microstates. As the paddle position is determined by conductivity of ions and their distribution, the physical entropy of the hydrogel is fundamentally linked to the informational entropy of the paddle states/positions, as $\Omega$ influences unique states $u$. Due to the resolution of the ball's position as applied to the MEA, When applied to the ball the number of unique states will remain constant, limited by the 6 regions the ball inhabits, so not providing usable information.

- Variance in frequency of unique states: The variance in quantity of occurrence of each unique state, used as a measure for uniformity in the distribution. Defined in equation set 6.1 as $\sigma^2$, where $c_i$ is the number of occurrences of the $i^{th}$ element of $O$, $barc$ is the mean value of $c$, $Q_j$ is the $j^{th}$ element of $Q$, and $q$ is the number of

elements in $Q$. Shown in figure 6.11 section A, the boundary states of 0 and 1000 greatly overshadow the central peak distribution. As the edge conditions are results of the interfacing algorithm and only represent a fraction of the paddle's motion, they can be ignored for the purposes of calculating variance in the paddle. This allows the uniformity in the central peak to be more accurately compared to that of the ball which is not subject to boundary conditions, as evidenced by figure 6.11 section B. Variance is linked to information entropy through information theory. Although not directly proportional, information entropy and variance are both measures of expected values and share trend directionality [264].

$$\sigma^2 = \frac{\sum (c_i - \bar{c})^2}{o - 1} \tag{6.1}$$

$$o = |O| \tag{6.2}$$

Where:

$$c_i = \sum_{j=1}^{q} f(Q_j, O_i)$$

$$f(Q_j, O_i) = \begin{cases} 1 & Q_j = O_i \\ 0 & Q_j \neq O_i \end{cases}$$

Due to the dynamic nature of the hydrogels, each sample will have slight variations in ion distribution, polymer density, and surface texture, this could lead to differences in recorded metrics. However, the learning behaviour is still driven by the same mechanics regardless of starting inconsistencies and, as a result, the trend shape of these metrics will be consistent between samples. To minimise the affect of gel synthesis inconsistencies, the metrics are normalised via feature scaling to better highlight the shape of the trends. The plot of these trends is shown in figure 6.12. The lines represent the mean between all samples with error bars representing the standard error between all samples used.

1. At t=200: The number of unique paddle states is low while the variance in both paddle and ball is high, showing few states with large variations in frequency. This matches the simulated distribution form figure 6.11 section A, expected as the ini-

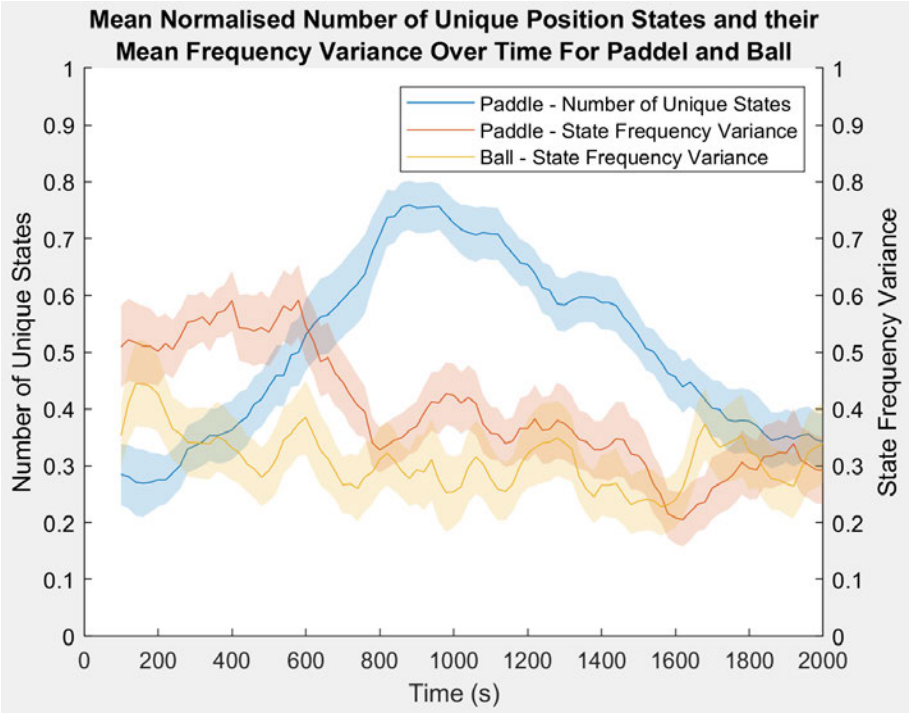


Figure 6.12: The mean of the normalised number of unique paddle states and the mean of the normalised variance between unique paddle state frequencies for both the paddle and ball, over the course of the game. Distributions were generated from each gel sample using a window size of 200 seconds, as in the plots in figure 6.10, sampled every 20 seconds from t=100 to t=2000. The number of unique paddle states and state frequency variance were then normalised and the mean between gel samples found. The standard error between gel samples is show by the shaded area.

tial distribution will be almost entirely driven by the boundary conditions, as no information has been gathered about the game environment and ions remain in a homogeneous distribution.

2. At t=600: The number of states increases as the variance decreases in both paddle and ball. This happens as more information about the environment is gathered and coincides with the rise in electric current seen in figure 6.7. With the application of an electric field the ions start to migrate within the hydrogel to represent the stimulation. As ion mobility increases the number of unique states increases and the paddle explores more of its working area. Simultaneously, as more of the working area is explored, paddle motion becomes more evenly distributed and so the variance decreases. As the ball is hit more often its variance decreases as it moves through more of the game environment before being reset on a miss. This is evident when comparing variance of simulations where the paddle always hits and always misses the ball shown in appendix figure A.23.

3. At t=1000: The number of states reaches its maximum and starts to decreases, this coincides with the behaviour of the electric current in figure 6.7 and can be explained though ion mobility. Initially the ions have total mobility as the gel is yet to change in structure, as the ions mobility increases hysteresis takes effect within the hydrogel opposing ion migration. Eventually ion mobility reaches its maximum causing the maximum peak in electric current seen in figure 6.7. After this point the hysteresis effect continues and ion mobility decreases causing the number of unique states to decrease, as ions start to settle into their final positions.

4. At t=1800: Both the number of states and variance in the paddle have reached their minimum, this coincides with the point of maximum performance shown in figure 6.8. The normalised variance in paddle and ball now match as the paddle and ball's behaviour have a stronger coupling. As the memory continues to saturate, the ion distribution comes to better represent the ball's motion. This leads to reduced paddle state variance and reduced number of unique paddles states, causing the behaviour of the paddle to become more like that of the ball. This causes the ball to be missed less often, resulting in a more homogeneous distribution of ball states and less variance,

as seen in appendix figure A.23 section B. The saturation of memory is caused by the hysteresis and so is linked to the breakdown of the polymer structure. Eventually, the same mechanic that allows the gel to retain memory causes the polymer structure to beak down to a point that it inhibits conductivity and performance reduces.

The trends shown in figure 6.12, and the way in which they coincide with features in other figures, adds another step to the chain of events leading to the increased performance. This highlights interesting forms of emergent behavior occurring as the ions migrate to reduce free energy.

**Control Experiments Via Interference of Information Translation**

Control results were collected, as described in the experimental description, to further show that the hydrogel's improved performance was a direct result of accurate environmental information fed into the hydrogels. The control experiments interfered with the translation of information as shown in figure 6.6. The first control experiment interfering with sensing at point 1, and the second control experiment interfering with stimulation at point 2.

Results for the control experiment that interfered with sensing can be seen in figure 6.13 section A. The performance in the Pong game is very poor, not reaching much beyond 0.3 in either the top or middle regions. The bottom region however remain consistent with the standard learning experiment. This is because the bottom region is being represented by the sensed electric current from the top region, after being rearranged. As explained earlier in this study the system contains a bias towards the top region allowing it to hit more often than any other. Although the sensing regions are rearranged this bias remains. This bias is then applied to the same region that the top region's sensed data is applied to, in this case the bottom region. Because of this the bottom region has a higher hit rate than the other regions, however still significantly less that the top region in the standard experiment. This allows that region's performance to remain consistent, however does not allow for learning due to the decoupling form the other regions after being rearranged.

Results for the control experiment that interfered with stimulation can be seen in figure 6.13 section B. Little improvement in performance can be seen, with no region achieving a hit rate beyond 30%. The middle region that showed the most improvement in the

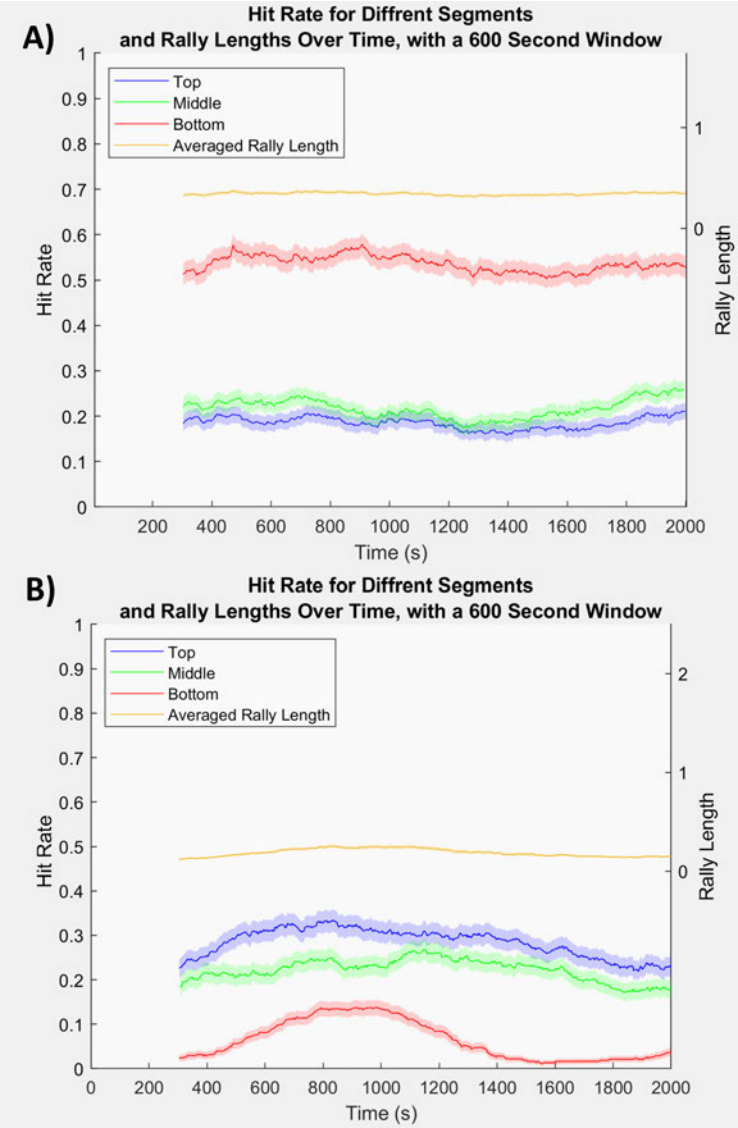


Figure 6.13: Performance of control experiments analysed via hit rate and rally lengths. **Left Axis)** The hit rate as hit to miss ratio over time for the combined impaired sensing feedback loop dataset, separated based on the region the hit/miss occurred in as described in the main text by figure 4 sections B. Smoothed using a moving average window of 600 seconds, as with previous figures. The standard error for each windowed sample was shown by the shaded area. **Right Axis)** The rally length (maximum score before a miss) against time for the combined impaired sensing feedback loop dataset. Smoothed using a moving average window of 600 seconds, as with previous figures. **A)** Performance of the Pong game where the sensing information is altered. The performance in the Pong game is very poor, not reaching much beyond 0.3 in either the top or middle regions. The bottom region however remain consistent with the standard learning experiment. The standard error was calculated for each windowed sample, with a maximum of 0.0259 The Pong game wasn't able to reach an average rally of 1 throughout the dataset. **B)** Performance of the Pong game where the stimulation information is altered. The performance in the Pong game is very poor, not reaching much beyond 0.3 for any of the regions. The standard error was calculated for each windowed sample, with a maximum of 0.0259. The Pong game wasn't able to reach an average rally of 1 throughout the dataset.

previous results shows little to no change in performance over the course of the game. Similarly, the top and bottom regions show some initial improvement but far too little to be considered significant especially given the low initial hit rate.

In both control experiments the lack of performance is even more evident when the rally lengths are plotted, also shown in figure 6.13 section A and B. From this little to no improvement can be seen in performance, with the average rally length well below 1 point. This means that the ball was missed far more often than hit throughout the game, with no consecutive hits achieved. The hit rate was below 33% in the vast majority of results so the null hypothesis is rejected as the performance was worse than if the paddle were moving randomly.

To further support these conclusions rally aces were plotted for both control experiments. These can be found in the appendix figure A.24, for both the inhibited sensing information and inhibited stimulation information as sections A and B respectively. These figures shown on average much longer rally aces for both control experiments, supporting that performance was reduced by the inhibited transfer of information. Additionally the trend of these figures is inverted when compared to those of the rally aces of the learning experiment shown in the appendix figure A.16. The rally aces start lower then increase toward the end of the run. This shows a decrease in performance over the course of the game.

Additionally, as with the previous experiment, the stabilisation of the standard deviation in the recorded hit rate of the dataset was analysed as more experimental results are added to the dataset. The standard deviation was applied to datasets over time, consisting of varied numbers of experimental runs (1 to 10), using the same 600 second window. As the dataset becomes larger the changing standard deviation becomes more stable and undergoes less change between datasets. With a dataset consisting of 9 experimental runs the trend of standard deviation does not appear to change any further and so has stabilised, requiring no further experimental runs. The plots of these standard deviations over time with varying dataset sizes can be seen in the appendix figures A.20 and A.21, for the first and second control experiment respectively.

Even with this incorrect environmental information, the hydrogel is still being provided stimulation. This means the hydrogel is still learning as the ions move to a distribution

representative of the information provided. Unfortunately, as the information provided is wrong, what is learnt by the hydrogel is also wrong. This observation helps to reinforce that the hydrogel's increase in performance is directly related to it being presented with an accurate representation of the virtual environment in which it is acting.

### 6.3.3 Discussion

From the results observed, there is a clear increase in performance of the hydrogel to play the Pong game, as shown in figure 6.8, when given information that is representative of the virtual game environment. When compared to the neural based systems of other MEA papers, the improved performance of the EAP hydrogel occurred despite the lack of any active feedback via a reward/punishment system. Over the course of the game the ball and paddle inhabit more areas of the game environment. This information is provided to the hydrogel via stimulation, and influences the polymer structure. In this way the hydrogel gathers information about the environment, and though this collection of information improves in performance. This supports use of unsupervised learning techniques, as patterns in the ball's motion are trained into the hydrogel via stimulation without external reward/punishment. This is possible due to the inference function defined in the encoding from hydrogel output to paddle position, shown in figure 6.4 section C. Continuing in the context of unsupervised learning, the inference function is how the error between internal states, of the ion distribution, and external states, of game dynamics, are applied to actions, of moving the paddle.

The development of the increased performance, based on the paddle state dynamics, can also be directly linked to the underlying mechanics of the EAP hydrogel through ion migration and memory mechanics due to hysteresis. Through this linking, via physical entropy of ion distribution and information entropy of paddle states, a logical similarity can be established between the properties of EAP hydrogels and theories of learning via FEP.

In FEP learning, external states of the environment influence internal states of the agent, in this case the EAP hydrogel, through a looped exchange of information called active inference. Active inference analogises an internal generative pseudo model used to predict inputs that represent the external world [189, 196, 193], based on theories of

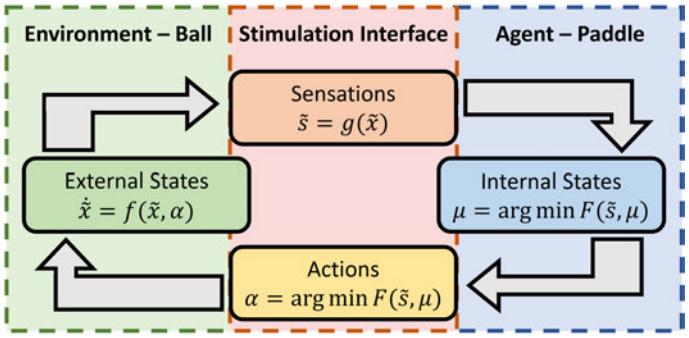


Figure 6.14: Diagram of information flow and dependency between states of the free energy minimisation task derived from FEP equations [189, 194, 195]. External states $\widetilde{x}$ are of the environment in which the agent acts, synonymous with the probability distribution of the ball. Sensations $\widetilde{s}$ are the interaction by which the agent gathers information, synonymous with the regional stimulation. Internal states $\mu$ are of the agent's internal model, synonymous with the probability distribution of the paddle. Actions $\alpha$ are the interactions between agent and environment, synonymous with measured electric current interpretation.

Bayesian inference [200, 201]. This feedback of information flow is illustrated in figure 6.14 with equations showing informational exchange. Environmental states $\widetilde{x}$ are described by the constraints of the game physics defining the motion of the ball. $\widetilde{x}$ translate to sensations $\widetilde{s}$ via the agent's interface. In this case the stimulation interface translates the ball's pixel positions into regional stimulations. As such, $\widetilde{s}$ is synonymous with the probability distribution of ball regions represented in figure 6.11 section B, appendix figure A.23, and used for state frequency variance of the ball in figure 6.12. $\widetilde{s}$ translate to internal states $\mu$ in the agent as a minimisation of the agent's internal free energy $F$. The EAP hydrogel's internal structure and ion distribution is representative of these internal states, synonymous with the pseudo internal model analogy of FEP learning, and altered as sensations of information are received. $\mu$ causes actions $\alpha$ via the minimisation of $F$ and as such $\mu$ is synonymous with the probability distribution of paddle states represented in figure 6.11 section A, and used for number of unique states and state frequency variance of the paddle in figure 6.12.

It is clear from 6.12 the minimisation of the unique number of states and state frequency variance in both paddle and ball coincide with improved performance, and through figure 6.14 their part in the feedback of information can be seen as $\widetilde{s}$ and $\mu$. This link can be further highlighted through formal definitions of free energy $F$ bound on Bayesian model evidence. $F$ is defined in equation 6.3 [194, 195], where $D_{kl}$ is the Kullback–Leibler

divergence, $Q(\mu)$ is the probability density of internal states $\mu$, and the joint probability distribution of $P(\widetilde{s}, \mu)$ is such that $P(\widetilde{s}, \mu) = P(\widetilde{s}|\mu)\, P(\mu)$.

$$F(\widetilde{s}, \mu) = \underbrace{D_{kl}[Q(\mu)||P(\mu|\widetilde{s})]}_{\text{relative entropy}} - \underbrace{lnP(\widetilde{s})}_{\text{log of evidence}} \tag{6.3}$$

$$= \underbrace{D_{kl}\ [Q(\mu)||P(\mu)]}_{\text{complexity}} - \underbrace{E_Q[\ln P(\widetilde{s}|\mu)]}_{\text{accuracy}} \tag{6.4}$$

Relative entropy cannot be less than zero, so that free energy is minimised when, in the Bayesian model, the approximate posterior becomes the true posterior and the free energy becomes the negative log of evidence for the internal pseudo generative model [265]. Through minimisation of free energy, the difference between the $\mu$ and $\widetilde{s}$ is minimised, as $\widetilde{x}$ is a component of $\widetilde{s}$ this results in environmental learning. The minimisation of relative entropy can be seen in figure 6.12 as the state frequency variance of both the paddle and ball become closer as performance increases. Log of evidence is representative of the hydrogel memory, linked to ion distribution, as information is collected the memory becomes saturated leading to less impact on the overall system. Via the definition of equation 6.3, minimising free energy is equivalent to maximising model evidence, and equivalent to minimising the complexity of accurate explanations for sensations [195], this is shown in the equivalent equation 6.4, where $E_Q$ is the expected outcome respect to $Q$. Minimisation of free energy equates to minimisation of complexity, observed in the simplification of distributions in figure 6.10, and maximisation of accuracy, observed in the improved performance of figure 6.8.

In this theory, entropy is a measure of surprise the system has about sensory information, acting as a measure of difference. A system will seek to minimise this surprise and thus minimise entropy [189, 194]. Through minimisation of entropy the system minimises the number of states it needs to inhabit, culling states that are not beneficial to acting within the environment, much like neural pathways in BNNs [266, 267]. The key difference between the hydrogel learning and that found in BNNs is the lack of an external feedback rewards structure. The feedback loop between the game and hydrogel leads actions by the hydrogel to influence the ball's trajectory. However, success or failure in the game

has no consequence on the hydrogel. There is, however, an additional internal feedback loop. Through free energy minimisation, the internal structure of the hydrogel changes both in polymer structure and ion distribution. What is initially a high entropy system of uniform polymer and ion distribution, becomes representative of not only the Pong game environment's x an y axis but also in terms of time, becoming a structural map of the ball's behavior and thus learning said behavior.

The experimental results, presented in figure 6.13 section A and B, also show that when an incorrect representation of the virtual environment is provided to the hydrogel or the actions of the hydrogel are altered, the performance is severely inhibited. This behaviour can be explained through the memory mechanics, as a result of ion interactions and migration. The hydrogel seeks to represent the information given via ion migration. If the information provided to the gel does not accurately represent the environment in which the gel's outputs are being applied, the ions will redistribute to represent this incorrect information. Thus the hydrogel's internal representation of the environment, via FEP, is incorrectly updated, inhibiting active inference, and so the gel does not perform the task accurately. The implications of these results also support the comparison to unsupervised learning. If the same inference function was used for a different goal the performance would decrease. This is because the goal is provided to the hydrogel via the inference function, and is how the error between internal and external states is used to alter actions. The control experiments show an example of altering the inference function without altering the goal, and the reduced performance that follows.

## 6.4 Conclusion

This chapter expanded on the computational implantation of Chapter 4, using the neuromimetic behaviour and approach initially investigated in Chapter 5. Using theories of FEP in BNNs in combination with reservoir computing to apply EAP hydrogels to a more complex continuous task.

Firstly, by measuring ion concentrations through conductivity of the EAP hydrogel after periods of stimulation, a new method of output extraction was established and the memory mechanics of the ionic EAP hydrogel were enforced.

Secondly, utilising techniques in reservoir computing and unsupervised learning, the ionic EAP hydrogel is embodied in the simulated game world of Pong, through the use of a custom MEA. The game environment was encoded into stimulations provided to the hydrogel and recorded ion concentrations were used as motor commands within the game world. Through analysis of the behaviour of the EAP hydrogel within this simulated environment, improved performance was observed through the course of the game. Additionally, through analysis of how performance improvement manifested through behavioural changes, the mechanisms of the EAP hydrogels were linked back to FEP.

By investigating the chain of events leading from ion migration to game performance, the way the theories of FEP present as learning in the case of ionic EAP hydrogels were clarified. This was achieved by recording the various layers of abstraction from electric field stimulation to rally length, analysing the connections between these layers. The Pong game acts as a problem to be solved. When this problem is provided to the hydrogel as an electric field, it causes an excess of free energy. Through FEP, the hydrogel created a pseudo internal model of the environment via ion migration, effectively learning to play the game. The ions within the hydrogel seek to minimise this free energy and redistribute, the redistribution of ions then becomes the solution to the problem.

The way in which the solution is interpreted allows it to be applied to the problem, in this case through conversion of localised ion concentration to paddle motion. As ions migrate to represent the game environment, presented as a series of changing electric fields, the memory in the hydrogel is filled resulting in an increase in electric current draw. This then causes a change in paddle motion to better intercept the ball, which in turn improves the hit rate in the regions, which in turn increases the rally lengths.

The results of this study demonstrate the significance of FEP in theories of learning, and in particular systems whose behaviour is more directly derived from free energy minimisation. BNNs themselves are only subject to FEP and active inference on a macro level, when the behaviour of a complete and embodied neural network is assessed. Furthermore, in reality BNNs are driven by many different interconnected electrical and chemical systems that rely on more than just free energy minimisation. Alternatively, EAP hydrogels are far more compatible with pure free energy approximations, and offer a system whose behaviour can be explained via FEP at a fundamental level. The fact that a medium,

whose fundamental mechanics rely on FEP, is able to exhibit emergent learning further implies that FEP may be more integral to emergent learning than previously thought.

Lastly, a set of baseline experiments were also performed. The goal of these experiments was to show that for the EAP hydrogel to learn it must be presented with information accurate to the environment in which it is embodied. By altering the mapping between regions and stimulation locations the 'vision' of the hydrogel was impaired. This impairment severely impacted the performance of the hydrogel within the game. The severe reduction in performance supports the claim that for the hydrogel, or any FEP based medium, to learn it must be supplied with information that accurately represents the problem being learned.

# Chapter 7

# Conclusion

The aim of this work was to show that EAP hydrogels, and by extension other similar materials, can be used uniquely in computational applications, potentially offering characteristics and abilities not exploited in other works in the field.

First, in chapter 3 by replicating previous EAP hydrogel works, the characteristics were explored and the basic interfacing structure defined. Through experimentation with different procedures, the bending motion, shown in other EAP works, was replicated and recorded, providing the base procedure for the experiments undertaken throughout this study. It was through this initial exploration that the memory like mechanics were observed and then later exploited for computational application.

Second, in chapter 4 through the structure of a Probabilistic Moore Automata, the output responses of the EAP hydrogels, combined with the observed memory mechanics, allowed the construction of a reservoir for the purpose of reservoir computing. Although this framework showed potential as a computational resource, and was used to train polynomial functions, it was limited by the discrete nature of the automaton structure. By expanding the input-output language and interfacing methodology, the computational ability of the EAP hydrogel could be more fully exploited.

Third, in chapter 5 the language expansion was approached by adding an additional degree of freedom in the form of another electrode. This also highlighted the similarities between the functional mechanics of the EAP hydrogels and biological neurons. Through experimentation, these similarities were further explored in order to find new ways to

better extract the computational ability of the EAP hydrogels. The experiments show very similar behaviour to the classic leaky integrator model used in basic neuron modeling [244, 245]. However, the response time and refractory period was observed to be much too slow to be of any beneficial use as a computational resource in the majority of real-world applications. Although the current method of extracting outputs was insufficient to be used as a computational resource, the underlying mechanics potentially allowed for interesting learning behaviour if the interfacing methodology could be improved.

Finally, in chapter 6 using the underlying concepts of ion migration, as explored initially in the study, a novel method of interfacing with the EAP hydrogel was developed and validated. This was inspired by those used in research with grown neuron cultures. Using a small voltage, applied via designated electrode pairs, the ion concretions could be monitored through conductivity in the electrical current draw. This allowed the stimulation to be applied in parallel to the output extraction and with a much faster response time. With this new interfacing method, the EAP hydrogels were applied to a real-world task making full use of the short period control loop and similarities to biological neurons to play the game Pong. Through this application, the EAP hydrogel was shown to exhibit learning behaviour similar to that of those shown in similar applications with BNN cultures [188]. This showed new insight into the potential application of EAP hydrogels as computational resources capable of emergent learning and also served to reinforce current theories of learning in neurology through free energy minimisation via FEP and active inference.

## 7.1 Contributions

The original contributions of this thesis to knowledge, inline with the original aims, include the following:

**Refined EAP Hydrogel Synthesis, Actuation, and Measurement Methodology.** In this study a detailed and reproducible methodology was created to synthesise, actuate, and measure EAP hydrogels. This methodology can be used with a much wider range of hydrogel shapes than those explored in current literature. These methods were developed by building on and refining current methods in the field via experimentation

and cross review of current literature.

**PMA Reservoir Framework.** In this study a new PMA reservoir framework was developed that allowed active matter behaviour to be used as a computational resource. This computational ability was shown through the PMA's ability to calculate polynomials using the stored EAP responses. The framework is diverse enough to be applied to any similar active matter systems and establishes the groundwork for the use of active matter systems as combined computational resources and actuators.

**Novel EAP Hydrogel Interface.** In this study a method for extracting output responses from EAP hydrogels while simultaneously applying input stimulation was developed. This was accomplished by designing a relatively easy to build MEA, with the approach inspired by MEAs used in BNN culture applications. This method of interfacing has never been used in this application before and offers new and interesting prospects for interfacing with EAP hydrogel materials as computational resources without the need for expensive equipment.

**Reinforcement of FEP and Active Inference.** In this study theories of FEP and active interference were shown to not only apply to learning in the biological brain but also other free energy based systems such as EAP hydrogels, and by association, other active matter systems. This was accomplished by building on the similarities found between the behaviour of EAP hydrogels and biological neurons. Furthermore, through this work, by showing learning behaviour in the EAP hydrogel system through task application, the importance of free energy minimisation in learning was reinforced.

**Application of EAP Hydrogel to Live Real-World Task.** This study provides a demonstrated example of active matter computational technology, that exhibits emergent learning behaviour and could be used to great effect in many real-world applications. In this study EAP hydrogels, and by association similar active matter systems, were shown to be capable of emergent learning behaviour when applied to a task. This was shown through the application of EAP hydrogels to a live real-world task, requiring a relatively fast control loop, and the resultant improvement in performance over time without the need for direct reinforcement.

## 7.2 Future Work

Although this work made significant contributions, there were areas and avenues of research that presented themselves through the work done in this study but lay beyond the scope of the aims of this study. This additional research areas are listed here, separated into sections based on the discoveries of the study that highlighted them. This study provides a strong foundation and evidence of the potential for EAP hydrogel's application in embodied computation in future work.

### 7.2.1 Real world PMA Application

Although the initial PMA was limited, it was still capable of computation and calculation thus shows potential in interesting applications. The EAP PMA is best suited to applications commonly used with probabilistic automata, such as statistical [139] or behavioural prediction [268, 269]. Reservoirs have also successfully been used in image analysis applications for data encoding [17]. As a demonstrated reservoir computing application, EAP hydrogels would also show potential in this area. Furthermore, due to the reservoir's probabilistic nature, there is the possibility for prediction [270] or recognition [271], such as in natural language translation [272]. Given the mechanisms behind the EAP hydrogel's computation, it would also offer benefits when applied to systems that themselves involve memory or consist of many active agents such as, for example, crowds of people [273].

### 7.2.2 Automaton and Reservoir Language Expansion

As shown in this study, the reservoir's complexity grows exponentially with additional inputs and outputs, although developing hardware to provide these inputs and outputs is time consuming and depends on scale. However, utilising encoding, the number of required inputs can be reduced. For example, compression techniques can be used. Regions or kernels can be applied to encode data via subsampling into fewer inputs, or far fewer complex EAP hydrogel reservoirs applied in parallel. Similar encoding techniques are used in many neural network image analysis applications [274, 275, 276]. This application of more dense encoding within the control scheme would prove an interesting path for study to further improve the computational potential.

### 7.2.3 Expansion of Active Matter FEP Learning to Other Applications

Foremostly, the results of this study demonstrate that a form of emergent learning is possible in mediums other than BNNs, when the behaviour of the medium in question is also subject to the principles of free energy. However, the application of Pong, as demonstrated, does not yet achieve the same resolution of ability that can be achieved with BNNs, as evidenced in current work [188]. As future work, higher resolution MEAs can be tested to investigate the limits of this form of reservoir computing. Similarly, additional applications can be attempted to investigate how the learning behavior is influenced by the task. Although FEP is found in BNNs, it only occurs in neurons as a network not individually. Comparatively, EAPs are subject to free energy on a more integrally at the physical chemistry level resulting in greater alignment with FEP theories. FEP is also found in many other forms of active matter and natural systems. Through exploration of these alternatives, a medium that is more capable, and just as accessible, can be found. All these avenues of research, however, fall outside the goals of this study but describe an interesting path for future work and application of this technology.

### 7.2.4 Expansion of EAP Computation Through Alternative Morphological Implementations

This study also employed relatively simple forms of hydrogel, utilising simple rod shapes and disks in experimentation. As is evident from the background and experimentation shown in this study, the interaction between the ions and the polymer structure impacts the responses of the EAP hydrogel. For this reason, experimentation with more complex hydrogel shapes would lead to interesting results. As a glimpse into the potential future of this technology EAP "computers" could be constructed/shaped for specific purposes, almost as a form of programming. Following this line of thinking, utilising the actuation mechanics of the material, robots could also be constructed that integrate the computational medium within the body material, giving the potential for smaller more complex compliant robotic platforms.

# Bibliography


[1] "computation, n.," in *OED Online*, p. sense 1.a., Oxford English Dictionary, 2023.

[2] E. Lamm and R. Unger, *Biological computation*. CRC press, 2011.

[3] E. Rich, *Automata, computability and complexity: theory and applications*. Pearson Prentice Hall Upper Saddle River, 2008.

[4] E. Katz, *Molecular and supramolecular information processing: from molecular switches to logic systems*. John Wiley & Sons, 2013.

[5] G. Tanaka, T. Yamane, J. B. Héroux, R. Nakane, N. Kanazawa, S. Takeda, H. Numata, D. Nakano, and A. Hirose, "Recent advances in physical reservoir computing: A review," *Neural Networks*, vol. 115, pp. 100–123, 2019.

[6] M. Ushio, K. Watanabe, Y. Fukuda, Y. Tokudome, and K. Nakajima, "Computational capability of ecological dynamics," *Royal Society Open Science*, vol. 10, no. 4, p. 221614, 2023.

[7] Y. Yin and J. A. Rogers, "Introduction: smart materials," 2022.

[8] M. Pishvar and R. L. Harne, "Foundations for soft, smart matter by active mechanical metamaterials," *Advanced Science*, vol. 7, no. 18, p. 2001384, 2020.

[9] K. Nakajima, H. Hauser, R. Kang, E. Guglielmino, D. G. Caldwell, and R. Pfeifer, "A soft body as a reservoir: case studies in a dynamic model of octopus-inspired soft robotic arm," *Frontiers in computational neuroscience*, vol. 7, p. 91, 2013.

[10] T. Zhu, H. Yang, and W. Zhang, "A spherical self-adaptive gripper with shrinking of an elastic membrane," in *2016 International Conference on Advanced Robotics and Mechatronics (ICARM)*, pp. 512–517, IEEE, 2016.

[11] R. Pfeifer and J. Bongard, *How the body shapes the way we think: a new view of intelligence*. MIT press, 2006.

[12] V. C. Müller and M. Hoffmann, "What Is Morphological Computation? On How the Body Contributes to Cognition and Control," *Artificial Life*, vol. 23, pp. 1–24, 02 2017.

[13] L. Shapiro and S. Spaulding, "Embodied Cognition," in *The Stanford Encyclopedia of Philosophy* (E. N. Zalta, ed.), Metaphysics Research Lab, Stanford University, Winter 2021 ed., 2021.

[14] A. Tero, S. Takagi, T. Saigusa, K. Ito, D. P. Bebber, M. D. Fricker, K. Yumiki, R. Kobayashi, and T. Nakagaki, "Rules for biologically inspired adaptive network design," *Science*, vol. 327, no. 5964, pp. 439–442, 2010.

[15] M. Dueñas-Díez and J. Pérez-Mercader, "How chemistry computes: language recognition by non-biochemical chemical automata. from finite automata to turing machines," *Iscience*, vol. 19, pp. 514–526, 2019.

[16] A. Wang, J. Gold, N. Tompkins, M. Heymann, K. Harrington, and S. Fraden, "Configurable nor gate arrays from belousov-zhabotinsky micro-droplets," *The European Physical Journal Special Topics*, vol. 225, no. 1, pp. 211–227, 2016.

[17] C. Fernando and S. Sojakka, "Pattern recognition in a bucket," in *European conference on artificial life*, pp. 588–597, Springer, 2003.

[18] G. Van der Sande, D. Brunner, and M. C. Soriano, "Advances in photonic reservoir computing," *Nanophotonics*, vol. 6, no. 3, pp. 561–576, 2017.

[19] S. Ramaswamy, "The mechanics and statistics of active matter," *Annu. Rev. Condens. Matter Phys.*, vol. 1, no. 1, pp. 323–345, 2010.

[20] M. Marchetti, J. Joanny, S. Ramaswamy, T. Liverpool, J. Prost, M. Rao, and R. A. Simha, "Hydrodynamics of soft active matter," *REVIEWS OF MODERN PHYSICS Rev Mod Phys*, vol. 85, no. 3, p. 1143, 2013.

[21] D. Harrison, W. Rorot, and U. Laukaityte, "Mind the matter: Active matter, soft robotics, and the making of bio-inspired artificial intelligence," *Frontiers in Neurorobotics*, p. 252, 2022.

[22] J. M. Parrilla-Gutierrez, A. Sharma, S. Tsuda, G. J. Cooper, G. Aragon-Camarasa, K. Donkers, and L. Cronin, "A programmable chemical computer with memory and pattern recognition," *Nature communications*, vol. 11, no. 1, pp. 1–8, 2020.

[23] V. Strong, W. Holderbaum, and Y. Hayashi, "Electroactive polymer gels as probabilistic reservoir automata for computation," *Iscience*, vol. 25, no. 12, p. 105558, 2022.

[24] M. Otake, Y. Kagami, M. Inaba, and H. Inoue, "Motion design of a starfish-shaped gel robot made of electro-active polymer gel," *Robotics and Autonomous Systems*, vol. 40, no. 2-3, pp. 185–191, 2002.

[25] T. Vicsek, A. Czirók, E. Ben-Jacob, I. Cohen, and O. Shochet, "Novel type of phase transition in a system of self-driven particles," *Physical review letters*, vol. 75, no. 6, p. 1226, 1995.

[26] S. Zhang, X. Ke, Q. Jiang, H. Ding, and Z. Wu, "Programmable and reprocessable multifunctional elastomeric sheets for soft origami robots," *Science Robotics*, vol. 6, no. 53, p. eabd6107, 2021.

[27] X. Fan, Y. Jiang, M. Li, Y. Zhang, C. Tian, L. Mao, H. Xie, L. Sun, Z. Yang, and M. Sitti, "Scale-reconfigurable miniature ferrofluidic robots for negotiating sharply variable spaces," *Science Advances*, vol. 8, no. 37, p. eabq1677, 2022.

[28] R. Yoshida, "Self-oscillating gels driven by the belousov–zhabotinsky reaction as novel smart materials," *Advanced Materials*, vol. 22, no. 31, pp. 3463–3483, 2010.

[29] Y. Horii, K. Inoue, S. Nishikawa, K. Nakajima, R. Niiyama, and Y. Kuniyoshi, "Physical reservoir computing in a soft swimming robot," *Artificial Life Conference Proceedings 33*, vol. 2021, no. 1, p. 92, 2021.

[30] Q. Zhao, K. Nakajima, H. Sumioka, H. Hauser, and R. Pfeifer, "Spine dynamics as a computational resource in spine-driven quadruped locomotion," in *2013 IEEE/RSJ International Conference on Intelligent Robots and Systems*, pp. 1445–1451, IEEE, 2013.

[31] V. Strong, W. Holderbaum, and Y. Hayashi, "Active matter as a path planning interpreter," in *2nd IMA Conference on Mathematics of Robotics 2*, pp. 66–77, Springer, 2022.

[32] A. Adamatzky, "A brief history of liquid computers," *Philosophical Transactions of the Royal Society B*, vol. 374, no. 1774, p. 20180372, 2019.

[33] M. Garrad, G. Soter, A. Conn, H. Hauser, and J. Rossiter, "A soft matter computer for soft robots," *Science Robotics*, vol. 4, no. 33, p. eaaw6060, 2019.

[34] L. Amico, M. Boshier, G. Birkl, A. Minguzzi, C. Miniatura, L.-C. Kwek, D. Aghamalyan, V. Ahufinger, D. Anderson, N. Andrei, *et al.*, "Roadmap on atomtronics: State of the art and perspective," *AVS Quantum Science*, vol. 3, no. 3, 2021.

[35] Z. Ezziane, "Dna computing: applications and challenges," *Nanotechnology*, vol. 17, no. 2, p. R27, 2005.

[36] A. Adamatzky, B. D. L. Costello, and T. Asai, *Reaction-diffusion computers*. Elsevier, 2005.

[37] "machine, n.," in *OED Online*, p. sense IV 6b, Oxford University Press, 2023.

[38] J. Henry, "Occult qualities and the experimental philosophy: Active principles in pre-newtonian matter theory," *History of science*, vol. 24, no. 4, pp. 335–381, 1986.

[39] E. F. Keller, "Active matter, then and now," *History and philosophy of the life sciences*, vol. 38, pp. 1–11, 2016.

[40] A. Sokolov and I. S. Aranson, "Physical properties of collective motion in suspensions of bacteria," *Physical review letters*, vol. 109, no. 24, p. 248109, 2012.

[41] D. Needleman and Z. Dogic, "Active matter at the interface between materials science and cell biology," *Nature reviews materials*, vol. 2, no. 9, pp. 1–14, 2017.

[42] I. Theurkauff, C. Cottin-Bizonne, J. Palacci, C. Ybert, and L. Bocquet, "Dynamic clustering in active colloidal suspensions with chemical signaling," *Physical review letters*, vol. 108, no. 26, p. 268303, 2012.

[43] A. Bricard, J.-B. Caussin, N. Desreumaux, O. Dauchot, and D. Bartolo, "Emergence of macroscopic directed motion in populations of motile colloids," *Nature*, vol. 503, no. 7474, pp. 95–98, 2013.

[44] S. Ramaswamy, "Active matter," *Journal of Statistical Mechanics: Theory and Experiment*, vol. 2017, no. 5, p. 054002, 2017.

[45] L. Berthier and J. Kurchan, "Lectures on non-equilibrium active systems," *arXiv preprint arXiv:1906.04039*, 2019.

[46] M. E. Cates and J. Tailleur, "Motility-induced phase separation," *Annu. Rev. Condens. Matter Phys.*, vol. 6, no. 1, pp. 219–244, 2015.

[47] J. Gorecki, K. Gizynski, J. Guzowski, J. Gorecka, P. Garstecki, G. Gruenert, and P. Dittrich, "Chemical computing with reaction–diffusion processes," *Philosophical Transactions of the Royal Society A: Mathematical, Physical and Engineering Sciences*, vol. 373, no. 2046, p. 20140219, 2015.

[48] T. Lister, C. O'Driscoll, and N. Reed, *Classic chemistry demonstrations*. Royal Society of Chemistry, 1995.

[49] I. Dasgupta and S. J. Gershman, "Memory as a computational resource," *Trends in Cognitive Sciences*, vol. 25, no. 3, pp. 240–251, 2021.

[50] P. Thagard, *Computational philosophy of science*. MIT press, 1988.

[51] R. Chaudhuri and I. Fiete, "Computational principles of memory," *Nature neuroscience*, vol. 19, no. 3, pp. 394–403, 2016.

[52] C. Majidi, "Soft-matter engineering for soft robotics," *Advanced Materials Technologies*, vol. 4, no. 2, p. 1800477, 2019.

[53] L. Wang and F. Iida, "Deformation in soft-matter robotics: A categorization and quantitative characterization," *IEEE Robotics & Automation Magazine*, vol. 22, no. 3, pp. 125–139, 2015.

[54] A. Chortos, J. Mao, J. Mueller, E. Hajiesmaili, J. A. Lewis, and D. R. Clarke, "Printing reconfigurable bundles of dielectric elastomer fibers," *Advanced Functional Materials*, vol. 31, no. 22, p. 2010643, 2021.

[55] H.-J. Chung, A. M. Parsons, and L. Zheng, "Magnetically controlled soft robotics utilizing elastomers and gels in actuation: A review," *Advanced Intelligent Systems*, vol. 3, no. 3, p. 2000186, 2021.

[56] J. A. Tracz, L. Wille, D. Pathiraja, S. V. Kendre, R. Pfisterer, E. Turett, C. K. Abrahamsson, S. E. Root, W.-K. Lee, D. J. Preston, *et al.*, "Tube-balloon logic for the exploration of fluidic control elements," *IEEE Robotics and Automation Letters*, vol. 7, no. 2, pp. 5483–5488, 2022.

[57] D. J. Preston, P. Rothemund, H. J. Jiang, M. P. Nemitz, J. Rawson, Z. Suo, and G. M. Whitesides, "Digital logic for soft devices," *Proceedings of the National Academy of Sciences*, vol. 116, no. 16, pp. 7750–7759, 2019.

[58] S. Park, K. Mondal, R. M. Treadway III, V. Kumar, S. Ma, J. D. Holbery, and M. D. Dickey, "Silicones for stretchable and durable soft devices: Beyond sylgard-184," *ACS applied materials & interfaces*, vol. 10, no. 13, pp. 11261–11268, 2018.

[59] Y. Jin, Y. Lin, A. Kiani, I. D. Joshipura, M. Ge, and M. D. Dickey, "Materials tactile logic via innervated soft thermochromic elastomers," *Nature communications*, vol. 10, no. 1, p. 4187, 2019.

[60] J. Binysh, T. R. Wilks, and A. Souslov, "Active elastocapillarity in soft solids with negative surface tension," *Science advances*, vol. 8, no. 10, p. eabk3079, 2022.

[61] A. K. Bastola, N. Rodriguez, M. Behl, P. Soffiatti, N. P. Rowe, and A. Lendlein, "Cactus-inspired design principles for soft robotics based on 3d printed hydrogel-elastomer systems," *Materials & Design*, vol. 202, p. 109515, 2021.

[62] G. Vorobyev, A. Vardy, and W. Banzhaf, "Supervised learning in robotic swarms: From training samples to emergent behavior," in *Distributed Autonomous Robotic Systems: The 11th International Symposium*, pp. 435–448, Springer, 2014.

[63] M. Otte, "An emergent group mind across a swarm of robots: Collective cognition and distributed sensing via a shared wireless neural network," *The International Journal of Robotics Research*, vol. 37, no. 9, pp. 1017–1061, 2018.

[64] I. Essafri, B. Ghosh, C. Desgranges, and J. Delhommelle, "Designing, synthesizing, and modeling active fluids," *Physics of Fluids*, vol. 34, no. 7, 2022.

[65] M. Wehner, R. L. Truby, D. J. Fitzgerald, B. Mosadegh, G. M. Whitesides, J. A. Lewis, and R. J. Wood, "An integrated design and fabrication strategy for entirely soft, autonomous robots," *nature*, vol. 536, no. 7617, pp. 451–455, 2016.

[66] G. W. Scherer, "Structure and properties of gels," *Cement and Concrete Research*, vol. 29, no. 8, pp. 1149–1157, 1999.

[67] J. Kim, J. A. Hanna, M. Byun, C. D. Santangelo, and R. C. Hayward, "Designing responsive buckled surfaces by halftone gel lithography," *science*, vol. 335, no. 6073, pp. 1201–1205, 2012.

[68] W. Hong, A. Almomani, and R. Montazami, "Electrochemical and morphological studies of ionic polymer metal composites as stress sensors," *Measurement*, vol. 95, pp. 128–134, 2017.

[69] Z. Liu, Y. D. Liu, Q. Shi, and Y. Liang, "Electroactive dielectric polymer gels as new-generation soft actuators: a review," *Journal of Materials Science*, vol. 56, no. 27, pp. 14943–14963, 2021.

[70] T. Tanaka, D. Fillmore, S.-T. Sun, I. Nishio, G. Swislow, and A. Shah, "Phase transitions in ionic gels," *Physical Review Letters*, vol. 45, no. 20, p. 1636, 1980.

[71] T. Tanaka, I. Nishio, S.-T. Sun, and S. Ueno-Nishio, "Collapse of gels in an electric field," *Science*, vol. 218, no. 4571, pp. 467–469, 1982.

[72] P. Atkins and J. De Paula, "Atkins' physical chemistry, volume 8. ed," 2006.

[73] M. Bassil, J. Davenas, and M. E. Tahchi, "Electrochemical properties and actuation mechanisms of polyacrylamide hydrogel for artificial muscle application," *Sensors and Actuators B*, vol. 134, pp. 496–501, 2008.

[74] D. De Tommasi, G. Puglisi, and G. Zurlo, "Hysteresis in electroactive polymers," *European Journal of Mechanics-A/Solids*, vol. 48, pp. 16–22, 2014.

[75] R. Kürsten, V. Sushkov, and T. Ihle, "Giant kovacs-like memory effect for active particles," *Phys Rev Lett*, vol. 119, p. 188001, 2017.

[76] A. Pourjavadi, M. Kurdtabar, G. R. Mahdavinia, and H. Hosseinzadeh, "Synthesis and super-swelling behavior of a novel protein-based superabsorbent hydrogel," *Polymer Bulletin*, vol. 57, pp. 813–824, 2006.

[77] I. Steinberg, A. Oplatka, and A. Katchalsky, "Mechanochemical engines," *Nature*, vol. 210, pp. 568–571, 1966.

[78] M. Suzuki and O. Hirasa, "An approach to artificial muscle using polymer gels formed by micro-phase separation," *responsive gels: volume transitions II*, pp. 241–261, 2005.

[79] R. Yoshida, K. Uchida, Y. Kaneko, K. Sakai, A. Kikuchi, Y. Sakurai, and T. Okano, "Comb-type grafted hydrogels with rapid deswelling response to temperature changes," *Nature*, vol. 374, no. 6519, pp. 240–242, 1995.

[80] I. Yannas and A. Grodzinsky, "Electromechanical energy conversion with collagen fibers in an aqueous medium," *Journal of mechanochemistry & cell motility*, vol. 2, no. 1, pp. 113–125, 1973.

[81] A. Grodzinsky and N. Shoenfeld, "Tensile forces induced in collagen by means of electromechanochemical transductive coupling," *Polymer*, vol. 18, no. 5, pp. 435–443, 1977.

[82] T. Mitsumata, A. Nagata, K. Sakai, and J.-i. Takimoto, "Giant complex modulus reduction of $\kappa$-carrageenan magnetic gels," *Macromolecular rapid communications*, vol. 26, no. 19, pp. 1538–1541, 2005.

[83] M. Zrínyi, L. Barsi, and A. Büki, "Deformation of ferrogels induced by nonuniform magnetic fields," *The Journal of chemical physics*, vol. 104, no. 21, pp. 8750–8756, 1996.

[84] S. Juodkazis, N. Mukai, R. Wakaki, A. Yamaguchi, S. Matsuo, and H. Misawa, "Reversible phase transitions in polymer gels induced by radiation forces," *Nature*, vol. 408, no. 6809, pp. 178–181, 2000.

[85] L. Engel, C. Liu, N. M. Hemed, Y. Khan, A. C. Arias, Y. Shacham-Diamand, S. Krylov, and L. Lin, "Local electrochemical control of hydrogel microactuators in microfluidics," *Journal of Micromechanics and Microengineering*, vol. 28, no. 10, p. 105005, 2018.

[86] C. Rivest, D. Morrison, B. Ni, J. Rubin, V. Yadav, A. Mahdavi, J. Karp, and A. Khademhosseini, "Microscale hydrogels for medicine and biology: synthesis, characteristics and applications," *Journal of Mechanics of materials and structures*, vol. 2, no. 6, pp. 1103–1119, 2007.

[87] H. L. Lim, J. C. Chuang, T. Tran, A. Aung, G. Arya, and S. Varghese, "Dynamic electromechanical hydrogel matrices for stem cell culture," *Advanced functional materials*, vol. 21, no. 1, pp. 55–63, 2011.

[88] Y. Bar-Cohen, "Electroactive polymers as artificial muscles-reality and challenges," in *19th AIAA Applied Aerodynamics Conference*, p. 1492, 2001.

[89] Y. Bar-Cohen, *Electroactive polymer (EAP) actuators as artificial muscles: reality, potential, and challenges*, vol. 136. SPIE press, 2004.

[90] Y. Bar-Cohen, "Eap as artificial muscles: progress and challenges," in *Smart Structures and Materials 2004: Electroactive Polymer Actuators and Devices (EAPAD)*, vol. 5385, pp. 10–16, International Society for Optics and Photonics, 2004.

[91] M. Otake, Y. Kagami, Y. Kuniyoshi, M. Inaba, and H. Inoue, "Inverse kinematics of gel robots made of electro-active polymer gel," in *Proceedings 2002 IEEE International Conference on Robotics and Automation (Cat. No. 02CH37292)*, vol. 3, pp. 3224–3229, IEEE, 2002.

[92] C. Moore and S. Mertens, *The nature of computation*. OUP Oxford, 2011.

[93] M. Mitchell, "Biological computation," *COMPUTER SCIENCE FACULTY PUBLICATIONS AND PRESENTATIONS*, 2010.

[94] L. N. de Castro, "Fundamentals of natural computing: an overview," *Physics of Life Reviews*, vol. 4, no. 1, pp. 1–36, 2007.

[95] L. N. De Castro, *Fundamentals of natural computing: basic concepts, algorithms, and applications*. CRC Press, 2006.

[96] T. Bäck, J. N. Kok, and G. Rozenberg, *Handbook of natural computing*. Springer, Heidelberg, 2012.

[97] E. W. Weisstein, "Elementary cellular automaton," *https://mathworld. wolfram. com/*, 2002.

[98] L. N. De Castro and J. Timmis, *Artificial immune systems: a new computational intelligence approach*. Springer Science & Business Media, 2002.

[99] T. Bäck, D. B. Fogel, and Z. Michalewicz, "Handbook of evolutionary computation," *Release*, vol. 97, no. 1, p. B1, 1997.

[100] J. Ledin, *Modern Computer Architecture and Organization: Learn x86, ARM, and RISC-V architectures and the design of smartphones, PCs, and cloud servers*. Packt Publishing, 2020.

[101] H. Hamann and H. Wörn, "Embodied computation," *Parallel Processing Letters*, vol. 17, no. 03, pp. 287–298, 2007.

[102] M. Li, *The Lived Body in Heidegger, Merleau-Ponty and Derrida*. Louisiana State University and Agricultural & Mechanical College, 2015.

[103] F. J. Varela, E. Thompson, and E. Rosch, *The embodied mind, revised edition: Cognitive science and human experience*. MIT press, 2017.

[104] A. Chemero, "Radical embodied cognitive science," *Review of General Psychology*, vol. 17, no. 2, pp. 145–150, 2013.

[105] L. Shapiro, *Embodied cognition*. Routledge, 2019.

[106] M. Wilson, "Six views of embodied cognition," *Psychonomic bulletin & review*, vol. 9, pp. 625–636, 2002.

[107] R. Pfeifer, M. Lungarella, and F. Iida, "Self-organization, embodiment, and biologically inspired robotics," *science*, vol. 318, no. 5853, pp. 1088–1093, 2007.

[108] L. Foglia and R. A. Wilson, "Embodied cognition," *Wiley Interdisciplinary Reviews: Cognitive Science*, vol. 4, no. 3, pp. 319–325, 2013.

[109] M. Sitti, "Physical intelligence as a new paradigm," *Extreme Mechanics Letters*, vol. 46, p. 101340, 2021.

[110] S. H. Sadati, M. ElDiwiny, S. Nurzaman, F. Iida, and T. Nanayakkara, "Embodied intelligence & morphological computation in soft robotics community: Collaborations, coordination, and perspective," in *IOP Conference Series: Materials Science and Engineering*, vol. 1261, pp. 1–9, IOP Publishing Ltd., 2021.

[111] K. Ghazi-Zahedi, J. Rieffel, S. Schmitt, and H. Hauser, "Recent trends in morphological computation," *Frontiers in Robotics and AI*, vol. 8, p. 708206, 2021.

[112] R. Pfeifer and G. Gómez, "Morphological computation–connecting brain, body, and environment," *Creating brain-like intelligence: From basic principles to complex intelligent systems*, pp. 66–83, 2009.

[113] K. Nakajima, T. Li, H. Hauser, and R. Pfeifer, "Exploiting short-term memory in soft body dynamics as a computational resource," *Journal of The Royal Society Interface*, vol. 11, no. 100, p. 20140437, 2014.

[114] A. Sadeghi, A. Tonazzini, L. Popova, and B. Mazzolai, "A novel growing device inspired by plant root soil penetration behaviors," *PloS one*, vol. 9, no. 2, p. e90139, 2014.

[115] C. Laschi and B. Mazzolai, "Lessons from animals and plants: The symbiosis of morphological computation and soft robotics," *IEEE Robotics & Automation Magazine*, vol. 23, no. 3, pp. 107–114, 2016.

[116] E. Brown, N. Rodenberg, J. Amend, A. Mozeika, E. Steltz, M. R. Zakin, H. Lipson, and H. M. Jaeger, "Universal robotic gripper based on the jamming of granular material," *Proceedings of the National Academy of Sciences*, vol. 107, no. 44, pp. 18809–18814, 2010.

[117] T. McGeer *et al.*, "Passive dynamic walking," *Int. J. Robotics Res.*, vol. 9, no. 2, pp. 62–82, 1990.

[118] H. Hauser, "Spiders' webs as computer." `https://www.morphologicalcomputation.org/the-spiders-web-as-a-computer/`, 2017. Accessed: 09-05-2023.

[119] M. S. Garrad, L. Renson, and H. Hauser, "Nonlinear dynamics of a synthetic spider web," in *NODYCON 2021*, 2021.

[120] A. Adamatzky, *Physarum machines: computers from slime mould*, vol. 74. World Scientific, 2010.

[121] A. Adamatzky, G. J. Martinez, S. V. Chapa-Vergara, R. Asomoza-Palacio, and C. R. Stephens, "Approximating mexican highways with slime mould," *Natural Computing*, vol. 10, pp. 1195–1214, 2011.

[122] A. Adamatzky and P. P. de Oliveira, "Brazilian highways from slime mold's point of view," *Kybernetes*, vol. 40, no. 9/10, pp. 1373–1394, 2011.

[123] A. Adamatzky and A. V. Kayem, "Biological evaluation of trans-african highways," *The European Physical Journal Special Topics*, vol. 215, no. 1, pp. 49–59, 2013.

[124] F. Ghanbari, J. Sgarrella, and C. Peco, "Emergent dynamics in slime mold networks," *Journal of the Mechanics and Physics of Solids*, vol. 179, p. 105387, 2023.

[125] E. Thelen, G. Schöner, C. Scheier, and L. B. Smith, "The dynamics of embodiment: A field theory of infant perseverative reaching," *Behavioral and brain sciences*, vol. 24, no. 1, pp. 1–34, 2001.

[126] K. Zahedi and N. Ay, "Quantifying morphological computation," *Entropy*, vol. 15, no. 5, pp. 1887–1915, 2013.

[127] K. Ghazi-Zahedi, C. Langer, and N. Ay, "Morphological computation: Synergy of body and brain," *Entropy*, vol. 19, no. 9, p. 456, 2017.

[128] K. Ghazi-Zahedi, D. F. Haeufle, G. Montúfar, S. Schmitt, and N. Ay, "Evaluating morphological computation in muscle and dc-motor driven models of hopping movements," *Frontiers in Robotics and AI*, vol. 3, p. 42, 2016.

[129] M. Kaminski and N. Francez, "Finite-memory automata," *Theoretical Computer Science*, vol. 134, no. 2, pp. 329–363, 1994.

[130] P. Torrens, "Cellular automata," in *International Encyclopedia of Human Geography* (R. Kitchin and N. Thrift, eds.), pp. 1–4, Oxford: Elsevier, 2009.

[131] A. Lindenmayer and G. Rozenberg, "Developmental systems and languages," in *Proceedings of the fourth annual ACM symposium on Theory of computing*, pp. 214–221, 1972.

[132] J. Wang, *Formal methods in computer science*. CRC Press, 2019.

[133] R. Grishman, *Computational linguistics: an introduction*. Cambridge University Press, 1986.

[134] G. H. Mealy, "A method for synthesizing sequential circuits," *The Bell System Technical Journal*, vol. 34, no. 5, pp. 1045–1079, 1955.

[135] E. F. Moore *et al.*, "Gedanken-experiments on sequential machines," *Automata studies*, vol. 34, pp. 129–153, 1956.

[136] R. Marinescu, C. Seceleanu, H. Le Guen, and P. Pettersson, "A research overview of tool-supported model-based testing of requirements-based designs," *Advances in Computers*, vol. 98, pp. 89–140, 2015.

[137] M. Droste, W. Kuich, and H. Vogler, *Handbook of weighted automata*. Springer Science & Business Media, 2009.

[138] E. Vidal, F. Thollard, C. De La Higuera, F. Casacuberta, and R. C. Carrasco, "Probabilistic finite-state machines-part i," *IEEE transactions on pattern analysis and machine intelligence*, vol. 27, no. 7, pp. 1013–1025, 2005.

[139] T. Marschall and S. Rahmann, "Probabilistic arithmetic automata and their application to pattern matching statistics," in *Annual symposium on combinatorial pattern matching*, pp. 95–106, Springer, 2008.

[140] S. Ghosh and S. Bhattacharya, "A data-driven understanding of covid-19 dynamics using sequential genetic algorithm based probabilistic cellular automata," *Applied Soft Computing*, vol. 96, p. 106692, 2020.

[141] A. Alaghi and J. P. Hayes, "Survey of stochastic computing," *ACM Transactions on Embedded computing systems (TECS)*, vol. 12, no. 2s, pp. 1–19, 2013.

[142] V. K. Mansinghka *et al.*, *Natively probabilistic computation.* PhD thesis, Massachusetts Institute of Technology, Department of Brain & Cognitive Sciences, 2009.

[143] C. M. Grinstead and J. L. Snell, *Introduction to probability.* American Mathematical Soc., 1997.

[144] P. A. Gagniuc, *Markov chains: from theory to implementation and experimentation.* John Wiley & Sons, 2017.

[145] P. Grivet, "Thermodynamics and statistical mechanics," *PHYSICS TODAY*, 1971.

[146] D. George and J. Hawkins, "Towards a mathematical theory of cortical micro-circuits," *PLoS computational biology*, vol. 5, no. 10, p. e1000532, 2009.

[147] A. Gupta and J. B. Rawlings, "Comparison of parameter estimation methods in stochastic chemical kinetic models: examples in systems biology," *AIChE Journal*, vol. 60, no. 4, pp. 1253–1268, 2014.

[148] D. G. Champernowne, "A model of income distribution," *The Economic Journal*, vol. 63, no. 250, pp. 318–351, 1953.

[149] H. A. Simon and C. P. Bonini, "The size distribution of business firms," *The American economic review*, vol. 48, no. 4, pp. 607–617, 1958.

[150] R. Fitzpatrick, *Thermodynamics and Statistical Mechanics.* World Scientific, 2020.

[151] D. Van Ravenzwaaij, P. Cassey, and S. D. Brown, "A simple introduction to markov chain monte–carlo sampling," *Psychonomic bulletin & review*, vol. 25, no. 1, pp. 143–154, 2018.

[152] A. Davis, "Markov chains as random input automata," *The American Mathematical Monthly*, vol. 68, no. 3, pp. 264–267, 1961.

[153] T. Nieh and J. Carlyle, "On the deterministic realization of stochastic finite-state machines," in *Proceedings of the Second Annual Princeton Conference on Information Sciences and Systems, Princeton University, Princeton, NJ*, 1968.

[154] D. LaBerge and S. J. Samuels, "Toward a theory of automatic information processing in reading," *Cognitive psychology*, vol. 6, no. 2, pp. 293–323, 1974.

[155] S. Zeki, "A massively asynchronous, parallel brain," *Philosophical Transactions of the Royal Society B: Biological Sciences*, vol. 370, no. 1668, p. 20140174, 2015.

[156] C. Van Der Malsburg, "Frank rosenblatt: Principles of neurodynamics: Perceptrons and the theory of brain mechanisms," in *Brain theory*, pp. 245–248, Springer, 1986.

[157] W. S. McCulloch and W. Pitts, "A logical calculus of the ideas immanent in nervous activity," *The bulletin of mathematical biophysics*, vol. 5, pp. 115–133, 1943.

[158] Y. Huang, "Advances in artificial neural networks–methodological development and application," *Algorithms*, vol. 2, no. 3, pp. 973–1007, 2009.

[159] W. H. Delashmit, M. T. Manry, *et al.*, "Recent developments in multilayer perceptron neural networks," in *Proceedings of the seventh Annual Memphis Area Engineering and Science Conference, MAESC*, 2005.

[160] X. Qiang, G. Cheng, and Z. Wang, "An overview of some classical growing neural networks and new developments," in *2010 2nd International Conference on Education Technology and Computer*, vol. 3, pp. V3–351, IEEE, 2010.

[161] A. Ajit, K. Acharya, and A. Samanta, "A review of convolutional neural networks," in *2020 International Conference on Emerging Trends in Information Technology and Engineering (ic-ETITE)*, pp. 1–5, IEEE, 2020.

[162] J. Misra and I. Saha, "Artificial neural networks in hardware: A survey of two decades of progress," *Neurocomputing*, vol. 74, no. 1-3, pp. 239–255, 2010.

[163] Y. Liao, "Neural networks in hardware: A survey," *Department of Computer Science, University of California*, 2001.

[164] T. Schoenauer, S. Atasoy, N. Mehrtash, and H. Klar, "Neuropipe-chip: A digital neuro-processor for spiking neural networks," *IEEE Transactions on Neural Networks*, vol. 13, no. 1, pp. 205–213, 2002.

[165] M. Verleysen, P. Thissen, J.-L. Voz, and J. Madrenas, "An analog processor architecture for a neural network classifier," *IEEE Micro*, vol. 14, no. 3, pp. 16–28, 1994.

[166] T. Francis, T. Lu, X. Yang, and D. A. Gregory, "Optical neural network with pocket-sized liquid-crystal televisions," *Optics Letters*, vol. 15, no. 15, pp. 863–865, 1990.

[167] S. Bellis, K. M. Razeeb, C. Saha, K. Delaney, C. O'Mathuna, A. Pounds-Cornish, G. de Souza, M. Colley, H. Hagras, G. Clarke, *et al.*, "Fpga implementation of spiking neural networks-an initial step towards building tangible collaborative autonomous agents," in *Proceedings. 2004 IEEE International Conference on Field-Programmable Technology (IEEE Cat. No. 04EX921)*, pp. 449–452, IEEE, 2004.

[168] J. Végh, "How amdahl's law limits the performance of large artificial neural networks," *Brain informatics*, vol. 6, no. 1, pp. 1–11, 2019.

[169] H. Jaeger, "The "echo state" approach to analysing and training recurrent neural networks-with an erratum note," *Bonn, Germany: German National Research Center for Information Technology GMD Technical Report*, vol. 148, no. 34, p. 13, 2001.

[170] W. Maass, T. Natschläger, and H. Markram, "Real-time computing without stable states: A new framework for neural computation based on perturbations," *Neural computation*, vol. 14, no. 11, pp. 2531–2560, 2002.

[171] W. Maass, "Networks of spiking neurons: the third generation of neural network models," *Neural networks*, vol. 10, no. 9, pp. 1659–1671, 1997.

[172] A. Patiño-Saucedo, H. Rostro-González, T. Serrano-Gotarredona, and B. Linares-Barranco, "Liquid state machine on spinnaker for spatio-temporal classification tasks," *Frontiers in Neuroscience*, vol. 16, p. 819063, 2022.

[173] D. E. Hyndman, *Analog and Hybrid Computing: The Commonwealth and International Library: Electrical Engineering Division*. Elsevier, 2016.

[174] J. Love, R. Msiska, J. Mulkers, G. Bourianoff, J. Leliaert, and K. Everschor-Sitte, "Spatial analysis of physical reservoir computers," *Physical Review Applied*, vol. 20, no. 4, p. 044057, 2023.

[175] B. Schrauwen, D. Verstraeten, and J. Van Campenhout, "An overview of reservoir computing: theory, applications and implementations," in *Proceedings of the 15th european symposium on artificial neural networks. p. 471-482 2007*, pp. 471–482, 2007.

[176] L. Larger, M. C. Soriano, D. Brunner, L. Appeltant, J. M. Gutiérrez, L. Pesquera, C. R. Mirasso, and I. Fischer, "Photonic information processing beyond turing: an optoelectronic implementation of reservoir computing," *Optics express*, vol. 20, no. 3, pp. 3241–3249, 2012.

[177] K. C. Chatzidimitriou and P. A. Mitkas, "Adaptive reservoir computing through evolution and learning," *Neurocomputing*, vol. 103, pp. 198–209, 2013.

[178] G. M. Hoerzer, R. Legenstein, and W. Maass, "Emergence of complex computational structures from chaotic neural networks through reward-modulated hebbian learning," *Cerebral cortex*, vol. 24, no. 3, pp. 677–690, 2014.

[179] O. Lee, T. Wei, K. D. Stenning, J. C. Gartside, D. Prestwood, S. Seki, A. Aqeel, K. Karube, N. Kanazawa, Y. Taguchi, *et al.*, "Task-adaptive physical reservoir computing," *Nature Materials*, pp. 1–9, 2023.

[180] K. Heiney, O. H. Ramstad, I. Sandvig, A. Sandvig, and S. Nichele, "Assessment and manipulation of the computational capacity of in vitro neuronal networks through criticality in neuronal avalanches," in *2019 IEEE Symposium Series on Computational Intelligence (SSCI)*, pp. 247–254, IEEE, 2019.

[181] M. Conrad, "Information processing in molecular systems," *BioSystems*, vol. 5, no. 1, pp. 1–14, 1972.

[182] P. Mateos-Aparicio and A. Rodríguez-Moreno, "The impact of studying brain plasticity," *Frontiers in cellular neuroscience*, vol. 13, p. 66, 2019.

[183] R. Von Bernhardi, L. E.-v. Bernhardi, and J. Eugenín, "What is neural plasticity?," *The plastic brain*, pp. 1–15, 2017.

[184] P. Aaser, M. Knudsen, O. Huse Ramstad, R. van de Wijdeven, S. Nichele, I. Sandvig, G. Tufte, U. S. Bauer, Ø. Halaas, S. Hendseth, *et al.*, "Towards making a cyborg: A closed-loop reservoir-neuro system," *ECAL 2017, the Fourteenth European Conference on Artificial Life*, vol. 14, pp. 430–437, 2017.

[185] Z. C. Chao, D. J. Bakkum, and S. M. Potter, "Shaping embodied neural networks for adaptive goal-directed behavior," *PLoS computational biology*, vol. 4, no. 3, p. e1000042, 2008.

[186] D. J. Bakkum, Z. C. Chao, and S. M. Potter, "Spatio-temporal electrical stimuli shape behavior of an embodied cortical network in a goal-directed learning task," *Journal of neural engineering*, vol. 5, no. 3, p. 310, 2008.

[187] T. B. DeMarse and K. P. Dockendorf, "Adaptive flight control with living neuronal networks on microelectrode arrays," in *Proceedings. 2005 IEEE International Joint Conference on Neural Networks, 2005.*, vol. 3, pp. 1548–1551, IEEE, 2005.

[188] B. J. Kagan, A. C. Kitchen, N. T. Tran, B. J. Parker, A. Bhat, B. Rollo, A. Razi, and K. J. Friston, "In vitro neurons learn and exhibit sentience when embodied in a simulated game-world," 2021.

[189] K. Friston, "The free-energy principle: a unified brain theory?," *Nature reviews neuroscience*, vol. 11, no. 2, pp. 127–138, 2010.

[190] D. Demekas, T. Parr, and K. J. Friston, "An investigation of the free energy principle for emotion recognition," *Frontiers in Computational Neuroscience*, vol. 14, p. 30, 2020.

[191] K. Friston, "The free-energy principle: a rough guide to the brain?," *Trends in cognitive sciences*, vol. 13, no. 7, pp. 293–301, 2009.

[192] K. Friston, "The history of the future of the bayesian brain," *NeuroImage*, vol. 62, no. 2, pp. 1230–1233, 2012.

[193] K. Friston, P. Schwartenbeck, T. FitzGerald, M. Moutoussis, T. Behrens, and R. J. Dolan, "The anatomy of choice: active inference and agency," *Frontiers in human neuroscience*, vol. 7, p. 598, 2013.

[194] K. Friston and G. Buzsáki, "The functional anatomy of time: what and when in the brain," *Trends in cognitive sciences*, vol. 20, no. 7, pp. 500–511, 2016.

[195] K. Friston, T. FitzGerald, F. Rigoli, P. Schwartenbeck, and G. Pezzulo, "Active inference: a process theory," *Neural computation*, vol. 29, no. 1, pp. 1–49, 2017.

[196] T. Parr and K. J. Friston, "Generalised free energy and active inference," *Biological cybernetics*, vol. 113, no. 5, pp. 495–513, 2019.

[197] K. Friston, J. Kilner, and L. Harrison, "A free energy principle for the brain," *Journal of physiology-Paris*, vol. 100, no. 1-3, pp. 70–87, 2006.

[198] W. R. Ashby, "Principles of the self-organizing dynamic system," *The Journal of general psychology*, vol. 37, no. 2, pp. 125–128, 1947.

[199] P. Schwartenbeck, T. H. FitzGerald, C. Mathys, R. Dolan, M. Kronbichler, and K. Friston, "Evidence for surprise minimization over value maximization in choice behavior," *Scientific reports*, vol. 5, no. 1, pp. 1–14, 2015.

[200] R. M. Neal, *Bayesian learning for neural networks*, vol. 118. Springer Science & Business Media, 2012.

[201] D. C. Knill and A. Pouget, "The bayesian brain: the role of uncertainty in neural coding and computation," *TRENDS in Neurosciences*, vol. 27, no. 12, pp. 712–719, 2004.

[202] T. Isomura, K. Kotani, and Y. Jimbo, "Cultured cortical neurons can perform blind source separation according to the free-energy principle," *PLoS computational biology*, vol. 11, no. 12, p. e1004643, 2015.

[203] T. Isomura and K. Friston, "In vitro neural networks minimise variational free energy," *Scientific reports*, vol. 8, no. 1, pp. 1–14, 2018.

[204] T. Parr and K. J. Friston, "The discrete and continuous brain: from decisions to movement—and back again," *Neural computation*, vol. 30, no. 9, pp. 2319–2347, 2018.

[205] G. Nicolis and I. Prigogine, *Self-organization in Nonequilibrium Systems: From Dissipative Structures to Order Through Fluctuations*. New York: John Wiley, 1977.

[206] J. Bruineberg and E. Rietveld, "Self-organization, free energy minimization, and optimal grip on a field of affordances," *Frontiers in human neuroscience*, vol. 8, p. 599, 2014.

[207] J. S. Kelso, *Dynamic patterns: The self-organization of brain and behavior*. MIT press, 1995.

[208] V. Pasquale, P. Massobrio, L. Bologna, M. Chiappalone, and S. Martinoia, "Self-organization and neuronal avalanches in networks of dissociated cortical neurons," *Neuroscience*, vol. 153, no. 4, pp. 1354–1369, 2008.

[209] W. Dou, G. Zhong, J. Cao, Z. Shi, B. Peng, and L. Jiang, "Soft robotic manipulators: Designs, actuation, stiffness tuning, and sensing," *Advanced Materials Technologies*, vol. 6, no. 9, p. 2100018, 2021.

[210] J. Cao, W. Liang, J. Zhu, and Q. Ren, "Control of a muscle-like soft actuator via a bioinspired approach," *Bioinspiration & biomimetics*, vol. 13, no. 6, p. 066005, 2018.

[211] V. V. Yashin, S. Suzuki, R. Yoshida, and A. C. Balazs, "Controlling the dynamic behavior of heterogeneous self-oscillating gels," *Journal of Materials Chemistry*, vol. 22, no. 27, pp. 13625–13636, 2012.

[212] O. Kuksenok, V. V. Yashin, and A. C. Balazs, "Mechanically induced chemical oscillations and motion in responsive gels," *Soft Matter*, vol. 3, no. 9, pp. 1138–1144, 2007.

[213] P. Atkins and J. De Paula, *Physical chemistry for the life sciences*. Oxford University Press, USA, 2011.

[214] P. Atkins, P. W. Atkins, and J. de Paula, *Atkins' physical chemistry*. Oxford university press, 2014.

[215] K. M. POLURI, "Fabrication of biopolymer-based organs and tissues using 3d bioprinting," *3D printing Technology in Nanomedicine*, p. 43, 2019.

[216] R. Yegappan, V. Selvaprithiviraj, S. Amirthalingam, and R. Jayakumar, "Carrageenan based hydrogels for drug delivery, tissue engineering and wound healing," *Carbohydrate polymers*, vol. 198, pp. 385–400, 2018.

[217] D. J. McHugh, "A guide to the seaweed industry," *FAO fisheries technical paper*, vol. 441, p. 105, 2003.

[218] M. Doble and A. Kumar, *Biotreatment of industrial effluents*. Elsevier, 2005.

[219] K. S. Soppirnath and T. M. Aminabhavi, "Water transport and drug release study from cross-linked polyacrylamide grafted guar gum hydrogel microspheres for the controlled release application," *European Journal of Pharmaceutics and Biopharmaceutics*, vol. 53, no. 1, pp. 87–98, 2002.

[220] B. B. Mandal, S. Kapoor, and S. C. Kundu, "Silk fibroin/polyacrylamide semi-interpenetrating network hydrogels for controlled drug release," *Biomaterials*, vol. 30, no. 14, pp. 2826–2836, 2009.

[221] R. C. Allen, C. A. Saravis, and H. R. Maurer, "Gel electrophoresis and isoelectric focusing of proteins," in *Gel Electrophoresis and Isoelectric Focusing of Proteins*, de Gruyter, 2019.

[222] E. A. Smith, S. L. Prues, and F. W. Oehme, "Environmental degradation of polyacrylamides. 1. effects of artificial environmental conditions: temperature, light, and ph," *Ecotoxicology and Environmental Safety*, vol. 35, no. 2, pp. 121–135, 1996.

[223] P. Menter, "Acrylamide polymerization—a practical approach," *Bio-Rad Laboratories*, 2013.

[224] Y. Seida and Y. Nakano, "Effect of salt on the property of adsorption in thermosensitive polymer hydrogel," *Journal of chemical engineering of Japan*, vol. 29, no. 5, pp. 767–772, 1996.

[225] E. Doi, "Gels and gelling of globular proteins," *Trends in Food Science & Technology*, vol. 4, no. 1, pp. 1–5, 1993.

[226] S. Ahmed, Z. Ounaies, and E. A. F. Arrojado, "Electric field-induced bending and folding of polymer sheets," *Sensors and Actuators A: Physical*, vol. 260, pp. 68–80, 2017.

[227] H. Li, A. Erbas, J. Zwanikken, and M. Olvera de la Cruz, "Ionic conductivity in polyelectrolyte hydrogels," *Macromolecules*, vol. 49, no. 23, pp. 9239–9246, 2016.

[228] Mathworks, "Curve fitting toolbox." `https://uk.mathworks.com/products/curvefitting.html`, 2014. Accessed: 13-03-2023.

[229] P. Liu, R. Lv, Y. He, B. Na, B. Wang, and H. Liu, "An integrated, flexible aqueous zn-ion battery with high energy and power densities," *Journal of Power Sources*, vol. 410, pp. 137–142, 2019.

[230] E. Wiyadi, A. Wati, Y. Hamzah, and L. Umar, "Simple iv acquisition module with high side current sensing principle for real time photovoltaic measurement," in *Journal of Physics: Conference Series*, vol. 1528, p. 012040, IOP Publishing, 2020.

[231] M. Oyen, "Mechanical characterisation of hydrogel materials," *International Materials Reviews*, vol. 59, no. 1, pp. 44–59, 2014.

[232] D. Grune, K. Van Reeuwijk, H. E. Bal, C. J. Jacobs, and K. Langendoen, *Modern compiler design*. Springer Science & Business Media, 2012.

[233] C. E. Shannon and J. McCarthy, *Automata Studies.(AM-34), Volume 34*, vol. 34. Princeton University Press, 2016.

[234] G. C. Goodwin, S. F. Graebe, M. E. Salgado, *et al.*, *Control system design*. Upper Saddle River, NJ: Prentice Hall,, 2001.

[235] M. N. I. Shiblee, K. Ahmed, M. Kawakami, and H. Furukawa, "4d printing of shape-memory hydrogels for soft-robotic functions," *Advanced Materials Technologies*, vol. 4, no. 8, p. 1900071, 2019.

[236] A. K. Denisin and B. L. Pruitt, "Tuning the range of polyacrylamide gel stiffness for mechanobiology applications," *ACS applied materials & interfaces*, vol. 8, no. 34, pp. 21893–21902, 2016.

[237] Y. Zhang, H. Wu, and L. Cheng, "Some new deformation formulas about variance and covariance," in *2012 Proceedings of International Conference on Modelling, Identification and Control*, pp. 987–992, IEEE, 2012.

[238] D. G. Altman, "Categorizing continuous variables," *Encyclopedia of Biostatistics*, vol. 1, 2005.

[239] M. C. Soriano, "Reservoir computing speeds up," *Physics*, vol. 10, p. 12, 2017.

[240] Mathworks, "Polyfit." `https://www.mathworks.com/help/matlab/ref/polyfit.html`, 2014. Accessed: 13-03-2023.

[241] P. Atkins, J. d. Paula, and J. Keeler, *Atkins' Physical Chemistry 11th Edition*. Oxford University Press, 2018.

[242] V. Vunder, A. Punning, and A. Aabloo, "Mechanical interpretation of back-relaxation of ionic electroactive polymer actuators," *Smart Materials and Structures*, vol. 21, no. 11, p. 115023, 2012.

[243] R. Knapp, M. Rubenzik, E. Malatynska, E. Varga, W. R. Roeske, and H. I. Yamamura, "Neurotransmitter receptors," in *Encyclopedia of the Neurological Sciences* (M. J. Aminoff and R. B. Daroff, eds.), pp. 602–614, New York: Academic Press, 2003.

[244] C. Eliasmith and C. H. Anderson, *Neural engineering: Computation, representation, and dynamics in neurobiological systems*. MIT press, 2003.

[245] M. A. Navarro, A. Salari, J. L. Lin, L. M. Cowan, N. J. Penington, M. Milescu, and L. S. Milescu, "Sodium channels implement a molecular leaky integrator that detects action potentials and regulates neuronal firing," *Elife*, vol. 9, p. e54940, 2020.

[246] D. Purves, R. Cabeza, S. A. Huettel, K. S. LaBar, M. L. Platt, M. G. Woldorff, and E. M. Brannon, *Cognitive neuroscience*. Sunderland: Sinauer Associates, Inc, 2008.

[247] J. Coombs, J. C. Eccles, and P. Fatt, "The specific ionic conductances and the ionic movements across the motoneuronal membrane that produce the inhibitory post-synaptic potential," *The Journal of physiology*, vol. 130, no. 2, pp. 326–373, 1955.

[248] L. F. Abbott, "Lapicque's introduction of the integrate-and-fire model neuron (1907)," *Brain research bulletin*, vol. 50, no. 5-6, pp. 303–304, 1999.

[249] M. A. Biederman-Thorson, R. F. Schmidt, and G. Thews, *Human Physiology*. Springer Science & Business Media, 2013.

[250] G. Schuszter, T. Gehér-Herczegh, Á. Szűcs, Á. Tóth, and D. Horváth, "Determination of the diffusion coefficient of hydrogen ion in hydrogels," *Physical Chemistry Chemical Physics*, vol. 19, no. 19, pp. 12136–12143, 2017.

[251] S. J. Martin, P. D. Grimwood, and R. G. Morris, "Synaptic plasticity and memory: an evaluation of the hypothesis," *Annual review of neuroscience*, vol. 23, no. 1, pp. 649–711, 2000.

[252] A. Rakitianskaia and A. Engelbrecht, "Measuring saturation in neural networks," in *2015 IEEE Symposium Series on Computational Intelligence*, pp. 1423–1430, IEEE, 2015.

[253] W. C. Abraham and M. F. Bear, "Metaplasticity: the plasticity of synaptic plasticity," *Trends in neurosciences*, vol. 19, no. 4, pp. 126–130, 1996.

[254] A. Soltoggio and K. O. Stanley, "From modulated hebbian plasticity to simple behavior learning through noise and weight saturation," *Neural Networks*, vol. 34, pp. 28–41, 2012.

[255] H. J. Ruskin and R. Walshe, "Emergent computing-introduction to the special theme," *ERCIM News*, vol. 64, pp. 24–25, 2006.

[256] S. Bondar, J. C. Hsu, A. Pfouga, and J. Stjepandić, "Agile digitale transformation of enterprise architecture models in engineering collaboration," *Procedia Manufacturing*, vol. 11, pp. 1343–1350, 2017.

[257] J. R. Gray, "Conductivity analyzers and their application," *Environmental instrumentation and analysis handbook*, vol. 1, pp. 491–510, 2004.

[258] R. Bourtchouladze, *Memories are made of this: How memory works in humans and animals.* Columbia University Press, 2002.

[259] G. Schiavone, X. Kang, F. Fallegger, J. Gandar, G. Courtine, and S. P. Lacour, "Guidelines to study and develop soft electrode systems for neural stimulation," *Neuron*, vol. 108, no. 2, pp. 238–258, 2020.

[260] K. Jia, X. Li, and Y. Wang, "Electrochemical breakdown in hydrogel ionotronic devices," *Soft Matter*, vol. 17, no. 4, pp. 834–839, 2021.

[261] Y. Mao, M. Cates, and H. Lekkerkerker, "Depletion force in colloidal systems," *Physica A: Statistical Mechanics and its Applications*, vol. 222, no. 1-4, pp. 10–24, 1995.

[262] H. N. Lekkerkerker and R. Tuinier, "Depletion interaction," in *Colloids and the depletion interaction*, pp. 57–108, Springer, 2011.

[263] D. V. Schroeder, *An introduction to thermal physic*, vol. 57. San Francisco, CA: Addison Wesley, 2000.

[264] N. Ebrahimi, E. Maasoumi, and E. S. Soofi, "Ordering univariate distributions by entropy and variance," *Journal of Econometrics*, vol. 90, no. 2, pp. 317–336, 1999.

[265] M. J. Beal, *Variational algorithms for approximate Bayesian inference.* University of London, University College London (United Kingdom), 2003.

[266] G. Chechik, I. Meilijson, and E. Ruppin, "Synaptic pruning in development: a computational account," *Neural computation*, vol. 10, no. 7, pp. 1759–1777, 1998.

[267] F. I. Craik and E. Bialystok, "Cognition through the lifespan: mechanisms of change," *Trends in cognitive sciences*, vol. 10, no. 3, pp. 131–138, 2006.

[268] J. Zylberberg and M. R. DeWeese, "How should prey animals respond to uncertain threats?," *Frontiers in computational neuroscience*, vol. 5, p. 20, 2011.

[269] L. Chittaro and M. Serra, "Behavioral programming of autonomous characters based on probabilistic automata and personality," *Computer animation and virtual worlds*, vol. 15, no. 3-4, pp. 319–326, 2004.

[270] A. Hu, F. Cotter, N. Mohan, C. Gurau, and A. Kendall, "Probabilistic future prediction for video scene understanding," in *European Conference on Computer Vision*, pp. 767–785, Springer, 2020.

[271] S. G. Wu, F. S. Bao, E. Y. Xu, Y.-X. Wang, Y.-F. Chang, and Q.-L. Xiang, "A leaf recognition algorithm for plant classification using probabilistic neural network," in *2007 IEEE international symposium on signal processing and information technology*, pp. 11–16, IEEE, 2007.

[272] A. S. Hsu, N. Chater, and P. M. Vitányi, "The probabilistic analysis of language acquisition: Theoretical, computational, and experimental analysis," *Cognition*, vol. 120, no. 3, pp. 380–390, 2011.

[273] A. Bottinelli, D. T. Sumpter, and J. L. Silverberg, "Emergent structural mechanisms for high-density collective motion inspired by human crowds," *Physical review letters*, vol. 117, no. 22, p. 228301, 2016.

[274] K. O'Shea and R. Nash, "An introduction to convolutional neural networks," *arXiv preprint arXiv:*, vol. 1511.08458, Nov 2015.

[275] J. Cong and B. Xiao, "Minimizing computation in convolutional neural networks," in *International conference on artificial neural networks*, pp. 281–290, Springer, 2014.

[276] T. Iakymchuk, A. Rosado-Muñoz, J. F. Guerrero-Martínez, M. Bataller-Mompeán, and J. V. Francés-Víllora, "Simplified spiking neural network architecture and stdp learning algorithm applied to image classification," *EURASIP Journal on Image and Video Processing*, vol. 2015, no. 1, pp. 1–11, 2015.

[277] S. Siegal, *Nonparametric statistics for the behavioral sciences.* McGraw-Hill, 1956.

[278] J. H. Zar, *Biostatistical Analysis.* New Jersey: Prentice Hall International, INC., 1998.

[279] H. Lehmann, Erich; D'Abrera, *Nonparametrics: Statistical Methods Based on Ranks.* Holden-Day, 1975.

# Appendix A

# Supplemental Information

## A.1 Reproducing EAP Hydrogel Actuation Results

### A.1.1 Step by Step Polyacrylamide Hydrogel Synthesis Procedure

Through these steps consistently shaped polyacrylamide hydrogels are able to be synthesised in batches for use in experiments. The steps for this synthesis, with chemical quantities for 9 10x10x30mm hydrogels, are written below:

1. Rinse out a flask then fill with 27ml of distilled water, fill a tub with ice and place the flask in ice to keep the water cold, below polymerisation initiation temperature
2. Add the following chemicals to the flask, measured using an analytical balance within a fume hood:
   (a) Acrylamide (1.3365 g), the linear constituent
   (b) N, N'- Methylenebisacrylamide (0.0356 g), the tetrafunctional crosslinking constituent
   (c) Ammonium Persulfate (0.0107 g), the initiator
3. After each chemical is added place in magnetic stirrer and mix solution until chemicals will not dissolve any further, normally 5-10 minutes depending on particle sizes
4. Cover the flask with plastic wrap, with a small hole to allow air to escape
5. Place ice in the degasser (vacuum chamber) then place flask in degasser chamber, place setup in fume hood (as degasser often leaks oil), pressurise and leave for 20 minutes
6. Using a pipette measure the TEMED into the flask containing the dissolved chemicals:
   (a) N, N, N, N-tetramethylethylenediamine (TEMED) (64µl), the accelerator
7. Gently stir the flask to distribute the TEMED without causing more micro bubbles within the solution
8. Using a serological pipette place solution into each subsection of the mould, enough to fill each subsection ( 3ml)

9. Place the mould on a hotplate set to minimum temperature until the base of the solution starts to solidify, then immediately remove mould from the hotplate
10. Leave to fully polymerise over 12-24 hours, longer period can cause the gel to dry out. Place a cover over the hydrogels to help prevent contamination while allowing ventilation
11. Remove hydrogels from mould by pouring a small amount of distilled water over as a mould release and run a metal spatula around the edge carefully
12. Completely submerge hydrogels into a beaker filled with distilled water and leave to equalize for 24 hours
13. Fill a beaker to a significate enough level to completely submerge the gel strips (150ml), in the fume hood add 1.2% TEMED using a serological pipette (1.8ml), mix the solution and the place the hydrogel strips in the beaker to undergo hydrolysis, leave for a 7 days to ionise
14. Pour solution away leaving the hydrogels. Fill beaker with distilled water to wash away any residual TEMED, then pour away remaining water
15. Place hydrogels into plastic sealed container and move to the area for experimentation

## A.2 Electroactive Polymer Gels as Probabilistic Reservoir Automata for Computation

### A.2.1 Post-Processing Experimental Results to Reduce Variance

To effectively judge consistency some post-processing is needed to filter noise caused by unavoidable inconsistencies between experiments e.g. positioning of gel, gel surface texture, slight synthesis differences between batches etc. To filter noise in the current setup a gain and offset parameter are used.

$$\boldsymbol{\Theta}_i = \alpha_{gain}\theta_i - \theta_0 \tag{A.1}$$

$$\boldsymbol{\Theta} = (\boldsymbol{\Theta}_1, \boldsymbol{\Theta}_2, \boldsymbol{\Theta}_3)\ \{\boldsymbol{\Theta}_i \in \mathbb{R}\} \tag{A.2}$$

$$\text{Where}\quad \alpha_{gain} = \arg\min_{a\in\mathbb{R}} \sum_{i=1}^{N} (a\theta_i - \bar{\theta_{\boldsymbol{I}}})^2 \tag{A.3}$$

Where $\bar{\theta_{\boldsymbol{I}}}$ is the average output angle in the collected data for input sequence $\boldsymbol{I}$

The offset parameter accounts for differences in surface texture that cause initial bending in the gel at t=0 [235], by subtracting the bending angle at t=0 from further angles all gels have the same zero reference, as shown in equation A.1. Where $\boldsymbol{\Theta}$ is the vector of processed angles as defined in equation A.2, $\alpha_{gain}$ is a gain parameter, $\theta_i$ is the angle after input symbol $i$, $\theta_0$ is the bending angle from the initial posture of the gel at t=0.

The gain parameter is used to reduce the effect of differences in synthesis between batches. Changing the chemical ratio changes swelling rate due to change in elasticity [236]. A gain parameter is applied to each gel to minimises its distance from the average output angle for that input sequence. This is shown in equation A.3 where $\bar{\theta_{\boldsymbol{I}}}$ is the average output angle in the collected data for input sequence $\boldsymbol{I}$. As only one gain and offset parameter is used per gel this method compensates for procedural flaws without forcing data into a fabricated pattern.

The variance [237] in output angles for each input sequence is used to evaluate the success of this post processing. Table A.1 shows variance for each input sequence $\boldsymbol{I}$, before and after the gain parameter along with the reduction, giving an average reduction of 33.5 degrees$^2$. This shows notable improvement, mitigating a significant portion of noise from the experimental procedure.

### A.2.2 Optimisation of Output Encoding Thresholds to Maximize Automaton Response

The selection of output thresholds alter the response of the gel as an automaton. The bending angle is converted to a symbol as shown in equation A.4 where; $\boldsymbol{O}$ is the output symbol, $\boldsymbol{\Theta}$ is the processed output angle. $t_1$ and $t_2$ are thresholds 1 and 2 respectively which remain constant for a given Moore machine. By altering threshold values and analysing the resultant probabilistic Moore machine the gel automaton's range of capability can be found. The ideal Moore machine would maximize certain evaluation criteria;

- Maximize predictability: Achieved by maximising the probability that each $\boldsymbol{I}$ vector will consistently result in the same $\boldsymbol{O}$ vector between activations of the probabilistic Moore machine.

- Maximise computational range: Achieved by realising equal distribution of output symbols in the $\boldsymbol{O}$ vectors generated by the probabilistic Moore machine.
- Maximize computational versatility: Achieved by maximising the number of unique $\boldsymbol{O}$ vectors given by the probabilistic Moore machine across all $\boldsymbol{I}$ vectors.

Altering the threshold values affects these criteria in the generated probabilistic Moore machines, thus every combination of 2 thresholds are used to generate graphs representing each criteria. The range of threshold values tested are bound by the maximum and minimum recorded bending angles (-31.3 and 29.3) with a step of 0.5 degrees ($\boldsymbol{\Theta}_{min}, \boldsymbol{\Theta}_{min} + 0.5, ..., \boldsymbol{\Theta}_{max} - 0.5, \boldsymbol{\Theta}_{max}$). The results of this can be seen in figure S3 of the supplementary document and show how thresholds affect each criteria.

$$\boldsymbol{O} = \omega\left(\boldsymbol{\Theta}, t_1, t_2\right) = \left\{ \begin{array}{cc} -1 & \boldsymbol{\Theta} < t_1 \\ 0 & t_1 \leq \boldsymbol{\Theta} \leq t_2 \\ 1 & \boldsymbol{\Theta} > t_2 \end{array} \right\} \tag{A.4}$$

Finding a value that fully maximises all these criteria is impossible as the number of unique output sequences increases inversely to the probability and standard deviation shown in figure A.1 A, B and C. The sum of squared errors is used to simplify this multi-objective optimisation into a single function to be minimized. The error graph, figure A.1 D, shows the threshold values that achieve the most significant ability from the probabilistic Moore machine at the minima of the graph. For data collected these thresholds were found to be -7.8 and 2.7 for threshold 1 and 2 respectively.

Table A.1: Related to Equations A.1, A.2, and A.3. Comparison of variance of angles for different input sequences ($\boldsymbol{I}$) with and without gain parameter

| $\boldsymbol{I}$ | Variance No Gain | Variance With Gain | Reduction |
|---|---|---|---|
| -1 | 35.28 | 14.81 | 20.48 |
| 1 | 30.92 | 21.27 | 9.65 |
| -1,-1 | 30.45 | 10.95 | 19.50 |
| -1,1 | 32.48 | 16.53 | 15.95 |
| 1,-1 | 23.30 | 8.71 | 14.59 |
| -1,-1 | 57.73 | 26.51 | 31.22 |
| -1,-1,-1 | 52.80 | 59.83 | -7.03 |
| -1,-1,1 | 161.57 | 85.23 | 76.35 |
| -1,1,-1 | 33.05 | 15.84 | 17.21 |
| -1,1,1 | 89.83 | 7.34 | 82.49 |
| 1,-1,-1 | 59.02 | 2.83 | 56.19 |
| 1,-1,1 | 5.02 | 4.25 | 0.76 |
| 1,1,-1 | 88.48 | 54.95 | 33.53 |
| 1,1,1 | 103.57 | 6.15 | 97.42 |

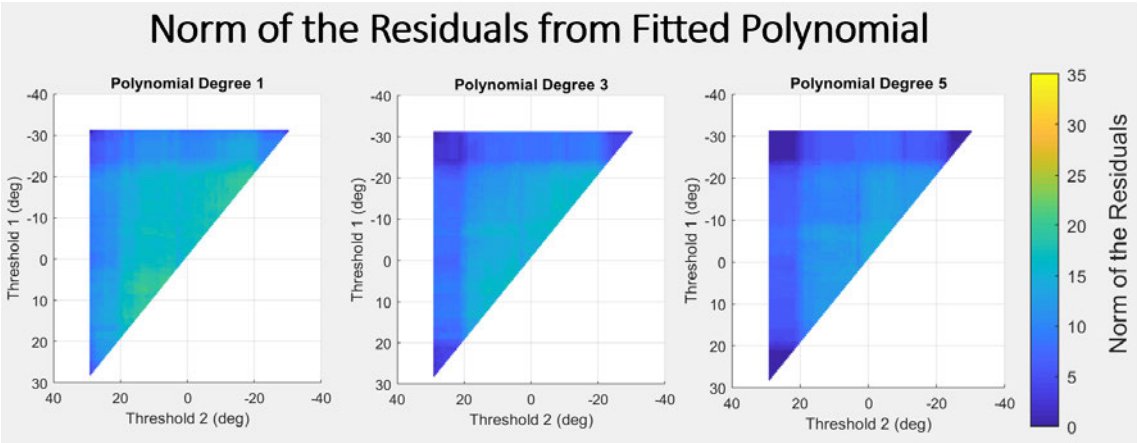


Figure A.2: Heat map for the norm of residuals error of fitted polynomials, against the threshold values used in the output layer of the PMA reservoir instance that the polynomial is fitted to. Each pair of threshold values is used to generate a PMA reservoir by being applied to the output layer and a polynomial is fitted to the mapping function of these reservoirs. These graphs show the results of polynomial fitting for polynomial degrees 1, 3 and 5. The colour bar shows the relative norm of residual values

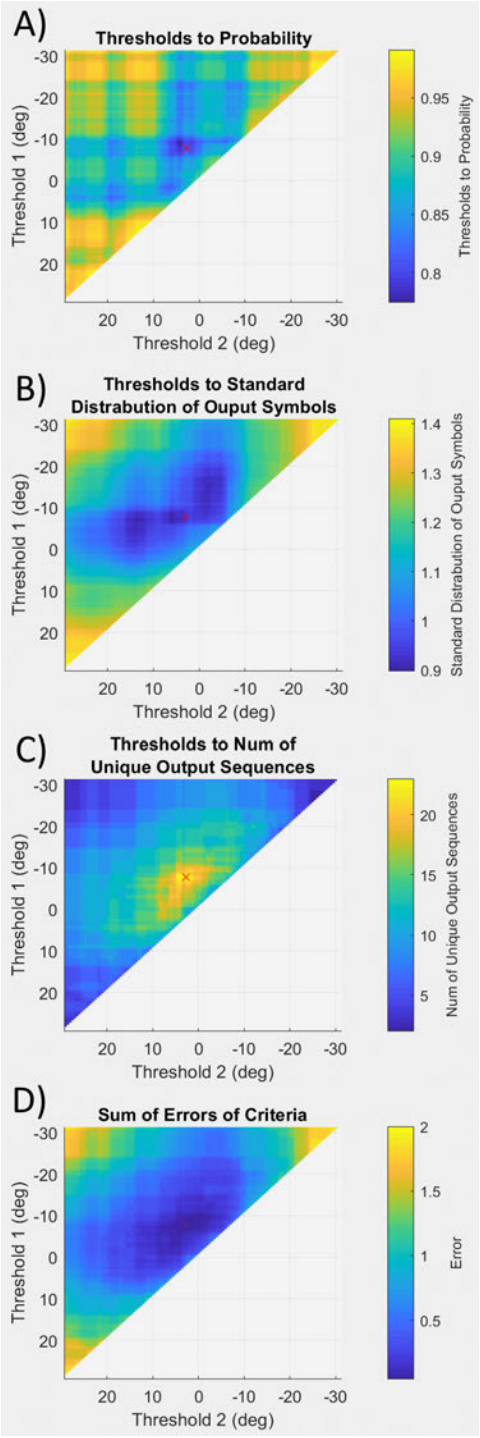


Figure A.1: Error results of criteria used to measure the affect of thresholds as described in the section titled Threshold Optimisation; **A)** Maximize predictability, **B)** Maximise computational range, **C)** Maximize computational versatility, **D)** Sum of errors of all evaluation criteria to indicate best threshold selection

## A.3 EAP Hydrogel Inspired Spiking Neural Network

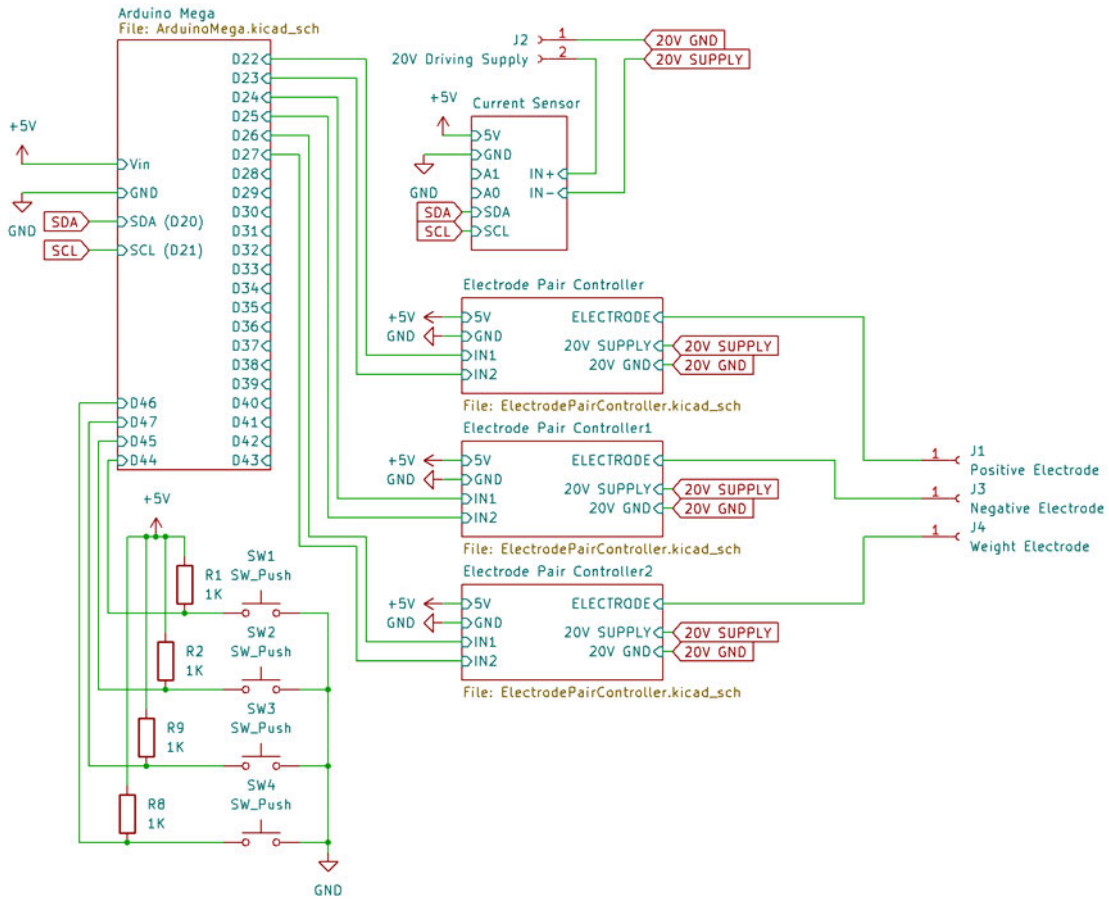


Figure A.3: Schematic of control electronics used in experiments. Sub-sheets for components of "Electrode Pair Controller", "Current Sensor", and "Relay" are found in figure A.4. The Arduino Mega module has had the number of outputs reduced to just those used in this circuit to improve readability.

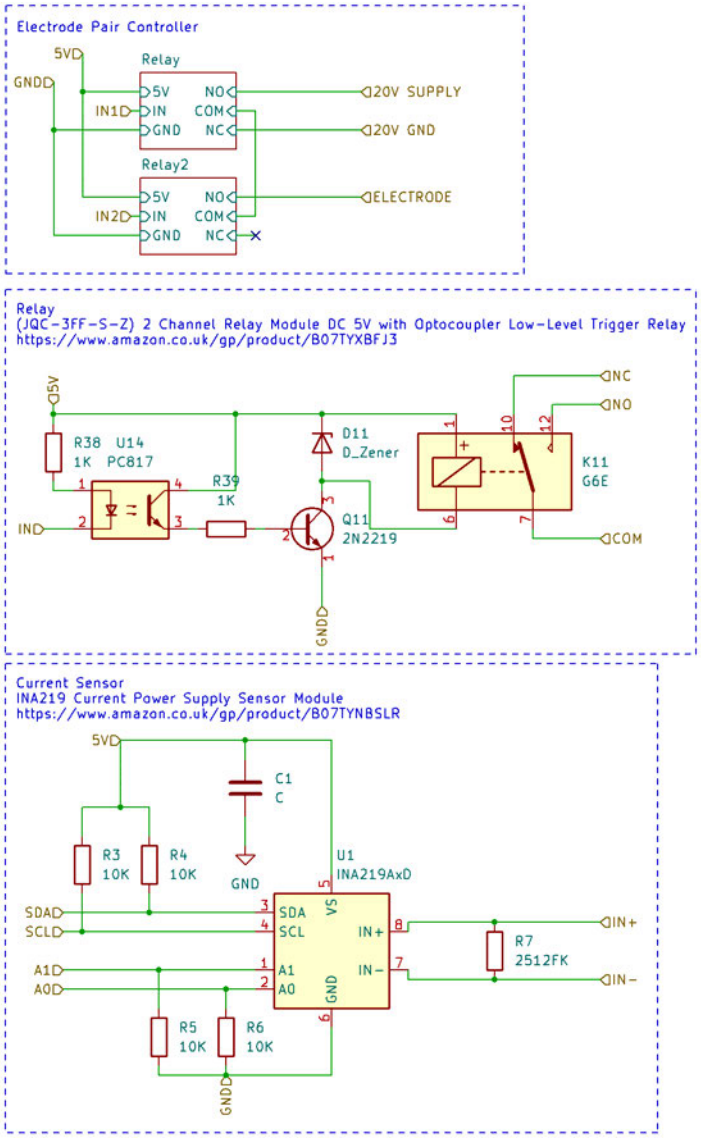


Figure A.4: Schematic of control electronics sub-sheets, main schematic found in figure A.3, for components of "Electrode Pair Controller", "Current Sensor", and "Relay". The electronics were constructed from commercially available modules which are shown here as blocks: "Relay" which represents one half of a 2-channel relay module with with Optocoupler Low-Level Trigger using the JQC-3FF-S-Z relay (https://www.amazon.co.uk/gp/product/B07TYXBFJ3). "Current Sensor" which is an I2C controlled power sensing module using the INA219 IC (https://www.amazon.co.uk/gp/product/B07TYNBSLR). The "Electrode Pair Controller" is a collection of Relay modules to make the layout simpler and to improve readability.

## A.4 Learning Behaviour When Embodied in a Simulated Game-World

### A.4.1 Gel Synthesis Procedure

This section details the procedure used to synthesise and mould the polyacrylamide hydrogels for use in the experiments. Polyacrylamide gels were prepared by free-radical polymerisation [70] following the basic procedure as described in "Collapse of gels in an electric field" [71]. The detailed synthesis procedure is written below.

1. Rinse out a flask then fill with 107ml of distilled water. Fill a tub with ice and place the flask in the ice to keep the water cold
2. Add the following chemicals measured using an analytical balance within a fume hood (make a note of final mass each time):
   - Acrylamide (5.3452 g), the linear constituent
   - N, N'- Methylenebisacrylamide (0.142 g), the tetrafunctional crosslinking constituent
   - Ammonium Persulfate (0.0428g), the initiator
3. After each chemical is added, shake the solution until the chemical will not dissolve any further
4. Cover the flask with plastic wrap with a small hole to allow air to escape
5. Place some ice in the degasser (vacuum chamber) then move flask to degasser chamber. Place setup in fume hood (as degasser often leaks oil), pressurise and leave for 20 minutes.
6. Using a pipette measure the TEMED into the flask containing the dissolved chemicals:
   - N, N, N, N-tetramethylethylenediamine (TEMED) (256.6112 µl), the accelerator
7. Using a serological pipette place 12ml of the solution steadily into glass beakers, or similar glass container, (ensuring they were rinsed and cleaned) with a base diameter measuring approximately 50mm across
8. Place the beakers on a hotplate set to 100C for 3 minutes or until the liquid at the bottom has just started to gel then remove them from the hotplate
9. Repeat until all the solution is used, this should result in 8 to 10 samples
10. Leave to fully polymerise over 12-24 hours, longer period can cause the gel to dry out. Place a cover over the gels and help prevent contamination while allowing ventilation.
11. To remove them from the moulds, add a small amount of distilled water to use as a mould release and run a metal spatula around the edge carefully.
12. Fill a beaker with 800ml of distilled water

13. Place gels into water to equalize for 24 hours
14. Fill a beaker to a significant enough level to completely submerge the gel strips (800ml), in the fume hood add 1.2% TEMED using a serological pipette (9.6ml), mix the solution and the place the gel strips in the beaker to undergo hydrolysis, leave for a week to ionise.
15. Pour solution away leaving the gels and the fill beaker with distilled water to wash away any residual TEMED, pour away water.
16. Place gel disks into plastic sealed container (watertight lunch box) and move to the lab for the Pong experiment, they can be left on a table or in a drawer and do not need to be refrigerated

### A.4.2 Pong Game Implementation and Behaviour

The closed loop between the Pong game and the MEA consists of four main components. These components are listed here in order of information flow, along with a description of the implementation of each component. The simulated environment controls the speed of the closed loop in this setup. The MEA provides electric current measurements at the same rate it is provided stimulation instructions. In this experiment this call and response rate is set to 0.5 seconds per loop.

1. Simulated Pong game environment:

   At the start of the Pong game the ball starts in the centre of the game area with a random speed and direction towards the right wall. The speed of the ball is measured in pixels moved per game update. For the random speed, a value between 4 and 8 pixels per game update was used for the x axis, and between 1 and 8 pixels per game update for the y axis. This allows the ability of the hydrogel to be assessed against various ball trajectories and speeds giving a more accurate measurement of performance. When the ball hits a surface, such as a wall or paddle, the speed perpendicular to the surface is reversed to allow it to bounce with approximate realism and allow the ball path to be predictable. If the ball hits the paddle the score is increased by 1. If the paddle misses the ball, and the ball hits the wall behind, the score resets to 0 and the ball resets position to the middle of the play area with a new random speed and trajectory.

   With this randomisation of starting trajectory, the top and bottom regions are equally hit by the ball, both twice as often as the middle section. This is expected in the course of a Pong game as the ball most often has a diagonal trajectory, and the top and bottom regions are the boundaries. This hit distribution was recorded and is shown in the supplementary information figure A.10 to show no bias in ball hit locations regardless of interaction with paddle or wall.

2. Conversion from ball position to stimulation via relays and regions:

   The position of the ball, based on the region it is currently within, is sent to the MEA as a binary string where each bit represents 1 of 6 regions. The MEA interprets the binary string into instructions for each region, activating the corresponding relays and applying the electric field accordingly. The ball is wide enough to be in multiple regions at once. As the ball passes between regions all regions the ball touches will be active until the ball is only in one region. These combinations allow for more states to represent ball positions and a greater resolution of positional information.

3. MEA and EAP hydrogel:

   The stimulation causes migration of ions as the electric field interacts with the EAP hydrogel. The shape of the electric field, governed by the combination of activated stimulation electrodes driven by the balls position, controls the spacial migration of ions. In this way the environmental information of the ball is applied to the EAP hydrogel. The specifics of this application and the associated theories of free energy that support it are described in more detail in the main text.

4. Conversion from ion migration to paddle position via current sensing:

   When the computer sends the stimulation instructions to the MEA, the MEA responds with the recorded electric current measurements at each of the current sensing electrodes. These electric current measurements provide information about the ion

concentrations, and migration, to the simulated game world. These measurements are then used to place the paddle as described in figure 6.5. The paddle then either hits or misses the ball, altering its trajectory, leading to the next iteration of the closed control loop.

As there can be small inconsistencies between gels the starting current value is measured, before the Pong game is started, using the average current value over a 75 second period. This value is used as a baseline to calibrate the sensor readings.

### A.4.3 MEA Hardware Implementation and Details

For application of stimulation, electro-mechanical relays were used to apply the electric field as they allow for a high impedance state where electrode pairs are not connected to either power or ground. This prevents electric field interference from electrode pairs that are not in use. Current sensors were used to measure the current draw at the sensing electrodes. These relays and sensors were coordinated by a microcontroller that sends and receives commands from the computer containing the Pong environment. A more detailed circuitry schematic can also be found in figure A.5, additionally an image of the physical hardware can be seen in figure A.7 with a diagram of the MEA apparatus shown in figure A.8. The MEA was designed so that the height between electrode pairs was adjustable to allow for differing hydrogel thicknesses. Additionally, pins were used as the electrode surface to allow for easy replacement so as to keep electrode surfaces consistent across experiments. The full setup of the computer game environment and MEA apparatus can be seen in the supplemental information figure A.9.

### A.4.4 Pong Game Experimental Procedure

This section details the procedure used to apply the polyacrylamide hydrogels (synthesised using the procedure in section A.4.1 "Gel Synthesis Procedure") to the simulated game world and record the results.

1. 2 gels are placed in a dish and submersed in a 0.08% sodium chloride salt-water solution (0.6417g in 800ml) for 20 minutes
2. A new set of electrodes are placed in the MEA
3. Each electrode is tested with a multimeter to ensure the connection between the electrode surface and the end of the associated pin connector is less than 10 ohms
4. The electrode array is then plugged into the driving rig with the connectors to the bottom electrodes placed at the front row of pins (closest to the 4 power supply sockets) and the top electrode connectors placed at the back row of pins (closest to the Arduino)
5. Ensure the stimulation and sensing power are plugged into the sockets on the front (stimulation 20v in the white socket holder, sensing 2v in the black socket holder)
6. The power to the driver rig via the barrel jack 5v power supply must be turned on before it is plugged into the computer via the USB
7. The gels are placed in the MEA so the bottom surface that would have been in contact with the bottom of the beaker during molding is in contact with the electrodes, with the top flat surface facing each other. Ensure that any air bubbles trapped between gels are removed.
8. The sprung screws are tightened until the entire surface of the electrodes are in contact with the gel and the top MEA is level with the base
9. The serial monitoring program (Serial_plot2.py) is run to record and average the current values of the 3 electrode pairs over a 100 second period
10. The 2v sensing voltage is applied and the average of each sensing electrode pair after 100 seconds is recorded
11. These values are entered into the Pong game software (Pong.py) to provide the base current values
12. The 2v sensing voltage and 20v stimulation voltage are turned on and the Pong software is started (threadedPong.py)
13. During this initial period of the game, the response of the measured current to the stimulation should be monitored to make sure it works as expected. Additionally, the stimulation power supply should be monitored to ensure that each segment draws a current when stimulated. If any errors in operation are discovered at the very start of the Pong game there is an opportunity to address the issue before the full trial.
14. The game is run for 4000 seconds or until the gel breaks down and no longer functions
15. The MEA is loosened, and the gel removed along with the electrodes
16. The MEA is cleaned ready for the next experiment

### A.4.5 Accuracy of Experiment Repetitions

To check the stability of results from the 21 experimental repetitions, the standard deviation in the recorded hit rate of the dataset was analysed as more experimental results are added to the dataset. The standard deviation was applied to datasets over time, consisting of varied numbers of experimental runs (1 to 21), using the same 600 second window. As the dataset becomes larger the changing standard deviation becomes more stable and undergoing less change between datasets. With a dataset consisting of 19 experimental runs, the trend of standard deviation does not appear to change any further and so has stabilised and no further experimental runs are necessary. The plots, showing the standard deviations over time with varying dataset sizes, can be seen in the figure A.13.

### A.4.6 Rally Length Subsampling for Learned and Unlearned States

To perform statistical analysis on the hydrogel's game performance over the course of the game, the samples, from the rally length dataset show in figure 6.8, representing before and after the learning need to be defined. Through the trend of rally lengths, the point at which learning starts and the point at which maximum learning occurs can be defined. To this end a 4th degree polynomial best fit line was applied to the data, shown in figure 6.8 as the blue dashed line. This was found to be the lowest degree polynomial that still visibly fit the data trend. Using the best fit line, the average rally lengths started around 4.4 and over the course of the game increased to 5.1, giving an increase of 0.7 over the course of 1700 seconds. With this trend, the samples can be extracted from the rally length dataset prior to smoothing.

The sample representing the learned state can be extracted by using the the point of maximum learning ans the center, marked in figure 6.8 as the black dot, at 1744 seconds. To ensure the largest sample possible, the extracted data set is symmetrical around the point of maximum learning with the maximum width limited by the cutoff at 2000 seconds. This means that the learned data set starts at $1744 - (2000 - 1744)$ =1488 seconds, represented in figure 6.8 by the green dashed line, and ends at 2000 seconds, giving 228 data points. The sample representing the pre-learned state can be taken from 0 seconds up to the point where performance starts to improve at 1000 seconds, as evidenced by the trend in figure 6.8. To accurately represent the pre-learned state the sample must span the largest range. However, to avoid compensation variables when dealing with data sets of unequal size and to more accurately compare the samples, the learned and pre-learned data sets must be of equal size. To achieve this the full data range from 0 to 1000 seconds was sub-sampled into 228 data points, making the range of the sample 0 to 838 seconds, shown in figure 6.8 by the orange dashed line.

### A.4.7 Statistical Significance and Mann–Whitney U Test Calculations

The significance of the learned and unlearned rally length samples is assessed via the p value of the comparison. Given the large size of the samples, critical limit theorem allows $p$ to be calculated from the z score $z$ using the normal distribution $\Phi$, as shown in equation A.5. The z score is calculated from the normal distribution and U statistic $U$ as shown in equation A.6, where $\mu_U$ is the mean of $U$ calculated using equation A.8 [277], $C_{cont}$ is $-0.5$ the continuity adjustment due to the direction of the one-tail distribution, and $\sigma_U$ is the standard deviation of $U$. The Mann–Whitney U test can be used to assess significance as both samples have non-normal distributions and independent variables. This is evident when the samples are represented via a density histogram as shown in the supplementary

information figure S8 where both follow an exponential distribution due to 0 being the most common rally length in both samples.

$$p = \Phi(z) \tag{A.5}$$

where:

$$z = \frac{U - \mu_U + C_{cont}}{\sigma_U} \tag{A.6}$$

and:

$$U = R_s - \frac{n(n+1)}{2} \tag{A.7}$$

$$\mu_U = \frac{n^2}{2} \tag{A.8}$$

$$\sigma_U = \sqrt{\frac{n^2}{12}(2n - C_{ties})} \tag{A.9}$$

$$C_{ties} = \frac{\sum_{k_{rank}=1}^{K_{rank}} ({t_{k_{rank}}}^3 - t_{k_{rank}})}{2n(2n-1)} \tag{A.10}$$

Following the Mann–Whitney U test, the ranked sum was calculated for each sample. Where ties were present the assigned rank was equal to the midpoint of unadjusted rankings. The summed ranks were calculated to be 47476.5 and 56719.5 for the pre and post learned samples respectively. The lower of the values was used to calculate the U statistic using equation A.7 [278], where $U$ is the U statistic, $R_s$ is the lowest ranked sum value, and $n$ is the size of the sample which here is equal in both samples. $\sigma_U$ is calculated using equation A.9 [279], where $C_{ties}$ is the adjustment due to the number of tied ranks. $C_{ties}$ is calculated in equation A.10 [279], where $t_{k_{rank}}$ is the number of ties for the ${k_{rank}}^{th}$ rank, and $K_{rank}$ is the total number of unique ranks with ties.

These calculations give a $z = -3.3433$ which, using equation A.5, gives a $p = 0.00041$. Using the z table for the negative score this places the probability below 0.05% and rejects the null hypothesis. This validates the improvement before and after learning is statistically significant.

### A.4.8 Paddle Motion and Standard Deviation Analysis

Two plots were made from the collected data, one to show the paddle's position over time, shown in figure A.19 section A, and a second to show the standard deviation of the paddle's position over time, shown in figure A.19 section B. The goal is to analyse how the paddle's motion in reaction to the ball's position changes over the course of the Pong game, and analyse how that behaviour change leads to improved performance. To better show this, the data representing the paddle's position was separated based on the region the ball was in at the time. Combinations of regions, when the ball is in more than one region at once, were not considered as these events happen far to infrequently to give any useful indication as to the paddle's change in behaviour. As with the previous plots an averaging window of 600 seconds was applied along with the cutoff at 2000 seconds.

From the plot of paddle position over time, shown in figure A.19 section A, the position of the paddle in reaction to the ball being in different regions can be seen to change as the game progresses, aligning with the increase in hit rate seen in figure 6.8. The change in

paddle positions were collected into table A.2 to show the position at the start (in this case at 300 seconds due to the sampling window of 600 seconds), the position when at the point of maximum performance (found in the hit rate in figure 6.8 as 1600 seconds), and the percentage change in paddle position between these points compared to the total height of the Pong environment of 1000 pixels. From table A.2 it can be seen that the paddle's reaction to the front regions each show little change (all less than 4% of the total game height), however the paddle's behaviour in reaction to the back regions show significantly more. The paddle's position in reaction to the ball being in the back top and back bottom regions show similar change over the course of the game of 10.5% the total game height. In reaction to both the top and bottom ball positions the paddle moves further into the region where the ball is, even while the ball is as far as it can be from the paddle. The back middle region shows the most change of 13%, where the paddle's average position moves further down. This paddle behaviour is beneficial in game performance. If the ball is in the back middle region, given ball's trajectory is never completely horizontal, it will most likely next enter the top or bottom regions. Thus if the paddle is in either the top or bottom regions it will be more likely to hit the ball on approach. All these changes in paddle behaviour occur due to the change in ion distribution, as it 'solves' the problem presented by the virtual environmental information. This solution seems to present itself as the paddle preempting the ball's location based on where it is in the back regions.

From the plot of standard deviation of the paddle's position over time, shown in figure A.19 section B, the precision of the paddle's motion was analysed over the course of the Pong game. The standard deviation is representative of the average deviation from the mean of a set of values. Higher standard deviation in the context of the paddle means that its motion, in response to a ball position, is more erratic and can be in a larger variation of positions covering a larger portion of the paddle's play space. Alternatively, if the standard deviation is lower than the paddle's position, in response to the ball's position, then the paddle has less varied motion and tends to a more precise location.

From the plot it can be seen that for every region there was a decrease in standard deviation of paddle position over time. Each region has a different starting standard deviation. However, each has a reduction in standard deviation over the course of the game, the values of these reductions are detailed in table A.3. The most pronounced decrease in paddle deviation can be seen in response to the back top, back middle, back bottom, and front middle regions, the same regions that showed the most pronounced change in average paddle position as seen in figure A.19 section A. This adds credence to the back regions allowing for the paddle to preempt the ball's hit location, as the change in precision of the paddle's motion in reaction to those regions is much greater over the course of the game. The results in table A.3 give an average standard deviation reduction of 43 pixels, with the average minimum standard deviation reached at 1290 seconds, which aligns with the change in paddle position in A.19 section A and the point at which performance increases in figure 6.8 for the rally lengths.

The changes in paddle position in reaction to the region of the ball, and the reductions in deviation of paddle position, align with the change in sensed current and increased hit rate. The most significant changes in paddle position, and reduction in standard deviation, occur between the peak in current at around 1100 seconds and the peak in hit rate at around 1600 seconds. This adds another step to the chain of events leading to the increased performance. This highlights interesting forms of emergent behavior occurring as the ions migrate to reduce free energy.

### A.4.9 Hit/Miss Baseline Comparison

Baseline results were collected to further show that the hydrogel's improved performance was a direct result of the environmental information received, and explore the null hypothesis that the improved performance is simple cause and effect within the gel and thus not a result of learning. As described in the experimental description, the electrode positions were rearranged to give incoherent environmental information to the hydrogel, effectively impairing its 'vision'. The hit rate was recorded in the same way, shown in figure 6.13 section A, using the same averaging window and cutoff point as with the previous plots. Additionally, as with the previous experiment, the stabilisation of the standard deviation in the recorded hit rate of the dataset was analysed as more experimental results are added to the dataset. The standard deviation was applied to datasets over time, consisting of varied numbers of experimental runs (1 to 10), using the same 600 second window. As the dataset becomes larger the changing standard deviation becomes more stable and undergoes less change between datasets. With a dataset consisting of 9 experimental runs the trend of standard deviation does not appear to change any further and so has stabilised and no further experimental runs are necessary. The plots of these standard deviations over time with varying dataset sizes can be seen in the figure A.22.

From the plots in figure 6.13 section A little improvement in performance can be seen, with no region achieving a hit rate beyond 30%. The middle region that showed the most improvement in the previous results shows little to no change in performance over the course of the game. Similarly, the top and bottom regions show some initial improvement but far too little to be considered significant especially given the low initial hit ratios. This lack of performance is even more evident when the rally lengths are plotted, shown in figure 6.13 section B. From this graph little to no improvement can be seen in performance, with the average rally length well below 1 point. This means that the ball was missed far more often than hit throughout the game, with no consecutive hits achieved.

Due to the hit rate not reaching above 33%, the null hypothesis can be rejected as the performance was worse than if the paddle were moving randomly, given the paddle length is a third the total game environment height. Even with this incorrect environmental information, the hydrogel is still being provided stimulation. This means the hydrogel is still learning as the ions move to a distribution representative of the information provided. Unfortunately, as the information provided is wrong, what is learnt by the hydrogel is also wrong, leading to its performance being worse than random motion. This observation helps to reinforce that the hydrogel's increase in performance is directly related to it being presented with an accurate representation of the virtual environment in which it is acting.

## Control Experiment Surrogate Data Simulation

The control experiment pong game was simulated using the real-world data, collected through the experimental runs of the EAP hydrogel embodied within the simulated environment, as a surrogate dataset. The pong game was run with the same game physics and logic however, as the hydrogel is not physically present the surrogate dataset stood in for this component. This dataset provided real world data representing the sensed electric current readings for specific locations of the ball at varying times throughout the hydrogel's experimental lifetime. The dataset consists of:

- The time, from start of game, at which the stimulation was applied to the hydrogel.
- Which combination of the 6 regions the ball was located at the time of stimulation.

- The electric current measured from each of the top, middle, and bottom sensing regions.

The surrogate dataset was implemented via the following steps, occurring once every simulated game loop:

1. The dataset is filtered based on the location of the ball within the 6 regions.
2. The resulting data is sorted based on time.
3. A window of 600 seconds, centered on the current game time, is applied to the dataset.
4. The resulting samples are averaged to give top, middle, and bottom sensed electric current values.
5. The electric current values are rearranged based on the requirements of the control experiment.
6. The electric current values are combined into a paddle position, using the method as described in figure 6.5 of the main text.

A window of 600 seconds was used to remain consistent with all other averaging applied in analysis thought this study. This is further enforced as 600 seconds was also found to be the width of the learned period in the T-test analysis of the main text.

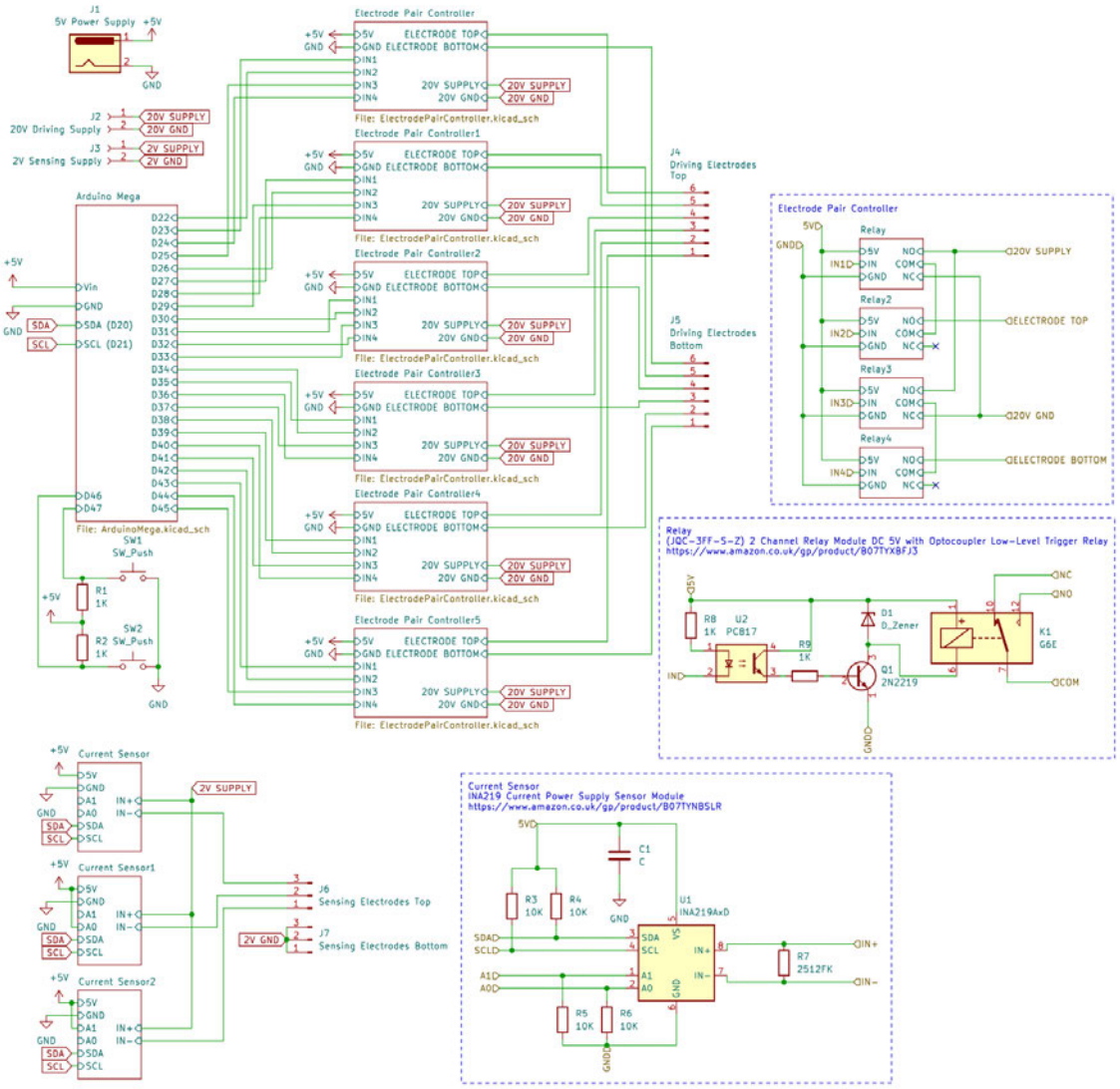


Figure A.5: Circuit diagram of the MEA driving apparatus. Sub-sheets for components of "Electrode Pair Controller", "Current Sensor", and "Relay" are found in figure A.6. The Arduino Mega module has had the number of outputs reduced to just those used in this circuit to improve readability.

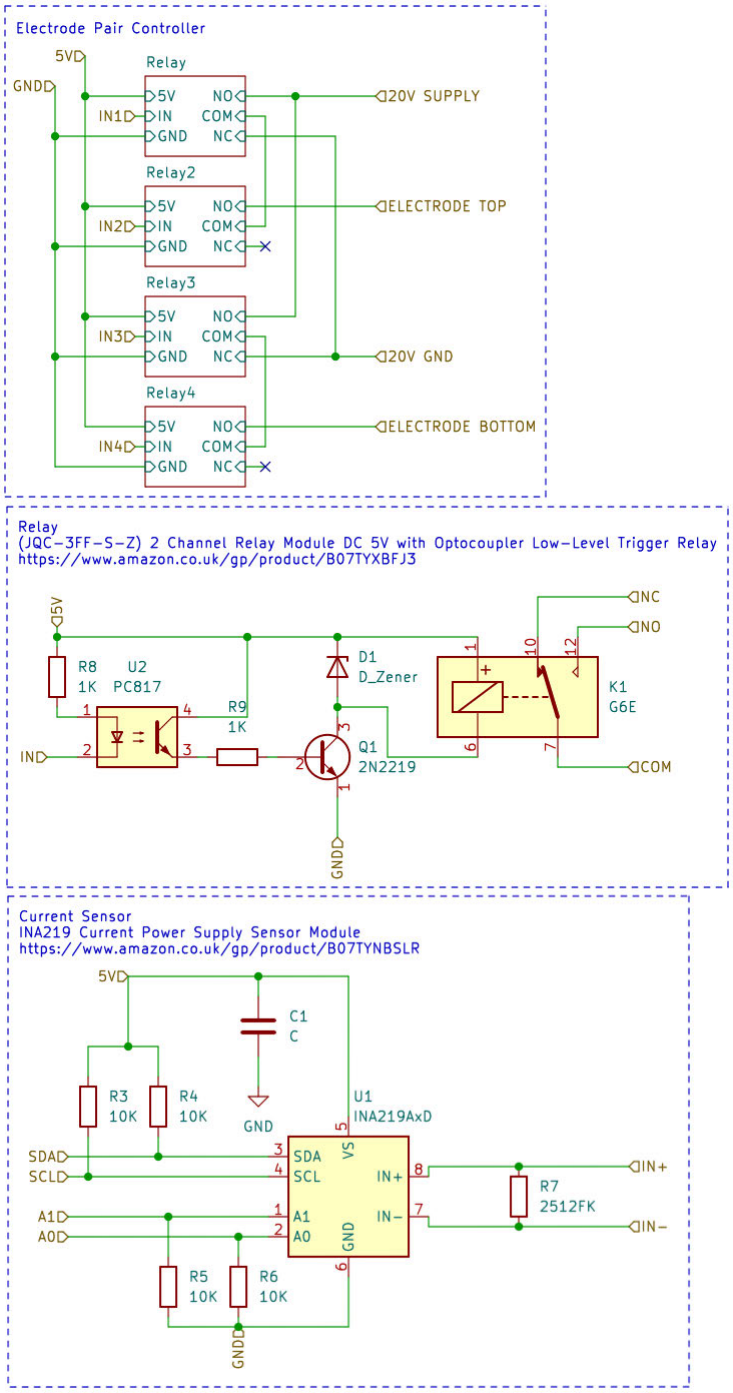


Figure A.6: Schematic of control electronics sub-sheets, main schematic found in figure A.5, for components of "Electrode Pair Controller", "Current Sensor", and "Relay". The electronics were constructed from commercially available modules which are shown here as blocks: "Relay" which represents one half of a 2-channel relay module with with Optocoupler Low-Level Trigger using the JQC-3FF-S-Z relay (https://www.amazon.co.uk/gp/product/B07TYXBFJ3). "Current Sensor" which is an I2C controlled power sensing module using the INA219 IC (https://www.amazon.co.uk/gp/product/B07TYNBSLR). The "Electrode Pair Controller" is a collection of Relay modules to make the layout simpler and to improve readability.

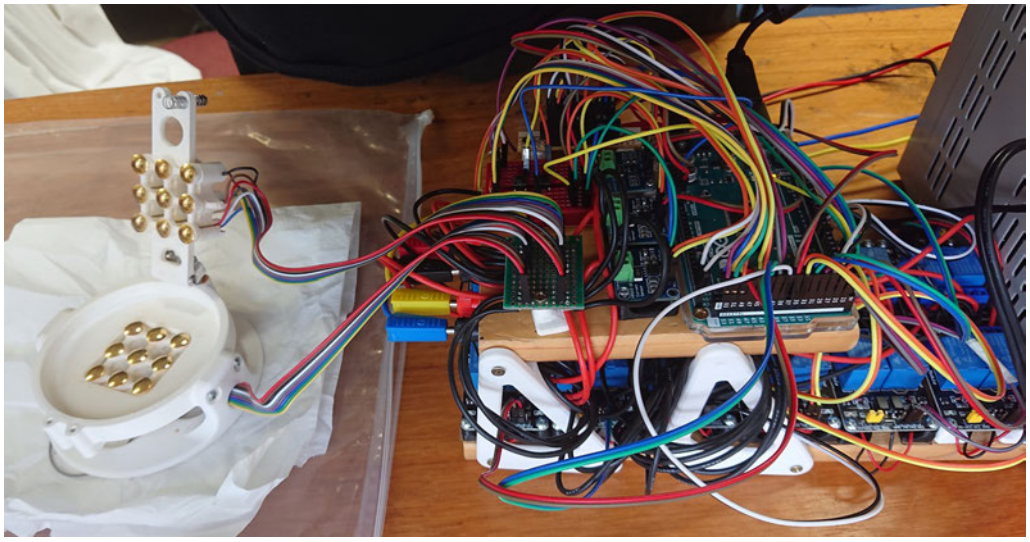

Figure A.7: Image showing the MEA gel holding apparatus and the driving electronics. The MEA was 3d printed and is shown on the left while the electronics were assembled from commercially available modules and is shown on the right.

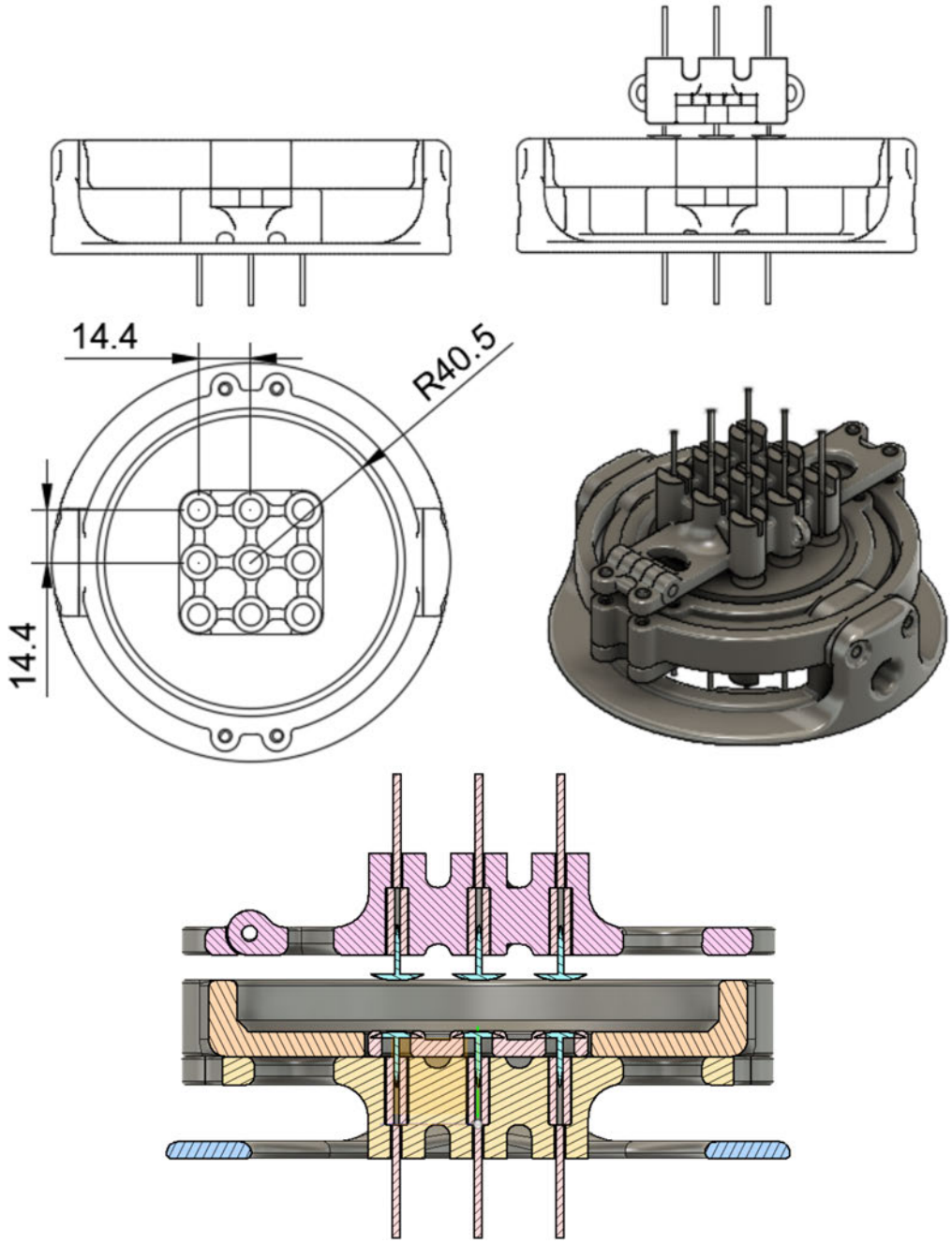


Figure A.8: Diagram of MEA gel holding apparatus, showing the electrodes and key dimensions. The height of the upper electrodes is adjustable using screws, much like with the previous suspension apparatus shown in figure 3.5, so as to allow for varied thicknesses of hydrogel.

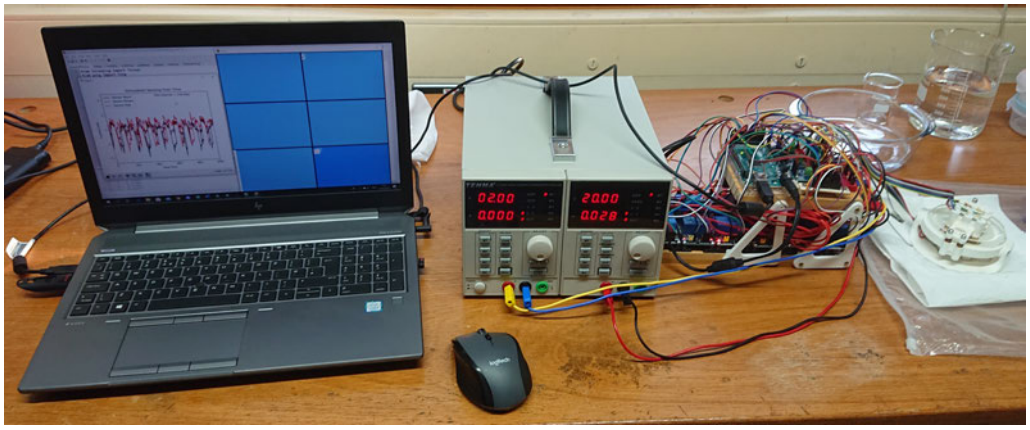

Figure A.9: Image showing the MEA apparatus (right) along with the power supply (middle) and control computer (left). The control computer shows the Pong game and sensor values on the desktop. The power supply provides the stimulation voltage (20v) and sensing voltage (2v) to the MEA apparatus.

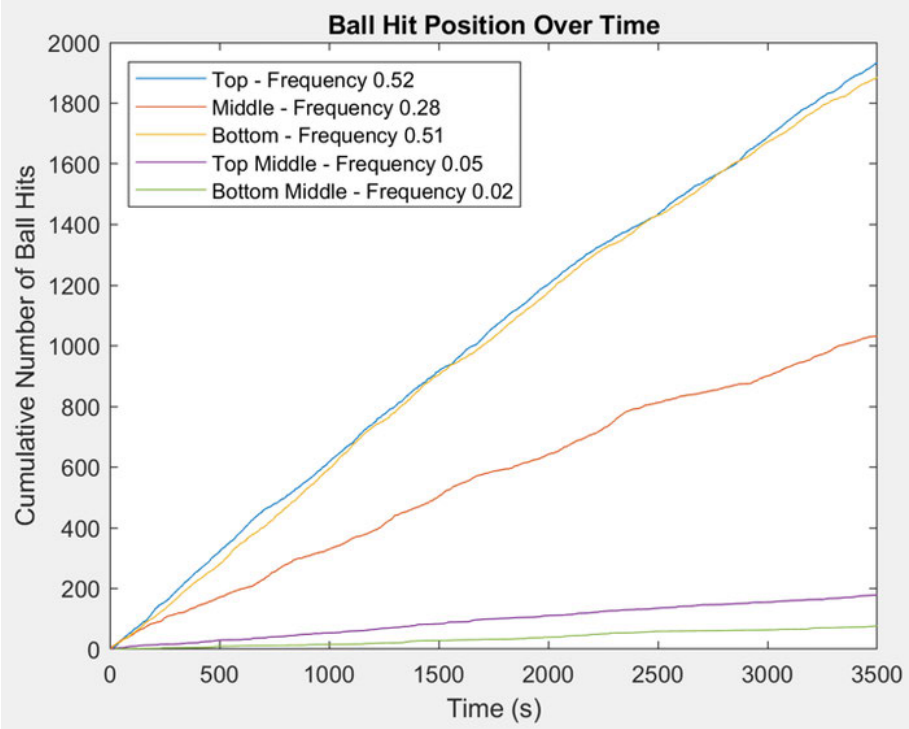


Figure A.10: The distribution of ball hits within the Pong game labelled by the region in which they occur as described in figure 6.4 section B. Situations where the hit occurred on the boundary between regions are denoted by "Top Middle" and "Bottom Middle". As the top and bottom represent the boundary conditions these are hit more often than the middle, likewise the top middle and bottom middle occur even less often. However all hit location show a steady rise over time leading to a consistent frequency which is noted next to the line label in the legend.

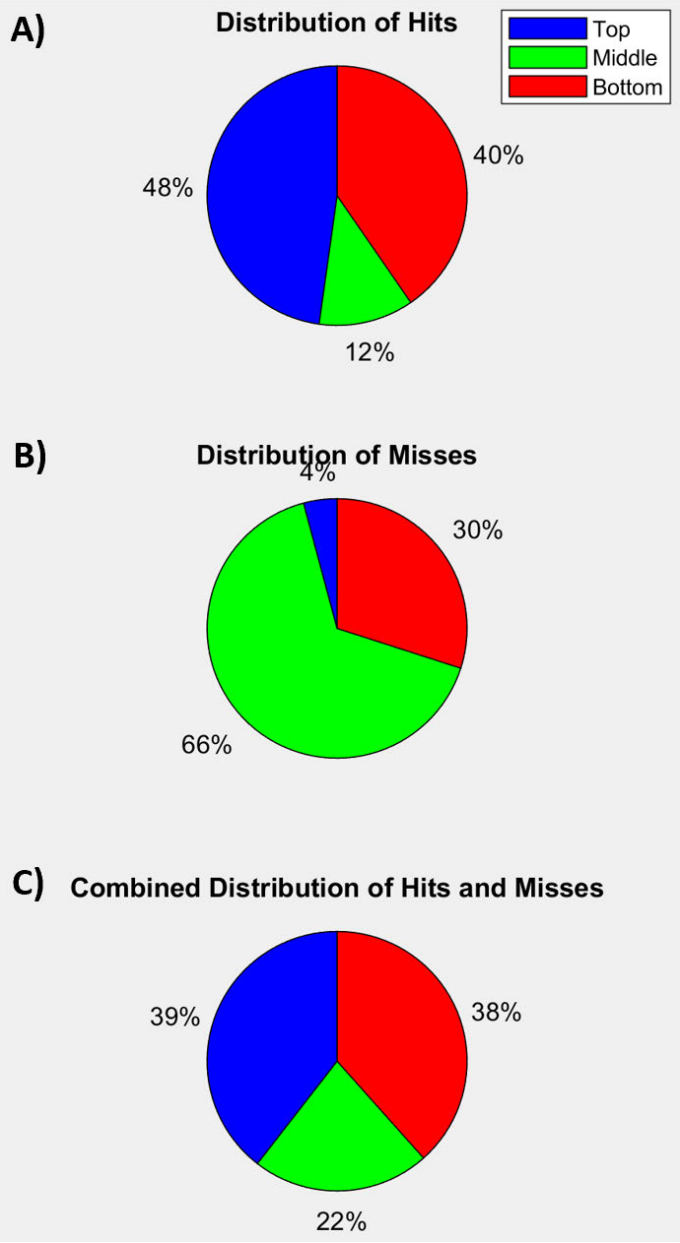


Figure A.11: **A)** The regional distribution of paddle hits summed across all 21 experimental runs. **B)** The regional distribution of paddle misses summed across all 21 experimental runs. **C)** The regional distribution of combined paddle hits and misses summed across all 21 experimental runs.

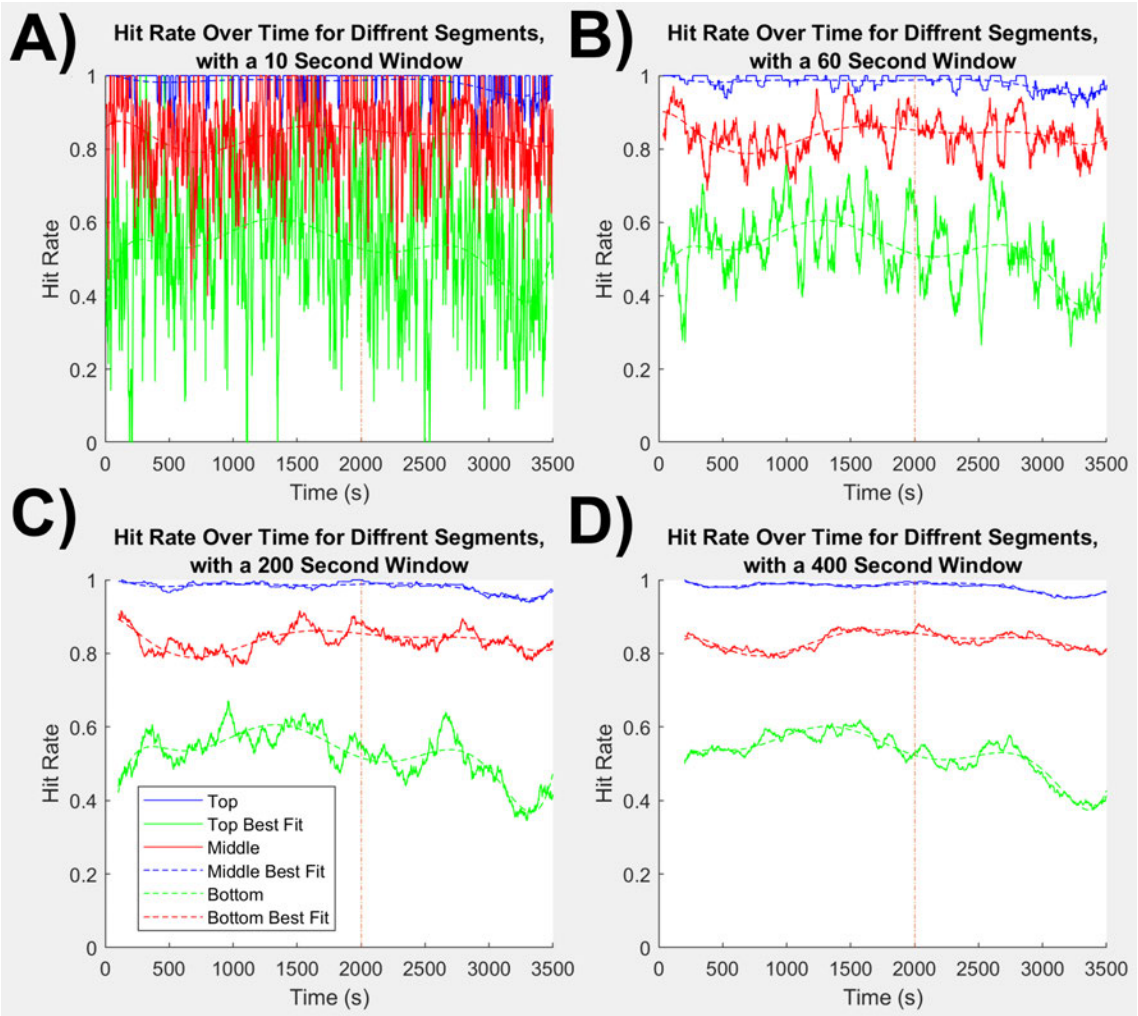


Figure A.12: The hit rate as hit to miss ratio over time for the unimpaired feedback loop, separated based on the region the hit/miss occurred in as described in figure 6.4 section B. The data has been smoothed using a moving average window of 10, 60, 200 and 400 in plots **A**, **B**, **C** and **D** respectively. From this as the averaging window is enlarged the trend of the dataset becomes more obvious, the windows size used though the analysis in this paper was 600 and can be seen in figures 6.8 and 6.7 . A best fit line was applied to the dataset using a 7th degree polynomial via the MATLAB Polyfit function [240] to visualize the smoothing's affect on the overall trend. The orange vertical dashed line marks the earliest point that the EAP gels broke down.

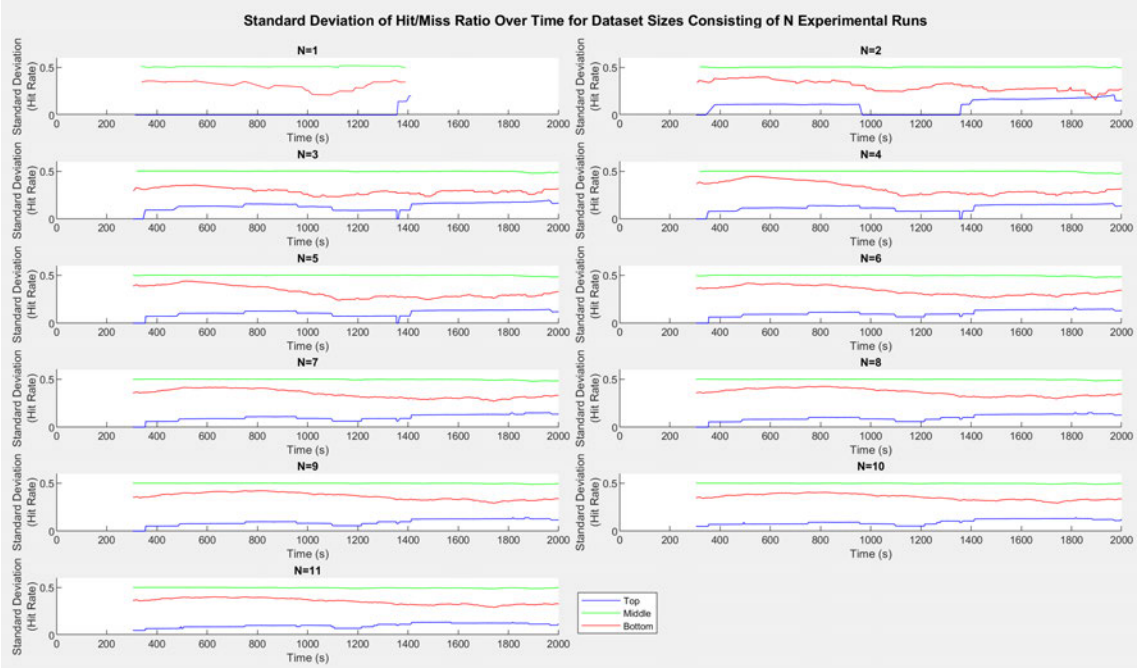


Figure A.13: Standard deviation of hit rate (for top, middle, and bottom regions) over time for the learning datasets consisting of N experimental runs. A moving window of 600 seconds, as with previous figures, was used to apply the standard deviation on the unsmoothed dataset. With a dataset consisting of 19 experimental runs the trend of standard deviation does not appear to change any further and so has stabilised and no further experimental runs are necessary. The first experiment run only recorded 1400 seconds worth of data so the plot of N=1 ends prior to the 2000 second cutoff, however all other experimental runs consist of over 2000 seconds worth of data.

Figure A.14: At the point of deterioration the EAP gel forms a large hole in the centre as a result of the repeated electric stimulation breaking down the EAP gel structure. Once the hole has formed the sensing electrode pairs are separated from the stimulation electrode pairs and so the EAP gel can no longer perform in the Pong game. Further degradation can be seen in the green/brown staining caused by contact with the electrodes over time.

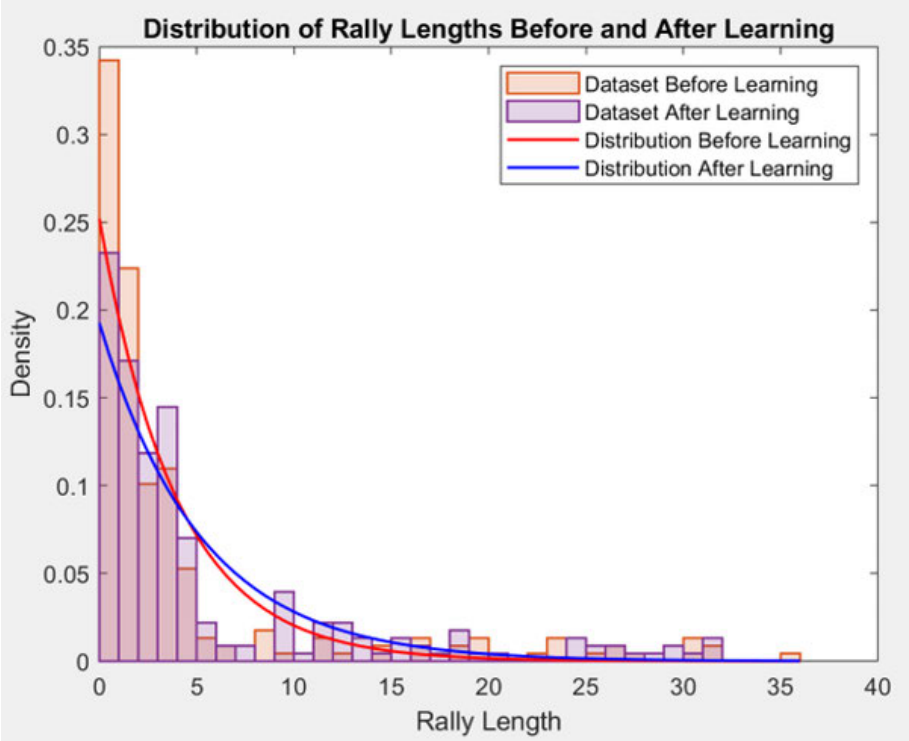


Figure A.15: Histograms showing the distributions of rally lengths before and after learning has occurred. An exponential trend is fit to the distributions and is shown by the solid line. The mean value for the dataset before and after learning is 3.97 and 5.19 respectively. The time-spans used to generate the datasets before and after the learning are shown in figure 6.8.

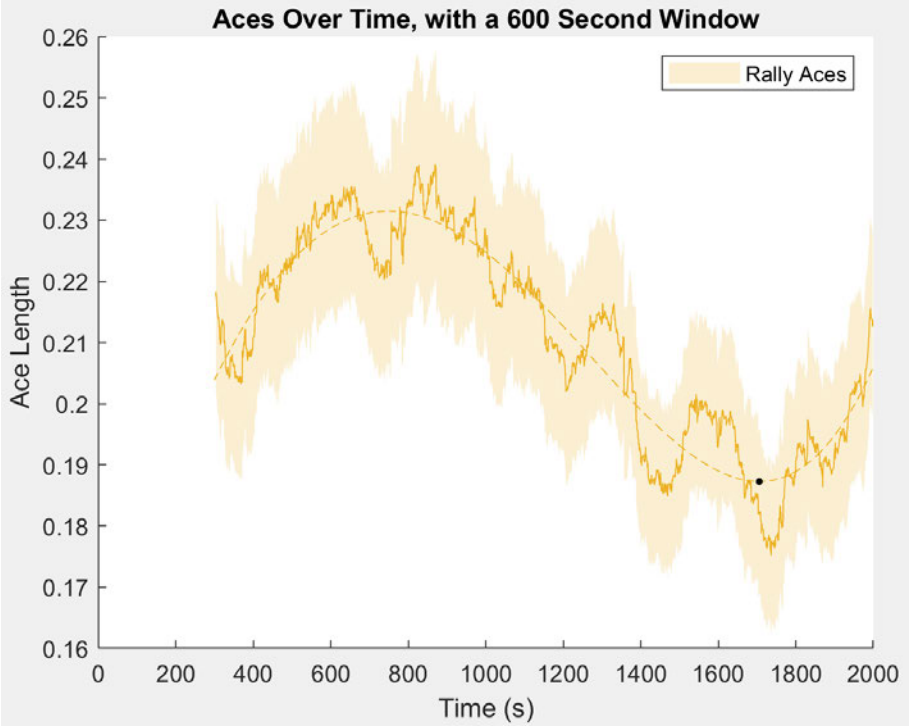


Figure A.16: Plot of rally aces, representing the number of times the paddle failed to intercept the ball without a single hit. Smoothed using a moving average window of 600 seconds. The standard error for each windowed sample is shown by the shaded area. A 4th degree polynomial best fit line was applied via the MATLAB Polyfit function [240]. This was the minimum order polynomial that fit the trend presented by the data. The maximum point of performance is marked by the black dot at 1706 seconds. This marks a decrease of 0.04, from 0.23 to 0.19.

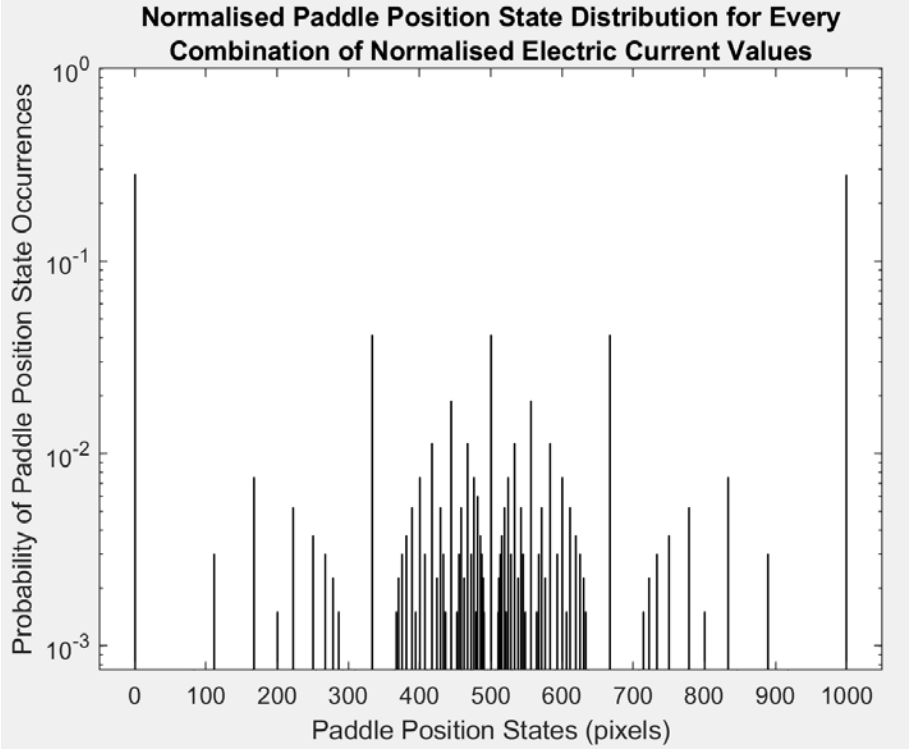


Figure A.17: The normalised distribution of paddle positions generated from every combination of normalised electric current values using the method as described in figure 6.5. The histogram shows that, due to the inference function, the paddle positions of 0 and 1000 pixels occur far more often, 28%, than any other as a result of the boundary condition. This also shows the interaction of the measurement locations with these boundary conditions, causing secondary peaks at 333, 500, and 667 pixels with percentages of 4

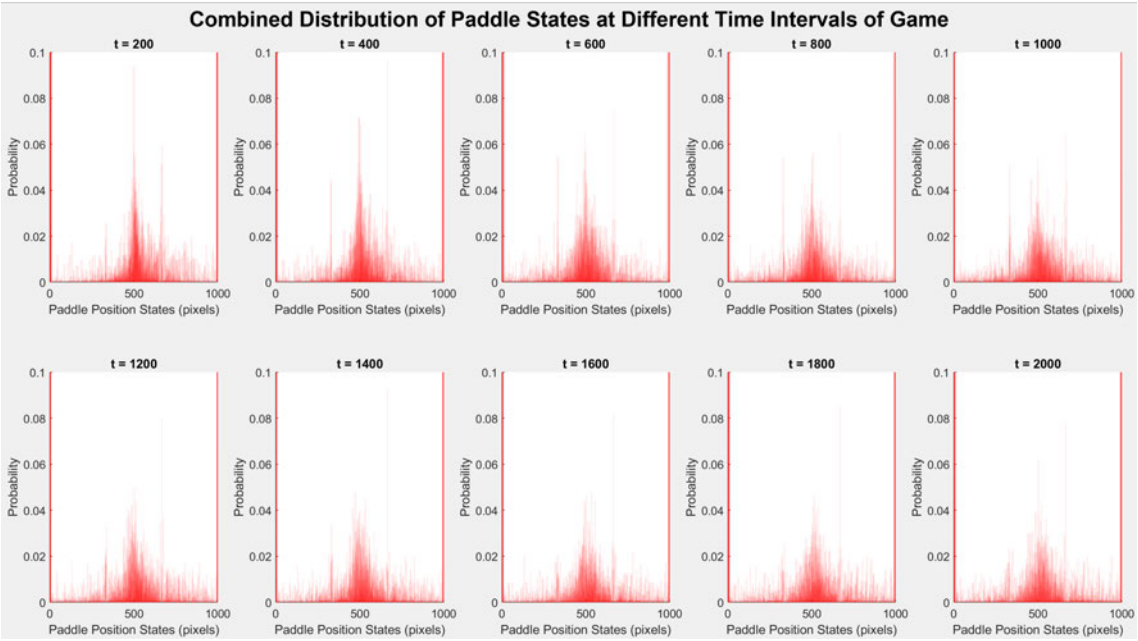


Figure A.18: A series of plots showing the changing distribution of paddle states over the course of the game. The results of each gel sample are made partially transparent and layered over each other to show the overall distribution between gels without obscuring the variation between gel samples. A window was applied over the data sets to capture the distributions, a window size of 300 seconds was used as it allowed the distribution at that point in time to captured without overlap and gave enough distributions to visually see change in behaviour.

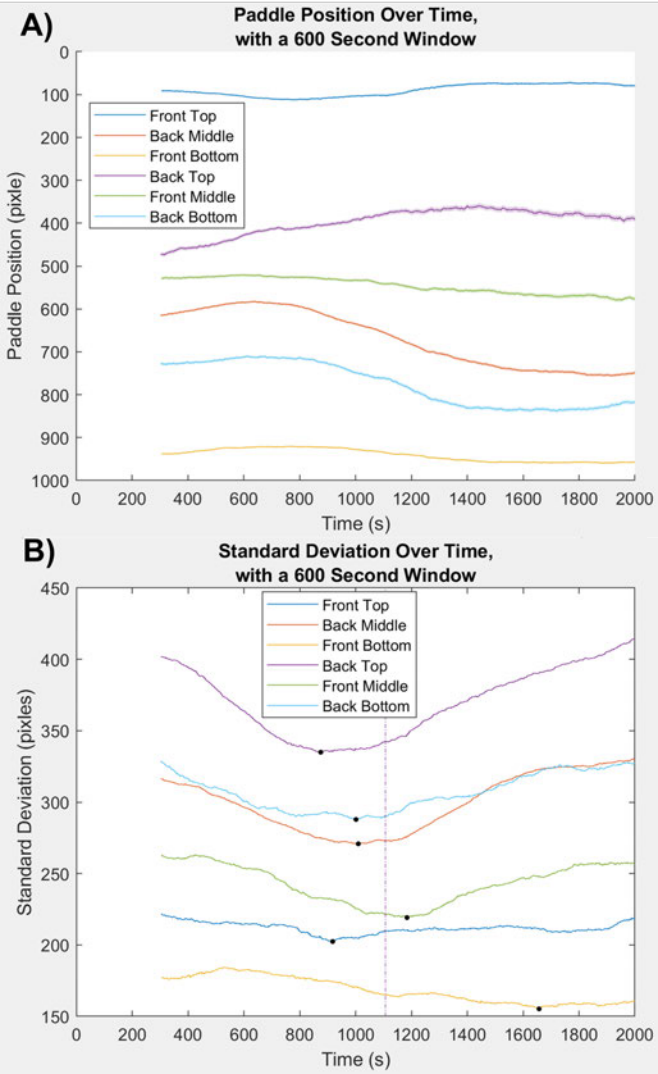


Figure A.19: **A)** Paddle position over time for the combined unimpaired feedback loop dataset, separated based on the region location of the ball as described in figure 6.4 section B. Smoothed using a moving average window of 600 seconds, as with previous figures. The standard error for each windowed sample is show by the shaded area. The y axis is inverted as the (0,0) origin in the Pong game environment is in the top left corner, with bottom right as (1000,1000). As time approaches the point of maximum learning, shown in figures 6.8 and 6.7, the paddle moves more appropriately given the position of the ball. This is most evident in the response of the back regions, where over time the back bottom causes the paddle to move down much more consistently and the back top causes the paddle to move up much more consistently, as the EAP gel "anticipates" the position of the ball coming toward the paddle. **B)** Standard deviation of paddle position over time for the combined unimpaired feedback loop dataset, separated based on the region location of the ball as described in figure 6.4 section B. A moving window of 600 seconds, as with previous figures, was used to apply the standard deviation on the unsmoothed dataset. The point of lowest standard deviation is marked on each dataset by the black dot. The purple vertical dashed line marks the average point of lowest standard deviation between all datasets, at 1107 seconds. Across all region responses, as time approaches the point of maximum learning shown in figures 6.8 and 6.7, the paddle's motion becomes less erratic as the standard deviation decreases.

Table A.2: Change in Paddle Position Over Learning per Region

| **Region** | **Paddle Position at t=300 (pixels)** | **Paddle Position at t=1600 (pixels)** | **Change in Paddle Position (% of 1000 pixels)** |
|---|---|---|---|
| Front Top | 91 | 75 | 1.6 |
| Back Middle | 615 | 743 | 12.8 |
| Front Bottom | 938 | 958 | 2 |
| Back Top | 473 | 370 | 10.3 |
| Front Middle | 529 | 567 | 3.8 |
| Back Bottom | 728 | 835 | 10.7 |

Table A.3: Reduction in Standard Deviation (SD) per Region

| **Region** | **Starting SD (pixels)** | **Lowest SD (pixels)** | **Time of lowest SD (seconds)** | **SD Reduction (pixels)** | **SD Reduction per Second (pixels per second)** |
|---|---|---|---|---|---|
| Front Top | 222 | 202 | 918 | 20 | 0.022 |
| Back Middle | 316 | 271 | 1010 | 45 | 0.045 |
| Front Bottom | 178 | 155 | 1657 | 23 | 0.014 |
| Back Top | 402 | 335 | 875 | 67 | 0.077 |
| Front Middle | 262 | 219 | 1184 | 43 | 0.036 |
| Back Bottom | 328 | 288 | 1001 | 40 | 0.040 |

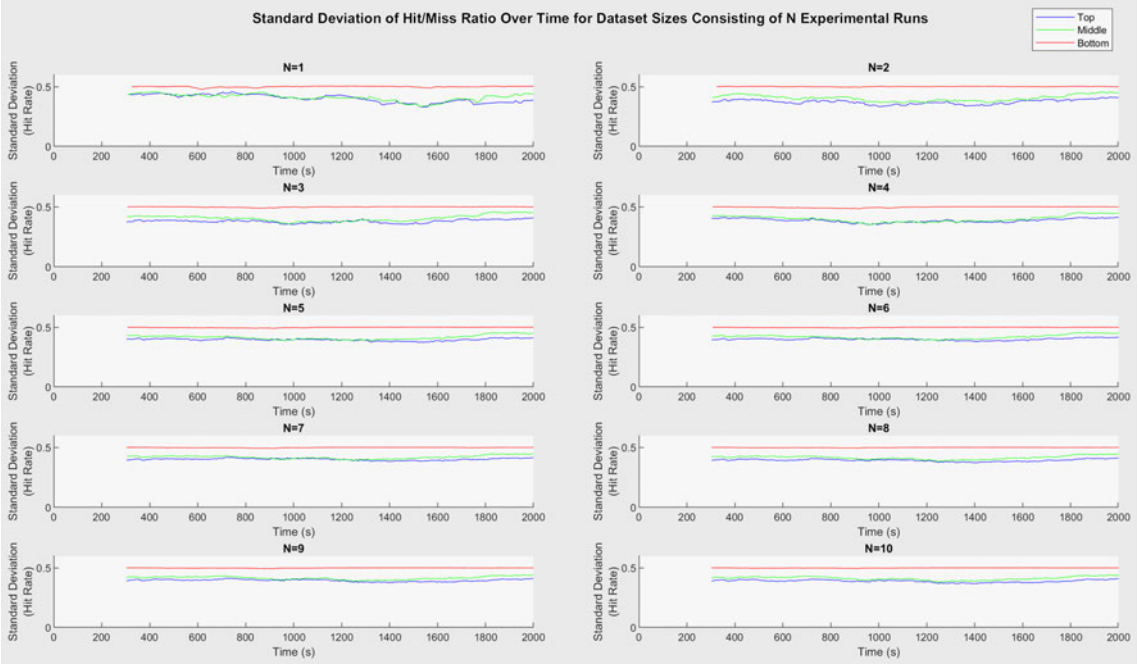


Figure A.20: Standard deviation of hit rate (for top, middle, and bottom regions) over time for the sensing impaired control experiment datasets consisting of N experimental runs. A moving window of 600 seconds, as with previous figures, was used to apply the standard deviation on the unsmoothed dataset. After 4 experimental runs the trend of standard deviation does not appear to change any further and so has stabilised. 10 experiments were run in total to ensure this stability.

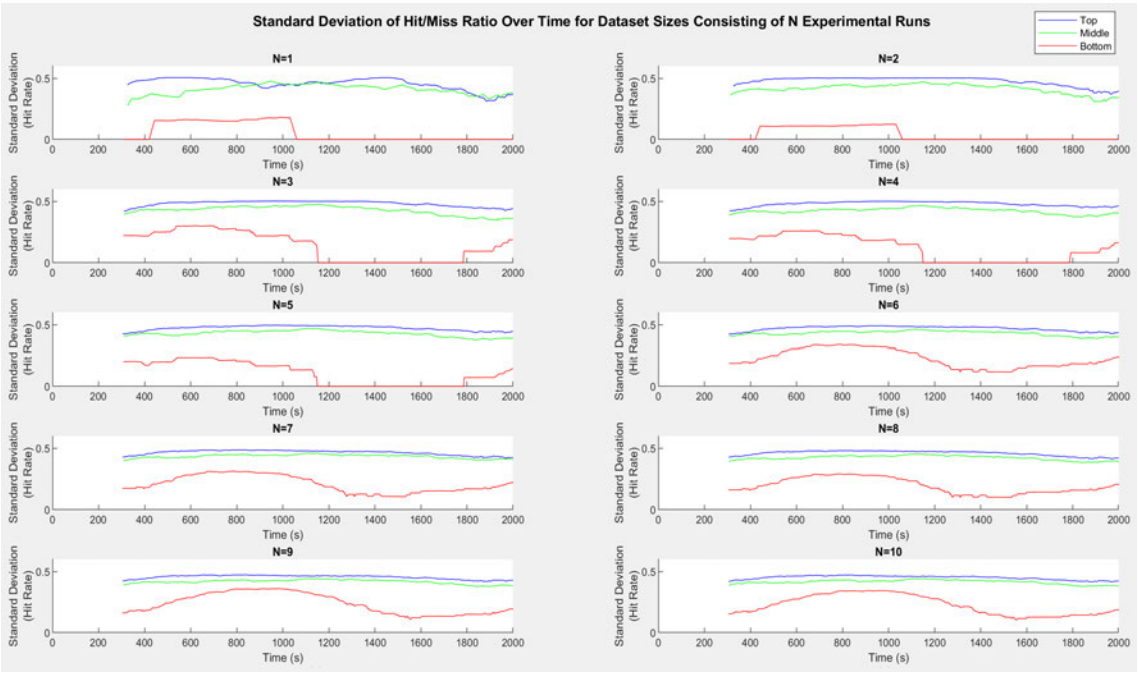


Figure A.21: Standard deviation of hit rate (for top, middle, and bottom regions) over time for the stimulation impaired control experiment datasets consisting of N experimental runs. A moving window of 600 seconds, as with previous figures, was used to apply the standard deviation on the unsmoothed dataset. With a dataset consisting of 9 experimental runs the trend of standard deviation does not appear to change any further and so has stabilised and no further experimental runs are necessary.

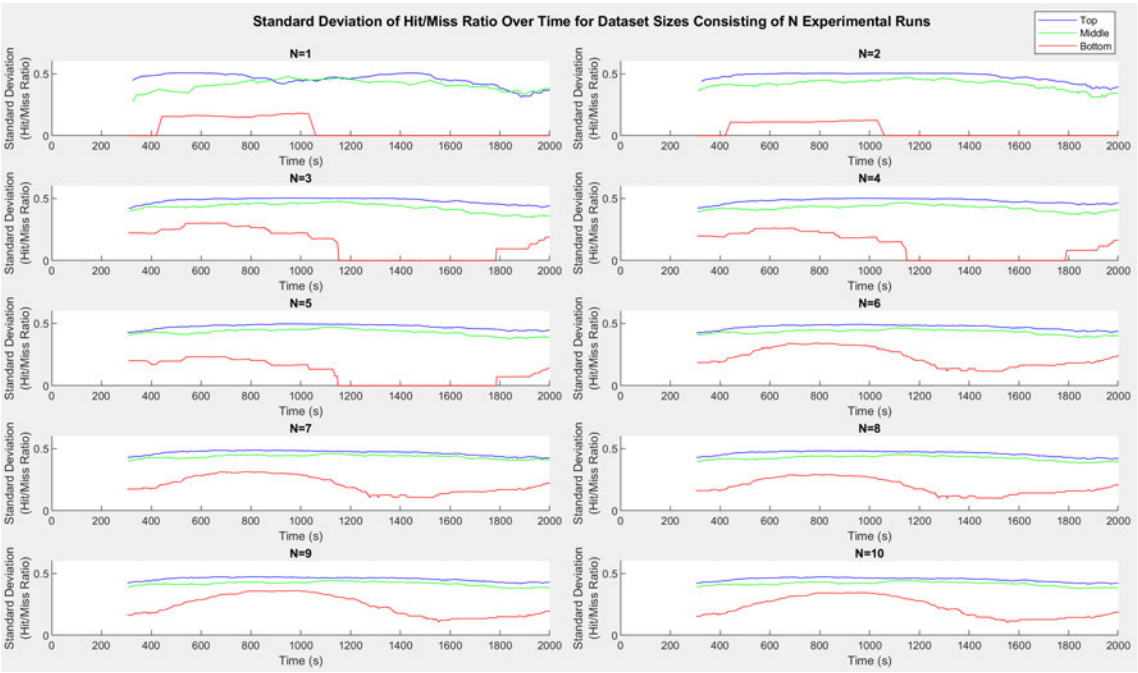


Figure A.22: Standard deviation of hit rate (for top, middle, and bottom regions) over time for the baseline datasets consisting of N experimental runs. A moving window of 600 seconds, as with previous figures, was used to apply the standard deviation on the unsmoothed dataset. With a dataset consisting of 9 experimental runs the trend of standard deviation does not appear to change any further and so has stabilised and no further experimental runs are necessary.

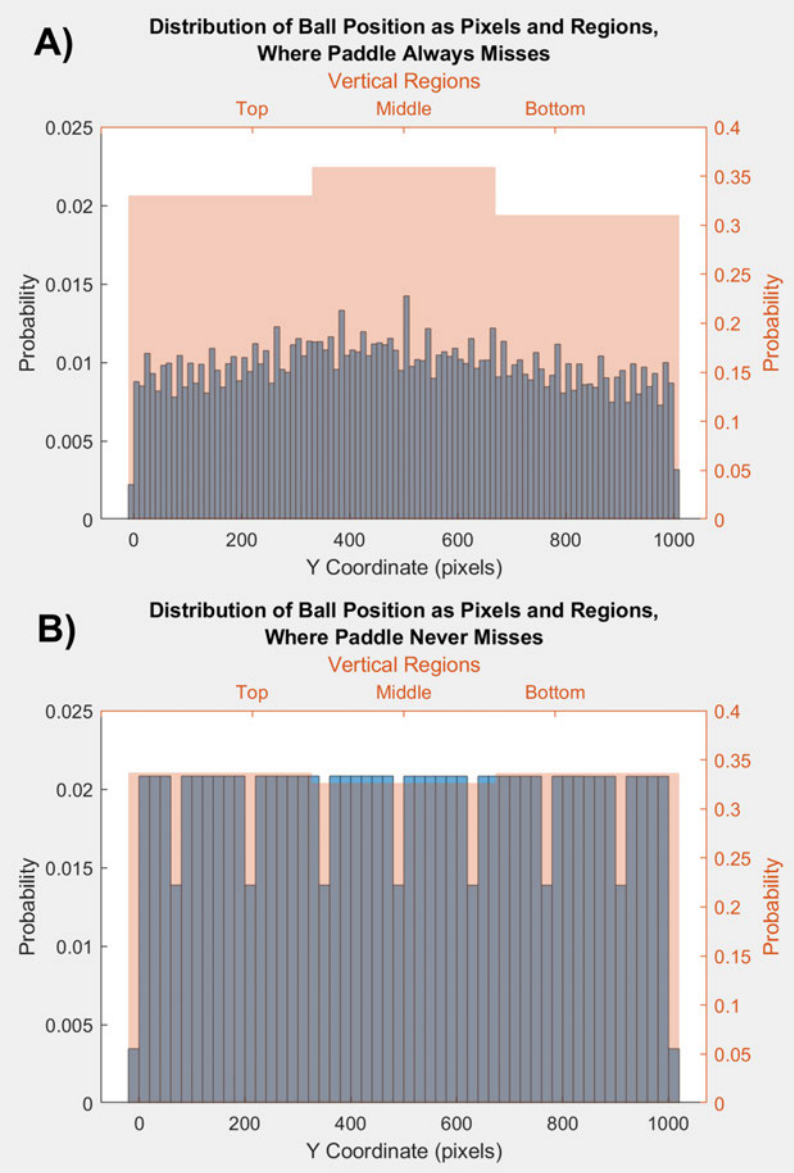


Figure A.23: The simulated distributions of vertical ball states. The ball was simulated with the same game environment physics, starting with a random direction and resetting to the centre on a miss. **A)** Distribution of ball states where the paddle never hits the ball and so the ball continually resets to it's starting position when hitting the left wall of the game area. This histogram had a Y coordinate position variance of 6.86e+04, and a vertical region position variance of 5.47e+07. **B)** Distribution of ball states where the paddle never misses the ball and so the ball is never reset to it's starting position, always being bounded back when hitting the left wall of the game area. This histogram had a Y coordinate position variance of 1.49e+04, and a vertical region position variance of 3.23e+07.

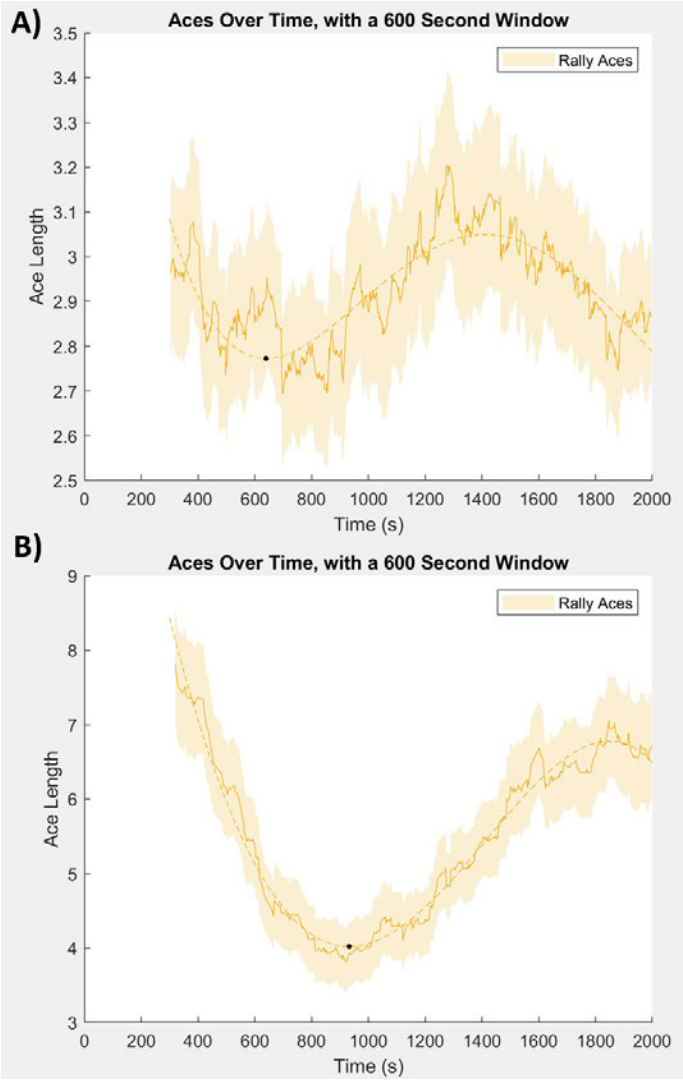


Figure A.24: Plot of rally aces, representing the number of times the paddle failed to intercept the ball without a single hit. Smoothed using a moving average window of 600 seconds. The standard error for each windowed sample is shown by the shaded area. A 4th degree polynomial best fit line was applied via the MATLAB Polyfit function [240]. This was the minimum order polynomial that fit the trend presented by the data. **A)** Rally aces of inhibited sensing information control experiment. The maximum point of performance is marked by the black dot at 639 seconds. The performance is however inverted as to what is shown in the learning experiment of figure A.16. The number of misses starts at a lower position then increases toward the point of maximum learning seen in other trends. The length of rally aces is also longer than that of the learning trend, showing that in this control experiment the paddle missed more often. **B)** Rally aces of inhibited stimulation information control experiment. The maximum point of performance is marked by the black dot at 933 seconds. As with the other control experiment the performance is inverted as to what is shown in the learning experiment of figure A.16. The number of misses, again, starts at a lower position then increases toward the point of maximum learning seen in other trends. The length of rally aces is also considerably longer than that of the learning trend, showing that in this control experiment the paddle missed far more often.

# Appendix B

# Code

The code used throughout this project would be far to long to include in its entirety and so is included via online repositories assigned to each chapter in which custom code is used. These repositories are made permanently available through Zenodo.org, the Zenodo badge is provided for each repository below along with the github link.

- Chapter 3 - Reproducing EAP Hydrogel Actuation Results
  - `https://github.com/VaStrong/Reproducing-EAP-Hydrogel-Actuation-Results.git`
  - `10.5281/zenodo.8006671`
- Chapter 4 - Electroactive Polymer Gels as Probabilistic Reservoir Automata for Computation
  - `https://github.com/VaStrong/Electroactive_Polymer_Gels_as_Computational_Probabilistic_Reservoir_Automata.git`
  - `10.5281/zenodo.7274655`
- Chapter 5 - EAP Hydrogel Inspired Spiking Neural Network
  - `https://github.com/VaStrong/EAP-Gel-Inspired-Spiking-Neural-Network.git`
  - `10.5281/zenodo.8006675`
- Chapter 6 - Learning Behaviour When Embodied in a Simulated Game-World
  - `https://github.com/VaStrong/EAP_Hydrogels_Exhibit_Emergent_Learning_When_Embodied_in_a_Simulated_Game-Environment.git`
  - `10.5281/zenodo.10615663`